

TECHNISCHE UNIVERSITÄT MÜNCHEN

Fachgebiet für Peptidbiochemie

**Synthesis, Characterization and Application of Stabilized Natural
Substrates as Protein Tyrosine Phosphatase Inhibitors**

Christoph Meyer

Vollständiger Abdruck der von der Fakultät Wissenschaftszentrum Weihenstephan für Ernährung, Landnutzung und Umwelt der Technischen Universität München zur Erlangung des akademischen Grades eines

Doktors der Naturwissenschaften (Dr. rer. nat.)

genehmigten Dissertation.

Vorsitzende:

Univ.-Prof. Dr. Iris Antes

Prüfer der Dissertation:

1. Univ.-Prof. Dr. Aphrodite Kapurniotu
2. Univ.-Prof. Dr. Dr. h.c. Horst Kessler

Die Dissertation wurde am 02.04.2012 bei der Technischen Universität München eingereicht und durch die Fakultät Wissenschaftszentrum Weihenstephan für Ernährung, Landnutzung und Umwelt am 09.07.2012 angenommen.

This Thesis was carried out under the supervision of Dr. Maja Köhn at the European Molecular Biology Laboratory (EMBL) in Heidelberg, Germany, between 2008 and 2012.

To Petra & my parents

Acknowledgments

First of all I want to thank Dr. Maja Köhn for providing me the opportunity to carry out this work in her laboratory and under her constant supervision. I am grateful to her for sharing her scientific expertise and experience with me. Her motivation, advice and support enabled me to acquire a wide variety of scientific skills spanning the areas of chemistry and biology. The experiences gained during my time in her laboratory are of invaluable importance for my future career and personal development.

I am thankful to the members of my Thesis Advisory Committee (TAC) Prof. Dr. Aphrodite Kapurniotu, Dr. Carsten Schultz and Dr. Jeroen Krijgsveld for their advice and support. I am especially grateful to Prof. Dr. Aphrodite Kapurniotu for taking part in the annual TAC meetings in Heidelberg and her support in the doctoral examination procedure.

I want to thank all members and alumni of the Köhn group for providing a truly pleasant working atmosphere characterized by mutual respect and support. Especially, I thank Dr. Jayanta Chatterjee for his constructive criticism, motivation and advice and for sharing his excitement about peptides with me. Furthermore, I want to thank him for many valuable scientific discussions and for his comments on the manuscript of this work. I want to thank my desk and hood neighbor Dr. Miriam Bru-Roig for the very nice atmosphere in “our” part of the lab and her patience and expertise in answering my chemistry and NMR related questions. Dr. Victoria Mcparland and Dr. Pablo Rios I would like to thank for their advice and help in cloning, protein expression and purification. Birgit Höger I thank for her contribution to this work during her internship.

I want to thank Dr. Jan Medenbach for generously sharing vectors and his experience in DNA cloning.

I am grateful to Kerstin Putzker and Dr. Peter Sehr from the chemical biology core facility at EMBL for their help with the enzyme assays and Dr. Nicole Jung for her collaborative efforts.

I want to thank Dr. Carsten Schultz and the members (and alumni) of his group for their input during our shared group meetings. I am especially thankful to Dr. Matthias Mentel, Dr. Adrian Neal, Dr. Oliver Wichmann, Dr. Gregor Reither, Dr. Amanda Cobos and Dr. Alen Piljic for helpful discussions and suggestions.

Publications

Parts of this thesis have already been published:

The Metastasis-Promoting Phosphatase PRL-3 Shows Activity toward Phosphoinositides. V. McParland, G. Varsano, X. Li, J. Thornton, J. Baby, A. Arvind, C. Meyer, K. Pavic, P. Rios, M. Köhn (2011) *Biochemistry*. **50**, 7579-7590.

Efficient Scaled-Up Synthesis of N- α -Fmoc-4-Phosphono(difluoromethyl)-L-phenylalanine and Its Incorporation into Peptides. C. Meyer, M. Köhn (2011) *Synthesis*. **2011**, 3255-3260.

Table of contents

List of abbreviations	X
List of figures	XV
1 INTRODUCTION	1
1.1 Cell signaling and protein phosphorylation	1
1.2 Control of phosphorylation by protein kinases and phosphatases	2
1.3 The protein tyrosine phosphatase (PTP) family	3
1.4 PTP1B (<i>PTPN1</i>) and its role in human disease.....	8
1.5 Inhibitors of PTP1B	12
1.6 Chemical probes to study PTP1B activity.....	17
2 AIM OF THE PROJECT	19
3 RESULTS	21
3.1 Determination of a substrate sequence for further derivatization	21
3.1.1 Selection of suitable substrate sequences for <i>in vitro</i> screening	21
3.1.2 Synthesis of phosphopeptides	22
3.1.3 Screening of the phosphopeptide library	22
3.2 Selection of a non-hydrolyzable phosphotyrosine analogue	24
3.2.1 Efficient scaled-up synthesis of N- α -Fmoc-4-Phosphono(difluoromethyl)-L-phenylalanine	25
3.2.2 Incorporation of F ₂ Pmp into peptides.....	27
3.3 Cyclization of F₂Pmp containing peptides	29
3.3.1 Cyclization trials using the thiol-ene reaction.....	29
3.3.2 Cyclization using the copper catalyzed azide-alkyne cycloaddition (CuAAC)	33
3.4 Binding and inhibition studies of F₂Pmp containing peptides	38
3.4.1 Measurement of inhibitory potencies using the pNPP inhibition assay.....	39
3.4.2 Affinity measurements with the fluorescence polarization assay.....	45
3.5 Evaluation of the cellular penetration, stability and activity of the peptidic inhibitors	47

3.5.1 Comparison of cellular penetration using confocal microscopy.....	47
3.5.2 Colocalization of a cell penetrating CF-Src-P(-2)A sequence with PTP1B	50
3.5.3 Stability of linear versus cyclic inhibitory peptides in cell lysate and human blood serum	53
3.6 Biotinylated F₂Pmp containing peptides as pull-down tools.....	55
4 DISCUSSION.....	65
4.1 Selection of a substrate sequence for further inhibitor development	65
4.2 Efficient synthesis of N-Fmoc-F₂Pmp and its incorporation into peptides.....	67
4.3 Cyclization of the inhibitory peptide	67
4.4 Analysis and binding studies of Src derived linear and cyclic sequences	68
4.5 Influence of cyclization on cell permeability and stability.....	73
4.6 Application of biotinylated F₂Pmp containing sequences as pull-down tools	74
5 CONCLUSIONS AND PERSPECTIVES	76
6 SUMMARY	79
7 EXPERIMENTAL SECTION.....	81
7.1 General.....	81
7.1.1 Chemicals.....	81
7.1.2 Instruments.....	81
7.1.3 Buffers and Media	83
7.1.4 Biological material	85
7.1.5 Software	87
7.1.6 Cloning, expression and purification of recombinant proteins.....	87
7.2 Experiments and methods to chapter 3.....	93
7.2.1 Experiments and methods to chapter 3.1.2.....	93
7.2.2 Experiments and methods to chapter 3.1.3.....	97
7.3.1 Experiments and methods to chapter 3.2.1.....	98
7.3.2 Experiments and methods to chapter 3.2.2.....	100
7.4.1 Experiments and methods to chapter 3.3.1.....	103
7.4.2 Experiments and methods to chapter 3.3.2.....	105
7.5.1 Experiments and methods to chapter 3.4.1.....	108
7.5.3 Experiments and methods to chapter 3.4.2.....	116

7.6.1 Experiments and methods to chapter 3.5.1	120
7.6.2 Experiments and methods to chapter 3.5.2	121
7.6.3 Experiments and methods to chapter 3.5.3	122
7.7 Experiments and methods to chapter 3.6	124
8 REFERENCES	133

List of abbreviations

Å	Ångström
AA	Amino acid
ABPP	Activity based protein profiling
Alloc	Allyloxycarbonyl
ATP	Adenosine triphosphate
AUC	Area under the curve
Bcr-Abl	Break point cluster region - Abelson
BPPM	Bis(para-phosphophenyl)methane
BSA	Bovine serum albumin
c-Src	cellular Src (“sarcoma”) kinase
cAMP	Cyclic adenosine monophosphate
Cdk	Cyclin dependent kinase
(c)DNA	(complementary) DNA
CF	5(6)-Carboxyfluorescein
CHO	Chinese hamster ovary
CML	Chronic myeloid leukemia
COSY	Correlation Spectroscopy
CPP	Cell penetrating peptide
CuAAC	Copper catalyzed azide alkyne cycloaddition
DAST	Diethylaminosulfur trifluoride
DCM	Dichloromethane
DIPEA	N,N-Diisopropylethylamine
DMAP	4-Dimethylaminopyridine
DMEM	Dulbecco’s modified eagle medium
DMF	Dimethylformamide
DSP	Dual-specific phosphatase

DTT	Dithiothreitol
EC ₅₀	Half maximal effective concentration
EDC	1-Ethyl-3-(3-dimethylaminopropyl)carbodiimide
EGF(R)	Epidermal growth factor (receptor)
EGFP	Enhanced green fluorescent protein
Equiv	equivalent
ER	endoplasmic reticulum
ErbB2 (Neu)	Member of the EGFR family
EtOAc	Ethylacetate
F2Pmp	Difluorophosphonomethylphenylalanine
FDA	Food and drug administration
FLIM	Fluorescence lifetime imaging microscopy
Fmoc	Fluorenylmethoxycarbonyl
FP	Fluorescence polarization
FPLC	Fast protein liquid chromatography
FRET	Förster resonance energy transfer
g	Gram
GST	Glutathione-S-transferase
HAD	Haloacid dehalogenase
HATU	2-(1H-7-Azabenzotriazol-1-yl)-1,1,3,3-tetramethyluronium hexafluorophosphate
HBTU	<i>O</i> -(Benzotriazol-1-yl)- <i>N,N,N',N'</i> -tetramethyluronium hexafluorophosphate
HEPES	4-(2-hydroxyethyl)-1-piperazineethanesulfonic acid
HMQC	Heteronuclear Multiple-Quantum Correlation
HOAt	1-Hydroxy-7-azabenzotriazole
HPLC	High pressure liquid chromatography
HRP	Horse radish peroxidase
IC ₅₀	Half maximal inhibitory concentration

IGF1R	Insulin-like growth factor 1 receptor
IR(K)	Insulin receptor (kinase)
IRS-1	Insulin receptor substrate-1
IZD	Isothiazolidinone
Jak	Janus kinase
K_d	Dissociation constant
kDa	Kilo Dalton
K_i	Inhibition constant
K_M	Michaelis-Menten constant
L	Liter
LB	Luria (Bertani) broth
LMPTP	Low molecular weight protein tyrosine phosphatase
m	Milli
M	Molar (mol/liter)
MALDI	Matrix-assisted laser desorption ionization
MeCN	Acetonitrile
MeOH	Methanol
MES	2-(<i>N</i> -morpholino)ethanesulfonic acid
Mmt	Monomethoxytrityl
(HR)MS	(High resolution) Mass spectrometry
Mtt	4-Methyltrityl
n	Nano
NMR	Nuclear magnetic resonance
OMT	O-malonyltyrosyl
OST-PTP	Osteotesticular protein tyrosine phosphatase
P-loop	Phosphate binding loop
PBS	Phosphate buffered saline
PCR	Polymerase chain reaction
PDB	Protein data bank

PDGFR	Platelet-derived growth factor receptor
pH	Negative decimal logarithm of the hydrogen ion concentration
Pi	Inorganic phosphate
PI(3,4,5)P ₃	Phosphatidylinositol-3,4,5-trisphosphate
PI(4,5)P ₂	Phosphatidylinositol-4,5-bisphosphate
PI3K	Phosphoinositide 3-kinase
PK	Protein kinase
pKa	Acid dissociation constant
Pmp	Phosphonomethylphenylalanine
PMSF	Phenylmethylsulfonylfluoride
pNPP	Para-nitrophenylphosphate
PP	Protein phosphatase
ppm	Parts per million
Pra	Propargylglycine
PRL-3	Phosphatase of regenerating liver-3
PSTP	Protein serine/threonine phosphatase
PTEN	Phosphatase and tensin homolog
PTK	Protein tyrosine kinase
PTP	Protein tyrosine phosphatase
PTP1B	Protein tyrosine phosphatase 1B
Q-loop	Glutamine loop
r.t.	room temperature
RNA	Ribonucleic acid
ROS	Reactive oxygen species
RP	Reversed phase
RPTP	Receptor protein tyrosine phosphatase
SDS-PAGE	Sodium dodecylsulfate polyacrylamide gel electrophoresis-
SFKs	Src family kinases

SH2-domain	Src homology 2 domain
SH3-domain	Src homology 3 domain
SO ₂ H	Sulphinic acid
SO ₃ H	Sulphonic acid
SOH	Sulphenic acid
SPPS	Solid phase peptide synthesis
TAE	Tris-actetate buffer
TBST	Tris-buffered saline + Tween 20
TBTU	O-(Benzotriazol-1-yl)-N,N,N',N'-tetramethyluronium tetrafluoroborate
<i>t</i> BuOH	Tertiary butanol
TCA	Trichloro acetic acid
TCPTP	T-cell protein tyrosine phosphatase
TEA	Triethylamine
TFA	Trifluoro acetic acid
TGS	Target guided synthesis
TIS	Triisopropyl silane
TLC	Thin-layer chromatography
TMSBr	Trimethylsilyl bromide
TMSE	2-(Trimethylsilyl)ethanol
TOF	Time-of-flight
UV	Ultra violett
v-Src	Viral Src ("Sarcoma") kinase
WPD-loop	Tryptophane-proline-aspartate-loop
YRD-loop	Tyrosine-arginine-aspartate-loop
δ	delta (chemical shift)
μ	micro

List of figures and schemes

Figure 1: Reversible Phosphorylation of proteins

Figure 2: Classification of the human protein tyrosine phosphatase family

Figure 3: Domain architecture of PTPs

Figure 4: Catalytic and regulatory mechanism of PTP1B

Figure 5: Structural features of PTP1B

Figure 6: Molecular structures of described PTP1B inhibitors

Figure 7: General strategy for the synthesis of potent, specific and bioavailable PTP inhibitors

Figure 8: K_M value comparison of PTP1B and TCPTP towards a panel of phosphopeptides

Figure 9: Phosphotyrosine (pTyr) and its non-hydrolyzable phosphonodifluoromethyl-L-phenylalanine (F₂Pmp).

Figure 10: F₂Pmp containing model peptide **45**

Figure 11: Structural considerations for the synthesis of peptides **50** and **51**

Figure 12: MALDI and HPLC analysis of peptides **59** and **60**

Figure 13: Trials to perform *in situ* ring closure.

Figure 14: Sequences and IC₅₀ values of the alanine scan peptides

Figure 15: Sequences and IC₅₀ values of the truncation scan peptides

Figure 16: IC₅₀ values of the peptides tested with the pNPP competition assay

Figure 17: Molecular structure of the cyclic peptides **84** (“cyclo-K(CF)-Src-1C”) and **85** (“cyclo-K(CF)-Src-5C”) carrying the 5(6)-carboxyfluorescein fluorescent label

Figure 18: K_d values obtained with the fluorescence polarization assay

Figure 19: Comparison of cellular uptake and localization of the linker containing sequences before and after cyclization

Figure 20: Comparison of cellular uptake and localization of peptides bearing increasing amounts of arginine residues

Figure 21: Peptide **91** (CF-Src-P(-2)A-R₆) but not **92** (CF-Src-Y-R₆) colocalizes with mKate-PTP1B in U2OS cells

Figure 22: Stability of the linear linker-containing and cyclic peptides in U2OS cell lysate

Figure 23: Comparison of the stability of the linear and cyclic peptides in human serum

Figure 24: Cyclic and linear biotinylated peptides used for the pull-down experiments

Figure 25: Comparison of the pull-down efficiency of several biotinylated peptides

Figure 26: Comparison of the results of three independent pull-down experiments of endogenous PTP1B by several biotinylated peptides

Figure 27: Fluorescence polarization assay against PTP1B with peptides bearing the fluorescein either at the N-terminus or in the side chain of an N-terminal lysine

Figure 28: Loading of biotinylated peptides to streptavidin beads determined by HPLC quantification

Figure 29: Comparison of pull-down efficiency of transiently overexpressed EGFP-PTP1B and EGFP-TCPTP

Figure 30: Pull-down of endogenous PTP1B from U2OS cell lysates on a silver stained gel

Figure 31: Visualization of alanine and truncation scan data

Figure 32: Expressed and purified recombinant proteins on a 4-12% Bis-tris SDS polyacrylamide Gel

Scheme 1: Synthesis of N-Fmoc-F₂Pmp-OH

Scheme 2: Solid phase Synthesis of model peptide **44** containing F₂Pmp

Scheme 3: Cyclization trials of F₂Pmp containing peptides **46** and **47** using the thiol-ene reaction

Scheme 4: Cyclization trials of phosphotyrosine containing peptides **50** and **51** using the thiol-ene reaction

Scheme 5: Azide functionalization of peptides

Scheme 6: Cyclization of peptides “Src-5C” (**57**) and “Src-1C” (**58**) using azide-alkyne 1,3-dipolar cycloaddition

Scheme 7: Theoretical considerations on the inhibitory mechanism

1 Introduction

1.1 Cell signaling and protein phosphorylation

Communication between individual cells is essential for the adaptation and response to changes in the (micro-) environment of multicellular organisms, as well as populations of single cells.¹ This process, often referred to as cell signaling, relies on the ability of a cell to receive signals from the outside, which is accomplished by specialized protein molecules, so called “receptors”.² The conceptual background that led to the appreciation of these specific molecular recognition processes was already formed in the late nineteenth century by Emil Fischer in his famous lock-and-key analogy.^{3,4}

External stimuli activating their specific receptor can be of physical or chemical nature. Depending on the physicochemical properties of a signaling molecule, it can either diffuse through the plasma membrane and bind its receptor in the cytoplasm, or bind to membrane-spanning receptors, which transfer the signal to the interior. Inside the cell the signal is propagated from the receptor to other proteins resulting in signaling pathways, which themselves are embedded in complex signaling networks.^{1,2}

A comprehensive understanding on how signals are transferred started to arise early in the second half of the 20th century with the discovery that posttranslational modifications can influence the activity of enzymes and the identification of the first second messenger, cyclic adenosine monophosphate (cAMP).² The role of one of the major posttranslational modifications in this context, reversible protein phosphorylation, was first described by Krebs and Beavo.^{5,6} The control over the momentary phosphorylation status of a protein is achieved by the concerted action of protein kinases (PKs) and phosphatases (PPs) (Figure 1).^{5,7} Whereas kinases catalyze the transfer of a phosphate group from the cofactor adenosine trisphosphate (ATP) to a specific residue on the target molecule, phosphatases are responsible for their removal conferring a similar level of specificity.⁷

The effect of phosphorylation on a given protein can vary between altering the enzymatic activity, change of conformation or binding to other (adaptor-) proteins, which ultimately may cause a change in cellular localization.² Modern proteomic approaches can help to understand these processes in greater detail and showed that many proteins have even multiple phosphorylation sites and could therefore be regarded as “integration platforms” in the context of signaling networks.⁶

Due to the vital importance of accurate signaling, perturbation of these events is consequentially contributing to the development of human diseases such as cancer and

diabetes.⁸ A very prominent example on how detailed knowledge about aberrant signaling in human diseases can lead to the discovery of treatments, is the development of the drug imatinib. It was rationally designed in the 1990s as inhibitor of the aberrant kinase activity of the BCR-Abelson (Abl) fusion protein, which is caused by the chromosomal abnormality “Philadelphia chromosome” and leads to the development of chronic myeloid leukaemia (CML).^{9–12} Since its approval by the U.S. food and drug administration (FDA) in 2001, it has proven to be superior to traditional, less selective, treatments in Philadelphia chromosome positive CML patients in terms of toleration and long-term survival.¹²

It is therefore highly desirable to generate molecular tools to interfere selectively with signaling processes to gain further knowledge about these complex systems and, ultimately, to develop treatments against human diseases.

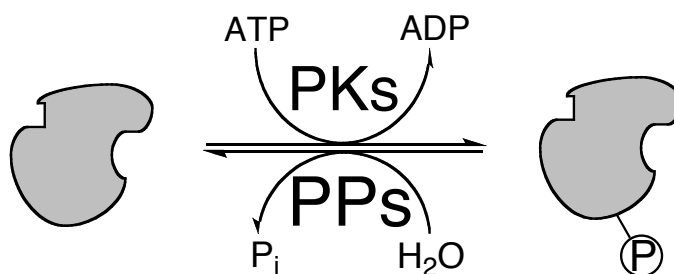


Figure 1: Reversible phosphorylation of proteins by protein kinases (PKs) and phosphatases (PPs).⁵

1.2 Control of phosphorylation by protein kinases and phosphatases

Although counteracting each other, kinases and phosphatases must not be regarded as opponents. Both enzyme classes are jointly responsible for the maintenance of a physiological phosphorylation equilibrium.⁷ An estimated one-third of all proteins in higher eukaryotes are phosphorylated at any given time and only a minor part changes its phosphorylation levels upon stimulation, highlighting the importance of a precisely regulated steady state.⁶

The most abundantly phosphorylated residues in proteins of eukaryotes are tyrosine, threonine and serine residues with a relative distribution of 1.8%, 11.8% and 86.4% as determined by Mann and coworkers in a human cancer cell line (HeLa).⁶ The kinases responsible for the phosphorylation of these residues can be grouped into one major class.^{13,14} The phosphatases, on the contrary, have evolved in two distinct families, which differ significantly in their domain structure as well as their catalytic mechanism.¹⁵ The two groups are termed according to their preferential substrate specificity as protein serine/threonine phosphatases (PSTPs) and protein tyrosine phosphatases (PTPs).¹⁵ The main characteristic of the PSTP family is the structure of their catalytic core domain, which requires

two complexed metal ions for catalysis. The control over their activity and substrate specificity is provided by a plethora of regulatory subunits.¹⁶

The characteristic feature of the PTP family is the presence of the active-site signature motif HCX₅R containing the essential cysteine residue required for catalysis.¹⁵ In contrast to the PSTPs, which are organized at the holoenzyme level, almost all PTPs are built up by multiple domains that determine their subcellular localization and/or substrate specificity. PTPs share this regulatory principle with PTKs, which may also reflect their similarity in the number of genes identified, 107 human PTPs are counteracting 90 PTKs.¹⁷ On the contrary, individual PSTPs can fulfill a variety of tasks through their regulation by the different subunits and, thus, it is not surprising that much fewer genes have been identified compared to their counteracting kinases, which are also regulated on the domain level.¹⁷

Interestingly, the use of tyrosine phosphorylation appears to be an almost exclusive feature of multicellular eukaryotes.¹⁷ And, although accounting for a much lower overall number of phosphorylations compared to serine and threonine residues, the impact of tyrosine phosphorylation on the proper function of signaling events is obvious considering the highly dynamic changes upon, for example, EGF stimulation.⁶ Thus, PTPs are of paramount importance for balancing signaling events and, consequently, human health. The functional and structural details of the enzymes belonging to this class will therefore be discussed in greater detail in the next chapter.

1.3 The protein tyrosine phosphatase (PTP) family

In a fundamental paper of *Alonso et al.* in 2004 the, at that time recently sequenced human genome, was scanned for genes encoding PTPs according to sequences of catalytic motifs or entire PTP domains of already known PTPs.¹⁷ The authors identified 107 human PTP genes, which were classified in 4 groups class I, II, III and IV (Figure 2).¹⁷

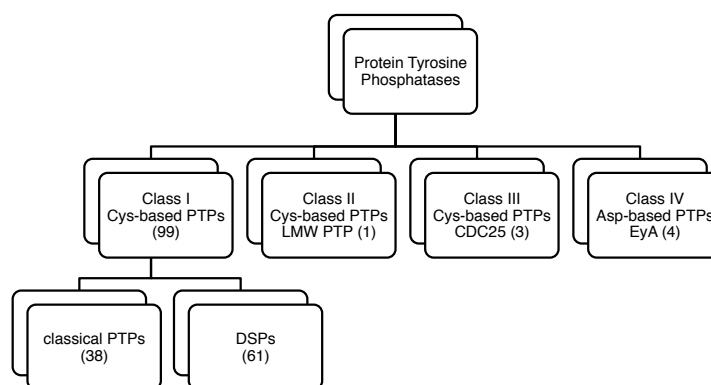


Figure 2: Classification of the human protein tyrosine family. (Adapted from reference 17.)

The highest number of genes (99) is represented in class I, which can be further subdivided into the dual-specificity phosphatases (DSPs) encoded by 61 genes and the so-called “classical” PTPs with 38 or 37 genes depending on whether or not osteotesticular PTP (OST-PTP) is regarded as pseudogene or not.^{15,17} The term “classical PTPs” refers on their specificity for tyrosine phosphorylated substrates. In contrast to that, DSPs can recognize and dephosphorylate a broader variety of substrates ranging from serine, threonine and tyrosine phosphorylated proteins and peptides to even other molecule classes like phosphoinositides or ribonucleic acid (RNA), which is caused by a much shallower architecture of the catalytic pocket compared to the one of classical PTPs.^{15,17,18}

The group of the classical PTPs includes membrane-spanning receptor-like PTPs (RPTP) and cytoplasmic enzymes (Figure 3). In 12 out of 21 RPTPs two catalytic domains, which consist of around 280 residues, are present with one being usually less or not active, but play important roles regarding specificity, stability and regulation for instance by dimerization.^{15,19–22} The extracellular part of the RPTPs is potentially involved in signaling processes by binding to extracellular ligands or cell-cell and cell-matrix contacts. Many advances have been and are still being made in understanding the influence of such interactions on the activity and specificity of the intracellular catalytic domain. Regulation of the cytoplasmic non-transmembrane PTPs (NTPTPs) is accomplished by specific domains, which can alter the activity either directly by inter- or intramolecular interactions, as described for the Src-homology-2 (SH2) domain-containing protein tyrosine phosphatase-2 (SHP-2), or indirectly by subcellular localization, as is the case for example with the C-terminal stretch of PTP1B, which localizes the enzyme predominantly to the cytoplasmic face of the endoplasmic reticulum.^{23,24}

A quite distinct characteristic of the active-site, which comprises a different residue (aspartate) being responsible for the nucleophilic attack in the catalytic mechanism, specifies the members of the class IV aspartic acid-based PTPs. The four haloacid dehalogenases (HAD) EyA1-4, which also function as transcription factors, have been grouped in this class due to their phosphatase activity against tyrosine and serine residues. A better understanding of structure and function of this class could potentially lead to the discovery of even more members of this group in the big family of HADs.^{17,26–28}

Apart from the enzymes belonging to class IV, the catalytically active domains of PTPs share the signature motif HCX₅R comprising the phosphate-binding loop (“P-loop”). The motif creates an environment that enhances the nucleophilicity of the essential cysteine residue, which has, due to the surrounding sequence, an extremely low pK_a, and hence is deprotonated at physiological pH.^{29–31} The catalytic cycle starts by a nucleophilic attack of the thiolate anion on the phosphorus atom of the substrate (Figure 4). The breakdown of the cysteinyl-phosphosubstrate intermediate is facilitated by protonation of the tyrosyl leaving group by a very important aspartate residue in the phosphatase. The very same residue functions in the next step as a base and abstracts a proton from a water molecule, which is coordinated by a glutamine residue, thereby initiating the hydrolysis of the phosphate thioester regenerating the active enzyme.^{29,32–34}

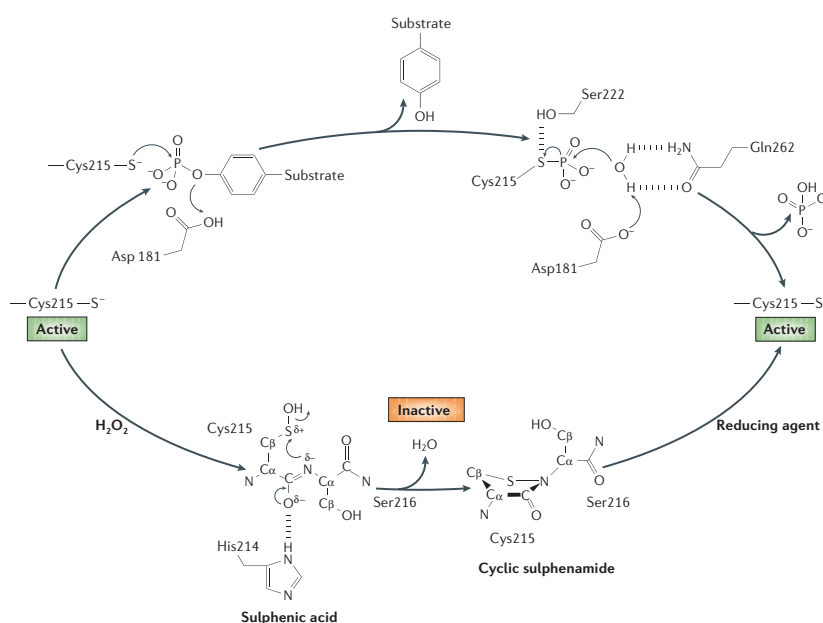


Figure 4: Catalytic and regulatory mechanism of PTP1B. (Taken from reference 15 with permission.)

The special biochemical properties of the active-site cysteine residue are not only responsible for its performance in the catalytic cycle, it is also being recognized as a feature involved in the control of enzymatic activity by oxidation (Figure 4).^{15,35–37} It has been shown that the sulfur can readily be oxidized to sulphenic (SOH), sulphinic (SO₂H) or sulphonic acid (SO₃H)

by reactive oxygen species (ROS) produced in response to many signaling events or cellular stress.^{38,39} Oxidation to sulphinic or sulphonic acid would inactivate the enzyme irreversibly, whereas the oxidative state of the sulphenic acid is reversible. Hence, in classical PTPs a mechanism has been discovered, which protects the cysteine residue from oxidation beyond the sulphenic acid state involving the formation of a cyclic sulphenamide with an adjacent backbone amide.⁴⁰ In some DSPs as well as the LMW PTP another mechanism of oxidative regulation has been unraveled, in which the active site cysteine forms a reversible disulfide bridge upon oxidation to a neighboring cysteine residue in the catalytic domain.³⁶

Considering the vast amount of signaling pathways PTPs are involved in, it is not surprising that impaired regulation of PTP activity has been linked to various human diseases.¹⁵ Along these lines, overexpression or gain-of-function mutations of certain PTP genes could be identified as a driving force in the development of certain types of cancers.⁴¹ One of the first oncogenic PTP genes identified was *PTPN11* (SHP-2). The activity and specificity of this cytoplasmic PTP is regulated by its N-terminal SH2 domain, which binds to phosphotyrosine residues of target proteins. The conformational change induced thereby promotes activation of the enzyme.²³ Various mutations in the SH2 region and PTP domain, causing higher basal activity of the enzyme, have been identified and linked to malignancies such as Noonan syndrome and leukaemias.⁴¹ Also, the Cdc25 phosphatases were identified to be involved in the development of many types of cancers, which can be directly correlated to their important role in cell cycle control.⁴² In addition to early events in tumorigenesis, PTPs have also been linked to later stages in cancer progression. The DSP phosphatase of regenerating liver-3 (PRL-3) for instance, was found to be highly overexpressed in metastases of colorectal cancer compared to the primary tumor suggesting a role in metastases formation.⁴³ Recently, PRL-3 was reported to act as phosphatidylinositol 5-phosphatase dephosphorylating PI(4,5)P₂. This activity suggests a direct role of the enzyme in metastases formation as depletion of PI(4,5)P₂ has been described to enhance cell motility.^{44,45}

But PTPs do not only promote cancer: Another DSP dephosphorylating phosphatidylinositols, the phosphatase and tensin homolog (PTEN), was identified as the first tumor suppressor gene in the PTP family. Its activity against the 3-position of PI(3,4,5)P₃ is balancing the oncogenic activity of phosphatidylinositol 3-kinase (PI3K).⁴⁶

PTPs, however, are involved in the development of many different diseases in addition to cancer, which include autoimmune diseases, like type I diabetes, Grave's disease, rheumatoid arthritis and systemic lupus erythematosus.¹⁵ Another level of complexity can be highlighted using the example of the classical non-receptor protein tyrosine phosphatases PTP1B, which was described to be involved in metabolic diseases, like type 2 diabetes and obesity, as well as in the development and suppression of cancer. This example clearly shows the challenge in phosphatase research and drug development to examine the (mis-)

regulation of an enzyme and its role in disease on the complex background of the respective cellular and signaling network environment. At the same time, investigation of this complexity bears the potential to find missing links between certain signaling events and different disease types on the molecular level and, hence, the discovery of new and effective strategies for therapeutic intervention.

1.4 PTP1B (*PTPN1*) and its role in human disease

As already mentioned at the end of the previous chapter, the cytoplasmic class I enzyme PTP1B is a very good example for the complexity of regulation and influence in signal transduction of PTPs. This might in part be due to “historical” reasons since PTP1B was the first enzyme of the family to be purified and characterized in 1988, and therefore, research on this particular member of the family had a head start.^{47,48}

Isolation of PTP1B encoding cDNA two years later revealed that the wild-type enzyme, in contrast to the 37 kDa catalytic domain purified in 1988, contains additional 114 residues at the C terminus.^{49,50} Another two years later in 1992, *Frangioni et al.* found that the 35 amino acid C-terminal sequence is localizing the enzyme to the endoplasmic reticulum with its catalytic domain facing the cytosol.²⁴ In a second article one year later the group reported that proteolytic cleavage of the C-terminal part of PTP1B by the protease calpain can relocate and augment the activity of the enzyme.⁵¹ In the same year several phosphorylation sites of serine residues in the protein were identified. Phosphorylation of these residues were shown to influence catalytic activity giving the possibility of an interconnection with serine/threonine phosphorylation networks.⁵² Very soon after in 1994, the first crystal structure of the catalytic domain (1-321) of PTP1B, and therewith, the first PTP crystal structure in general, was published by Barford and coworkers.⁵³ Due to being the first PTP that was isolated and the rapid gain of knowledge in the beginning, with a time span of only six years between the first isolation of the protein to first major breakthroughs in deciphering regulatory mechanisms and successful structure determination, PTP1B is often referred to as the “prototypic PTP”.

The structural studies of the catalytic domain of PTP1B and other PTPs together with detailed kinetic analyses revealed the general catalytic mechanism already discussed in the previous chapter (Figure 4).⁵⁴ Also, the structural architecture of the catalytic domain comprising central β -sheets surrounded by α -helices is very similar comparing individual PTPs.⁵⁵

The catalytically active cysteine, which initiates the catalytic mechanism, lies at the bottom of a 9 Å deep cleft at position 215. The signature motif HCX₅R around the active cysteine makes up the phosphate binding P-loop (Figure 5). The depth of the cleft determines the specificity of PTP1B towards tyrosine phosphorylated substrates, since phosphoserine or -threonine are too short to reach the essential cysteine residue.⁵³ The aspartate residue, which serves as

general acid in the first step of the dephosphorylation reaction, is at position 181 in PTP1B. It is located in the so-called WPD-loop and serves in the second step of the catalytic cycle as general base, facilitating the regeneration of the active cysteine by hydrolysis of the phosphate thioester intermediate through a water molecule, which is coordinated by glutamine 262 in the “Q-loop” (Figure 4 and 5).⁵³

The first crystal structure of catalytically inactive PTP1BC215S mutant together with a phosphopeptide, which was in this case derived from the autophosphorylation site of the epidermal growth factor receptor (EGFR), revealed that a conformational rearrangement of the phosphatase is made upon substrate binding. The WPD-loop is closing over the substrate, thereby creating a binding pocket and enabling π -stacking interactions of phenylalanine 182 with the phosphotyrosine substrate (Figure 5 (C)).⁵⁶ The discovery of another non-catalytic binding site, the so-called “second aryl phosphate-binding site”, by cocrystallization of PTP1B with the unnatural substrate bis(*para*-phosphophenyl)methane (BPPM) gave important implications for subsequent design of small molecule inhibitors of the active site.⁵⁷ Kinetic analysis and cocrystallization of PTP1B with doubly phosphorylated stretches of the insulin receptor kinase (IRK), a reported substrate of PTP1B, revealed also a physiological role of the second binding site. Whereas pTyr-1162 of the IRK binds to the active site, the more C-terminal pTyr-1163 was found to bind the secondary site. The binding is predominantly mediated by the arginines 24 and 254 of PTP1B. A dramatic drop of affinity was observed, when Tyr-1163 was not phosphorylated.⁵⁸

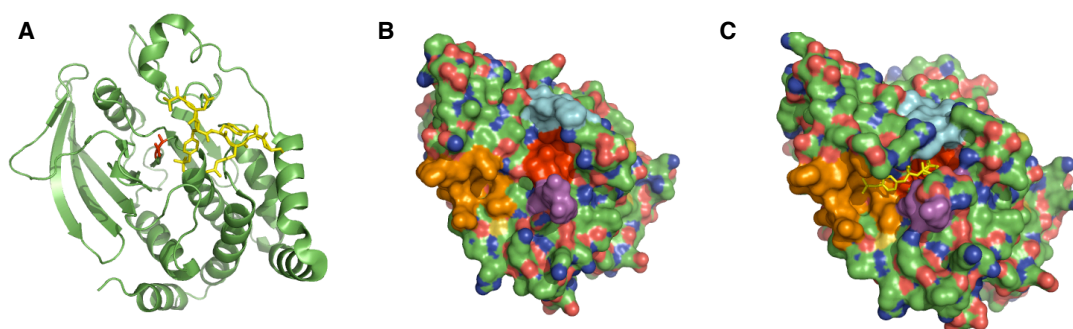


Figure 5: Structural features of PTP1B. (A) The catalytic domain of PTP1B (1-321) has the typical arrangement of secondary structure elements, central β -sheets are flanked by α -helices. The active cysteine (marked in red) is located in a 9 Å deep cleft, which allows access of tyrosine phosphorylated substrates (yellow). (B) The phosphate binding P-loop (red) is surrounded by the YRD-loop (magenta), the second aryl-phosphate-binding site (orange) and the WPD-loop (cyan), all of which are important for substrate recognition and/or catalysis. (C) Upon binding the substrate (yellow), the WPD-loop closes over the substrate (yellow), creating a binding pocket. (PDB entry 1G1H for (A) and (C), and 1OEM for (B))

The mutation of the active site cysteine to serine or alanine provided a good strategy that allowed the observation of complex formation with substrate sequences, which is otherwise not possible due to the very transient nature of the phosphatase-substrate interaction in the

wild-type phosphatase. An even stronger interaction between phosphatase and substrate can be generated, when the invariant and highly conserved aspartate residue (D181 in PTP1B) is mutated to alanine. This so-called “substrate trapping” mutants bind the substrate, but lack almost completely the ability to turn over the substrate, and thus, can even be used for the identification of physiological substrates.⁵⁹

Using the substrate trapping approach, *in vitro* dephosphorylation or cell based assays, numerous targets of PTP1B could be identified.⁶⁰ Especially prominent amongst the identified substrates or receptor tyrosine kinases (RTKs). An early example identified *in vitro* was the β subunit of the insulin receptor (IR).⁴⁸ The specificity of this interaction was later verified by solving the crystal structure of the protein substrate complex and the substrate trapping approach.^{58,61} The breakthrough that linked PTP1B to RTK activity on a physiological level was the generation of PTP1B-null mice in 1999.⁶² The knockout animals show no apparent phenotype, are healthy and fertile and display enhanced insulin sensitivity as well as increased phosphorylation of the IR receptor and possibly insulin receptor substrate 1 (IRS-1).^{62,63} Furthermore, *PTP1B*^{-/-} mice are protected from getting obese or developing insulin resistance, when fed a high fat diet in part due to increased energy expenditure.^{62,63} The obesity resistance could be especially linked to a brain-specific deletion of *PTP1B* causing hyperphosphorylation of the RTK Jak2, which is regulated in part by leptin, a hormone associated with obesity.^{64,65}

In cells derived from *PTP1B* knockout mice higher phosphorylation of the IR, the EGFR, the platelet-derived growth receptor (PDGFR) and insulin-like growth factor 1 receptor (IGF1R) compared to wild-type cells after stimulation with the respective ligand could be detected.⁶⁶⁻⁶⁹

These and other studies solidly established the role of PTP1B in RTK dephosphorylation. However, the question on when and how the interaction of the predominantly endoplasmic reticulum (ER) bound phosphatase with the plasma membrane bound substrates occurs, is still a matter of intensive research. Interestingly, PTP1B is the only member of the PTP family showing this localization with the exception of a minor fraction of the very close related T-cell protein tyrosine phosphatase (TCPTP). This enzyme, which shares 72% primary sequence identity in the catalytic domain and some of the known substrates with PTP1B, exists *in vivo* in two splicing variants.⁶⁶ The shorter 45 kDa isoform shuttles in and out the nucleus, whereas the longer 48 kDa variant localizes, like PTP1B, to the ER facing the cytosol.⁶⁶ Nevertheless, although being very similar enzymes in the catalytic site, PTP1B and TCPTP action is tightly regulated and very specific. In addition to substrate specificity over the catalytic pocket, sub-cellular localization and features like a proline-rich domain in PTP1B, which is required for the interaction with Src homology (SH3) domain-containing substrates, are responsible for regulation.⁷⁰

There is evidence for three different scenarios on how the interaction of the ER bound form of PTP1B could take place with the plasma membrane bound targets, and all three are not mutually exclusive. One possibility is that the phosphorylation status of RTKs is controlled by PTP1B during their biosynthesis in vesicles in the cytoplasm. It could be shown that the level of phosphorylation of this fraction of RTKs is sensitive to PTP1B overexpression and that the enzyme plays an important role in the control of their maturation.⁷¹⁻⁷⁵

A single study has shown by means of fluorescence complementation that a direct interaction of the ER bound PTP1B with plasma membrane localized RTK is possible.⁷⁶ Interaction of PTP1B with the IR after insulin stimulation could be observed in distinct spots, which can be explained as contact points of the ER network, which stretches out to the cell periphery with the plasma membrane.⁷⁶

The best studied scenario, however, is that RTK dephosphorylation by PTP1B takes place by endocytosis after ligand stimulation. PTP activity has been found to take place at endosomal membranes and this activity can be found in punctured areas throughout the ER.^{77,78} The activity of plasma membrane proximal PTP1B has even been found to be down-regulated, potentially by oxidation through the localized production of reactive oxygen species maintaining an area of low PTP1B activity close to the membrane, which could facilitate spatial RTK activity.^{79,80} Recent findings point to the fact that PTP1B not only dephosphorylates endocytosed RTKs, but also actively regulates the endocytosis event by dephosphorylating endocytotic regulators like STAM2.^{60,81}

Its negative role in growth-promoting RTK signaling pathways and the fact that cells lacking PTP1B become highly sensitive to these stimuli, led to the speculation that PTP1B was a tumor suppressor.⁶⁷ Indeed, PTP1B overexpression in fibroblasts could prevent transformation by several oncogenic stimuli like ErbB2 (Neu), v-Src, v-Ras, v-Crk and Bcr-Abl.^{70,82-84} Furthermore, there is evidence for PTP1B to be involved in apoptosis and cell-cell adhesion.^{85,86} However, although there are hints of a tumor suppressive role of PTP1B on a molecular level, the *ptp1b* gene has not been found to be impaired in human or in mouse models of cancer.⁸⁷

On the contrary, PTP1B has been found to be overexpressed especially in breast and ovary cancer.^{88,89} In mouse models of ErbB2 induced breast cancer it could be shown that overexpression of PTP1B promoted tumorigenesis, rather than being a consequence of increased tyrosine phosphorylation in general.^{90,91} A recent study in a 3D cell culture model of human breast cancer could link this tumor promoting activity with increased Src kinase activation by dephosphorylation of its inactivating pTyr-530 by PTP1B.⁹² This is consistent with clinical data reporting decreased phosphorylation levels of this site in Src in combination with increased PTP1B expression.⁹³

The positive role of PTP1B in the onset of type 2 diabetes, obesity and several types of cancers made it an interesting target for drug development. Many efforts have been undertaken so far in this respect, which will be summarized in the next chapter. However, in spite of these efforts, in which also many big pharmaceutical companies were involved in, having started as early as in the 1990's a marketed drug is still missing. Furthermore, although a PTP1B inhibitor seems an attractive drug for many different pathological conditions, care has to be taken since PTP1B inhibition cannot be excluded to cause unwanted effects like tumor formation. Especially, the effect of PTP1B inhibition in long-term treatment schemes, which would certainly be required for the treatment of chronic diseases, like diabetes, need to be considered critically. Therefore, more research and especially chemical tools are required to deepen our knowledge about the molecular (inter-) actions of PTP1B on different biological backgrounds.

1.5 Inhibitors of PTP1B

Selectivity and bioavailability are the two major challenges in the development of PTP1B inhibitors as drugs or tools in cell biological research.⁹⁴ Especially, targeting the active site is problematic in this respect, since the catalytic domains of PTPs are highly conserved. Double knock-out of PTP1B and its most closely related enzyme TCPTP is lethal, whereas *PTP1B*^{-/-} mice appear healthy, highlighting the need for specific inhibitors, especially as drugs.⁹⁵ Furthermore, the active site of PTPs has evolved to accommodate the highly negatively charged phosphate group of its substrates, hence, many inhibitors targeting the active site are negatively charged, explaining their often poor membrane permeability.⁹⁴

The PTP active site targeting mechanism of Vanadium containing compounds, like vanadate and pervanadate, could explain their earlier observed insulin-mimetic activity in biological systems.⁹⁶ The tetrahedral structure of Vanadate in the +5 oxidation state mimics a phosphate group very well, which is continuously used to develop vanadium complexes with insulin-enhancing effects.⁹⁷

Examples for rationally derived active site binding moieties mimicking the phosphotyrosyl group (**1**) are the O-malonyltyrosyl (OMT) (**2a**), fluoro O-malonyltyrosyl (**2b**), sulfotyrosyl (**3**), thiophosphoryltyrosyl (**4**), O-dithiophosphoryltyrosyl (**5**), O-boranophosphoryltyrosyl (**6**), phosphonomethylphenylalanine (Pmp) (**7a**) and difluorophosphonomethylphenylalanine (F₂Pmp) (**7b**) groups (Figure 6 (A)).⁹⁸⁻¹⁰⁵ These moieties mimic structurally phosphotyrosine, but impair the second step of the catalytic cycle. In addition to these at physiological pH doubly negative charged structures, neutral or at most simply negative charged mimetics were developed including saturated (**8a**) and unsaturated isothiazolidinones (IZDs) (**8b**), or very recently N-(4-carboxyphenyl)trifluoromethylsulfonamide (**9**) (Figure 6 (A)).¹⁰⁶⁻¹⁰⁸

12/7/12 11:08 AM By incorporation of non-hydrolyzable pTyr mimetics into peptide sequences or peptidomimetics, high affinity binders can be obtained. F₂Pmp is representing the most potent one, when used as pTyr mimetic in the sequence of the dephosphorylation site of known PTP1B substrates. The hexapeptide NH₂-Asp-Ala-Asp-Glu-pTyr-Leu-COOH derived from the dephosphorylation site of the EGFR (988-993) has been most widely used for the determination of the inhibitory strength of these molecules. The F₂Pmp containing sequence showed an IC₅₀ of 0.2 μM against PTP1B in an insulin receptor dephosphorylation assay, which was 3 orders of magnitude superior to the sequence containing the fluorine-less Pmp derivative.¹⁰⁴ The same peptide sequence has been used to synthesize linear (**10**) and cyclic variants (**11a**, **11b** and **12**) containing the OMT group (Figure 6 (**B**)). The linear peptide (**10**) had a K_i value of 13 μM against PTP1B. The ring closure was performed as head-to-tail cyclization via one or two glycines with K_i values of 25.2 (**11a**) and 2.6 μM (**11b**), respectively, showing that the longer linker, giving rise to a less constrained peptide, provides better inhibitory performance. This could even be further increased to 0.73 μM when the ring closure was performed via a sulfide ether linkage (**12**), but with the same backbone size than the two glycine containing peptide (Figure 6 (**B**)).¹⁰⁹

Maybe due to limited access to these moieties, comprehensive binding studies of different sequences containing the same non-hydrolyzable pTyr mimetic are limited. In one report, a library of peptides based on the F₂Pmp containing EGFR sequence in which every position was exchanged sequentially for all naturally occurring L-amino acids except cysteine, was synthesized.¹¹⁰ In a second project, a combinatorial library of malonyltyrosine containing peptides was screened for binding to PTP1B.¹¹¹ However, more data about preferred substrate sequences of PTP1B was gained from dephosphorylation assays of chemically synthesized or phage-display derived libraries of phosphopeptides. The interactions were obtained in solution or with microarray strategies by either measuring dephosphorylation efficiency or binding to a substrate-trapping mutant of PTP1B.¹¹²⁻¹¹⁵ The results obtained do not point to the fact that a general consensus sequence for PTP1B in the sense of a linear motif exists. However, quite consistently a preference for aromatic residues at the -1 and acidic residues in general, especially at positions -2 and -3, was suggested. *Ren et al.* report also a preference for multiple pTyr sites, but not necessarily adjacent to each other, which might be expected from the notion that the doubly phosphorylated site of the insulin receptor (pYpY-1162,1163) is a physiological substrate of PTP1B.^{58,116}

As peptides are generally stigmatized to be poor candidates for drug development due to poor bioavailability and stability, research in the area of medicinal chemistry has been more focused on the development of small molecules. These efforts, with a major part being pursued by the pharmaceutical industry, are manifold and cannot be discussed here in depth, but some important examples shall be highlighted to provide an overview over the most important developments.

Although aiming for a different kind of molecule, the approaches to detect a good small molecule inhibitor were partially very similar to the screening for good substrate sequences. Zhang and coworkers generated a library of compounds, which possessed a pTyr as active site-binding fragment, a linker moiety (23 members) and an aryl group targeting the peripheral site (8 members), after identification of a second, non-catalytic binding site also capable of binding to arylphosphates, consistently with the observation that PTP1B prefers aromatic residues at the -1 position in peptide substrates.^{57,117} The library was screened for binding to the catalytically impaired PTP1BC215S and the best candidate identified was converted to a remarkably potent inhibitor ($K_i = 2.4$ nM against PTP1B) by exchange of the pTyr by an F_2Pmp group generating compound **13** (Figure 6).¹¹⁷ This compound showed also 10fold selectivity towards the most closely related TCPTP highlighting the importance of the strategy to target the peripheral site as well.¹¹⁷

This principle was also employed in the so-called “linked-fragment approach” in which X-ray crystallographic data was used as basis for an NMR screen to identify compounds that bind either the active or the secondary site.¹¹⁸ By fusing the best two fragments identified, the highly potent and at least 2-fold selective inhibitor over TCPTP compound **14** with a K_i of 22 nM against PTP1B could be generated (Figure 6 (C)).

But also these compounds are poorly cell permeable, since they still contain highly negatively charged groups necessary for active site inhibition. Therefore, compound **15** (Figure 6 (C)) was developed on the basis of **14** in which all acidic groups are masked as methyl or ethyl esters, which resembles a basic prodrug strategy.¹¹⁹ This compound showed increased cell permeability and cellular activity.¹¹⁹ By excluding doubly negatively charged fragments from the library and repeating the NMR screen, compound **16** (Figure 6 (C)) was developed from the same research group. Although this compound showed with $6.9 \mu M$ a significantly weaker K_i against PTP1B it was 30 times more selective to PTP1B over TCPTP and showed also cellular activity.¹²⁰ Zhang and coworkers followed a completely different strategy to enhance the cellular availability of their “two-site binder” **13**. Fusion of the compound to a stretch of 8 D-arginines, which resembles a cell penetrating peptide sequence (CPP), via a disulfide bridge did not only enhance cell membrane permeation of the molecule, the polybasic sequence also reduced the inhibitory potency for 3 orders of magnitude. But reduction of the disulfide bond between compound **13** and its CPP upon cell entry releases the active molecule inside the cell, explaining the increased phosphorylation levels of IR and IRS-1 by treating chinese hamster oocyte (CHO) cell lines with only 5 nM of the cell penetrating compound.¹²¹

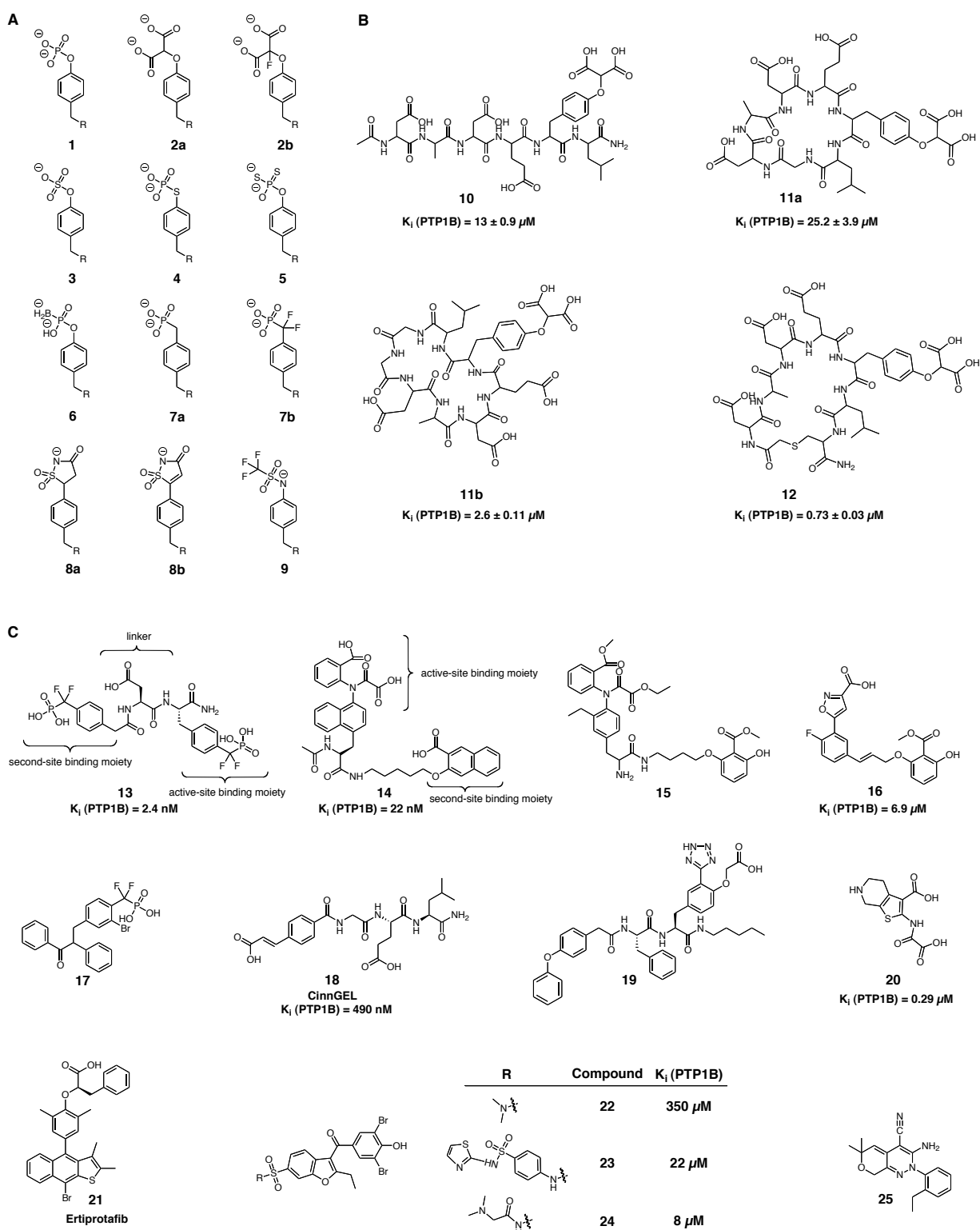


Figure 6: Molecular structures of described PTP1B inhibitors. **(A)** Phosphotyrosine and its various non-hydrolyzable analogues. **(B)** Linear and cyclic O-malonyltyrosyl (OMT) containing peptides. **(C)** Small molecule inhibitors of PTP1B.

Unexpectedly, the *ortho*-bromo substituted small molecule derivative of F₂Pmp compound **17** (Figure 6 (C)) showed oral bioavailability and insulin-mimetic activity in rats.¹²² Apparently, the high lipophilicity with a deoxybenzoin and a phenyl group attached to the non-hydrolyzable pTyr mimetic promotes uptake, although the molecule is highly negatively charged at physiological pH. The cinnamic acid derivative “CinnGEL” **18** (Figure 6 (C)) is a highly potent PTP1B inhibitor *in vitro* with a K_i of 490 nM against PTP1B.¹²³ The methyl ester of the cinnamic acid fused to the tripeptide of glycine, glutamate and leucine is commercially available as cell permeable prodrug of CinnGEL from Biomol (Hamburg, Germany).

Compound **19** (Figure 6 (C)) is a cell active, insulin-mimicking molecule, which was developed on the basis of an OMT derivative. First, the malonyltyrosyl group was replaced by a 2-carboxymethoxybenzoic acid, which resulted in higher activity. The additional replacement of the 2-carboxy group with a tetrazole as bioisostere was the key to enhance cell permeability.¹²⁴

The thiophene **20** (Figure 6 (C)) is also targeting the active site and was reported to be highly potent with an IC₅₀ of 0.29 μM against PTP1B. The diethyl ester prodrug is active in cell based assays.^{125,126}

Weyth developed the benzothiophene derivative Ertiprotafib **21** (Figure 6 (C)), which showed good activity in a mouse model of diabetes. The compound went into clinical trials but had to be withdrawn in phase II due to side effects, caused by multiple off-target effects of the drug, and low efficacy.¹²⁷

Several natural products like Tannins and Caffeoyl derivatives of *Cichorium intybus*, Papaverine, Berberine, 1,2,3,4,6-Penta-O-galloyl-D-glucopyranose from *Paeonia lactiflora* and Curcumin are known to target PTP1B directly, to increase IR phosphorylation in cells or to lower blood glucose in animal models.¹²⁸ Further development of these molecules and thorough characterization of their mode of action could be a potential source of innovation in the field of small molecule inhibitors.^{112–115,129}

In a library screen for new pTyr mimetics *Wiesmann et al.* detected a benzbromarone derivative **22** (Figure 6 (C)), which was a weak (IC₅₀ = 350 μM) and non-competitive inhibitor of PTP1B suggesting an alternative mode of inhibition to the classical pTyr mimetics.¹³⁰ Further development led to compounds **23** and **24** (Figure 6 (C)) with higher potency (IC₅₀ = 22 μM (**23**) and 8 μM (**24**)), but still non-competitive mode of inhibition. Structural analysis revealed that the compounds indeed were not binding the active site, but a shallow hydrophobic pocket 20 Å away from the active site formed by Leu 192, Phe 196 and Phe 280. Binding of the compounds to this pocket prevents the closure of the WPD loop and therefore locks the enzyme in an inactive state. Interestingly, this site seems not as highly conserved in the PTP family as the active site and compound exhibits 5-fold selectivity over TCPTP.

Another type of inhibition is underlying the activity of pyridazine analogues like compound **25** (Figure 6 (C)). These analogues act on PTP1B by reversible oxidation, are cell permeable and some molecules show a good degree of selectivity (up to 20-fold) towards TCPTP.¹³¹

Both alternative inhibitor strategies hold the potential to outperform classical active site-targeting inhibitors due to better cell permeability, as these inhibitors do not need to be charged intrinsically, and better selectivity, as the binding sites could be less conserved among the enzyme family.

ISIS pharmaceuticals is following a completely different approach by aiming to develop an antisense drug against PTP1B. However, the phosphorothioate antisense oligomer ISIS 113715, which entered phase 2 clinical trials was withdrawn from clinical studies according to ISIS' annual report from 2010 (10k) in favor of another potentially more potent oligomer. The development of an antisense drug holds the potential to reduce expression levels of PTP1B very specifically.

However, the answer if impairment of PTP1B activity has therapeutic potential to treat diabetes, obesity and/or several types of cancers, and which would be the best strategy to follow, can only be answered by clinical investigations.

1.6 Chemical probes to study PTP1B activity

As outlined in the previous chapter, selective and cell permeable inhibitors are the basis for successful drug development. Furthermore, they are indispensable tools for cell biologists to study biological aspects of the target enzyme. However, along with the evolution of more sophisticated experimental techniques, especially in the area of fluorescent microscopy and mass spectrometry-based proteomics, the possibilities of interrogating biological questions with the help of chemically synthesized probes have become more versatile.

A fluorescently labeled and photo-caged phosphopeptide with the EGFR substrate sequence, for example, has been used together with enhanced green fluorescent protein (EGFP) labeled PTP1B in a fluorescent lifetime imaging microscopy (FLIM) to visualize the presence of a stable enzyme substrate gradient throughout cells by Förster resonant energy transfer (FRET).⁷⁹ This data indicated spatial regulation of PTP1B activity with a less active membrane-proximal fraction.⁷⁹

Another approach, which bears potential for the usage in proteomic-based studies, are so-called activity-based protein profiling (ABPP) probes. These molecules are designed to covalently modify the targeted enzyme in an activity dependent fashion.^{132,133} Zhang and coworkers were the first in 2004 to apply this principle specifically to the PTP family.¹³⁴ Their

α -bromobenzylphosphonate was binding covalently to various PTPs at the active site. The probe was attached to a biotin molecule via a linker moiety and, thus, can be used for the visualization or enrichment of the “PTPome” of a cell.¹³⁴ *Shen et al.* were using a phosphotyrosine derivative, which generated a highly reactive quinone methide upon dephosphorylation, to crosslink PTP1B. Due to the coupling of a glutamate and a difluorophosphonomethylbenzoyl to the N-terminus of the active group and C-terminal attachment of a biotin via a linker, the probe could be used to selectively label PTP1B in *E.coli* lysates. When applied in low concentrations (20 μ M) the probe could specifically label PTP1B in the presence of PTP3A4.¹³⁵ In another approach, a very similar phosphotyrosine derivative, which also generates a quinone methide, was used to crosslink. The group was incorporated into a tripeptide and a biotin group was coupled via a linker to the N-terminus. By varying the amino acid between the linker and the active moiety subtle differences in the intensity of the labeling between individual PTPs could be demonstrated. The authors suggest to extend the variable region in order to gain more specificity in future approaches.¹³⁶

Skorey et al. reported unspecific crosslinking of PTP1B and TCPTP with inhibitors containing a photolabile diazirine moiety upon UV radiation. The molecules were used to detect the phosphatases after immunoprecipitation with antibodies.¹³⁷

In addition to their usage for the detection of the enzymes, these probes could be used to isolate the phosphatases from cell lysates. This would enable a big variety of proteomic analysis, which could lead to the detection of allosteric binders or posttranslational modifications and therefore contribute to a deeper understanding of regulation and activity of PTPs. Although representing high affinity binders, peptides with non-hydrolyzable pY mimetics have not been evaluated for the isolation of PTPs from cell lysates. These molecules, however, could be valuable tools to isolate and analyze the native enzymes since they would not modify the phosphatases covalently.

2 Aim of the project

Although proven to be extremely potent in converting natural substrate sequences into high affinity binders and inhibitors of PTP1B, the non-hydrolyzable pTyr mimetic F₂Pmp has almost exclusively been used in the sequence of the dephosphorylation site of the epidermal growth factor receptor (EGFR). Application of these peptide-based inhibitors in cell experiments and *in vivo* has been limited in the past due to their poor cell permeability and, supposedly, stability. Nevertheless, the amino acid residues around the pTyr mimetic in these inhibitors can potentially modulate potency and selectivity. Furthermore, the relatively easy and selective access of functional groups in peptides, through orthogonal protection strategies, allows various modifications to convert a peptide inhibitor into a chemical tool for the usage in biological experiments. This represents, together with affinity and selectivity modulation through the sequence, a major advance of peptide based inhibitors compared to small molecules.

The aims of this work were: I) to study the influence of the amino acid residues of a natural substrate sequence around the non-hydrolyzable pTyr mimetic in terms of potency and selectivity, II) to tackle the issue of poor bioavailability by chemical modification of the peptide and III) to introduce fluorescent labels and affinity tags to convert the peptide into a chemical tool and to validate its potential in cell experiments.

Initially, multiple phosphorylation sites of known substrates in varying length for their dephosphorylation efficiency towards PTP1B and the most closely related member of the PTP family TCPTP would be screened for their dephosphorylation efficiency. The most promising candidate of this screen would be converted to a high affinity binder by exchange of the pTyr for F₂Pmp. Thorough analysis of the binding mode of this sequence by alanine and truncation scan against both phosphatases would be performed to reveal the influence of the amino acids around the dephosphorylated residue for binding and selectivity.

To enable these studies, a fast and efficient synthetic pathway to prepare gram amounts of N-Fmoc-F₂Pmp-OH for its use in solid phase peptide synthesis (SPPS) would be devised.

As cyclization of peptide molecules has been described to improve both cellular uptake and stability, this strategy would be applied, and analysis of its potential, in the context of stabilized natural PTP substrates, would be conducted. Although cyclic peptides containing non-hydrolyzable pTyr mimetics were synthesized before, a full characterization of their cell permeability and stability in relevant biological media was missing.

For the ring closure the potential of bioorthogonal reactions would be explored, allowing the cyclization to take place *in situ* by co-incubating the linear precursor peptide with the targeted

enzyme. Validation of such a reaction would enable the screening of preferred molecular arrangements, regarding ring size and linker length, and molecular configurations, which could enhance affinity and selectivity of the obtained cyclic peptide.

Furthermore, fluorescently labeled or biotin tagged variants of the optimized inhibitory peptide would be used in microscopy or pull-down experiments to demonstrate their applicability in cell biology experiments and to further characterize the potential of the developed inhibitor in a cellular context.

As this approach is in principle applicable to all members of the PTP family dephosphorylating protein substrates on Tyr residues, this work can be regarded as a model study to devise a workflow to generate specific inhibitors and experimental tools for individual PTPs (Figure 7).

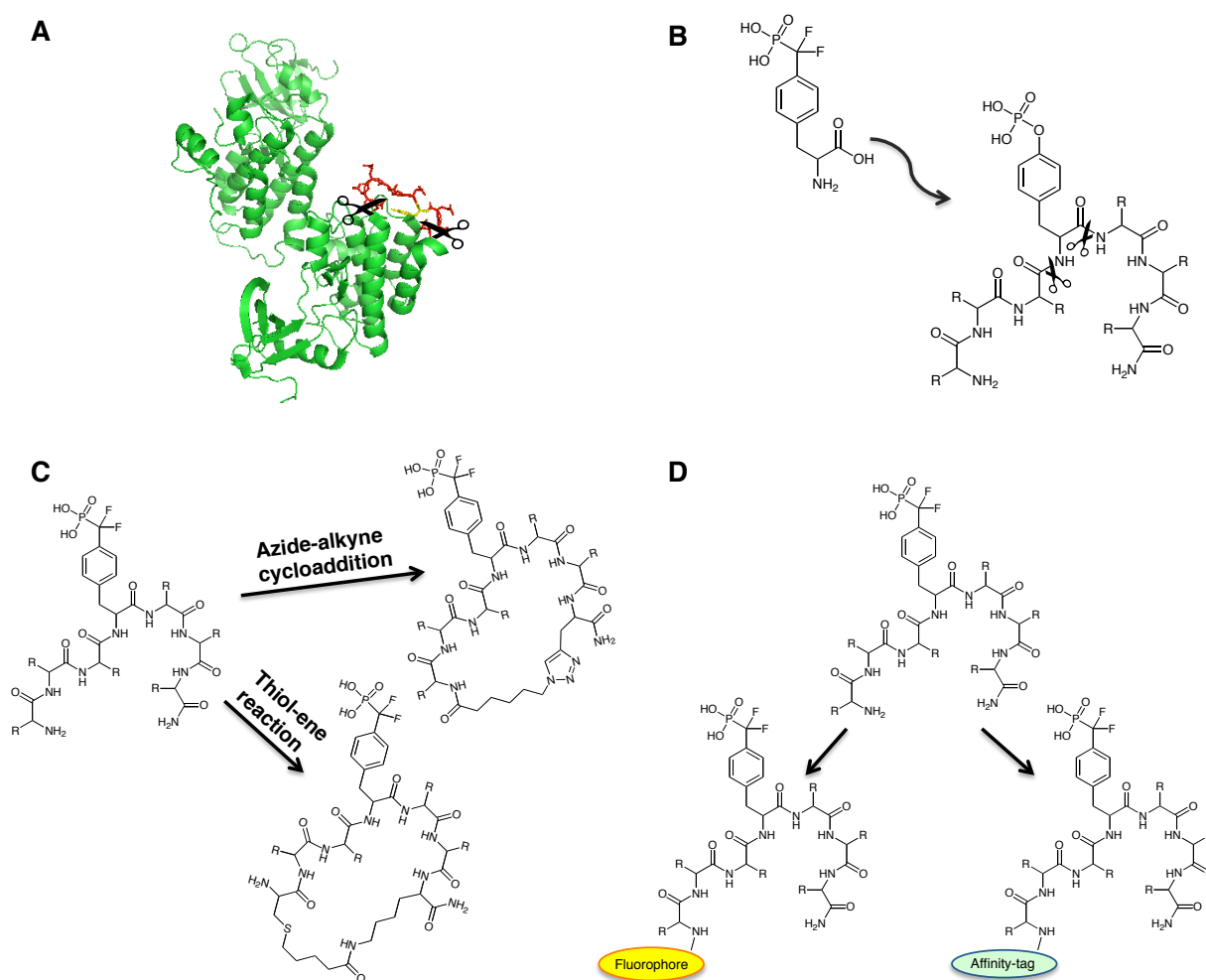


Figure 7: General strategy for the synthesis of potent, specific and bioavailable PTP inhibitors and the development of biological tools. **(A)** First, the dephosphorylation site of a potent and specific substrate needs to be identified. **(B)** Exchange of the pTyr for a non-hydrolyzable pTyr mimetic is needed to convert the substrate sequence in a potent inhibitor. **(C)** Evaluation of strategies to enhance bioavailability of the inhibitor, by e.g. cyclization. **(D)** Labeling of the peptidic inhibitor with fluorescence and affinity tags to study its activity and selectivity in cell experiments.

3 Results

3.1 Determination of a substrate sequence for further derivatization

3.1.1 Selection of suitable substrate sequences for *in vitro* screening

In an initial screen the dephosphorylation efficiency of PTP1B and TCPTP towards different phosphopeptides was compared in order to find the best candidate sequence for the subsequent inhibitor development. The sequences chosen were derived from the dephosphorylation sites of reported *in vivo* substrates of PTP1B (Table 1).¹³⁸

Aiming for an inhibitor that is as selective as possible for PTP1B, peptides **26-29** were synthesized corresponding to the doubly phosphorylated site of the receptor tyrosine kinase (RTK) Jak2 (pYpY-1007/1008). Four sequences varying in length (7mer, 10mer, 13mer and 17mer) around the phosphotyrosine were synthesized. Whereas Jak2 was reported as PTP1B substrate, explaining the negative effect of PTP1B on leptin signalling, TCPTP was shown to dephosphorylate Jak1 and 3 but not 2, making the Jak2 sequences interesting candidates to achieve selectivity between the two phosphatases.¹³⁹⁻¹⁴³

In several reports the role of PTP1B in Src kinase activation, and thus cancer progression, by dephosphorylating the C-terminal autoinhibitory phosphotyrosine pY-530 was described.^{92,93,144-149} TCPTP, on the contrary, was reported in the inactivation of Src family kinases (SFKs) by controlling the phosphorylation status of the activating phosphotyrosine, which is pY-416 in the case of c-Src.^{150,151} Therefore, the 10mer **30**, corresponding to the C-terminal stretch of c-Src was tested and evaluated in terms of selectivity in this screening.

To benchmark the strength of the interactions and the provided selectivity of the peptides chosen so far, control sequences of proteins representing *bona fide* substrates of both PTP1B and TCPTP were also synthesized and tested. Peptides **31** (4mer) and **32** (7mer) were derived from the activation segment of the insulin receptor kinase (IRK) pYpY-1162/1163. PTP1B and TCPTP are known to regulate insulin signaling in a concerted fashion by controlling the phosphorylation of the cytoplasmic segment.^{58,61,62,66,152-157}

The 6mer peptide **33** originates from the site around pY-992 of the EGFR, also a target of both phosphatases, and was previously used as a template for the synthesis of high-affinity binders.^{56,59,67,78,158-161}

The 10mer peptide **34**, however, is not a blueprint of a physiological substrate, but was synthesized on rational considerations about the substrate recognition of the phosphatases. The *in vivo* substrates identified so far, and screenings of combinatorial peptide libraries, especially the work of *Ren et al.*, point to the fact that the enzyme prefers charged amino

acids in proximity to the phosphotyrosine targeted.¹¹⁶ Thus, **34** comprises only residues, which are neutral at physiological pH and should therefore exhibit poor performance in the dephosphorylation assay.

Table 1: Phosphopeptides derived from reported *in vivo* substrates of PTP1B.

Peptide	Protein of origin	Peptide length	Sequence
26	Jak2	7mer	Ac-KEpYpYKVK-NH ₂
27	Jak2	10mer	Ac-KEpYpYKVKEPG-NH ₂
28	Jak2	13mer	Ac-DKEpYpYKVKEPGES-NH ₂
29	Jak2	17mer	Ac-VLPQDKEpYpYKVKEPGES-NH ₂
30	c-Src	10mer	AC-EPQpYQPGENL-NH ₂
31	IRK	4mer	Ac-DpYpYR-NH ₂
32	IRK	7mer	Ac-TDpYpYRKG-NH ₂
33	EGFR	6mer	Ac-DADEpYL-NH ₂
34	Random	10mer	Ac-ASGApYAGGSA-NH ₂

3.1.2 Synthesis of phosphopeptides

The phosphopeptides were synthesized with solid phase peptide synthesis (SPPS) according to Merrifield using 9-Fluorenylmethoxycarbonyl (Fmoc) protection strategy.^{162–164} The synthesis was performed with a Syro I automated peptide synthesizer and Rink amide resin was chosen as solid support. After the final Fmoc deprotection, the N-termini of all peptides were acetylated using a mixture of acetic anhydride/pyridine (1:9). Cleavage from the resin with a mixture of trifluoro acetic acid (TFA)/triisopropyl silane (TIS) (20:1) and subsequent HPLC purification yielded the pure phosphopeptides. N-terminal acetylation and C-terminal amidation were carried out to avoid electrostatic interactions with the enzymes in the dephosphorylation assay.

3.1.3 Screening of the phosphopeptide library

The kinetic profiles of all phosphopeptides against recombinantly produced PTP1B (1-321) and TCPTP (1-307) were measured using the malachite green assay, in which the amount of inorganic phosphate (P_i) released is determined chromogenically (Figure 8).^{113,165} For comparison of the affinities and selectivities, the Michaelis-Menten constants (K_M) were

extracted from the saturation curves of product generated (P_i) against substrate concentration.¹⁶⁶

In general, all peptides showed very similar K_M values (between 5 – 30 μM), confirming the quite broad *in vitro* substrate specificity of PTP1B and TCPTP (Figure 8).¹¹⁶ In addition, the differences between PTP1B and TCPTP activity were quite low. Whereas the averaged values gave differences that are statistically not significant, consistency in the trends in substrate preferences for both phosphatases were nevertheless observed.

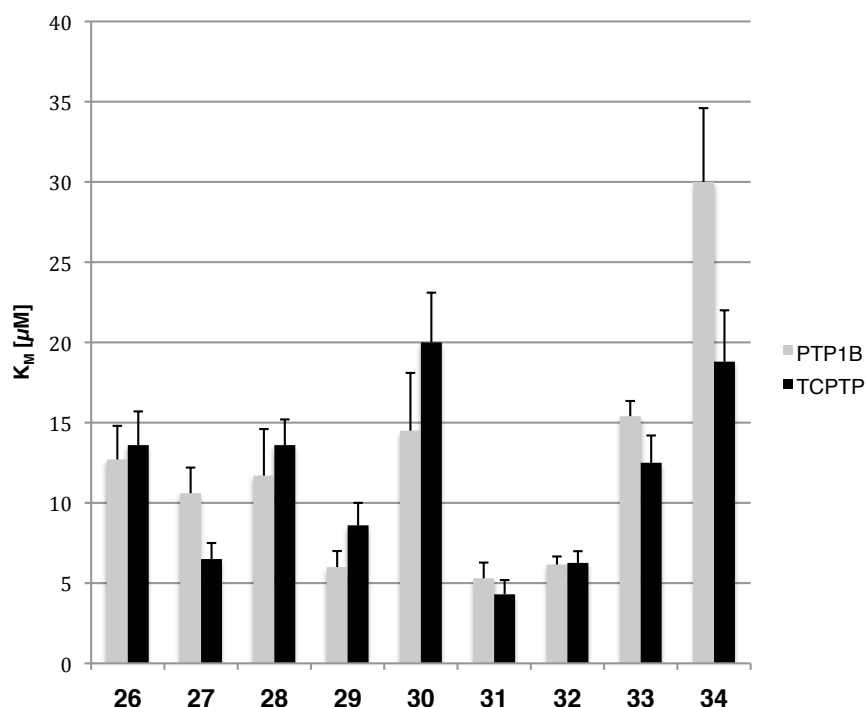


Figure 8: K_M value comparison of PTP1B and TCPTP towards a panel of phosphopeptides.

The 4mer and 7mer peptides derived from the IRK (**31** and **32**) were clearly among the best substrates with K_M values around 5 μM for both PTP1B and TCPTP.

The non-charged peptide **34**, on the contrary, showed the weakest K_M for PTP1B (30 ± 4.6 μM), as expected. The different peptides derived from Jak2 **26-29** showed no general trend regarding their length. Neither affinity nor selectivity seemed to benefit from either a longer or a shorter sequence. Nevertheless, the 17mer **29** was with a K_M of 6.0 μM (± 1.0 μM) a good substrate for PTP1B and was a slightly worse substrate for TCPTP ($K_M = 8.6 \pm 1.4$ μM). The 10mer of the Src sequence **30** showed slightly better selectivity for PTP1B, but the K_M in general was rather low with 14.5 μM (± 3.6 μM) compared to for example the Jak2 17mer **29**.

However, considering that the Jak2 and the IRK sequences had two phosphotyrosines in their sequence, which could not be distinguished by the assay used since the generation of inorganic phosphate was measured, the activity of the Src peptide was compared with the sequence from the second well established control substrate EGFR, because this peptide (**33**) also bore only one phosphotyrosine. The K_M value of the EGFR peptide against PTP1B was with $15.4 \mu\text{M}$ ($\pm 0.95 \mu\text{M}$) very similar. The consideration that the long and doubly phosphorylated Jak2 peptide **29** would cause additional difficulties in terms of pharmacokinetic behaviour of the resulting inhibitor due to the additional negative charges, the Src peptide sequence was chosen for the subsequent inhibitor development. Additionally, peptide **30** showed beneficial behaviour concerning selectivity when compared to **33** in this assay. Whereas the EGFR-derived peptide had a lower K_M against TCPTP compared to PTP1B, **30** showed better activity with PTP1B. At the same time, the K_M of **30** against TCPTP ($20 \pm 3.1 \mu\text{M}$) was even worse than the one of the random peptide **34** ($18.8 \pm 3.2 \mu\text{M}$).

3.2 Selection of a non-hydrolyzable phosphotyrosine analogue

To convert the identified substrate sequence into a high affinity binder and good inhibitor, the phosphotyrosine, which interacts only transiently with the phosphatase, had to be replaced by a non-hydrolyzable biomimetic.^{54,167} As outlined in chapter 1.5, several groups for this purpose had already been developed (Figure 5).^{98-104,127} By incorporating these building blocks into the peptide sequence high affinity binders can be obtained, with $F_2\text{Pmp}$ representing the most potent one against PTPs (Figure 9).¹⁰⁴ Therefore, $F_2\text{Pmp}$ was chosen to be synthesized and incorporated into the substrate sequence, well knowing that the, at physiological pH, doubly negatively charged phosphonic acid group represents a major obstacle regarding cell membrane permeation.¹²⁷

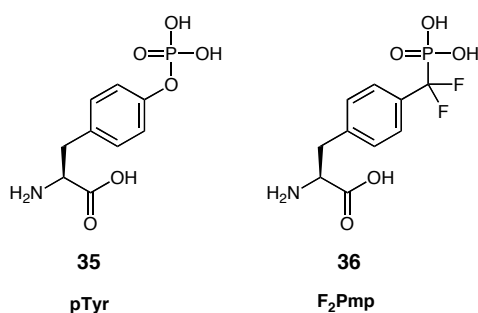


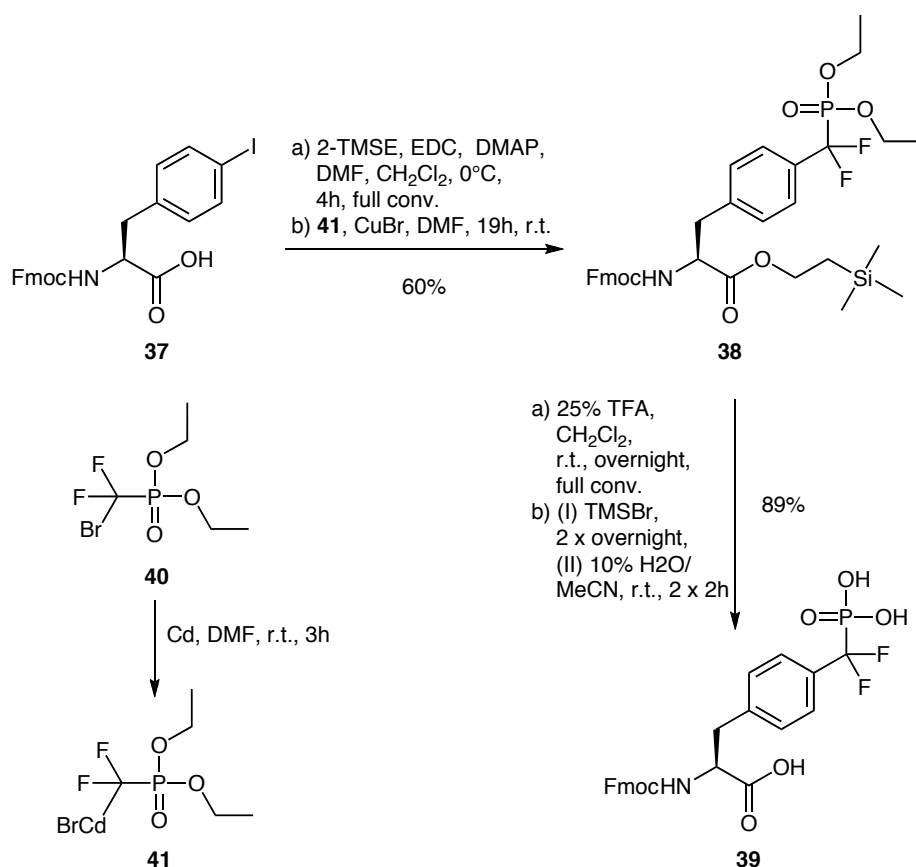
Figure 9: Phosphotyrosine (pTyr) (**35**) and its non-hydrolyzable analogue phosphonodifluoromethyl-L-phenylalanine ($F_2\text{Pmp}$) (**36**).

3.2.1 Efficient scaled-up synthesis of N- α -Fmoc-4-Phosphono(difluoromethyl)-L-phenylalanine

To enable the incorporation of the biomimetic building block by conventional Fmoc-solid phase peptide synthesis, N-Fmoc-L-F₂Pmp-OH (**39**) or its respective protected diethylphosphonate (**38**) can be used (Scheme 1).^{117,168} Also, an on-resin direct conversion of 4-iodophenylalanine into F₂Pmp(OEt₂) was reported.¹⁶⁹ However, the preferred method of F₂Pmp-incorporation into peptides is exploiting the free phosphonate building block due to potential side reactions caused by the harsh conditions needed to remove the ethyl protecting groups.^{168,169}

Several different synthetic routes to N-Fmoc-L-F₂Pmp-OH had been described thus far.^{117,168-174} Albeit very useful, these routes had individual drawbacks in that they required either several steps that needed purification, or provided relatively low overall yields.^{117,168,171-174} Often the highly explosive fluorinating agent diethylaminosulfur trifluoride (DAST) or diazomethane were used, which are difficult to scale-up.^{169,171-174} In addition, these routes had only been described on mg scale (in case the scale was reported). Therefore, the synthesis of N-Fmoc-L-F₂Pmp-OH needed to be optimized and scaled-up to provide enough material for the subsequent experiments.

Due to its high coupling efficiency the approach of Qabar and coworkers, adapted from Burton and coworkers, was chosen as starting point, which was based on CuCl-promoted coupling of diethyl phosphonodifluoromethyl-CdBr (**41**) to commercially available N-Fmoc-L-4-iodophenylalanine (**37**) (Scheme 1).^{169,175}



Scheme 1: Synthesis of N-Fmoc-F₂Pmp-OH **39**. 2-TMSE: 2-(Trimethylsilyl)ethanol; EDC: N-ethyl-N'-(3-dimethylamino-propyl)carbodiimide; DMAP: 4-(N,N-dimethylamino)pyridine; TMSBr: trimethylsilyl bromide

In the first step of the synthesis, the carboxylic acid moiety of **37** (4.8 g) was protected as an ester of 2-trimethylsilylethanol (TMSE). This protecting group was chosen because the ester bond can be removed using mild acidic conditions. Thus, after coupling of the phosphonogroup the subsequent deprotection was expected to be easier to control with respect to the integrity of the Fmoc group than the previously described basic removal of a methyl ester with LiOH.¹⁶⁹

The esterification showed complete conversion of the starting material after four hours by TLC. Subsequent aqueous work-up and drying in high vacuum yielded a brown oil, which was used in the next step without further purification.

In the next reaction the Cd-containing compound **41**, obtained by treatment of diethyl bromodifluoromethylphosphonate (**40**) with Cd, was coupled to TMSE-protected **37** in the presence of a copper halide.¹⁶⁹ Like Qabar and coworkers, it was also observed that an excess of copper (2-3 equiv) was needed for the reaction. Additionally, it was found that CuBr performed superior to CuCl and that a second addition of the cadmium reagent (1.7 equiv)

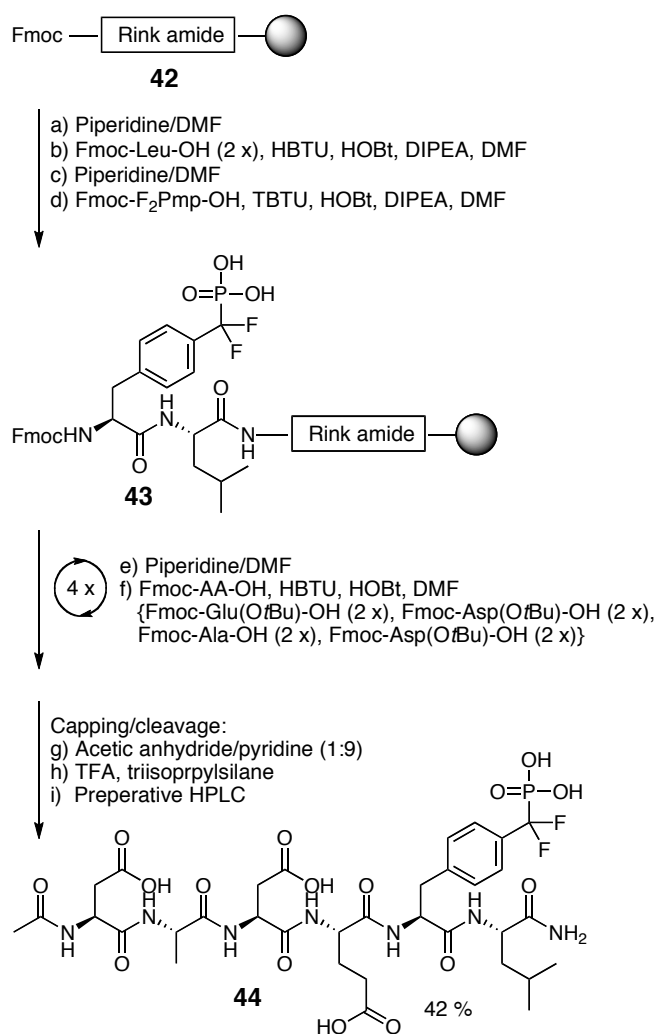
and CuBr (2 equiv) helped to drive the reaction faster to completion. Already after 19 hours, the conversion to the product was >93% (determined by analytical HPLC).

After aqueous work-up and column chromatography 3.8 g (60% over 2 steps) of compound **38** were isolated. Minor impurities were still visible after this purification, two in the ^{31}P and one in the ^1H NMR spectrum of compound **38**, which correspond to an impurity in starting material **40** and presumably to a side product derived from compound **41**. These impurities were not further removed, as they did not interfere with the purpose of the final product N-Fmoc-L-F₂Pmp-OH, which was to be incorporated into peptide- or peptide-mimic-based binders of PTPs. This is evident because the impurities in the ^{31}P NMR are absent in the spectrum of the corresponding peptides.

The subsequent hydrolysis of the trimethylsilylethyl ester took place quantitatively overnight in 25% trifluoroacetic acid (TFA) in CH₂Cl₂. After coevaporation of the acid with toluene and drying, the N-Fmoc-F₂Pmp(OEt₂) building block was obtained and directly used in the next step without purification. The phosphonic acid diethyl esters were hydrolyzed quantitatively without the need of adding scavengers by treatment with trimethylsilyl bromide (TMSBr) in CH₂Cl₂. Single repetition of the treatment lead to the highest purity of the final product **39**. Thus, 2.6 g of N-Fmoc-L-F₂Pmp-OH (**39**) were isolated as yellowish glass in >90% purity (determined by analytical HPLC), resulting in an overall yield of 54% based on the amount of starting material **37**.

3.2.2 Incorporation of F₂Pmp into peptides

Without further purification N-Fmoc-L-F₂Pmp-OH (**39**) was then directly used in solid phase peptide synthesis and, at first, the peptide sequences derived from the EGFR (**44**) and the random sequence (**45**) were prepared to test the applicability of the building block. The coupling took place efficiently on Rink amide resin using only 3 equivalents of the standard coupling reagents TBTU, HOBt and DIPEA and N-Fmoc-L-F₂Pmp-OH (Scheme 2). After cleavage from the resin, HPLC analysis showed no dominant fragments due to incomplete coupling and model peptides **44** (Scheme 2) and **45** (Figure 10). The 2 peptides represent sequences with quite distinct physicochemical properties in the side chains, and were obtained in good yield after HPLC purification (yield (**44**) = 42%, yield (**45**) = 37%).



Scheme 2: Scheme 2: Solid phase Synthesis of model peptide **44** containing F₂Pmp. HBTU: O-(1H-benzotriazol-1-yl)-N,N,N',N'-tetramethyluronium hexafluorophosphate; HOBT: 1-hydroxybenzotriazole; DIPEA: N,N-diisopropylethylamine

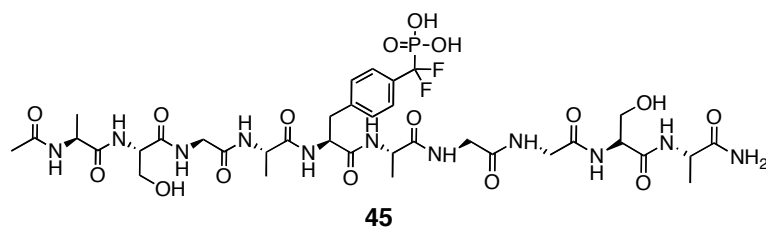


Figure 10: F₂Pmp containing model peptide **45**.

3.3 Cyclization of F₂Pmp containing peptides

In the previous part, a strategy to stabilize and protect the phosphotyrosine moiety of peptides from degradation by phosphatases has been outlined by means of introducing a non-hydrolyzable phosphotyrosine mimetic with the aim of creating high affine binders of this enzyme class.

As the usage of these inhibitors in biological experiments was aspired, also the remaining peptidic part of the molecule needed to be considered critically, since the peptide backbone itself could be prone to degradation by proteases. Several approaches have been applied successfully to enhance the biological stability of peptides. Amongst these are incorporation of D-amino acids, the use of peptidomimetics or cyclization.^{176–184}

For the stabilization of F₂Pmp containing peptides, cyclization via a hydrocarbon linker appeared as an especially interesting strategy, since it had been reported previously that a hydrocarbon-stapled peptide derived from the BH3 segment of the Bcl-2 protein, whose α -helical structure was stabilized by a carbon linker introduced with grubbs metathesis, provided not only enhanced protease stability, but also increased its cell membrane permeation.¹⁸⁵ Although non-hydrolyzable phosphotyrosine mimetics containing cyclic peptides had been synthesized before, only their inhibitory behaviour compared to their linear counterparts had been analyzed and studies regarding their cellular activity, uptake and stability were missing.^{109,186} In addition, these peptides were head-to-tail cyclized and did not contain a hydrocarbonlinker.

Therefore, it was sought to synthesize cyclic derivatives of the in chapter 3.1 identified sequence derived from c-Src and to study subsequently their inhibitory potency as well as membrane permeation and stability.

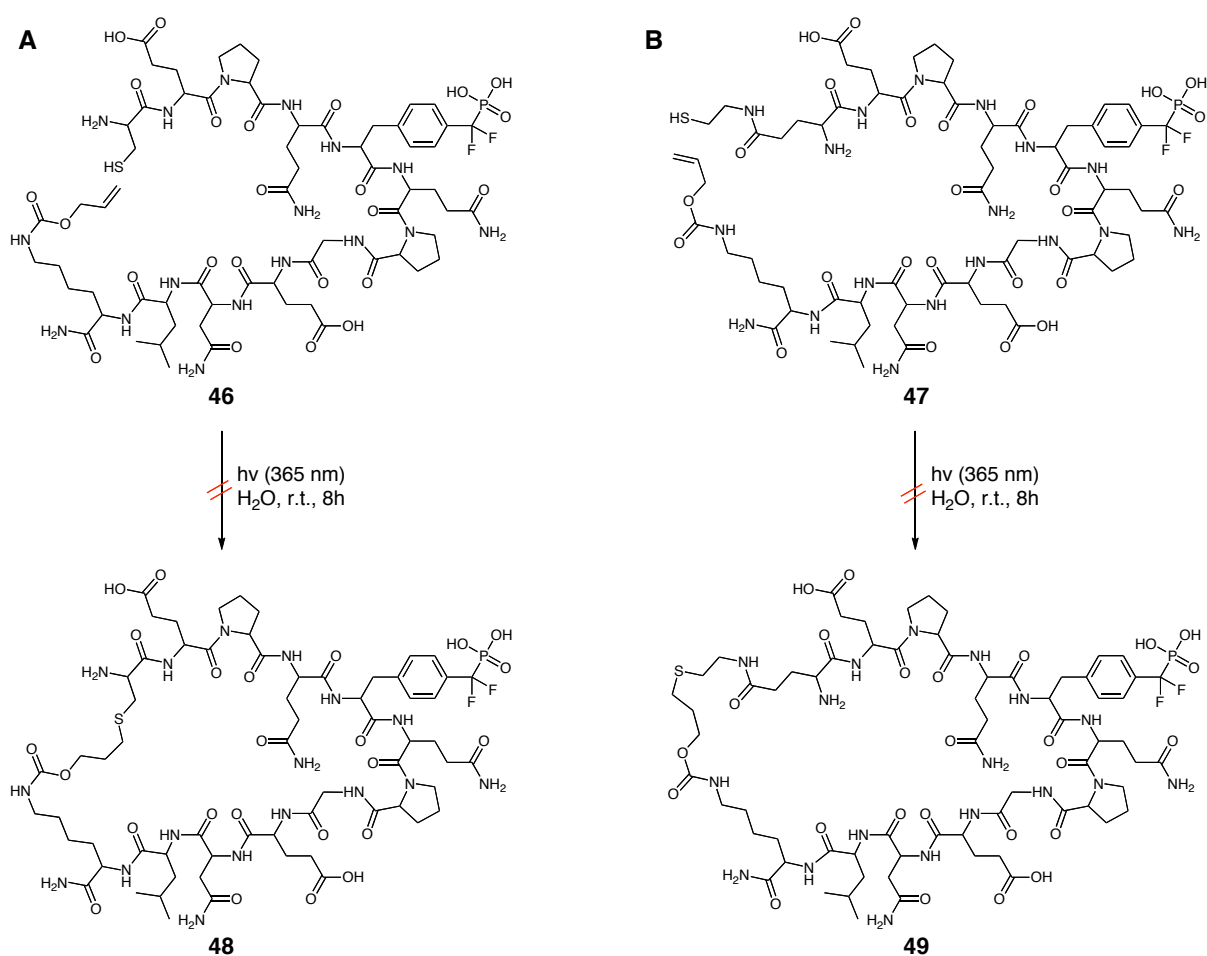
3.3.1 Cyclization trials using the thiol-ene reaction

Initially, the light induced thiol-ene reaction was tried to accomplish the aspired ring closure. This reaction proceeds via a radical mechanism between a sulfhydryl group and a double bond upon irradiation with UV light at a wavelength close to the visible spectrum ($\lambda = 365 - 405 \text{ nm}$).^{187–191} It was chosen due to its mild reaction conditions (the reaction proceeds readily at room temperature), the compatibility with aqueous media, the high yields obtained previously, without the generation of side products or the need of addition of catalysts, and the proven bio-orthogonality in complex biological samples.^{188,191} Especially, the possibility to perform the reaction in aqueous buffer would provide the chance to perform the ring closure *in situ* by incubating the peptide with the phosphatase. Thus, it could be possible to select for the most eligible conformers of the cyclopeptides, which bind the enzyme with the highest affinity, given that the generated ring system is rigid enough to cause conformational homogeneity.¹⁸¹

The first cyclization trials were performed with the peptides **46** and **47** (Scheme 3). Both peptides are based on the Src derived sequence identified in chapter 3.1. The core sequence was synthesized on solid phase as described. The double bond needed for the thiol-ene reaction was introduced by loading the resin first with a C-terminal allyloxycarbonyl (alloc) protected L-lysine. This side-chain would not be deprotected by the acidic cleaving conditions applied. The thiol was introduced in two different ways to implement two different possible linker lengths. An additional cysteine was coupled at the N terminus of peptide **46**. In **47** the N-terminal glutamate was introduced as γ -2-Phenylisopropyl ester. This side-chain protection was selectively removed on the solid support by treatment with 1% TFA in DCM. The free carboxy group was then activated with EDC, HOBT and DIPEA in DCM and cystamine was coupled by addition of cystamine, DIPEA and DMAP in DMF. Subsequent reduction of the cystamine with DTT, TEA in DCM, created the free thiol group. The peptides were cleaved from the solid support and purified by HPLC.

For the cyclization reactions the peptides were diluted in argon-purged water and irradiated with a mercury lamp for up to 8 hours. In order to favour the cyclization over the possible polymerization reaction, very low peptide concentrations between 7.5 and 200 μ M were tested. As water was used as solvent, the pH of the solutions was controlled to be below 7 to ensure that the thiol group is protonated, enabling the homolytic cleavage between the sulfur and the hydrogen.¹⁸⁷ After the respective reaction time the samples were analyzed by HPLC. If the reaction would have taken place, a new peak at a different retention time was expected.¹⁹² However, this could not be observed for both peptides. Also, co-incubation with 1.1 or 4 equivalents of PTP1B, in order to preform the peptide from its unstructured linear in a presumably more rigid and potentially loop like enzyme bound structure, did not yield positive results.

In order to exclude the possibility that the chromatographic behaviour of the linear and cyclic variants were too similar and, thus, the results were judged as a false negative, the samples were basified (pH \sim 10) and 1.5 equivalents of the thiol-reactive agent N-Ethylmaleimide was added. Only the free thiol group from the linear version would react with this reagent causing a shift in the chromatogram of samples containing the linear peptide. But both, irradiated and non-irradiated, samples reacted in the same way, thereby proving that the cyclizations failed and that peptides **48** and **49** were not obtained.



Scheme 3: Cyclization trials of F_2Pmp containing peptides **46** (A) and **47** (B) using the thiol-ene reaction. Both reactions did not yield any cyclic product, thus, peptides **48** and **49** could not be obtained.

Since the thiol-ene reaction conditions applied here had been used successfully in the literature, it was anticipated, that an unfavourable configuration for the cyclizations was most likely to be the cause for the failure of the reactions.¹⁸⁸ An analysis of the crystal structure of the C-terminal part of the Src kinase (PDB entry 1YOJ) revealed, that it might be favourable for a ring closure via the side chains to position the double bond in an amino acid mimicking the side chain of the N-terminal leucine, rather than next to it (Figure 11). In this situation the two side chains of the amino acids containing the reactive groups required for the thiol-ene reaction (positions -4 and +6 from the tyrosine) would point in the same direction. Of course, the major configurations adopted by the free peptide in solution were very likely to be different than the situation in the protein crystal structure. Nevertheless, the crystal structure is one of the possible configurations that can be adopted.

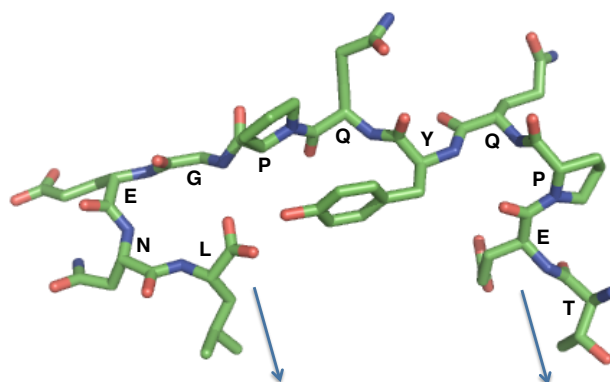
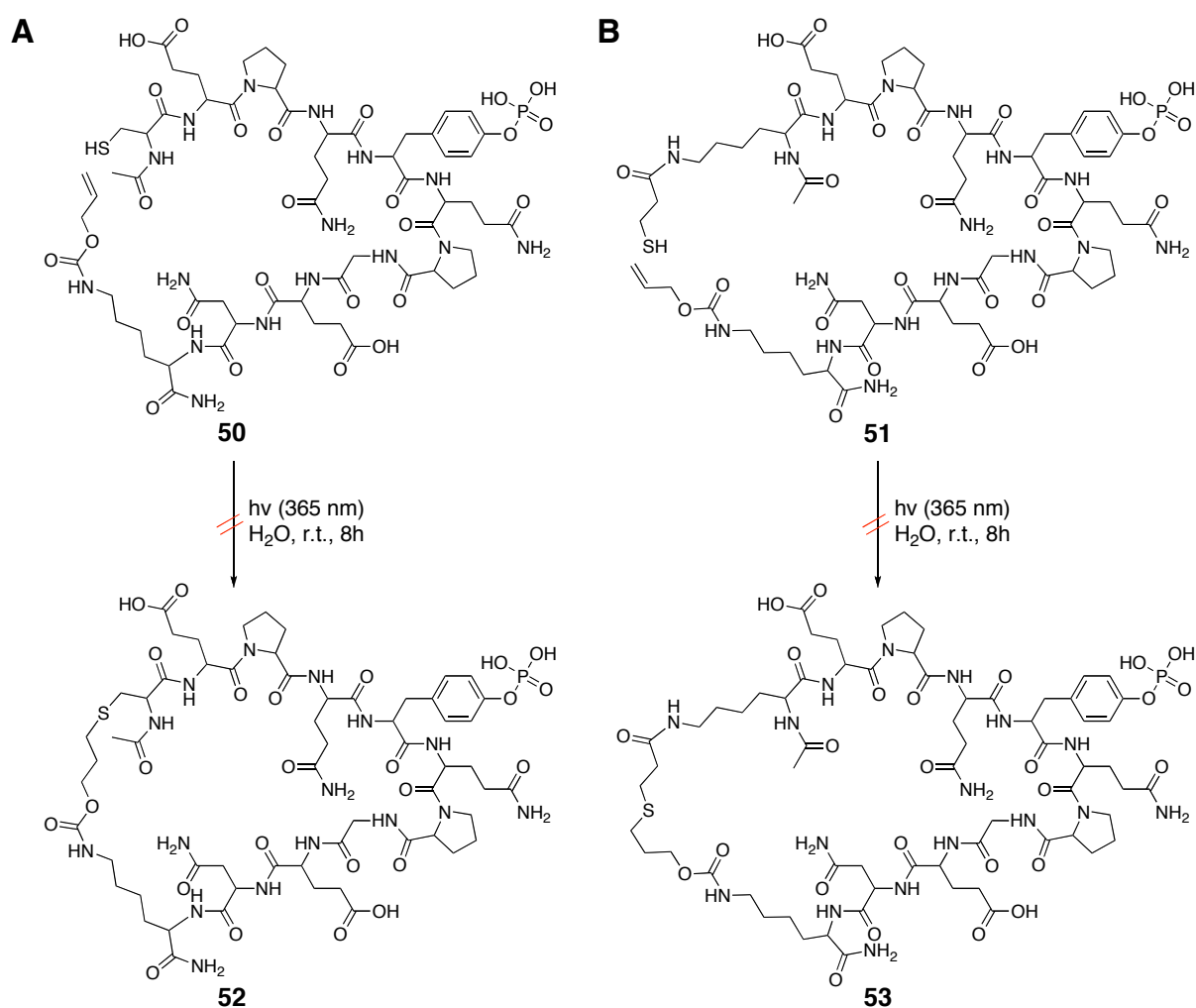


Figure 11: Structural considerations for the synthesis of peptides **50** and **51**. In the crystal structure of c-Src (PDB entry 1YOJ) the side chains of T at position -4 and L at position +6 point to the same direction suggesting that a cyclization via these side chains could be feasible.

Based on these considerations two additional peptides missing the N-terminal leucine were synthesized and tested (Scheme 4). Peptides **50** and **51** contained a phosphotyrosine residue instead of the F₂Pmp group, due to economic considerations and the fact that the thiol-ene reaction was successfully applied to phosphopeptides.¹⁸⁸ Nevertheless, pTyr and F₂Pmp containing peptides were expected to behave similar in these experiments. In **51** the thiol group was introduced by selective removal of the 4-methyltrityl (Mtt) protecting group of the C-terminal lysine with 1.8% TFA in DCM and coupling of Mtt protected mercaptopropionic acid, using HATU, HOAt and DIPEA in DMF. Both peptides were subjected to the same cyclization trials as **46** and **47**, except the *in situ* trials, which were not possible for the phosphotyrosine containing peptides. But also these candidates did not yield any cyclization and generation of peptides **52** and **53** was not observed.



Scheme 4: Cyclization trials of phosphotyrosine containing peptides **50** (A) and **51** (B) using the thiolene reaction. Generation of the cyclic peptides **52** and **53** could not be observed.

3.3.2 Cyclization using the copper catalyzed azide-alkyne cycloaddition (CuAAC)

Another highly selective and bioorthogonal - so termed - “click” reaction is the copper catalyzed 1,3-dipolar cycloaddition reaction between azides and alkynes, which was implemented as such by Sharpless and coworkers based on fundamental work by Rolf Huisgen.^{193,194} In contrast to the Huisgen protocol, which requires thermal activation of the reaction and mostly results in a mixture of 1,4- and 1,5-disubstituted 1,2,3-triazoles, the copper catalyzed variant of the reaction proceeds readily at room temperature and proved to be regioselective, yielding only 1,4-disubstituted 1,2,3-triazoles.¹⁹⁵

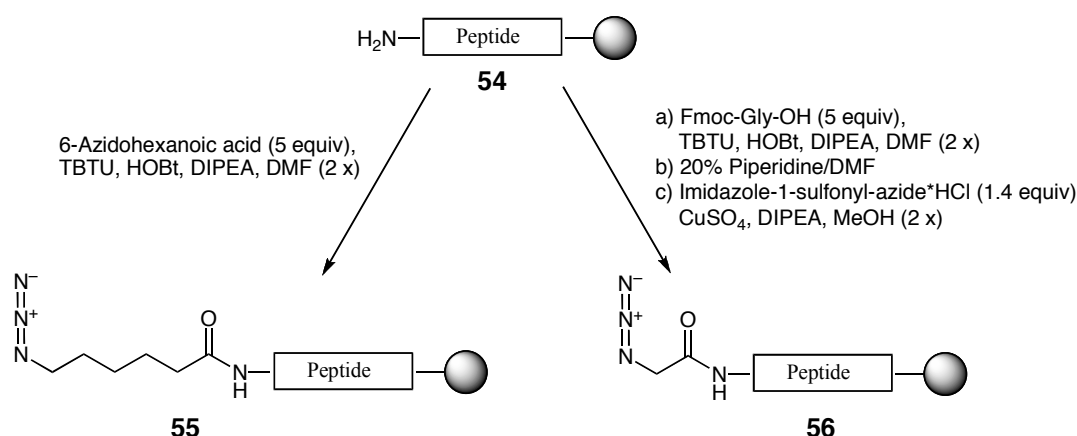
The applications of this type of chemistry are manifold and range from material science to medicinal chemistry.^{196,197} Interestingly, i to i+4 side chain-to-side chain or head-to-tail cyclizations and cyclodimerizations had already been conducted successfully using this strategy.^{192,198} In this manner Burke and coworkers synthesized macrocycles containing the phosphotyrosine mimetic Pmp as binders of the SH2 domain of Grb2.¹⁹⁹

Especially valuable for the usage of this type of reactions in biological settings is its compatibility with water and the “inertness” of the reaction partners in biological surroundings.¹⁹⁶ Additionally, it was shown that the reaction mechanism does not need the addition of a Cu(I) catalyst per se, which facilitates the reaction and determines its regioselectivity by the formation of a 6-membered copper(III) metallacycle intermediate, but rather any type of reagent that brings the azide and alkyne group in close proximity would be suitable.^{195,200–203} This finding had been exploited to generate inhibitors of the enzymes acetylcholine esterase or carbonic anhydrase II in a fragment based approach by target-guided synthesis (TGS), whereby the target protein itself selects two molecules from a fragment library that bind closely to each other at the surface of the protein and, thereby, undergo the cycloaddition reaction.^{200,201} This would also enable the use of this reaction, like the thiol-ene reaction, to create conformers of the macrocycles preferred by the enzyme *in situ*. Therefore, the azide-alkyne cycloaddition was chosen next to try the synthesis of a cyclic variant of the F₂Pmp containing sequence derived from the Src kinase.

In contrast to peptides **46** and **47**, which contain both groups needed for the cyclization reaction in the side-chain, the azide in **57** and **58** was introduced at the N-terminus, which initializes the ring closure as a head-to-side chain type of reaction together with the triple bond in the side chain of the C-terminally coupled propargylglycine (Pra). In **57** the azide was coupled to the N-terminal amine group using the building block 6-azidohexanoic acid (Scheme 5). This peptide (**57**) was termed “Src-5C”, because of the 5 methyl groups (“5 carbon”) containing spacer between the reactive azide and the last amide bond (Scheme 6). The deprotected N-terminus of **58** was directly converted to the azide using imidazole-1-sulfonylazide, which was synthesized as HCl salt according to the method described by Goddard-Borger and Stick (Scheme 5), resulting in a “1 carbon” linker between azide and amide bond (“Src-1C”) (Scheme 6).²⁰⁴

As the usage of this inexpensive, stable and safe diazotransfer reagent directly on solid phase has not been reported earlier, the reaction conditions needed to be transferred from solution to solid phase. Like in the solution phase approach, a small excess of imidazole-1-sulfonylazide hydrochloride (1.4 equiv) in MeOH was used, but instead of adding copper(II) sulfate pentahydrate in 1 mol % to the solvent (MeOH), a saturated solution of the copper salt in MeOH was added. The non-nucleophilic base potassium carbonate (2 equiv) was replaced by DIPEA (1.8 equiv) (Scheme 5).²⁰⁴ The diazotransfer was performed either with a single addition of the reagents over night or with 2 additions for 1 hour. HPLC-MS analysis showed quantitative conversion of the starting material to the functionalized peptide.

After introduction of the azide groups, both peptides were cleaved from the resin and purified by HPLC, which yielded 13 mg (20%) **57** (Src-5C) and 7.8 mg (13%) **58** (Src-1C).



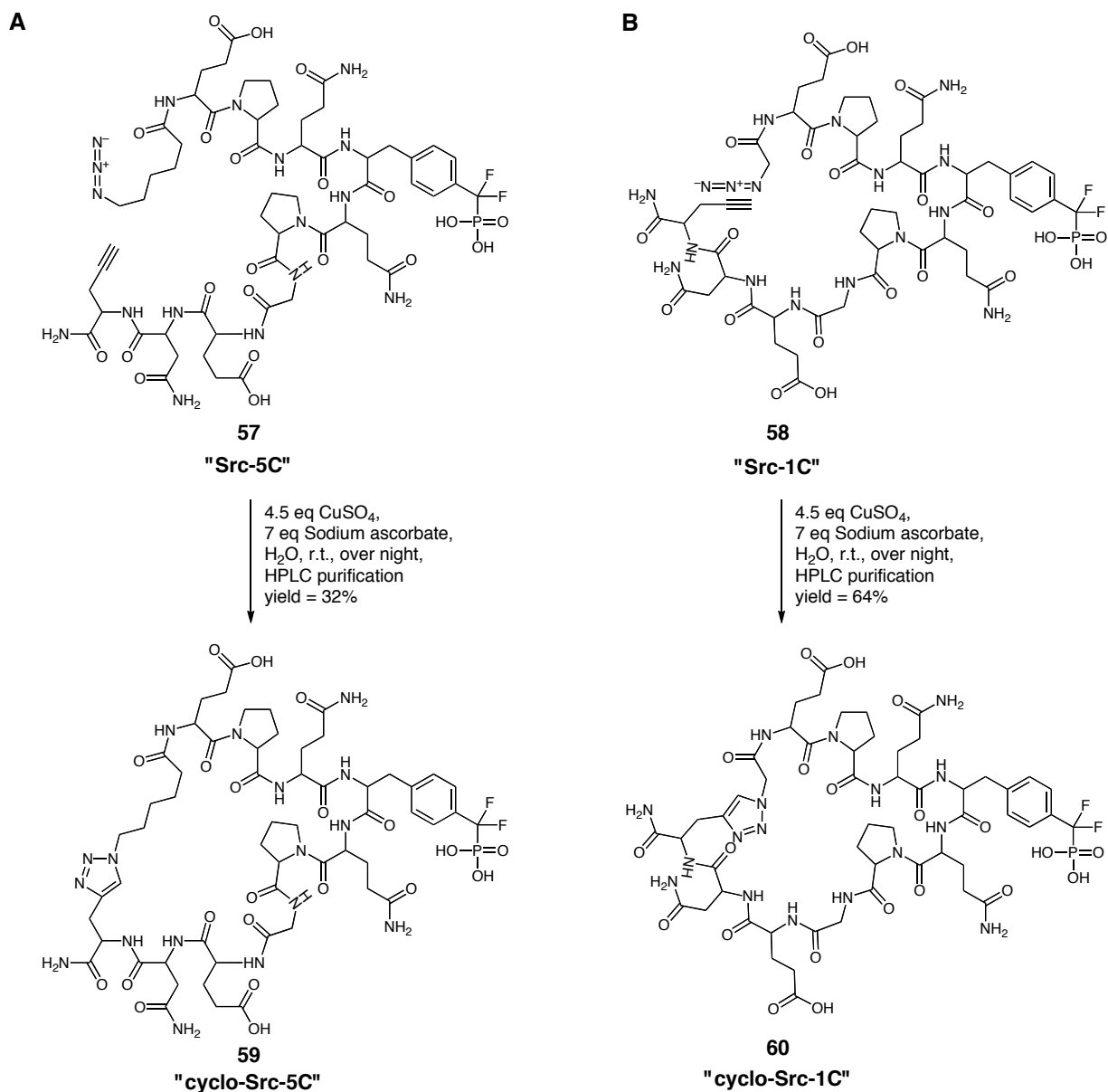
Scheme 5: Azide functionalization of peptides (**54**). The peptides were modified by N-terminal coupling of 6-azidohexanoic acid (**55**) or by N-terminal coupling of Fmoc protected glycine, Fmoc deprotection and conversion of the free amine bond to the azide on solid support (**56**).

The cycloaddition reactions were performed very similar to the protocol introduced by *Cantel et al.*, however, instead of a mixture of *t*BuOH/H₂O, water was used as solvent.¹⁹⁸ Both peptides were diluted to a concentration of 200 μ M to avoid polymerization or cyclodimerization, and copper sulfate pentahydrate (4.5 equiv) and ascorbic acid (7 equiv) were added to generate Cu(I) ions as catalyst. The reaction mixtures were stirred at room temperature over night. HPLC analysis showed complete conversion of the starting material and, in both cases, a peak with a shorter retention time compared to the respective precursor peptide was generated, a chromatographic behaviour typical of monomeric cyclopeptides relative to their linear precursors, as described in the literature.^{192,198}

After HPLC purification, MALDI mass spectrometry identified the reaction products “cyclo-Src-5C” (**59**) and “cyclo-Src-1C” (**60**) as monomeric macrocycles of “Src-5C” (**57**) and “Src-1C” (**58**), since the respective reaction products showed the same *m/z* ratios as the starting material and their isotopic pattern did not indicate di- or oligomerization (Figure 12). Analytical HPLC of the purified products confirmed a significant shift to shorter retention times (Figure 12). Additionally, the azide-alkyne cycloaddition conditions were applied to an equimolar mixture of the linear or cyclized peptides and Fmoc-propargylglycine. In contrast to the linear precursors, the cyclized peptides did not show an additional mass corresponding to the peptide/Fmoc-propargylglycine cycloaddition product in the MALDI MS-spectrum, thereby proving successful ring closure.

Due to overlapping signals the ¹H NMR data of the peptides before and after the reaction were not conclusive. Nevertheless, differences of peak patterns in 2 dimensional NMR experiments (COSY, TOCSY, NOESY, HMQC) indicated conversion of the linear peptides. However, due to the symmetrical nature of the Src sequence a sequential alignment by these data was not possible.

The yields after purification were 32 and 64% for “cyclo-Src-5C” (**59**) and “cyclo-Src-1C” (**60**), respectively. Both cyclic peptides contain an 1,4-disubstituted-1,2,3-triazole, which is connected to the former N-terminus via an amide bond and either a 5- or 1-carbon atoms containing hydrocarbon linker.



Scheme 6: Cyclization of peptides “Src-5C” (**57**) and “Src-1C” (**58**) using azide-alkyne 1,3-dipolar cycloaddition gave the cyclic products “cyclo-Src-5C” (**59**) and “cyclo-Src-1C” (**60**). The peptides differ in the length of the hydrocarbon linker between the triazole/azide and the amide bond.

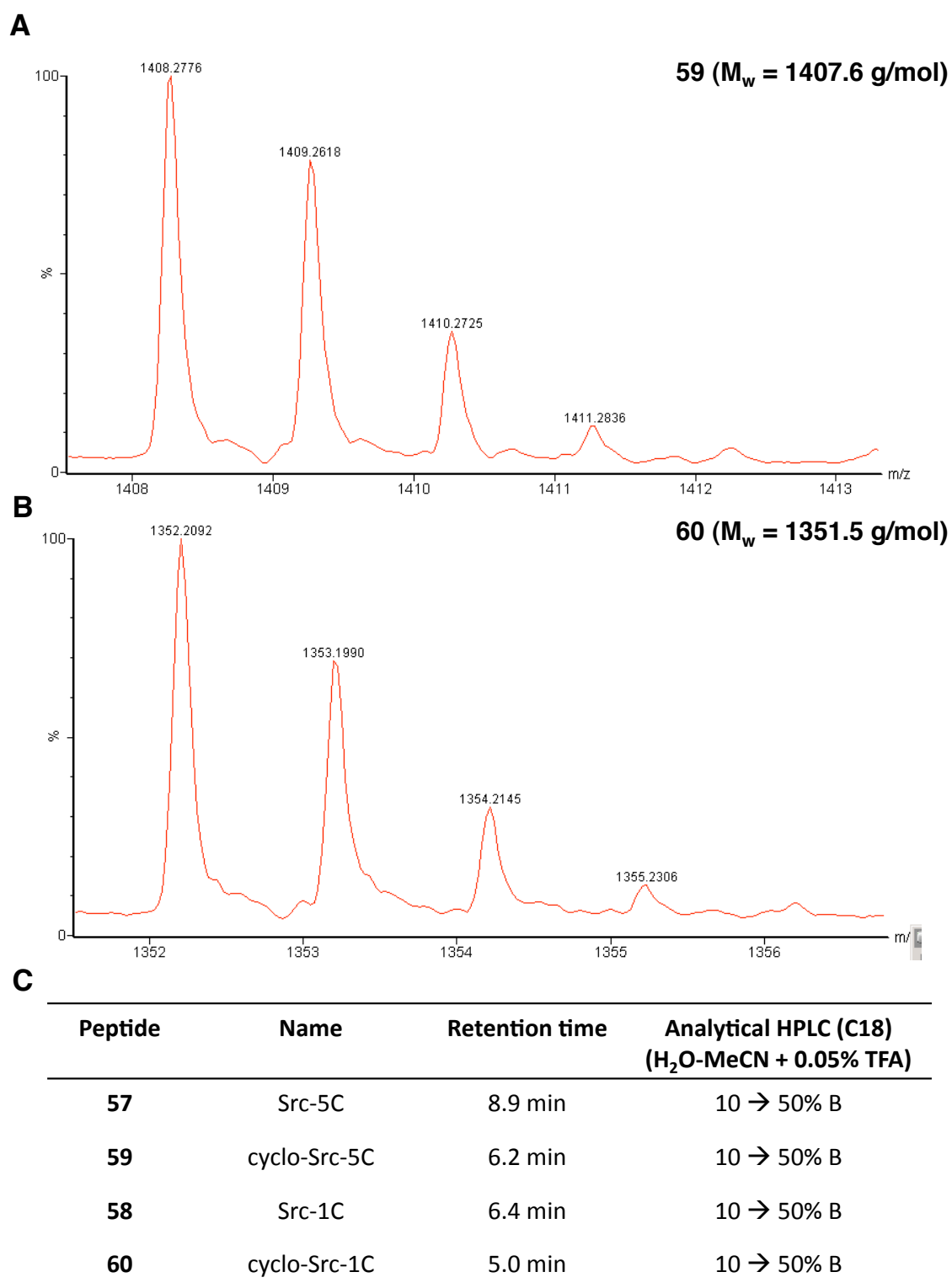


Figure 12: MALDI and HPLC analysis of peptides **59** and **60**. MALDI spectra of cyclopeptides **59** (“cyclo-Src-5C”, **(A)**) and **60** (“cyclo-Src-1C”, **(B)**). The difference of 1 m/z between the isotope peaks confirms the peptides to be monomeric. HPLC analysis **(C)** shows a shift to shorter retention times of the cyclopeptides compared to their linear precursors.

Additionally, the cyclizations were tried *in situ*, by incubating the linear peptides with PTP1B without the addition of a copper catalyst. But generation of cyclic product could not be observed in these experiments (Figure 13), which indicated that the peptides, while binding to the phosphatase (see chapter 3.4), do not adopt a 3D arrangement that would bring the reactive groups in close proximity.

Although this result could indicate that the cyclopeptides **59** and **60** did not have the optimal configuration to bind to PTP1B, these molecules were used for proof-of-concept experiments to study the influence of the hydrocarbon/triazole backbone linkers for cell entry and protease stability and to collect more information of their molecular configuration, binding ability and -mode to PTP1B, all of which are valuable data for further optimization of these kind of compounds. Another reason for the failure of the *in situ* reaction could be that the linkers were too flexible, even after binding of the peptides to the phosphatase, to allow the ring-closure reaction to take place.

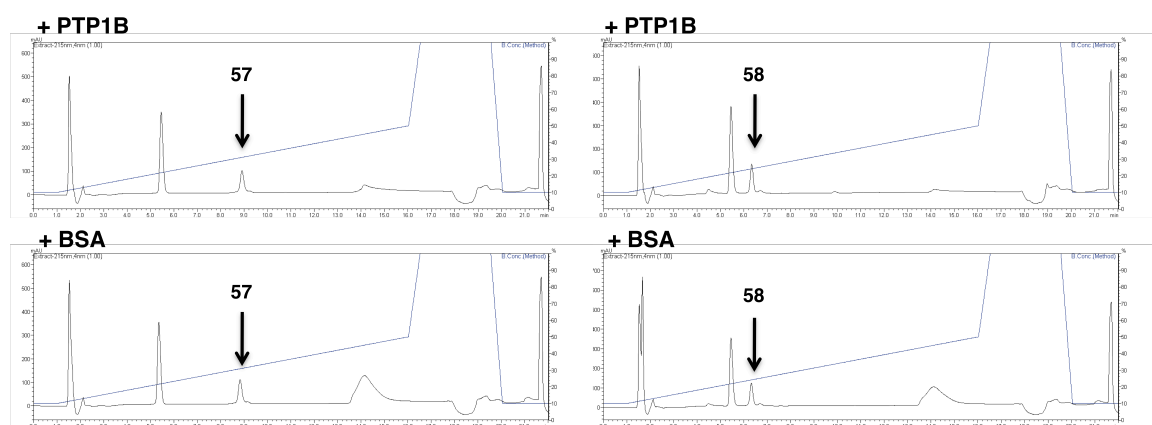


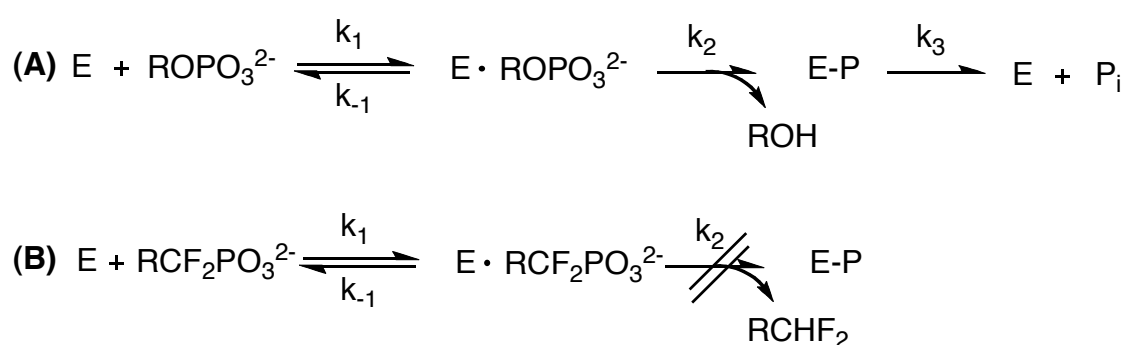
Figure 13: Trials to perform *in situ* ring closure. HPLC traces (C18; H₂O-MeCN + 0.05% TFA, 10 → 50% B) of the linear precursor peptides **57** and **58** incubated with PTP1B (0.4 equiv) or BSA (0.4 equiv) as control at 37°C over night. Generation of the cyclopeptides **59** (retention time 5.0 min, see Figure 12) or **60** (retention time 6.2 min, see Figure 12) in the PTP1B treated samples could not be observed.

3.4 Binding and inhibition studies of F₂Pmp containing peptides

For a characterization of the inhibition and binding strengths of the synthesized peptides two different types of assays were conducted.

An inhibition assay with the unnatural substrate para-nitrophenolphosphate (pNPP) was performed to compare the inhibitory constants (IC₅₀ values) of the synthesized cyclic and linear F₂Pmp containing peptides.^{109,205} It was shown that F₂Pmp containing peptides inhibit PTPs competitively by blocking the active-site cysteine and thereby disrupting the enzymatic mechanism due to their non-hydrolyzable C-P bond (Scheme 7).^{109,205} To gain further insight

in how the Src peptide binds to PTP1B and TCPTP and which residues are most important, an alanine and truncation scan library was synthesized and tested. Since all the peptides contain F₂Pmp and therefore inhibit the enzyme in the same manner, differences in the inhibitory potency of the individual peptides most likely reflect differences in the dissociation constant ($K_d = k_1/k_{-1}$). Therefore, the results obtained in the inhibition assay can be very well compared to the additionally performed binding assay. However, as the IC₅₀ is dependent on experimental parameters like substrate, inhibitor and enzyme concentration, only the relative changes between the individual peptides and not the absolute values can be compared. In this assay, the K_d of fluorophore-labeled derivatives of the F₂Pmp containing peptides was directly measured by means of fluorescence polarization.^{206–208}



Scheme 7: Theoretical considerations on the inhibitory mechanism of PTPs. Catalytic mechanism described by Zhang (A).⁹² The hydrolysis step (k_2) is blocked by non-hydrolyzable pTyr mimetics (B), thus, the enzyme-substrate-complex formation, described by the K_d (k_1/k_{-1}), determines mainly the relative interaction strength of different peptides containing the same pTyr mimetic.

3.4.1 Measurement of inhibitory potencies using the pNPP inhibition assay

Initially, the inhibitory potency (IC₅₀) of the Src sequence containing the non-hydrolyzable phosphotyrosine mimetic towards PTP1B and TCPTP was measured. The influence of the amino acid composition around the F₂Pmp to the overall binding of the peptide was assessed by synthesizing and comparing an alanine scan library of the Src sequence, in which every amino acid except F₂Pmp has been replaced by alanine (Figure 14).

This principle had successfully been used to map important amino acid residues for the activity in peptides and proteins.^{209–212} Alanine is usually chosen as replacement in this kind of analysis, since it is mimicking the geometry and flexibility of almost all canonical amino acids without having any functionality in β position except a methyl group. Therefore, the contribution of functionalities in certain side chains can be studied. In the Src sequence this was the case for the glutamate, asparagine, leucine and glutamine residues. At the same time, two proline and one glycine were present in the sequence, which are the amino acids differing in geometry and flexibility from the remaining canonical amino acids. Therefore,

replacement of these amino acids by alanine rather provides information on the importance of geometrical constraint at the respective position than side chain functionality.

Furthermore, a truncation scan library was synthesized and tested (Figure 15). By shortening the sequence from either the N- or C-terminus or from both termini it was aimed to study the influence of the N- and C-terminally residues as well as how many residues around the F₂Pmp are needed to promote efficient binding.

The measurements were performed in pNPP assay buffer with a pH value of 7.2 and physiological salt concentration, as described in previous publications.^{130,213} In order to be able to compare the binding to the phosphatases, the IC₅₀ values were obtained with an enzyme concentration of 40 nM for both PTP1B and TCPTP.

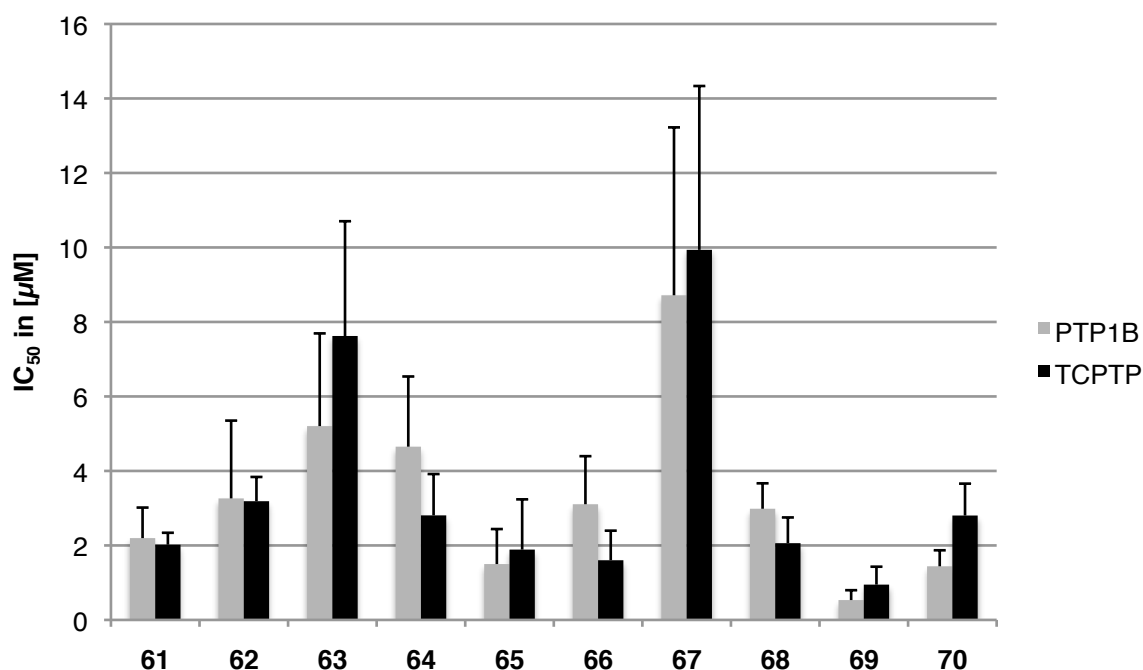
The original Src sequence peptide containing F₂Pmp (**61**) showed an IC₅₀ value of around 2 μM for both PTP1B (2.2 μM ± 0.82) and TCPTP (2.02 μM ± 0.32) (Figure 14). Thus, the slight preference of the sequence towards PTP1B as seen in chapter 3.1.3 was not observed with the inhibitory peptide in the inhibition assay.

The highest drop in activity (4-5-fold) in the alanine scan library was observed with peptide **67**. In this peptide the N-terminal adjacent glutamine to F₂Pmp at position +1 was exchanged.

Interestingly, exchanging two C-terminal residues of the peptide (+5 N and +4 E) resulted also in decreased inhibition strength with the replacement of the asparagine at position +5 causing the biggest change. This indicated that also residues further away from the non-hydrolyzable phosphotyrosine mimetic take part in binding to the protein justifying the use of the decamer sequence for the inhibitor development.

The residues at positions +2, +3, +6, -1 and -3 changed the inhibitory potency of the peptide only very moderately by replacement with alanine and thus might be interesting to consider, when alternative positions to place functional groups for cyclization are desired in the future.

The exchange of the proline at position -2 (peptide **69**) is the only candidate in the alanine scan library, which resulted in the (4-fold) increase of potency. As mentioned earlier, an exchange for proline to alanine reflects a change in conformation and backbone flexibility, which can also influence side chain interactions. Thus, the increase in binding could also potentially been caused by residues neighbouring the replaced proline. An exchange of the rigid proline for alanine could allow the neighbouring residues more “freedom” to adopt a conformation needed to interact with the protein.



Peptide	Sequence	IC ₅₀ [μM] (PTP1B)	IC ₅₀ [μM] (TCPTP)
61	Ac-EPQXQPGENL-NH ₂	2.20 ± 0.82	2.02 ± 0.32
62	Ac-EPQXQPGENA-NH ₂	3.26 ± 2.09	3.19 ± 0.65
63	Ac-EPQXQPGEA-NH ₂	5.20 ± 2.49	7.62 ± 3.08
64	Ac-EPQXQPGA-NH ₂	4.65 ± 1.88	2.81 ± 1.11
65	Ac-EPQXQPAENL-NH ₂	1.50 ± 0.94	1.89 ± 1.35
66	Ac-EPQXQAGENL-NH ₂	3.11 ± 1.29	1.60 ± 0.79
67	Ac-EPQXAPGENL-NH ₂	8.72 ± 4.51	9.94 ± 4.40
68	Ac-EPAQXQPGENL-NH ₂	2.38 ± 0.68	2.06 ± 0.69
69	Ac-EAQXQPGENL-NH ₂	0.53 ± 0.26	0.95 ± 0.48
70	Ac-APQXQPGENL-NH ₂	1.44 ± 0.43	2.80 ± 0.86

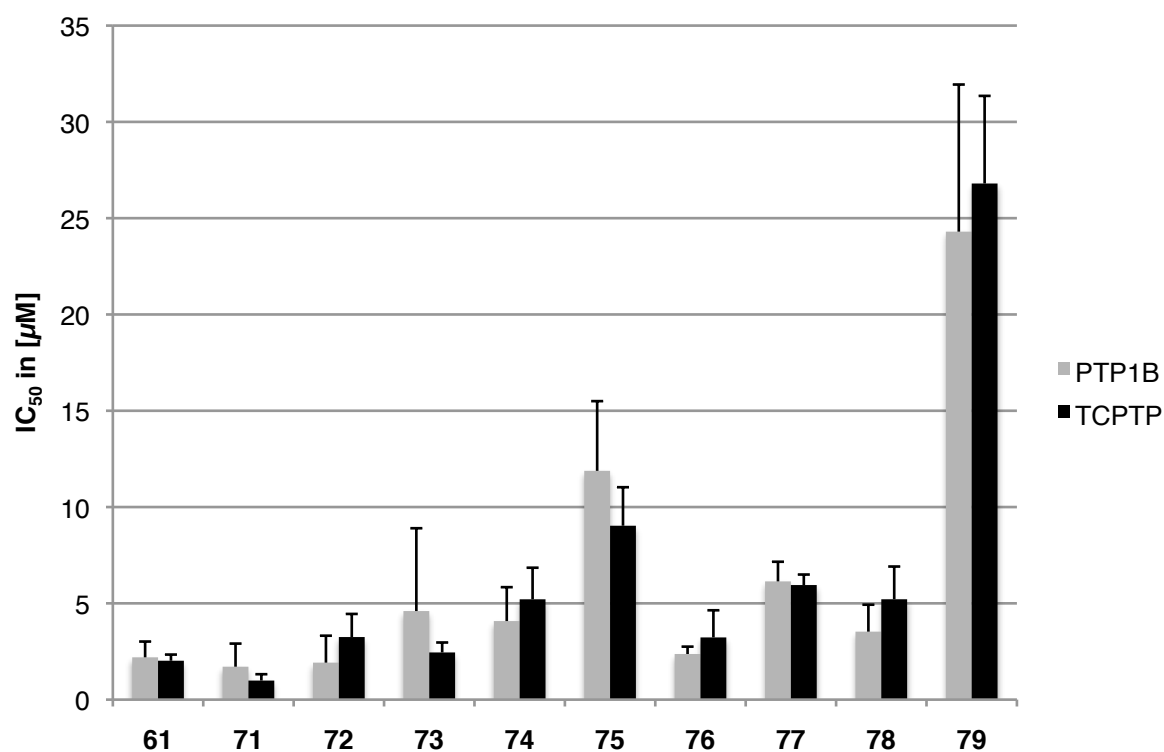
Figure 14: Sequences and IC₅₀ values of the alanine scan peptides (X = F₂Pmp).

The values obtained from the truncation scan library showed a gradual decrease of potency when the sequence was shortened from the N or C terminus or both (Figure 15). For the longer C terminal end a drop in activity was observed beginning from deletion of position +4. In contrast to the results from the alanine scan, which showed that substitution of asparagine at position +5 causes a drop in activity, no decrease in activity was observed when deleting this residue in peptide **72**.

Results

Shortening the peptide from both sides caused a decrease in inhibitor potency of about 2-fold when all residues except two on either side of F₂Pmp were deleted, and a decrease of more than 10 fold when only both adjacent glutamines were left.

This study suggested that for most efficient binding of the Src sequence 3 amino acids at the N- and 4 at the C-terminus were needed. However, due to the contrasting result that exchange of the asparagine at position +5 to alanine caused a decrease in potency, the original peptide length was kept for further experiments.



Peptide	Sequence	IC ₅₀ [μM] (PTP1B)	IC ₅₀ [μM] (TCPTP)
61	Ac-EPQXQPGENL-NH ₂	2.20 ± 0.82	2.02 ± 0.32
71	Ac-EPQXQPGEN-NH ₂	1.71 ± 1.2	0.99 ± 0.33
72	Ac-EPQXQPGE-NH ₂	1.92 ± 1.4	3.25 ± 1.20
73	Ac-EPQXQPG-NH ₂	4.6 ± 4.3	2.45 ± 0.52
74	Ac-EPQXQP-NH ₂	4.08 ± 1.76	5.21 ± 1.64
75	Ac-EPQXQ-NH ₂	11.88 ± 3.62	9.03 ± 2.00
76	Ac-PQXQPGENL-NH ₂	2.37 ± 0.38	3.23 ± 1.41
77	Ac-QXQPGENL-NH ₂	6.14 ± 1.02	5.95 ± 0.55
78	Ac-PQXQP-NH ₂	3.53 ± 1.4	5.21 ± 1.7
79	Ac-QXQ-NH ₂	24.30 ± 7.64	26.80 ± 4.55

Figure 15: Sequences and IC₅₀ values of the truncation scan peptides (X = F₂Pmp).

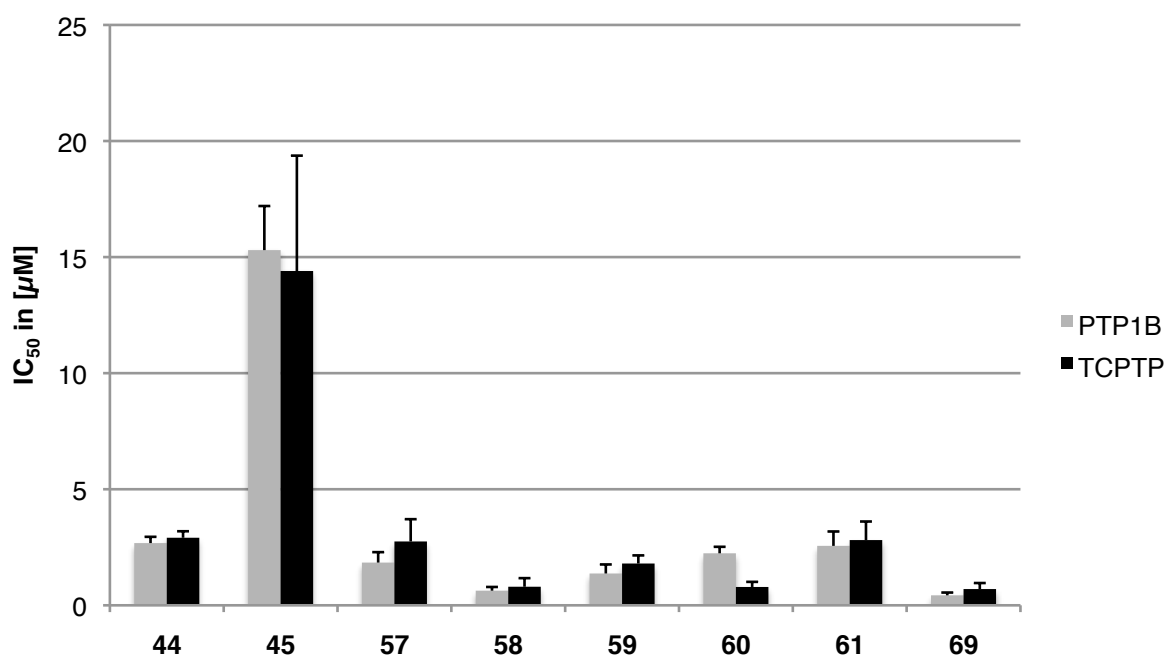
In another set of experiments the inhibitory potency of the original Src sequence was compared to the sequences containing the functionalities for the azide-alkyne cycloaddition before (**57** and **58**) and after cyclization (**59** and **60**) (Figure 16). Additionally, the IC₅₀ values of the best performing sequence from the alanine scan (**69**) and of the EGFR (**44**) and random sequence (**45**) from chapter 3.1.3 with a non-hydrolyzable F₂Pmp instead of phosphotyrosine were compared.

As in the K_M measurements, the resulting values were very close to each other and were ranging between 0.4 and 15 μM suggesting that the majority of the inhibitory potency was conferred by the F₂Pmp group.

Consistent with the previous measurements the IC₅₀ of the Src sequence without linker groups (**61**) was fairly similar towards PTP1B and TCPTP and in the range between 2 and 3 μM. Both linker-containing sequences showed slightly increased potency compared to the original sequence, with the 4-fold increase of the Src-1C peptide (**58**) resulting in a statistically difference (t-test, p < 0.05) compared to the Src sequence (**61**). The potency of Src-1C (**58**) against TCPTP remained constant upon cyclization, whereas a drop in activity was observed against PTP1B. Overall, a tremendous positive effect of cyclization on inhibitory potency could not be seen, which is in line with the finding that cyclization did not take place *in situ* by incubating with the enzyme without the addition of copper (chapter 3.3.2).

Comparable with the enzyme kinetic measurements (chapter 3.1.3) the 6mer sequence derived from the EGFR (**44**) performed very similar towards PTP1B as the Src sequence (**61**). The absolute value of 2.68 ± 0.27 μM of the EGFR peptide (**44**) differed with a factor of 10 from the described literature value of 0.2 μM.¹⁰⁴ However, absolute IC₅₀ values, especially between different experiments, are difficult to compare, as outlined in the beginning of chapter 3.4. In contrast to the inhibitory assay described herein, using the unnatural substrate pNPP, Burke and coworkers determined the IC₅₀ by the dephosphorylation of ³²P-labeled autophosphorylated insulin receptor. Therefore, especially differences in substrate concentrations and/or in the K_M of the substrate (-preparation) to the enzyme were difficult to assess retrospectively and could contribute to the observed difference of the absolute values. The random 10mer (**45**) was by far the least active and with 6-fold loss of potency statistically significant different (t-test, p < 0.05) from the Src sequence (**61**).

Like in the alanine scan, the Src-P(-2)A peptide (**69**) is with an IC₅₀ of 0.43 μM (± 0.12) against PTP1B and 0.7 μM (± 0.26) against TCPTP the most potent inhibitory peptide. Compared the Src (**61**) and the EGFR (**44**) peptide, this sequence is around 6-fold more potent and statistically significant different (t-test, p < 0.05) from both peptides.



Peptide	Name	IC ₅₀ [μM] (PTP1B)	IC ₅₀ [μM] (TCPTP)
44	EGFR	2.68 ± 0.27	2.91 ± 0.28
45	Random	15.3 ± 1.9	14.4 ± 4.97
57	Src-5C	1.84 ± 0.45	2.75 ± 0.96
58	Src-1C	0.63 ± 0.16	0.8 ± 0.37
59	cyclo-Src-5C	1.37 ± 0.39	1.8 ± 0.35
60	cyclo-Src-1C	2.24 ± 0.28	0.79 ± 0.22
61	Src	2.56 ± 0.62	2.81 ± 0.8
69	Src-P(-2)A	0.43 ± 0.12	0.7 ± 0.26

Figure 16: IC₅₀ values of the peptides tested with the pNPP competition assay.

To benchmark these values “CinnGEL” (**18**, Figure 6) a commercially available PTP1B inhibitor from Biomol (Hamburg, Germany) was tested with the pNPP competition assay.¹²³ Using this tripeptide with an N-terminal para-carboxycinnamic acid an IC₅₀ value of 3.62 μM could be measured in sodium acetate buffer at pH 6.0, which is in the same range as the described value of 1.3 μM by *Moran et al.* However, when pNPP assay buffer at pH 7.2 and physiological salt concentration was used, no inhibition was observed at the concentrations tested suggesting a higher potency of the inhibitory peptides described herein compared to CinnGEL (**18**) in physiologically more relevant conditions.

3.4.2 Affinity measurements with the fluorescence polarization assay

The underlying principle of fluorescence polarization (FP) was described in the early 1950's. It was observed that light emitted by a fluorescent molecule in solution, which was excited by polarized light, can be polarized depending on the rotational rate of the molecule and the fluorescence lifetime of the fluorophore.²⁰⁷ The larger a molecule gets, the slower its rotational rate. Very small molecules, like peptides, rotate so fast, that polarization of an attached fluorophore cannot be observed (rotational Brownian diffusion). However, binding of these fluorescently labeled molecules to larger macromolecules, like proteins, slows down their rotational rate and polarization of emitted light can be observed. This principle can be used to measure binding events, e.g. antibody antigen interactions.²⁰⁶

5(6)-Carboxyfluorescein (CF) labeled derivatives of the F₂Pmp containing EGFR sequence (**80**; CF-EGFR), the random 10mer sequence (**81**; CF-Random), the linker containing Src sequences before (**82** and **83**; K(CF)-Src-5C and K(CF)-Src-1C) and after cyclization (**84** and **85**; cyclo-K(CF)-Src-5C and cyclo-K(CF)-Src-1C) (Figure 17), the Src sequence without a linker moiety (**86**; CF-Src) and the Src sequence with proline at -2 position exchanged for alanine (**87**; CF-Src-P(-2)A) were synthesized and tested for binding to PTP1B and TCPTP based on the FP principle (Figure 18). Since in the linker-containing sequences the N termini were used to introduce an azide group, an additional Mtt protected lysine residue was incorporated at the N terminus to enable the attachment of the fluorophore. The fluorophore was coupled to the amine group in its side chain on solid support after selective removal of the Mtt group. In all the other sequences CF was coupled directly to the N-terminus.

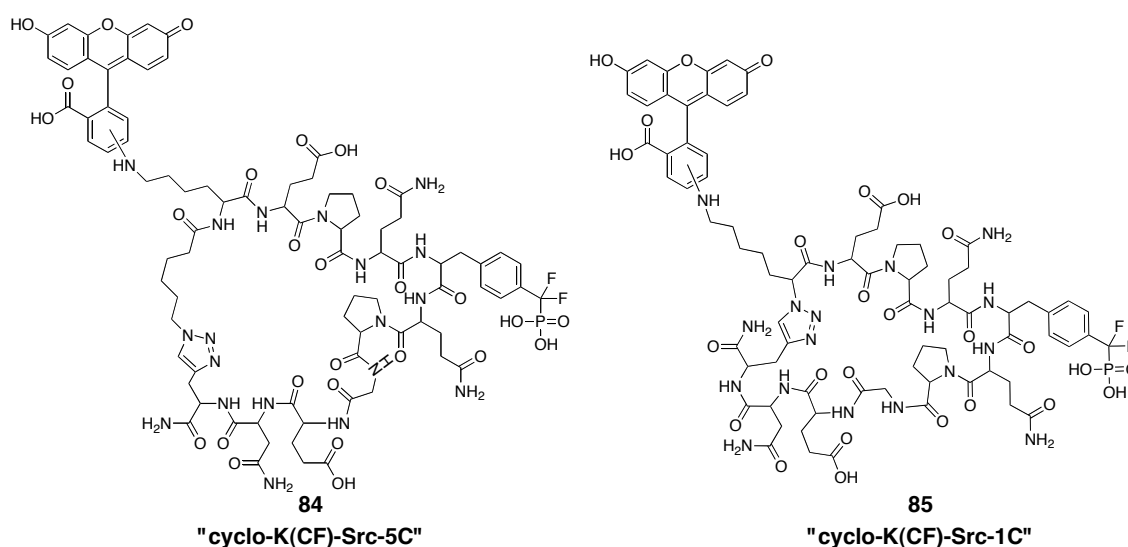
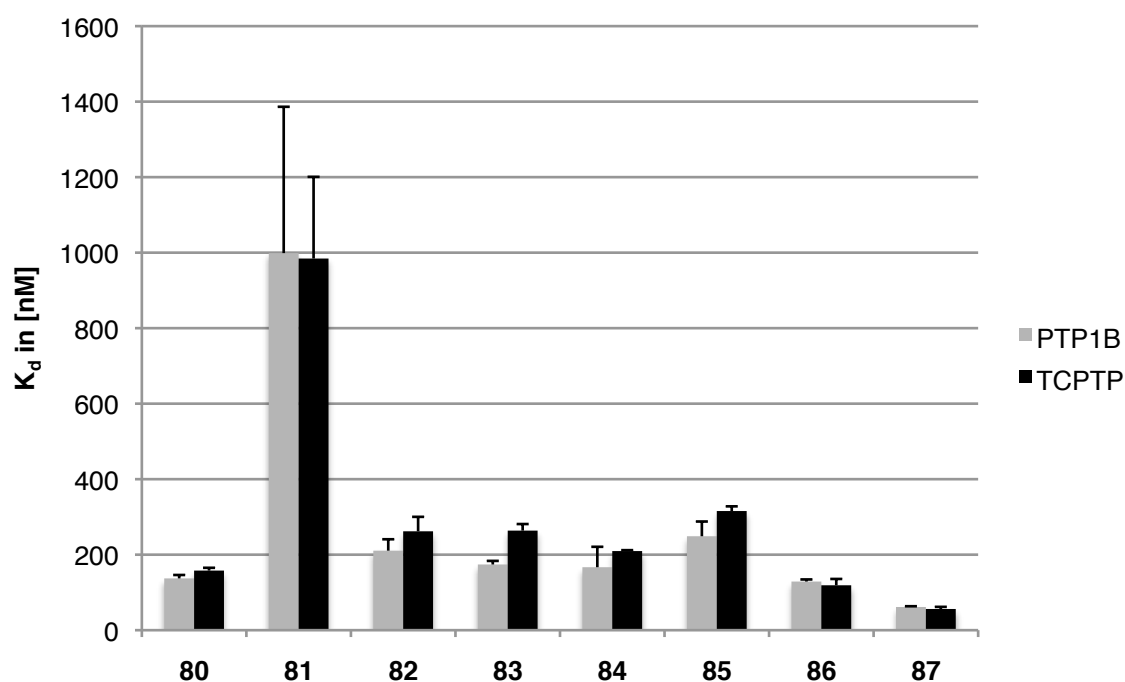


Figure 17: Molecular structure of the cyclic peptides **84** ("cyclo-K(CF)-Src-1C") and **85** ("cyclo-K(CF)-Src-5C") carrying the 5(6)-carboxyfluorescein fluorescent label in the lysine side chain.

Results



Peptide	Name	K _d [nM] (PTP1B)	K _d [nM] (TCPTP)
80	CF-EGFR	137.1 ± 9.1	157.9 ± 7.4
81	CF-Random	998.8 ± 387.6	984.4 ± 216.4
82	K(CF)-Src-5C	210.6 ± 30.2	261.9 ± 38.3
83	K(CF)-Src-1C	174.0 ± 17.4	263.7 ± 17.4
84	cyclo-K(CF)-Src-5C	166.8 ± 54.1	209.6 ± 2.4
85	cyclo-K(CF)-Src-1C	248.8 ± 39.0	315.6 ± 12.4
86	CF-Src	128.8 ± 5.6	118.9 ± 16.8
87	CF-Src-P(-2)A	61.4 ± 2.0	56.2 ± 5.6

Figure 18: K_d values obtained with the fluorescence polarization assay. The control proteins VHR, PTPα and the SH2 domain of the Src kinase did not show any polarization at the concentrations tested.

In order to obtain the dissociation constants for the interaction of peptide and phosphatase, the fluorophore labeled peptides were incubated in PBS buffer with a dilution series of protein and the emission of polarized light was measured.

As seen in K_M and IC₅₀ measurements, the obtained K_d values laid in a narrow range of ~100 – 300 nM with the exception of the random peptide **81** (~1000 nM).

The original Src sequence **86** binds with a K_d of 120 to 130 nM to PTP1B and TCPTP (Figure 18). Also in the FP assay, the Src-P(-2)A sequence **87** is the best binding peptide with an

affinity of around 60 nM to both phosphatases. In agreement with the pNPP assay is furthermore the comparable performance of the EGFR peptide **80** with the Src sequence **86** and the poor binding of the random 10mer **81**, which bound 7-8 times less strong than the Src sequence **86**. The similar relative performance of the control peptides in the pNPP and FP experiments showed that the FP assay could very well be used to compare binding affinities between several F₂Pmp containing peptides and that the N-terminal attachment of fluorescein did not interfere. Furthermore, the relative difference in binding was directly reflecting the relative difference in inhibitory potency.

Different to the pNPP assay is the fact that all linker containing sequences (**82**, **83**, **84** and **85**) bound less strong than the original Src sequence, which could be an artefact caused by the different positioning of the fluorophore in the linker containing peptides. The effect of the cyclization, however, is comparable to the effect observed in the pNPP assay. Whereas the binding got slightly better upon cyclization of the 5 carbon linker containing sequence obtaining peptides **84**, it got worse for the 1 carbon linker containing cyclic peptide **85**. But also in this experiment the effect of cyclization upon binding is a minor one. All linker containing or cyclized peptides show a slight preference for PTP1B in the FP assay, this difference, however, is statistically not significant.

Additionally, all peptides were tested against the dual specificity phosphatase VHR to determine their selectivity against a member of this phosphatase subfamily and no polarization was observed for the concentration range tested. The receptor-like phosphatase RPTP α was also reported to dephosphorylate the Src kinase at the C-terminal position and was therefore also tested, but no peptide showed polarization against its recombinantly produced and purified catalytic D1 domain (212-503).^{214,215}

Physiologically, the phosphorylated C terminus of the Src kinase binds to Src's SH2 domain intermolecularly and thereby inactivates the kinase domain. Therefore, binding of the F₂Pmp containing peptides against the recombinantly produced SH2 domain and the GST-fused SH2 domain of Src was studied, but also in case of these proteins no binding was observed in the concentration range tested.²¹⁶

3.5 Evaluation of the cellular penetration, stability and activity of the peptidic inhibitors

3.5.1 Comparison of cellular penetration using confocal microscopy

As mentioned earlier in this work, it was shown by Verdine and coworkers that the BH3 domain of the Bcl-2 protein, whose helical structure was stabilized with a hydrocarbon linker,

showed improved proteolytic resistance and plasma membrane penetration.¹⁸⁵ Therefore, the cyclization of the Src sequence via a hydrocarbon linker and a 1,2,3-triazole was not only performed to enhance stability against proteolytic degradation, a principle already known, but also to test if the cyclization of relatively short and more loop-like peptides via a hydrocarbon linker could potentially enhance their permeation through cell membranes, similar to the hydrocarbon-stapled helical structures mentioned.^{177,178}

To test this hypothesis, cultured HeLa Kyoto cells were incubated with fluorescently labeled linker containing linear and cyclic versions of the Src sequence K(CF)-Src-5C (**82**), K(CF)-Src-1C (**83**), cyclo-K(CF)-Src-5C (**84**) and cyclo-K(CF)-Src-1C (**85**), all containing the non-hydrolyzable F₂Pmp group. After washing the cells with PBS (3 x) to minimize background signal, the efficiency of uptake and the cellular localization of the peptides were compared by examination with a Leica SP2 confocal microscope (Figure 19). The fluorophore was excited with the argon laser ($\lambda = 488$ nm) and emission was collected from 500-650 nm. The Laser intensity, photomultiplier and pinhole settings were kept constant throughout a single experiment to be able to compare the signal intensities.

As expected, a homogenous fluorescent signal derived from the linear sequences, which would indicate cellular uptake in the cytoplasm, was low. The peptides most likely could not pass the plasma membrane efficiently due to their size and most importantly the highly negative charged nature of the F₂Pmp group, which was potentially repelled by the negative potential on the inner leaflet of the cell membrane. The peptide bearing the 1 carbon linker (**83**) showed a weak, but more homogenous distribution than the K(CF)-Src-5C (**84**) peptide, which exhibited a dotted staining and showed almost no signal in the cytoplasm. This dotted staining was caused by entrapment of the fluorescent peptide in small rounded up structures inside the cells, which most likely represent endocytotic vesicles. Since the only difference of the two linear peptides was the length of the carbon linker between the azide group and their N terminus, it seemed that the linker groups were causing this difference.

The cyclized peptides did not show a striking difference compared to their linear precursor molecules (Figure 19). The cyclized variant of the 1 carbon linker peptide **85** (cyclo-K(CF)-Src-1C) showed a rather less intense homogenous staining and a bit more dotted staining, but this difference was not very obvious. The staining of the cyclic peptide **84** (cyclo-K(CF)-Src-5C) looked very similar to its linear precursor **82**. Thus, cyclization did not lead to better cell penetration of the peptides in this experiment.

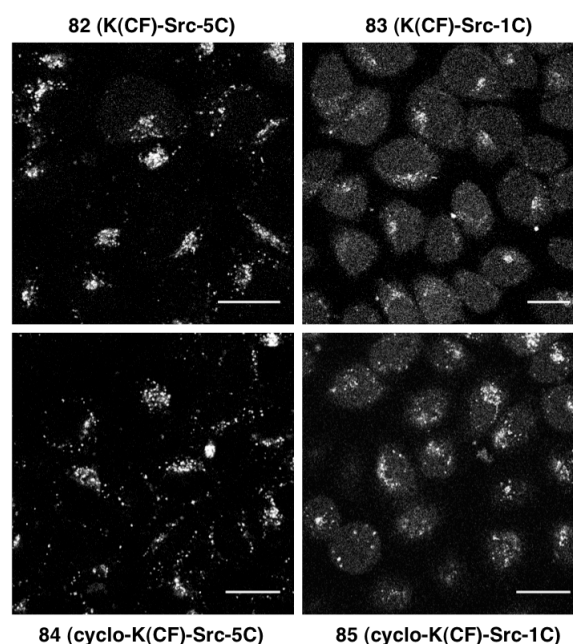


Figure 19: Comparison of cellular uptake and localization of fluorescein labeled linker containing Src sequences before and after cyclization. (Hela Kyoto cells were incubated with the peptides (50 μ M) for 12 hours at 37°C. Pictures were taken with a 63x oil immersion objective., scale bar = 20 μ M)

Previously, it was shown that addition of polybasic sequences, so-called cell penetrating peptides (CPPs), to peptides or small molecules can enhance the degree of uptake. Additionally, the guanidinium group of the amino acid arginine had been shown to be crucial for this effect.^{217–220}

Since the cyclization did not yield the anticipated improvement in cell penetration, the fluorescein labeled linear F₂Pmp containing Src sequence was synthesized carrying additional 4, 6 or 8 arginine residues at their C-termini, resulting in CF-Src-R₄ (**88**), CF-Src-R₆ (**89**) and CF-Src-R₈ (**90**). These peptides were used in the same experimental setup as the cyclized ones to compare their cellular uptake (Figure 20 (A)). Different amounts of arginine residues were added in order to find the number of arginines needed for the uptake, probably accompanied by a shift of the net charge of the peptide avoiding repulsion of the negative membrane potential.

Indeed, the degree of uptake correlated with the amount of arginine residues added. A gradual increase of cells with a brighter and more homogenous staining could be observed (Figure 20 (A)).

Since the change of the net charge of the poly-arginine peptides was not only expected to change the penetration behaviour but also the interaction strength of the peptide with the target protein, binding affinities against PTP1B were measured using the fluorescence polarization assay (Figure 20 (B)). It was observed, that with an increasing number of arginine

residues the binding strength dropped with peptide **88** (CF-Src-R₄) being around 5 times, **89** (CF-Src-R₆) 10 times and **90** (CF-Src-R₈) around 20 times less potent than CF-Src.

As a compromise between more efficient permeation and still decent binding behaviour of F₂Pmp containing peptides, 6 C-terminal arginines were used to promote cellular uptake of the peptide sequences in the subsequent colocalization experiment (chapter 3.5.2).

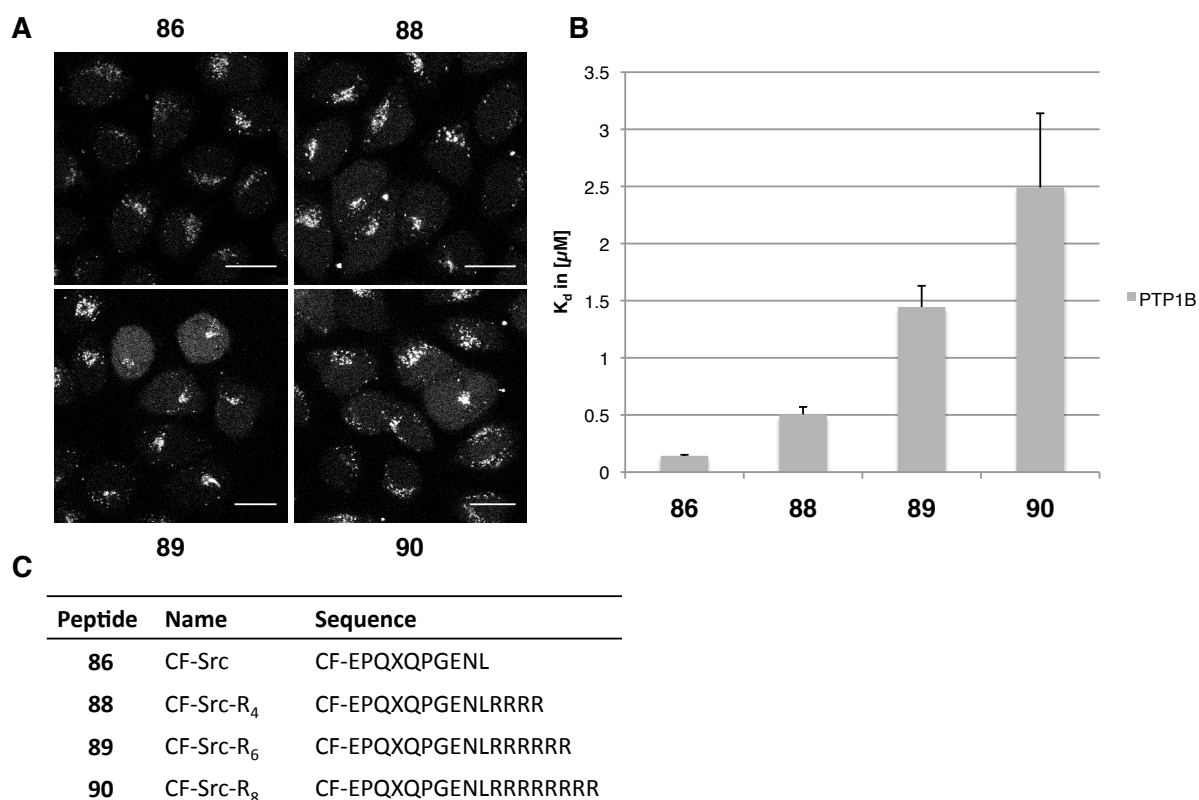


Figure 20: Comparison of cellular uptake and localization of fluorescein labeled Src sequences bearing increasing amounts of C-terminal arginine residues. **(A)**. (HeLa Kyoto cells were incubated with the peptides (50 µM) for 12 hours at 37°C, pictures were taken with a 63x oil immersion objective, scale bar = 20 µM) Affinity measurement of the poly-arginine peptides against PTP1B with the fluorescence polarization assay **(B)**. Table **(C)** displaying the sequences of peptides **86**, **88**, **89** and **90** (X = F₂Pmp).

3.5.2 Colocalization of a cell penetrating CF-Src-P(-2)A sequence with PTP1B

Next, it was investigated whether a cell penetrating, F₂Pmp containing and fluorescein labeled peptide shows colocalization with PTP1B in living cells. Due to the loss of binding affinity, when several arginines were added to the peptide, the strongest binding sequence identified in the FP and pNPP screen with the proline at position -2 exchanged for alanine (Src-P(-2)A) was used and peptide **91** (CF-Src-P(-2)A-R₆) was synthesized accordingly. The K_d towards PTP1B of the Src-P(-2)A sequence equipped with 6 C-terminal arginine residues (peptide **91**) was 1.3fold better than the K_d of the original Src sequence bearing the same number of arginines (**89**), as determined with the FP assay. As negative control the 5(6)-carboxyfluorescein labeled Src sequence comprising also 6 C-terminal arginines, but a

tyrosine instead of F₂Pmp, peptide **92** (CF-Src-(Y)-R₆), was synthesized. This peptide can also enter the cells but does not bind to PTP1B, as tested by fluorescence polarization.

Furthermore, a fusion protein of PTP1B with an N-terminal mKate fluorescent protein was generated, by cloning full length PTP1B in an mKate-C1 vector. A C-terminal anchor sequence determines PTP1B's natural cellular localization mainly to the ER membrane with the catalytic domain facing to the cytosol.^{24,81,82} Hence, the N-terminal fusion was chosen to not interfere with the normal distribution of the protein.

U2OS cells were transformed with the mKate-PTP1B vector and incubated with the peptides over night. After the incubation time the cells were washed with PBS (3 x) and pictures were taken with a confocal microscope. The fluorescein labeled peptides were excited using the 488 nm beam of the argon laser and emission was recorded from 500 to 525 nm. The mKate labeled protein was excited with 532 nm light of the helium-neon laser and emission was collected between 599 and 658 nm. The overexpressed protein showed normal subcellular distribution at the perinuclear/ER region as it was described for full length PTP1B before.²⁴

For both peptides homogenously distributed fluorescent signal in the fluorescein channel was detected inside all cells (Figure 21). Additionally, the pictures showed that in cells that overexpressed the protein, an accumulation of green fluorescence of peptide **91** (CF-Src-P(-2)A-R₆) could be found in the perinuclear/ER area where the protein is located, whereas this was not observed in cells treated with the F₂Pmp lacking control peptide **92**. This indicated that peptide **91** (CF-Src-P(-2)A-R₆) indeed could enter the cells and bind to PTP1B. This result was confirmed by a quantification of the colocalization signal of 10 individual cells from 3 different experiments, which were incubated with peptide **91** (CF-Src-P(-2)A) or the control peptide **92** (CF-Src-(Y)-R₆). Using the colocalization finder plugin of the ImageJ software a significant higher degree of colocalization ($p = 0.002$) for peptide **91** (CF-Src-P(-2)A-R₆) compared to the control peptide **92** (CF-Src-(Y)-R₆) could be detected, which proved that the F₂Pmp containing peptide **91** entered the cells and bound to PTP1B at its normal site of localization.

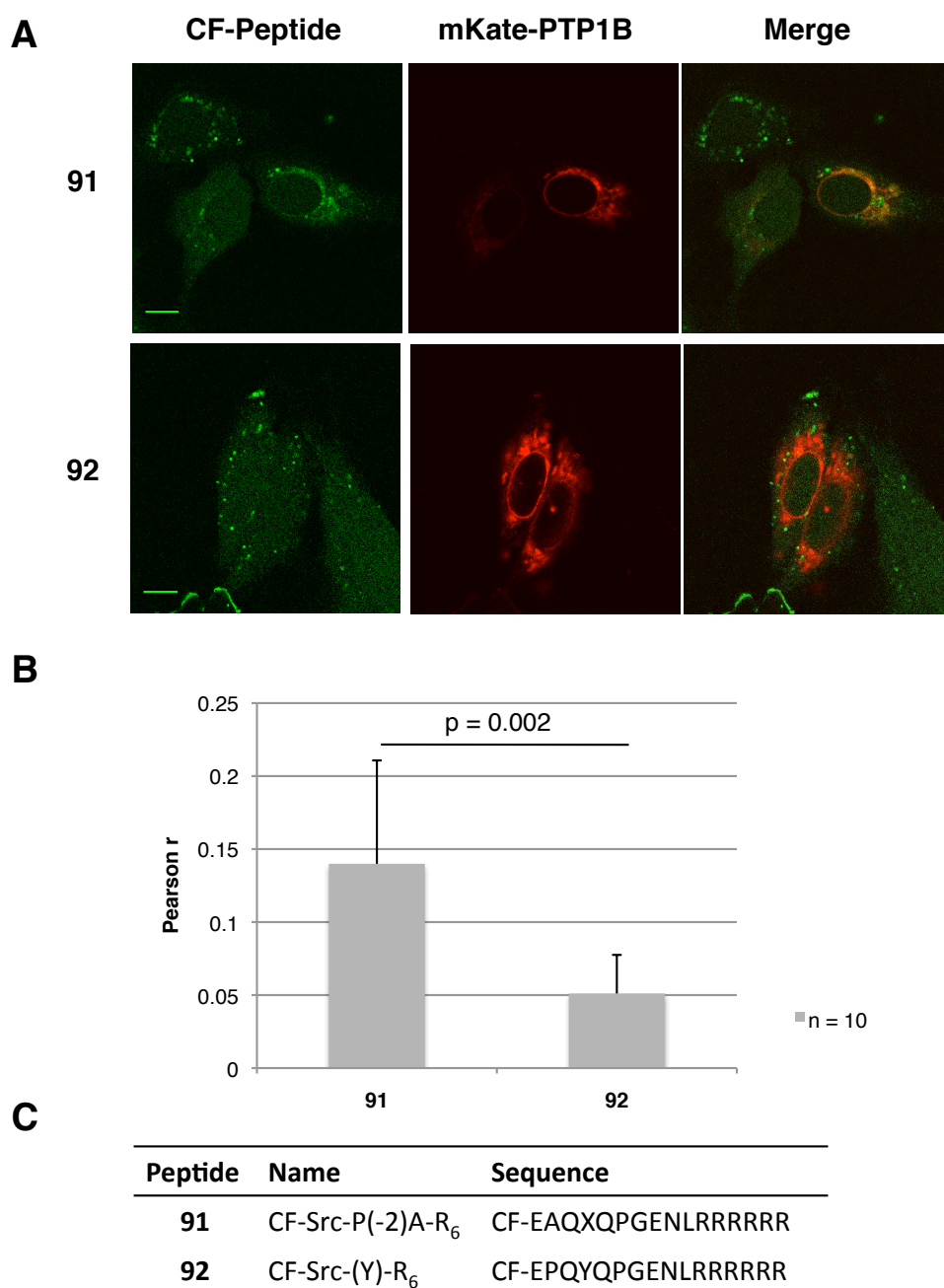


Figure 21: Peptide **91** (CF-Src-P(-2)A-R₆) but not **92** (CF-Src-Y-R₆) colocalizes with mKate-PTP1B in U2OS cells, as observed under the confocal microscope (**A**) (U2OS cells were incubated with the peptides (50 μ M) for 12 hours at 37°C. Pictures were taken with a 63x oil immersion objective, scale bar = 10 μ m). Quantification of the degree of colocalization using the “Colocalization Finder” plugin of ImageJ (**B**). Statistical analysis (t-test) revealed a significant increase in colocalization in cells treated with the F₂Pmp containing peptide **91** compared with the F₂Pmp free control **92** ($p = 0.002$, $n = 10$). Table (**C**) shows the sequence of peptides **91** and **92** (X = F₂Pmp).

3.5.3 Stability of linear versus cyclic inhibitory peptides in cell lysate and human blood serum

The second major obstacle of peptides limiting their usage as drugs or biological tools, together with poor membrane permeation, is their susceptibility to degradation by proteolytic enzymes, such as esterases and peptidases. These enzymes are present in large amounts in the digestive tract of all kinds of organisms, which poses a great challenge in the development of especially orally available peptidic drugs for human patients.¹⁷⁶

But also every individual cell is equipped with a characteristic set of endo- and exopeptidases, which are, together with the proteasome, part of the cellular protein degradation machinery. These intracellular enzymes do not only rapidly clear the cytoplasm from peptides generated by the proteasomal degradation of proteins, but are also highly active against any externally administered peptide entering the cell.¹⁷⁷⁻¹⁷⁹

Thus, the same problem of proteolytic degradation has to be considered, when developing peptides as tools for cell biology experiments.

As mentioned earlier in this work, cyclization is one of the possible strategies for an increased biological stability. Although cyclic F₂Pmp-containing peptides have been synthesized previously with the aim of enhancing inhibitory potency and proteolytic stability, the latter was not addressed experimentally.¹⁰⁹

To study the effect of cyclization on proteolytic stability, both fluorescently labeled linker and F₂Pmp containing peptides before (**82**; K(CF)-Src-5C and **83**; K(CF)-Src-1C) and after cyclization (**84**; cyclo-K(CF)-Src-5C and **85**; cyclo-K(CF)-Src-1C) were tested for degradation in U2OS cell lysate. Compared to the N-terminally fluorescein labeled control peptide (CF-Control-peptide), which contained only canonical amino acids and possessed a basic net charge, all four F₂Pmp containing peptides were remarkably stable over the course of 22 hours (Figure 22). This suggested, that already incorporation of unnatural constituents like the non-canonical amino acids (propargylglycine and F₂Pmp) or the azide bearing N-terminal linker enhanced the stability of the peptides dramatically. It is therefore not possible to draw conclusions about the effect of cyclization on these model peptides.

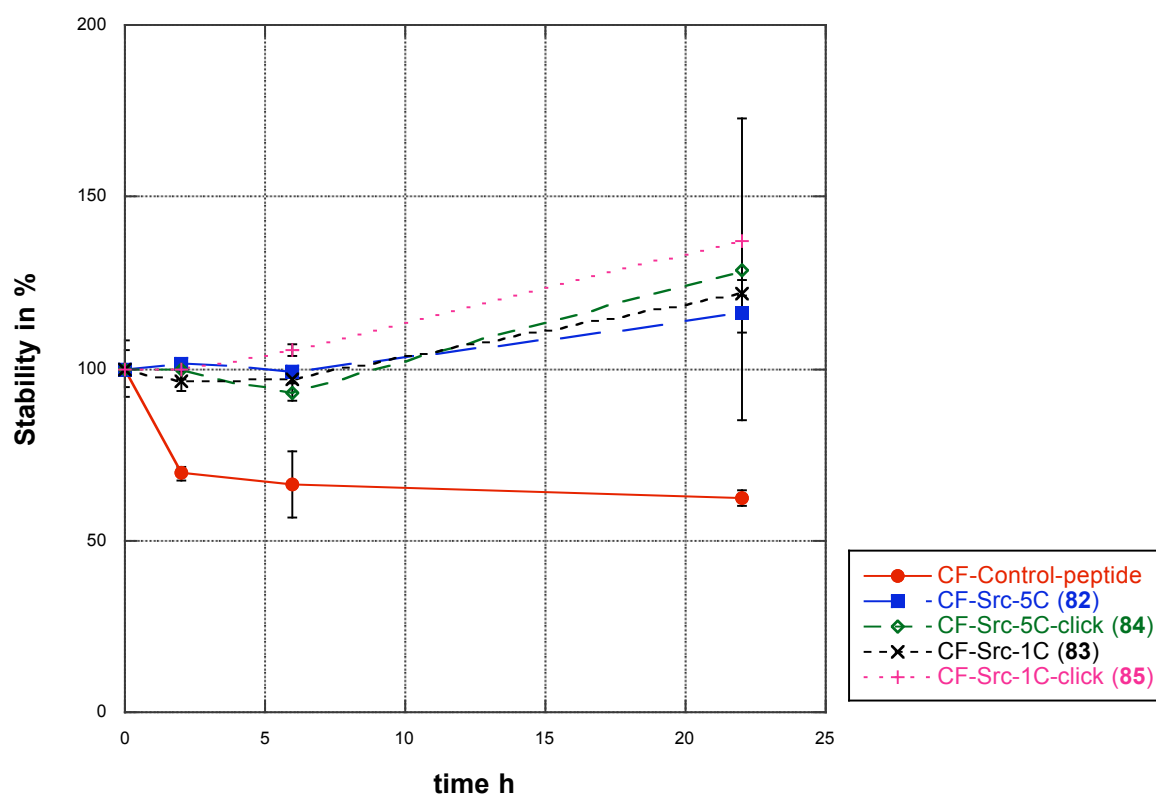


Figure 22: Stability of the linear linker-containing and cyclic peptides in U2OS cell lysate compared to a control peptide, composed solely of canonical amino acids.

In another experiment the stability of the two cyclic peptides **84** (K(CF)-Src-5C) and **85** (K(CF)-Src-1C) in human serum was compared to the fluorescein labeled and F₂Pmp-containing Src sequence without the linker moieties (**86**; CF-Src). Also in this experiment all three F₂Pmp containing peptides are strikingly stable over the entire time course (Graph 3.5.2 A). This indicated that rather the F₂Pmp group than the linker moieties is responsible for the increased stability.

This hypothesis was further supported when the stability of the CF-Src peptide **86** in human serum was compared to the fluorescein labeled Src sequence which contained a tyrosine instead of F₂Pmp **93** (CF-Src-(Y)) and a fluorescein labeled control sequence which contained only naturally occurring amino acids (CF-Control-peptide). Since the F₂Pmp-containing peptide was the most stable one in this experiment. The peptide bearing the tyrosine instead of F₂Pmp was less stable, but not as strongly degraded as the control peptide, which suggested that also the sequence derived from the Src kinase itself could contribute in part to a high proteolytic stability of the tested peptides.

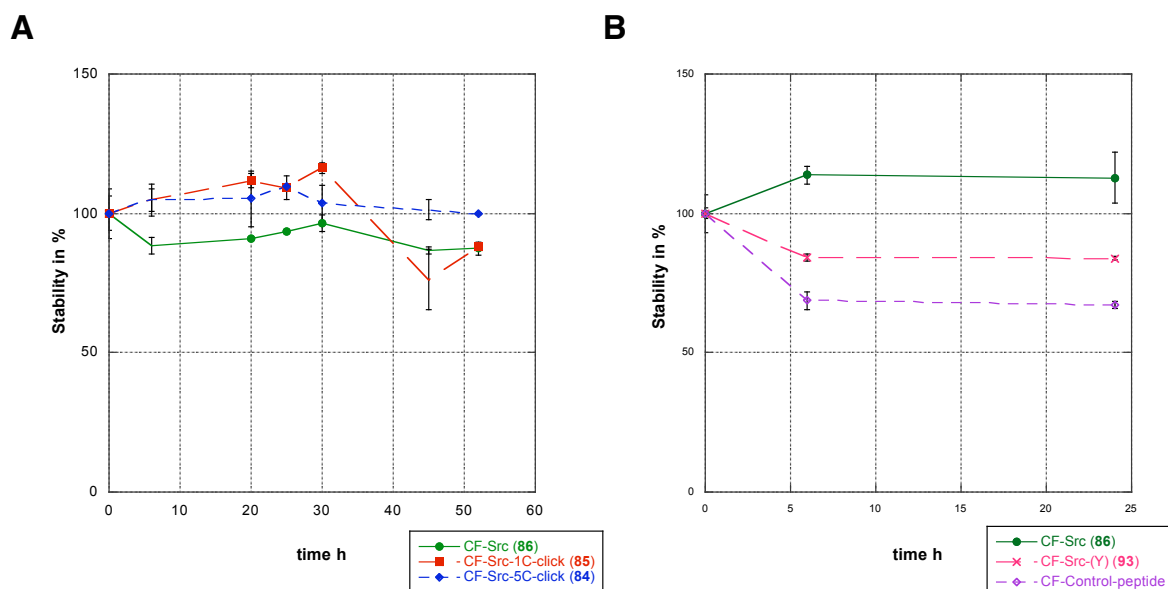


Figure 23: Stability of the linear Src sequence without linker moieties in human serum compared to the cyclic peptides (**A**) and the linear Src sequence with F₂Pmp exchanged to tyrosine or a control peptide composed solely of canonical amino acids (**B**).

3.6 Biotinylated F₂Pmp containing peptides as pull-down tools

Despite their high affinity to PTP1B, F₂Pmp containing peptides have not been used to isolate the enzyme from a complex biological sample such as a cell lysate. However, it has been demonstrated that the phosphatase SHP-1 shows enhanced binding to the adaptor protein Grb-2, when semisynthetic versions of the phosphatase were used, which contained either Pmp or F₂Pmp in positions 536 or 564 instead of tyrosine, thereby mimicking the natural phosphorylation at these sites.²²¹ The non-hydrolyzable pTyr mimetics were introduced by expressed protein ligation and the pull down experiments were performed with GST-Grb2 immobilized on glutathione-agarose and incubation with the semisynthetic proteins. Higher pull down efficiency of the phosphorylated proteins proved the interaction of phosphorylated SHP-1 with Grb-2 and that this principle can indeed be applied for pull down experiments.

Therefore, biotinylated versions of the F₂Pmp containing peptides were synthesized and tested for their efficiency to pull down PTP1B when bound to streptavidin-sepharose, a principle widely used in biochemistry.²²² Successful enrichment of PTP1B could potentially be used for the isolation of endogenously produced and posttranslationally modified protein from mammalian cells without the need of overexpression and tagging or for the simultaneous identification of allosteric binding partners. Especially, the highly affine but non-covalent nature of the interaction of F₂Pmp containing peptides with phosphatases could potentially be exploited to isolate the native protein, in contrast to the activity based probes introduced in chapter 1.6, which covalently modify the enzyme.^{133–137}

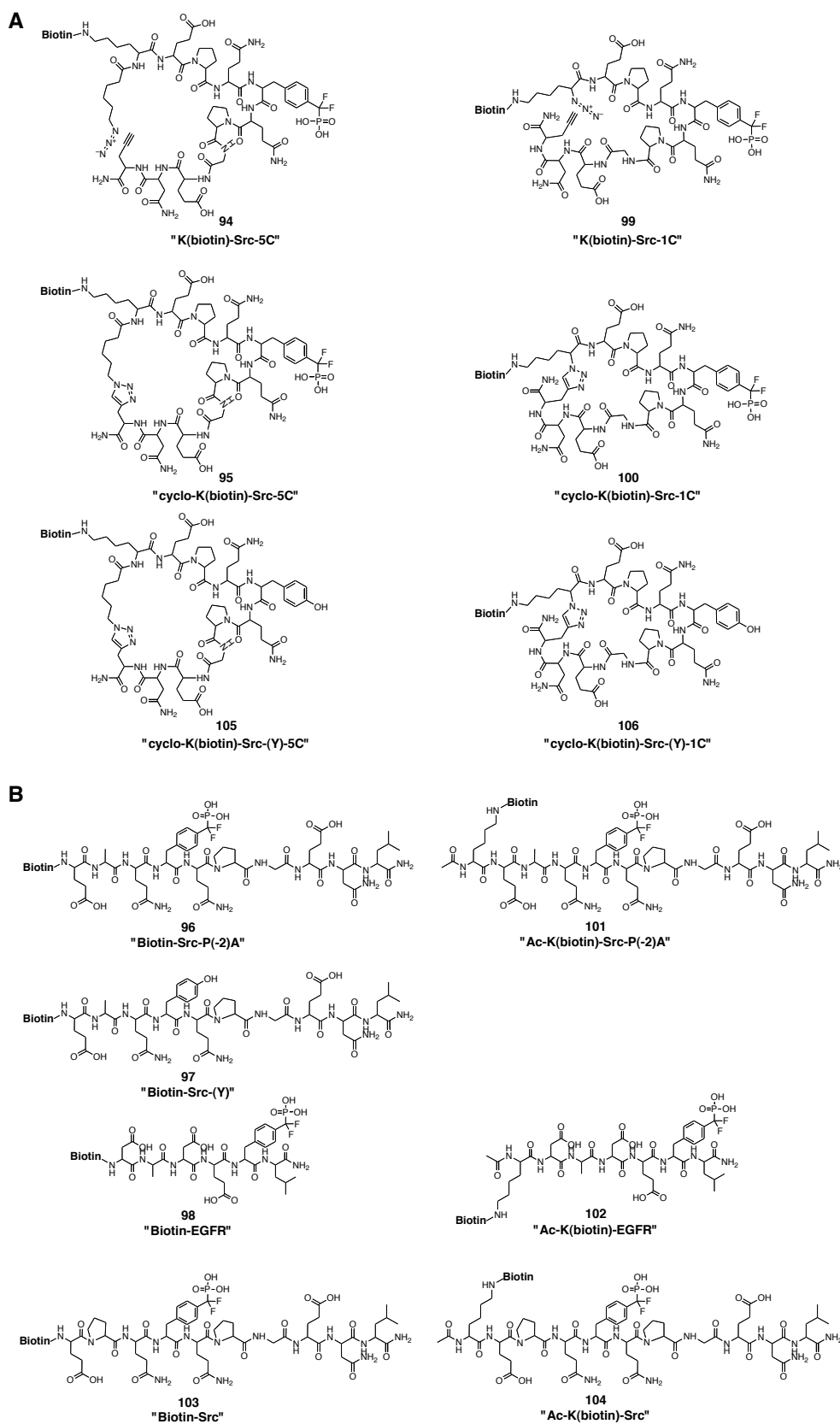


Figure 24: Cyclic (A) and linear (B) biotinylated peptides used for the pull down experiments.

Initially, the biotinylated F₂Pmp containing Src sequences with the 5-carbon linker before (**94**; K(biotin)-Src-5C) and after the cyclization reaction (**95**; cyclo-K(biotin)-Src-5C), the proline to alanine in the -2 position substituted peptide (**96**; Biotin-Src-P(-2)A), the F₂Pmp exchanged to Y peptide (**97**; Biotin-Src-(Y)) and the biotinylated EGFR sequence peptide (**98**; Biotin-EGFR) were synthesized (Figure 24). To the N-termini of the linear and no-linker-containing sequences (**96**, **97** and **98**), the biotin group was coupled directly using biotin, HATU, HOAt and DIPEA in NMP (Figure 24). Coupling was performed twice for at least 2 hours each. Similar to the fluorescein labeled peptides, sequences with an N-terminal linker (**94** and **95**) were equipped with an additional Mtt protected lysine at the N-terminus. After selective removal of Mtt with 1.8% TFA in DCM, the biotin group was coupled to the free side chain amine in the same manner as described above (Figure 24).

The biotinylated peptides were immobilized on streptavidin-sepharose (GE healthcare) by incubation of 30 μ L streptavidine bead medium (binding capacity biotin > 300 nmol/ml medium) with 400 μ L of the respective peptide in a 50 μ M concentration in washing buffer (50 mM Tris-HCl, pH 7.5, 125 mM NaCl, 5% Glycerol, 1.5 mM MgCl₂) over night at 4°C. The beads were washed before twice with 400 μ L washing buffer. The preloaded beads were incubated for 2 hours at 4°C either with recombinant PTP1B or lysates of U2OS, Hela Kyoto or HEK 293 cells (Figure 25). After 3 washing steps, the proteins were boiled off the beads and subjected to SDS-PAGE. Western blotting with PTP1B antibody FG6-1G (Calbiochem, La Jolla, USA) revealed that in all tested systems peptide **95** (cyclo-K(biotin)-Src-5C) was the most efficient in pulling down PTP1B, followed by its linear precursor **94** (K(biotin)-Src-5C). As expected, no signal was observed for the negative controls, peptide **97** (Biotin-Src-(Y)) and the “No peptide” control. However, no signal was detected also for the linear F₂Pmp containing sequences **96** (Biotin-Src-P(-2)A) and **98** (Biotin-EGFR), which was rather unexpected, since the fluorescence polarization experiments (Figure 18) showed that the linear peptides were binding stronger to PTP1B than the peptides containing the linker.

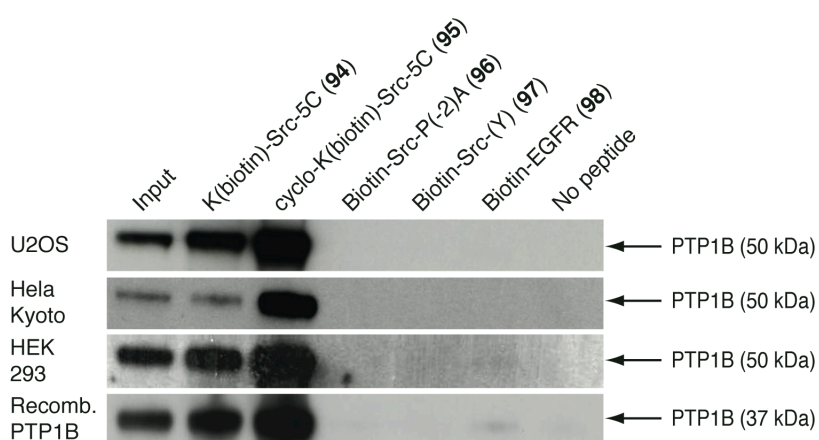


Figure 25: Comparison of the pull down efficiency of several biotinylated peptides of endogenous PTP1B in U2OS, Hela Kyoto and HEK 293 cell lysates and recombinant protein.

Based on these results more peptides were tested in pull down experiments from U2OS cell lysates (Figure 26). To find out if cyclization in general improves the pull down efficiency also the respective 1-carbon linker peptides before (**99**; K(biotin)-Src-1C) and after cyclization (**100**; cyclo-K(biotin)-Src-1C) were synthesized by introducing the biotin moiety to an additional N-terminal lysine, similarly to the 5-carbon linked peptides, and converting the amine group of this lysine into an azide using the method described in chapter 3.3.2 (Figure 24).

As mentioned before, the poor performance of the linear peptides in comparison to the cyclic and non-cyclic 5-carbon linked peptides was unexpected due to the stronger binding of the linear peptides in the FP assay. A difference amongst these peptides, which could have contributed to this, was the different way of attaching the biotin (N-terminal amine versus lysine side chain amine). Therefore, the Src-P(-2)A and EGFR peptides were synthesized also with an additional N-terminal lysine, in which the N-terminal amine group was acetylated and the biotin was attached to the amine group in the side chain, leading to the peptides **101** (Ac-K(biotin)-Src-P(-2)A) and **102** (Ac-K(biotin)-EGFR). Additionally, the wild type F₂Pmp containing Src sequences with biotin at the N-terminus (**103**; Biotin-Src) and in the lysine side chain (**104**; Ac-K(biotin)-Src) were synthesized accordingly (Figure 24). The peptides **105** (cyclo-K(biotin)-Src-(Y)-5C) and **106** (cyclo-K(biotin)-Src-(Y)-1C), which contain the 5- or 1-carbon linker but not F₂Pmp were synthesized and tested, to investigate whether cyclization per se, without contribution of the F₂Pmp group, enhances pull down efficiency.

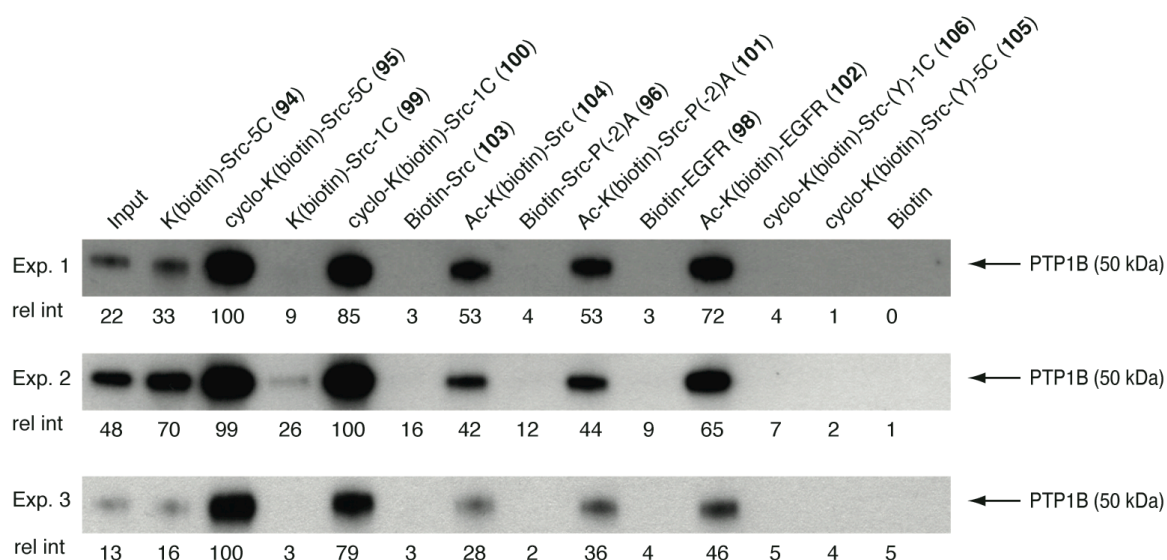


Figure 26: Results of three independent pull-down experiments of endogenous PTP1B from U2OS cell lysate using several biotinylated peptides. Note that the two cyclopeptides containing F₂Pmp (cyclo-K(biotin)-Src-5C and cyclo-K(biotin)-Src-1C) show the highest efficiency.

The individual pull down experiments showed in general good reproducibility of relative signal intensities (Figure 26). Also in these experiments the cyclized peptides **95** and **100** were pulling down PTP1B with the highest efficiency, whereby the 5-carbon linked peptide **95** performed best overall. Both non-cyclized linker-containing peptides **94** and **99** were performing worse than their cyclic counterparts, thereby proving again the benefit of the ring closure for pull down performance, with the 5-carbon linked **95** being more efficient compared to the 1-carbon linked peptide **100**.

Cyclization alone, as shown with the cyclic peptides **105** and **106**, which do not contain F₂Pmp, the most important residue for phosphatase binding, did not create peptides capable of pulling down PTP1B and no signal in these two lanes as well as in the biotin control was observed.

For the linear peptides without a hydrocarbon linker, a striking difference between biotinylation at the N-terminus to biotin attachment in the lysine side chain was observed. The peptides with the biotin in the side chain (**101**, **102** and **104**) pulled down PTP1B, whereas no signal was observed with the N-terminal biotinylated peptides (**96**, **98** and **103**), as in the initial pull-down experiments.

The sequences of the peptides **104** (Ac-K(biotin)-Src) and **101** (Ac-K(biotin)-Src-P(-2)A) differ in the exchange of the proline in -2 position of the original Src sequence to alanine. A slight difference can be seen in their pull down efficiency (Figure 26), which reflects the higher affinity of the Src-P(-2)A version observed in the pNPP and FP assays (chapter 3.4.1). However, when all the linear peptides biotinylated in the lysine side chain (**101**, **102** and **104**) were compared it was found that the EGFR sequence **102** performs best in the pull-down, which is in clear contradiction to the observed binding affinities in the FP assay, where the Src-P(-2)A sequence was the best binder. This demonstrated that the difference in affinity of the peptides to the phosphatase was not sufficient to explain their relative pull down efficiencies. Also, the higher pull down efficiency of the cyclic peptides **95** and **100** compared to the linear Src sequence **104** was contradictory to the observed binding affinities in FP assay (Figure 18) in the same manner.

To investigate further the influence of binding affinity on pull down efficiency, peptides **107** (Ac-K(CF)-Src), **108** (Ac-K(CF)-Src-P(-2)A) and **109** (Ac-(CF)-EGFR), which bear a 5(6)-carboxyfluorescein molecule in the N-terminal lysine side chain instead of a biotin, were synthesized. These peptides are comparable to the lysine side chain biotinylated versions used in the pull down experiment and their binding affinity to PTP1B was measured and compared to their N-terminal labeled counterparts **80**, **86** and **87** already used in chapter 3.4.3 (Figure 18). The obtained K_d values (Figure 27) showed that the affinities of the N-terminal compared to the lysine side chain labeled peptides were very similar, thus proving that the difference observed in pull-down efficiency were most likely not due to better binding affinities

of the side chain labeled peptides. It seems that rather a better orientation on or loading efficiency to the beads plays a more important role. This could also explain why the side chain labeled EGFR sequence **102** is more efficient than the Src derived sequences **101** and **104**, since in this sequence one additional amino acid residue between the biotin group and the F₂Pmp moiety exists, which could potentially allow better access of the phosphatase to the important F₂Pmp group. This could also be the reason for the better performance of the side chain labeled peptides, in which the peptide potentially adopts a better orientation for protein binding and/or is sterically less hindered, due to the additional spacer provided by the lysine side chain, when loaded to the beads, compared to the N-terminally modified peptides.

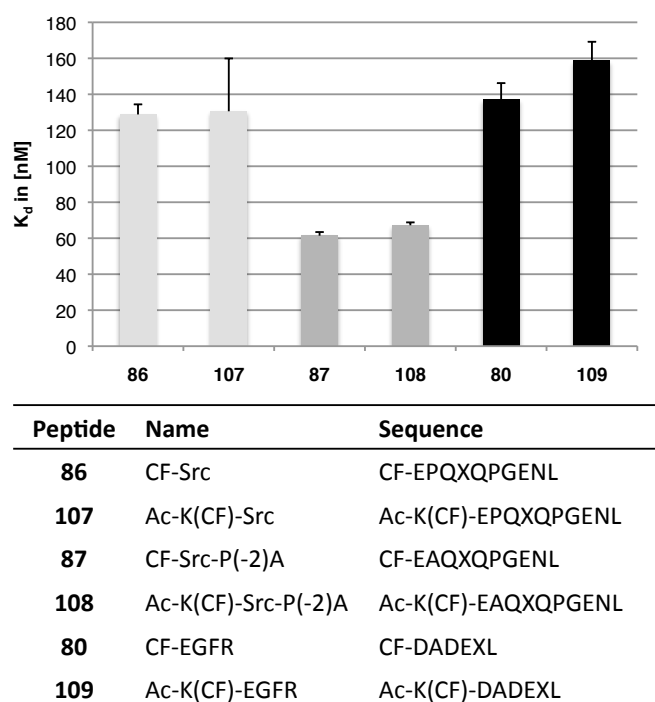


Figure 27: Fluorescence Polarization assay against PTP1B with peptides bearing the fluoresceine moiety either at the N terminus or in the side chain of an N-terminal lysine. The differently labeled peptides with the same sequence show similar binding affinities (X = F₂Pmp).

In order to investigate if a varying loading efficiency of the different peptides to the streptavidin beads influences pull-down efficiency, solutions of the peptides (50 μM) were injected to the HPLC before and after incubation with the beads. Each sample was injected twice, the area under the curves (AUCs) of the peptide peaks were measured and the values of the solutions prior to incubation were normalized to 100%. Reduction of the AUC after incubation with beads indicated depletion of peptide and is an indirect measure of binding efficiency to the beads (Figure 28).

For both linker containing peptides the cyclised versions **95** and **100** showed higher depletion and, therefore, better loading to the beads than the linear versions **94** and **99**, which

correlates well with the higher pull-down efficiency of the cyclic versions compared to their respective linear counterpart. However, if both linker containing linear sequences **94** and **99** were compared amongst each other, the 5-carbon linker containing peptide **94** was loaded less efficient to the beads than the 1-carbon linker peptide **99**, which is in contradiction to the observed differences in pull down efficiencies of these two peptides (Figure 26). Also, both linker-containing linear peptides **94** and **99** were loaded less efficiently than the N-terminal biotinylated Src sequence **103** (Biotin-Src), which is also contradictory, as a very poor pull down efficiency of **103** was observed. The N-terminal biotinylated Src sequence **103** showed in fact the same depletion as the Src sequence with the biotin in the lysine side chain (**104**; Ac-K(biotin)-Src), which was clearly superior in terms of pull-down efficiency compared to **103** (Figure 26).

Therefore, it seems that a better peptide loading to the beads could explain the better performance of the cyclic peptides compared to their linear counterparts or in other words, that cyclization of the peptides went along with a better loading efficiency. However, loading efficiency could not explain the differences in pull down performance between the individual peptide sequences, which indicated that those differences were caused by additional variables as, for example, orientation of the peptides on the beads.

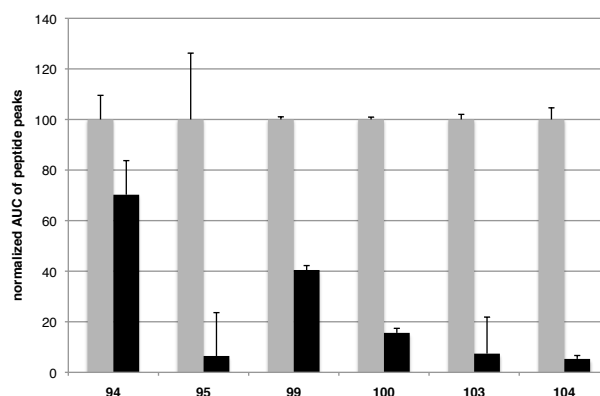


Figure 28: Loading of biotinylated peptides to streptavidin beads, determined by HPLC quantification. The AUC of the peptide in the chromatograms of the loading solution (dark grey) and after the incubation with the beads (black) was compared.

Next, it was investigated if the pull-down efficiency of the biotinylated peptides shows differences when pulling down PTP1B compared to TCPTP. The affinities of the peptide sequences to both phosphatases were not significantly different as seen with fluorescein labeled variants in the FP measurements in chapter 3.4.3. However, as it has been observed that rather orientation and/or loading of the biotinylated peptides to the streptavidin beads affects pull-down efficiency rather than binding affinity, it was tested if the pull down efficiencies differ between the two enzymes, which could also themselves be subject to variations, e.g. through a different orientation or accessibility of their catalytic pocket.

For this purpose, U2OS cells were transfected with a vector containing either EGFP-PTP1B (~65 kDa) or EGFP-TCPTP (~72 kDa) and allowed to grow for another 12 hours. In the case of PTP1B the catalytic domain (AAs 1-321) and for TCPTP the 45 kDa variant were used to create the fusion protein, because both of these variants localize similarly in the cytoplasm, thus, an effect of different subcellular distribution on pull-down efficiency could be minimized. Furthermore, that way both fusion proteins had comparable sizes.

The cells were lysed and the peptides immobilized to streptavidin-sepharose were incubated with either EGFP-PTP1B or EGFP-TCPTP containing cell lysate for 2 hours. The proteins were boiled off the beads and subjected to SDS-PAGE and Western-blotting with anti-GFP antibody, and the signal intensities of the bands were quantified (Figure 29). The relative intensities of the EGFP-PTP1B signals are in line with the pull downs of endogenous PTP1B before, showing that the modification of the protein did not influence the outcome of the experiments.

Relative intensities of the different EGFP-TCPTP signals were also very similar to those observed with endogenous PTP1B or EGFP-PTP1B (Figure 29). Solely, the signal of the pull-down by peptide **102** (Ac-K(biotin)-EGFR) was consistently higher in the EGFP-TCPTP pull-down relatively to the other signals compared in the EGFP-PTP1B pull-down, indicating that the EGFR derived sequence co-precipitates TCPTP better than the Src derived sequences. When the relative intensities of the cyclic (**95** and **100**) and linear linker-containing peptides (**94** and **99**) were compared, it could be seen that the cyclization leads to a 1.3-fold (**94** compared to **95**) or a 2-fold (**99** compared to **100**) enhancement in the EGFP-PTP1B pull-down, whereas in the EGFP-TCPTP pull down the enhancement was 3.8-fold (**94** compared to **95**) or 4.4-fold (**99** compared to **100**), respectively. This relative better performance of the cyclic versions (**95** and **100**) compared to the linear precursors (**94** and **99**) in the EGFP-TCPTP pull-down was not consistently observed in repetition experiments and was most likely caused by a saturation of the high signals of the cyclic peptides (**95** and **100**) in the EGFP-PTP1B pull down.

A selective pull-down of PTP1B in the presence of TCPTP, however, could not be expected, since all peptides, which co-precipitate PTP1B efficiently also pull-down TCPTP. Although both enzymes are expressed ubiquitously, their relative expression levels may vary from cell type to cell type. In cells or tissues where one of the phosphatases is expressed at a much higher level than the other, the use of these F₂Pmp containing peptides, especially peptide **95** (cyclo-K(biotin)-Src-5C), may enable a selective pull down of the higher abundant protein.

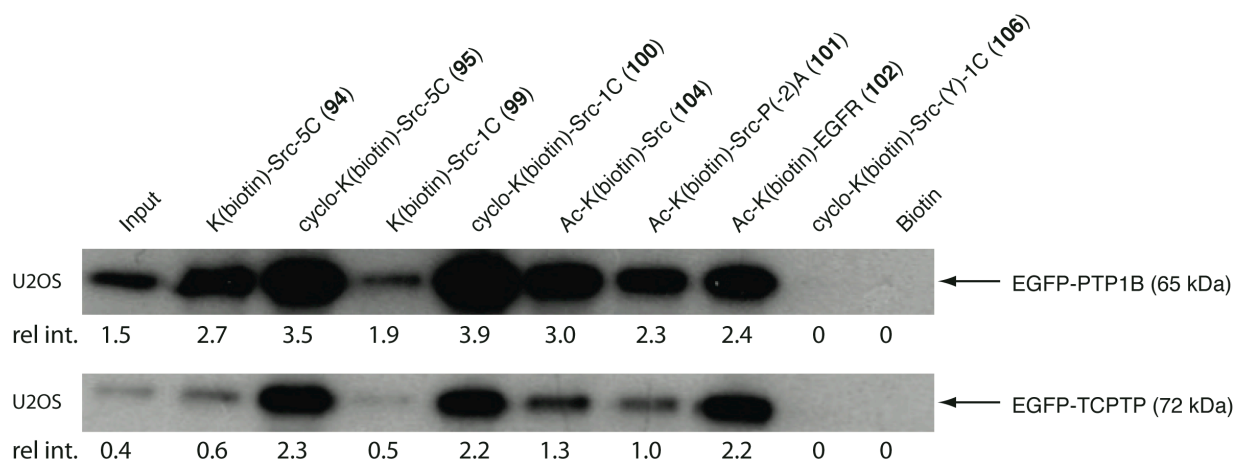


Figure 29: Comparison of relative pull-down efficiency of transiently overexpressed EGFP-PTP1B and EGFP-TCPTP in U2OS cells with several biotinylated peptides. EGFP antibody was used for detection on the western blot in both cases.

Interestingly, the silver stain of a pull-down from U2OS cell lysate using peptide **95** (cyclo-K(biotin)-Src-5C) showed only 2 signals under 100 kDa, which both stained for a specific PTP1B antibody (FG6-1G) and corresponded in their size to full length PTP1B (50 kDa) and the shorter version (42 kDa) potentially generated by calpain cleavage (Figure 30). In the control lane, where beads without a peptide loaded were used in the pull-down experiment, several bands were visible in the silver stain, but none of them stained for the PTP1B antibody. The antibody was tested for specificity against TCPTP and detected PTP1B selectively when the recombinantly produced catalytic domains of both enzymes were blotted on nitrocellulose. Hence, endogenous PTP1B could be immunoprecipitated very cleanly from U2OS cell lysates. Since peptide **95** was shown to indiscriminately co-precipitate also TCPTP, it seems likely that the protein was not, or only at very low levels, expressed in these cells. However, this needs to be addressed in future experiments.

Another band in the western blot at around 100 kDa is most likely a PTP1B dimer. Whether or not the smeared band at 225 kDa visible in the silver stain was also due to multimers or a different protein, potentially co-precipitated with PTP1B, has not yet been addressed experimentally.

Notably, peptide **95** (cyclo-K(biotin)-Src-5C) proved to effectively co-precipitate its target protein PTP1B and could be used to isolate the enzyme at endogenous levels for subsequent analysis of activity, posttranslational modifications or allosteric interaction partners.

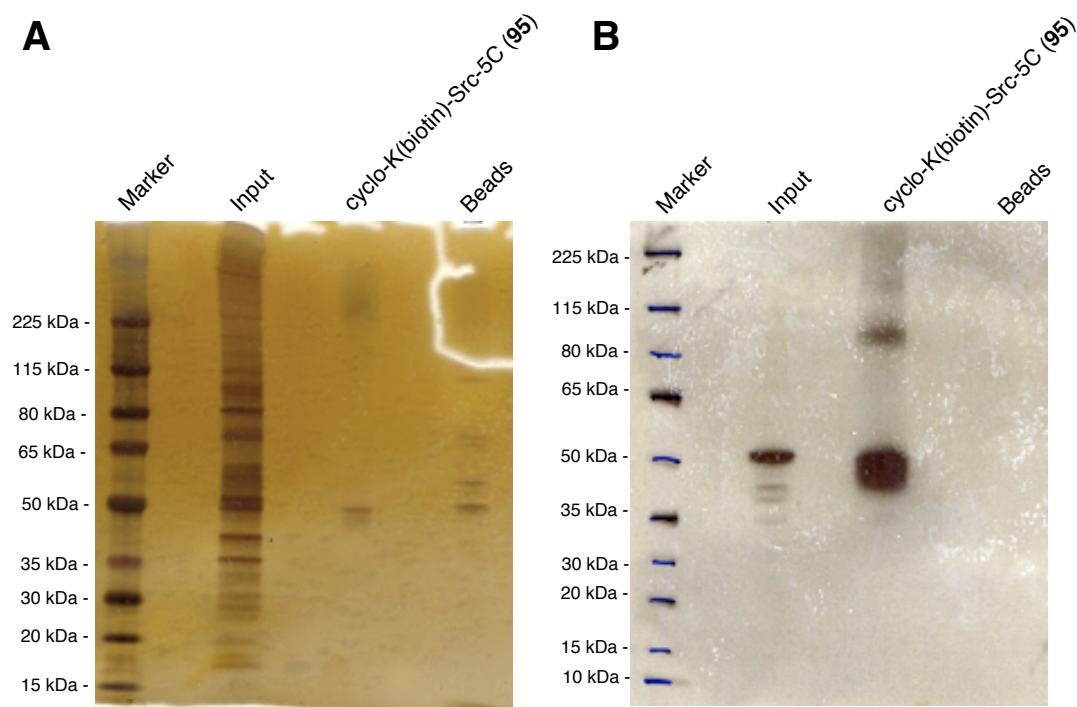


Figure 30: Pull-down from U2OS cell lysates with peptides cyclo-K(biotin)-Src-5C bound to streptavidine beads in a silver stain (A) or western blot (B) with PTP1B antibody FG6-1G.

4 Discussion

4.1 Selection of a substrate sequence for further inhibitor development

PTP1B is a very active phosphatase against multiple tyrosine phosphorylated peptides *in vitro*.^{56,112–115} Although this is pointing to the fact that PTP1B activity is unspecific for the substrate sequence around the phosphotyrosine, many studies involving combinatorial libraries or selections of naturally occurring phosphopeptides showed preferences of the enzyme for amino acids with certain characteristics at distinctive sites.^{56,112–115} The report about acidic residues at the -2 and aromatic residues at the -1 position is strikingly consistent, whereas reports about preferred positions at the C-terminal end are more controversial. Consensus sequences representing the by far optimal recognition site for the enzyme could not be detected and, therefore, are likely to not exist at least not in the sense of simple linear motifs.¹¹⁵ Furthermore, preferred motifs reported by combinatorial studies are often unrelated to natural substrate sequences.

Taken together, these studies imply that optimization of the amino acid sequence around the phosphorylated site can modulate potency and selectivity of a non-hydrolyzable inhibitor, since the surrounding residues are clearly involved in binding. However, this modulation should be regarded in the sense of a “fine-tuning” since the phosphatase can recognize a large variety of phosphorylated peptides.

In this work, it was anticipated to perform the inhibitor development on the basis of a natural substrate sequence. In this regard it can be seen as a model study with the “prototypic” PTP1B and its strategy being potentially applicable also to other members of the PTP family dephosphorylating tyrosine phosphorylated substrates. Therefore, phosphopeptides derived from four different literature known substrates were synthesized and tested against PTP1B and TCPTP. Two of the selected substrates were known to be physiological targets of both enzymes (IRK, EGFR), whereas the other two sequences (Jak2, Src) were reported substrates for PTP1B only.^{56,58,59,61,62,66,67,78,92,93,139–161} The doubly phosphorylated site of Jak2 was synthesized in different lengths (7 mer, 10 mer, 13 mer and 17 mer) to determine if increasing the length of a substrate peptide would be beneficial for the potency of the inhibitor (peptides **26** – **29**). The influence of peptide length in this context had not been studied in detail thus far. Additionally, peptide **34** containing only non charged amino acids (Ala, Ser, Gly) at physiological pH was designed with the notion that PTP1B prefers acidic residues around the pTyr and needs them for efficient binding and, therefore, should represent a weak binding sequence.

Indeed, the rationally designed non-substrate (“random”) sequence **34** performed worst in the dephosphorylation assay. Similar sequences were detected as weak substrates in an on-bead screening of a combinatorial phosphopeptide library.¹¹⁶ The difference to the best performing sequence was in the case of PTP1B about 6fold. The K_M values of the 7 (**31**) and 10 mer (**32**) IRK sequences (5.3 ± 0.98 and $6.2 \pm 0.5 \mu\text{M}$) compare very well to the value obtained by *Salmeen et al.* when measuring the K_M of the triple phosphorylated IRK peptide (RDIpYETDpYpYRKGGKGLL) against PTP1B ($7.5 \pm 1.9 \mu\text{M}$).⁵⁸ As expected, TCPTP showed comparative activity against the IRK peptides since both enzymes share a high degree of sequence similarity in the active site and have both been reported as IRK dephosphorylating enzymes.⁶⁶ However, activity of the phosphatase against the four Jak2 (**26-29**) sequences, which was reported to be a substrate for PTP1B but not for TCPTP, also did not show significant selectivity for PTP1B. Also, increasing the length of the peptide derived from this substrate did not show a benefit for activity or selectivity conclusively.

The doubly phosphorylated sequences performed collectively better than the monophosphorylated sequences from the EGFR (**33**) or the Src kinase (**30**). It could be argued that the malachite green assay cannot distinguish whether the enzymes dephosphorylated both phosphate groups in this sequences and that the better performance is dependent on this. However, it has been convincingly described that PTP1B selectively targets the C-terminal pTyr in the double phosphorylated IRK sequence. Furthermore, the better performance could also be explained by the preference of PTP1B for aromatic residues in the -1 position, described by several groups.^{58,115}

In the case of the monophosphorylated sequences the EGFR was known to be a substrate of both phosphatases, whereas c-Src was only reported as a PTP1B substrate and this fact seemed to be reflected in the selectivity in this data set. As the EGFR sequence (**33**) is preferentially the better substrate for TCPTP, PTP1B is performing better in case of the Src sequence (**30**). Furthermore, the K_M of PTP1B for the Src sequence ($14.5 \mu\text{M}$) is 2-fold better than for the random sequence, whereas TCPTP is dephosphorylating both equally well. This notion and the fact that it would be even more challenging to render a double phosphorylated peptide cell permeable, which would be the case if one of the Jak2 or IRK sequences would have been chosen, led to the decision to use the Src derived peptide **30** for the inhibitor development. As this study represents the first detailed analysis of this sequence used for the generation and characterization of a peptide base PTP1B inhibitor, its characteristics were compared to the literature known EGFR sequence throughout this work.

In summary, the above described possible “fine-tuning” of the peptide sequence surrounding the pTyr to enhance potency of the peptide could be confirmed in this part of the work.

4.2 Efficient synthesis of N-Fmoc-F₂Pmp and its incorporation into peptides

Since the non-hydrolyzable pTyr mimetic N-Fmoc-L-F₂Pmp-OH (**39**) was not commercially available and substantial amounts were needed for the optimization of the inhibitory peptide, existing synthetic strategies were evaluated and further optimized to gain efficient access to gram amounts of the building block.

Therefore, all reported synthetic schemes that required many steps, were low yielding or required hazardous reagents were excluded.^{117,168,170–174}

On the basis of the strategy reported by *Qabar et al.*, a synthetic scheme could be devised, which fulfilled the necessary requirements (Scheme 1).¹⁶⁹ Especially, the choice of the TMSE protecting group for the carboxyl group of the starting material N-Fmoc-L-4-I-Phe-OH (**37**) proved to be beneficial to earlier strategies, since this group coupled extremely well and no purification before the CuBr promoted coupling of diethyl phosphonodifluoromethyl-CdBr (**41**) building block was necessary, which was performed as described.¹⁶⁹ Furthermore, the mild acidic cleavage conditions and volatility of the TMSE group facilitated to proceed directly after evaporation with the hydrolysis of the diethyl esters using TMSBr. Simple repetition of the TMSBr cleavage yielded the final product **39** in high purity (> 90 %), so that a final purification was not required, even on a multi-gram scale.

Therefore, the N-Fmoc-L-F₂Pmp-OH (**39**) building block can be synthesized in gram scale with only one purification step required after coupling of the diethyl phosphonodifluoromethyl group.

This building block can be directly used for the synthesis of F₂Pmp containing peptides and no protection of the phosphonic acid groups is required, excluding the risk for sequence specific side reactions which could occur under the harsh deprotection conditions required for diethyl phosphonic acid esters.^{168,169}

4.3 Cyclization of the inhibitory peptide

Cyclization of the identified peptide sequence was desired to study if ring closure could improve cell membrane permeation and stability of the peptide. Although cyclic peptides containing different non-hydrolyzable pTyr mimetics had been synthesized and beneficial properties of these molecules were postulated, a detailed analysis remained elusive.^{109,199}

After unsuccessful attempts to perform the ring-closure via the thiol-ene reaction, (Schemes 3 and 4), the potential of the copper (I) catalyzed azide-alkyne 1,3-dipolar cycloaddition, representing another bioorthogonal click reaction, was explored.^{187–191,194,223} Using this reaction, which is highly regioselective for the 1,4-disubstituted 1,2,3-triazole under

the conditions described by Sharpless, two head-to-side chain cyclized variants of the Src sequence with different linker lengths peptide **59** (“cyclo-Src-5C”) and **60** (“cyclo-Src-1C”) could be synthesized in solution (Scheme 6).²²³ HPLC and MS (MALDI) analysis was used, as described in the literature to confirm the purified cyclic products to be monomeric.^{192,198} It was chosen to perform the ring closure in solution since the generation of monomeric cycles was anticipated and the reaction was expected to be easier to control in this respect rather than on solid phase as interpreted from the experience of other groups.^{192,198}

For the synthesis of the azide group in the one carbon linker precursor peptide **58**, the mild and efficient transformation of an amine group with imidazole-1-sulfonyl-azide hydrochloride was chosen (Scheme 5), which had previously been described for this kind of reactions in solution.²⁰⁴ Slight modifications of the protocol described by *Goddard-Borger et al.* enabled efficient transformation of the N-terminal amine groups to the azide, and, thus, the described conditions show potential for a general usage in amine to azide transformation on solid support.

As described by two groups independently, the biocompatible cycloaddition reaction takes also place between two fragments that bind to the same protein even without the need of addition of copper, when the azide and alkyne groups are aligned closely enough in space.^{200,201} In this type of so-called “target-guided synthesis” the targeted enzyme, instead of copper (I), acts as the catalyst needed to drive the reaction, which is otherwise very slow at room temperature. Therefore, the cyclization reaction with the different linear precursor peptides was also tried by incubation of the peptides with PTP1B, but without the addition of copper. Whereas joining of fragments to generate a good binder/inhibitor was successfully performed before, a target-guided cyclization of a peptide inhibitor to generate a macrocyclic version with improved characteristics was not described. However, cyclization could not be observed with both peptides upon incubation with the enzyme (Figure 13). This could implicate that either the linker groups are too long and flexible or that the cycles formed do not possess the optimal configuration for binding to the phosphatase. Both possible reasons could provide an explanation for the failure of the cyclization trials via the thiol-ene reaction, since this reaction is dependent on spontaneous contacts of the functional groups by diffusion, which is potentially limited by the intrinsic configuration provided by the peptide.

4.4 Analysis and binding studies of Src derived linear and cyclic sequences

Comparison of the influence of substitution or truncation of residues of the Src sequence on the IC₅₀ values of the resulting peptides can give valuable information about its binding mode (Figure 31 (A)).

The strongest loss in potency in the alanine scan was observed when the glutamine at the +1 position was replaced. Consistently, it has been reported that residues directly adjacent to the dephosphorylation site are predominantly involved in binding. However, the biggest influence in this respect was expected to be exhibited from the N-terminally located -1 position, because residues at this site were described to bind the secondary binding site of the enzyme, but the replacement of the residue in this position only modestly changed inhibitory potency.^{57,58} A possible explanation for this discrepancy could be deduced from the increase in binding upon exchange of the proline at the -2 position. It may be speculated that this proline prohibited binding of the glutamine at -1 in the original peptide caused by its structural rigidity and/or different dihedral backbone angle. Exchange of the proline for the more flexible alanine residue could allow the glutamine to bind to the secondary site, which could explain the only modest change upon replacement of the glutamine and the strong increase in binding upon exchange of the proline. This hypothesis is supported by the fact that replacement of this proline leads to a slight preference of the peptide to PTP1B in comparison to TCPTP, which is in line with the notion that binding to the secondary site can confer selectivity between these two phosphatases.⁵⁷

Furthermore, exchange of positions +2, +3 and -3 was either slightly increasing or only very modestly decreasing the inhibitory potency, which could make them interesting positions for attachment of linker groups in future efforts to optimize the configuration of cyclic variants. Interestingly, two of the very C-terminal residues (+5 N and +4 E) seemed to contribute to binding of the sequence since their replacement decreased potency. This suggests additional interactions of the C-terminal part of the peptide with the enzyme further away from the catalytic pocket, a fact that had only been poorly described in the literature.

The results from the truncation scan (Figure 31 **(B)**) showed that the inhibitory potency was strongly impaired (~9fold) if only two adjacent residues on either site of the F₂Pmp were left and modestly decreased if two residues were surrounding this site. Stepwise truncation of the C terminus revealed that deletion of the glutamate at the +4 position led to ~2fold drop of inhibitory potency. These results suggested additionally that at least three residues on either site of F₂Pmp and the glutamate at position +4 are involved in binding of the Src sequence. Furthermore, the modest change of inhibitory potency by replacement or truncation of the C-terminal leucine points to the fact that it is not involved in binding of the peptide to the enzyme and could provide an explanation why further elongation of the peptide sequences, as it was performed with the Jak2 peptides (**26-29**) (Figure 8), seems not to improve the interaction.

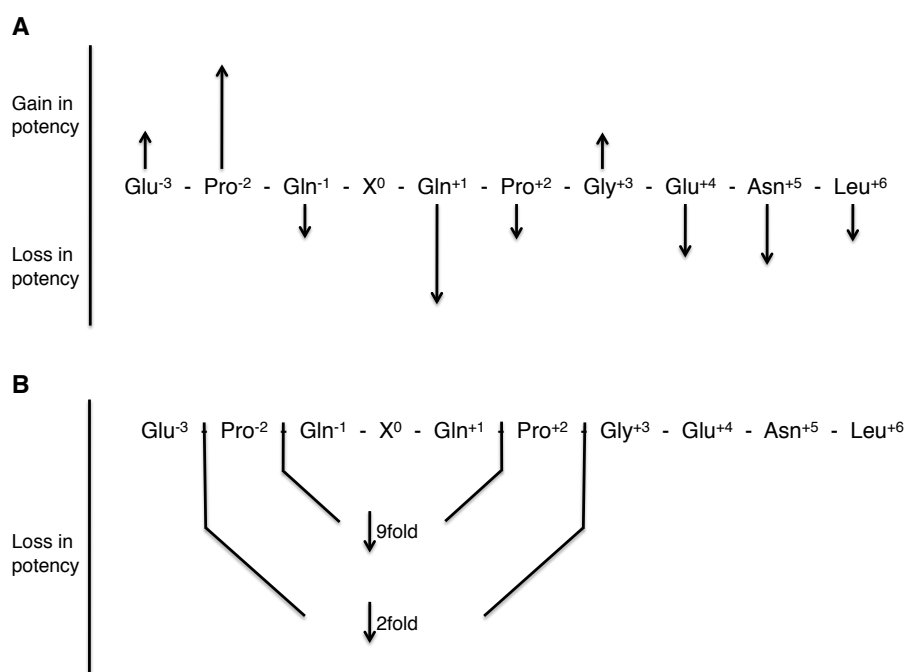


Figure 31: Visualization of alanine and truncation scan data. Relative change in inhibitory potency against PTP1B of the peptides derived from the alanine scan (**A**). Loss in potency against PTP1B upon truncation of the Src sequence (**B**). (X = F₂Pmp)

Also, the IC₅₀ values of the F₂Pmp containing Src (**61**), Src-5C (**57**), cyclo-Src-5C (**59**), Src-1C (**58**), cyclo-Src-1C (**60**), the EGFR (**44**), the random (**45**) and the Src-P(-2)A (**69**) sequence were compared. As expected from the dephosphorylation experiments, the EGFR sequence (**44**) showed very similar potency in inhibiting PTP1B as the Src derived sequence (**61**). However, a better selectivity towards PTP1B of the Src sequence (**61**) compared to TCPTP could not be observed. The random sequence (**45**) performed, consistent with the dephosphorylation experiments, worst. Its inhibitory potency was 6-fold less than the one of the Src sequence (**61**) reflecting the contribution of the F₂Pmp surrounding residues to binding of the peptide. The linker containing sequences (**57** and **58**) were performing both better than the original Src sequence (**61**), but not as good as the Src-P(-2)A peptide (**69**), discovered in the alanine scan. Cyclization of the linker containing sequences did not dramatically change the potency of the linker containing peptides, showing that cyclization did not hamper binding or inhibition. At the same time, cyclization did not improve the inhibitory potency dramatically, which was not fully unexpected regarding the failure of the *in situ* cyclization trials.

As mentioned earlier in this work, IC₅₀ values are dependent on many experimental factors, like enzyme, substrate and inhibitor concentration and are therefore often not suited for

comparison of absolute values with literature data, since the conditions used are varying or even not reported. Therefore, fluorescein labeled variants of the same sequences were used to determine their K_d values in a fluorescence polarization experiment. This value is, like the K_i , independent on enzyme concentration and could be used to compare the potency of these sequences with K_i values of literature known F_2Pmp containing peptides, as outlined in section 3.4. Advantageously, less inhibitor and material in general is required for the FP assay than for measuring K_i values with a competition assay and more peptides can be tested in the same microtiter plate, thereby reducing experimental variations.

Relative binding/inhibition strengths on the other hand can be very well compared especially if the same chemical entity, as in the case of this work is F_2Pmp , is responsible for the majority of the inhibitory potency/binding strength. The relative differences of the values obtained by the FP assay were very similar to the results obtained in the inhibition assay with the original Src **86** and EGFR sequence **80** showing comparable binding in the nanomolar range (128.8 ± 5.6 nM and 137.1 ± 9.1 nM). The IC_{50} value reported by Burke and coworkers for the F_2Pmp containing EGFR sequence against PTP1B, which was determined in a dephosphorylation experiment of autophosphorylated insulin receptor and already mentioned in chapter 3.4 lies in a very similar range ($0.2 \mu M$) than the K_d obtained by the FP assay.¹⁰⁴ The absolute value of determined by the pNPP assay, however was a factor of 10 higher. This may implicate that indeed a different substrate concentration/substrate affinity is the reason for the divergence in the IC_{50} values, whereas the substrate concentration independent K_d value is very similar to the reported literature data.

Seven to eight fold less strong was the binding of the random sequence (**81**), whereas the Src-P(-2)A (**87**) was the best binding sequence with an K_d of 61.4 ± 2.0 nM, which is in the same range as other (small molecule) PTP1B inhibitors targeting the active site with one non-hydrolyzable group, but somewhat less potent than the two-site binder (compound **13**) developed by the Zhang group ($K_i = 2.4$ nM).¹¹⁷ Also, the modest selectivity against TCPTP observed in the inhibition assay could not be confirmed in this experiment. Cyclization of the linker containing sequences did not show improvement, but also not decrease of binding strength as in the inhibition assay. Interestingly, all linker containing and cyclic fluorophore labeled variants (**82**, **83**, **84** and **85**) seemed to prefer slightly PTP1B over TCPTP by trend, however, this difference was not statistically significant. Overall binding affinities of all linker containing peptides (**82**, **83**, **84** and **85**) was decreased relative to the Src sequence (**86**) in contrast to the inhibition assay. This could be an artefact of the FP assay as all linker containing sequences bear the fluorophore molecule in the side chain of a lysine residue due to the N-terminal modification to the azide, whereas in the sequences without linker the fluorescein is attached to the N-terminus. This different localization of the fluorophore molecule might cause a subtle difference in binding or the read-out as the attachment to the lysine side-chain allows greater flexibility of the fluorophore.

Using the fluorescence polarization setup also the dual specificity phosphatase VHR was screened against the same panel of sequences, but no binding was observed in the concentration range tested (up to 10 μ M protein). Consistent with this, F₂Pmp containing PTP1B inhibitors have been described as selective against VHR.¹¹⁷

Activation of Src kinase by PTP1B was shown to contribute to ErbB2 triggered transformation of breast cancer cells.⁹² Hence, a PTP1B inhibitor could have therapeutic potential in the onset of Src kinase activity dependent malignancies.

Regarding the therapeutic potential of a PTP1B inhibitor on the basis of the C-terminal Src sequence it has to be considered that the molecule could hypothetically also activate Src itself. The mechanism of Src's intermolecular inactivation by phosphorylation of the Tyr 530 residue is based on binding of Src's internal SH2 domain to the phosphorylated tyrosine, which blocks the active site.²¹⁶ Competition of the peptide modeled on the C-terminal site, which could potentially bind to the SH2 domain, could open-up and activate the kinase. Therefore, Src's SH2 domain was also tested in the FP assay, which was possible since binding and not inhibition was measured. No binding was observed in the concentration range tested. This is line with a previous report measuring the competition of the phosphopeptide derived from the Src C-terminus with other phosphopeptides, the authors reported an apparent EC₅₀ of 66 μ M.²²⁴ This is a difference of 2-3 orders of magnitude to the affinity of the F₂Pmp peptide to PTP1B. The exchange of pTyr to F₂Pmp is most likely not causing the same dramatic increase in binding for the SH2 domain compared to PTPs as SH2 domains are only recognizing and not dephosphorylating the substrate. An affinity difference in this range should allow selective targeting of the phosphatase.

Additionally to PTP1B, the phosphatases RPTP α , RPTP η , RPTP ϵ , SHP-1 and LMW-PTP are reported in the literature to activate Src by dephosphorylation of the C-terminal phosphotyrosine.^{214,215,224-229} From these phosphatases the membrane proximal catalytic D1 domain of RPTP α has been included in the FP experiment, but also for this enzyme no binding was observed. However, it has been reported before, that RPTP α is only weakly active *in vitro* and that the second, less active, catalytic domain (D2) is involved in binding and needed for efficient dephosphorylation of Src.^{116,230} The expressed enzyme was proven to be active with the unnatural substrate pNPP and a K_M value of 23.9 \pm 4.1 mM could be determined, which was 3 times higher than the K_M of PTP1B against pNPP (7.9 \pm 0.4 mM). Therefore, this negative result needs to be considered critically and binding of the sequence to other, especially membrane associated, phosphatases should be determined in cell-based assays. Chemical tools like the fluorescently or biotin labeled compounds described in chapter 3.5 and 3.6 could potentially be used for this purpose.

However, therapeutically it might even be desired to target multiple phosphatases at the same time, which all potentially activate Src by dephosphorylation of pY 530, in certain cell types or

disease states thereby inhibiting an overshooting Src activation more efficiently than by selectively targeting only one phosphatase involved in this process.^{231,232}

4.5 Influence of cyclization on cell permeability and stability

Analysis of the influence of cyclization on cell permeability was performed with fluorescence microscopy using the fluorescein labeled and F₂Pmp containing peptides synthesized for the fluorescence polarization assay. The linker containing linear sequences **82** (CF-Src-5C) and **83** (CF-Src-1C) showed weak fluorescent signal even after over night incubation with the cells (Figure 19). Whereas **83** (CF-Src-1C) showed weak but homogenous staining, the cells showed dotted, vesicular-like staining after incubation with **82** (CF-Src-5C). The cyclic versions **84** (cyclo-Src-5C) and **85** (cyclo-Src-1C) were behaving very similar to their linear counterpart and no indication for stronger and more homogenous staining, indicating increased uptake, could be observed. The Verdine group used this principle successfully to render the BH3 domain of a Bcl-2 protein (a 23 mer peptide) cell permeable. However, their cyclization approach involved stabilization of the α -helical secondary structure of the domain, which could be a necessity to succeed in enhancing stability and cell permeability as supported by subsequent publications which reported also the stabilization of peptides with α -helical secondary structure elements.^{185,233} Phosphorylation sites, however, are most often found in unstructured regions and therefore do not possess secondary structure elements. On the other hand, molecules with negatively charged moieties, like F₂Pmp, are poorly cell permeable per se, which might prohibit cell entry even if ring closure would contribute positively.

The importance of charge on cell penetration is further highlighted by the fact that C-terminal attachment of an increasing number of arginines (4,6 and 8) resulted in increased cell penetration of the negatively charged Src peptide (Figure 20 (A)). This principle of cell penetrating peptide sequences (CPPs) was described before and partially relies on rendering the sequence net positively charged, but also especially on the presence of guanidinium groups in the arginine residues.²¹⁷⁻²²⁰

However, multiple positive charges in the same molecule influenced the binding of the F₂Pmp containing peptide to its target protein negatively (Figure 20 (B)). This was also described for small molecule inhibitors containing F₂Pmp, and was employed by the Zhang group to develop so-called self-silenced inhibitors, which contain a poly arginine stretch via a disulfide bridge. These inhibitors gain their full activity when the arginine stretch is released by reduction in the cytosol upon cell penetration.¹²¹

Nevertheless, the best binding F₂Pmp containing Src derived sequence, in which the proline at the -2 position was exchanged for alanine, equipped with 6 C-terminal arginines **91** (CF-Src-P(-2)A-R₆) proved to be cell permeable and colocalized with PTP1B inside cells, whereas the sequence without F₂Pmp **92** (CF-Src-(Y)-R₆), which does not bind to the protein, did not colocalize (Figure 21).

Analysis of the stability of linear and cyclic F₂Pmp containing peptides **82**, **83**, **84** and **85** showed that all four peptides are stable in cell lysate or human serum over the time course of 24 hours, whereas a control peptide, which contained canonical amino acids exclusively and had a net positive charge, was degraded to under 75% in the first 6 hours (Figure 22). The unexpected stability of the linear peptides did not allow to draw conclusions about the protective properties of the cyclization. Nevertheless, it demonstrated that the F₂Pmp containing Src sequence is extraordinarily stable in biological media and that inhibitors and tools could be used in cell biological and *in vivo* experiments without doubts about the stability of the peptides. The intermediate performance of the Src peptide without F₂Pmp but tyrosine may imply that the stability was caused by both, the unnatural and highly negative charged F₂Pmp group as well as the surrounding sequence. The special arrangement of two prolines to either end of the tyrosine, may contribute to the stability due to the specific structural features of the proline residue.

4.6 Application of biotinylated F₂Pmp containing sequences as pull-down tools

In chapter 3.6 it was shown that biotinylated variants of the Src peptide can be used in combination with streptavidin-beads to efficiently pull-down PTP1B expressed at endogenous levels from cell lysates. Potency in the pull-down was shown to rely on several aspects including loading to and orientation of the peptides on the beads as well as affinity of the peptide to the target enzyme. Peptides bearing the biotin group in the side chain of a lysine and even more the cyclic variants were shown to be especially potent (Figure 26). Using this strategy in combination with proteomic approaches many different aspects of phosphatase biology and inhibitor development could be addressed. In chapter 4.4 it was mentioned that the C-terminal pTyr of the Src kinase is targeted by many more phosphatases than PTP1B and that selectivity of the inhibitory peptides is difficult to address *in vitro* since some enzymes might not show the same activity as *in vivo*. Due to toxicity, stability or solubility issues, truncated versions of the enzymes need to be expressed and tested. Immunoprecipitation with the inhibitor from cell lysates represents a more global way of testing selectivity. The suspected proteins are all in their native form and compete at their physiological expression levels for binding with the inhibitor. Furthermore, selectivity can be tested in several different

cell or disease model systems, which is desirable since expression levels or isoform variation may change during different stages in development or disease.

In the case of the cyclized F₂Pmp containing Src sequence with the 5 hydrocarbon-linker **95** two bands, which both stained for a selective PTP1B antibody in the western blot were visible in a silver stained gel after pull-down with the peptides from U2OS cell lysate (Figure 30). However, a smeared band at 225 kDa was not characterized fully, yet. Further investigations will be necessary to find out if this band represents multimers of PTP1B or indeed another enzyme. Furthermore, many of the other phosphatases known to target Src are membrane associated and modifications of the pull down protocol, like variation of detergents and detergent concentrations used, might be necessary to try if differences can be observed.

At the same time variation of the pull-down protocol, especially the amount of washing steps and salt concentration, could be used to address open questions in phosphatase research, like the quest of additional allosteric interactors and the change and origin of posttranslational modifications in different stages of the cell cycle or after exogenous stimulation. In the basic protocol, described in chapter 3.6, the beads were washed twice with washing buffer containing 50 mM Tris-HCl (pH 7.5), 125 mM NaCl, 5% Glycerol and 1.5 mM MgCl₂ and once more with lysis buffer containing 0.2% of the detergent NP-40 additionally. These washing conditions might already be too stringent to detect transient allosteric interactors of the protein, since the silver stain showed only 2 dominant bands, which both stained for the PTP1B antibody. Especially, lowering the salt concentration and the amount of washing steps could be tried to detect interacting proteins.

Furthermore, increasing the salt concentration, varying the pH or eluting the peptide/protein complex with avidin and subsequent dialysis of the peptide could be tried to release the enzyme from the peptide-loaded beads mildly and, thus, the technique could be validated to purify endogenously expressed and modified phosphatases to study their modifications and activity. This possibility can be regarded as an advantage towards the activity-based probes introduced in chapter 1.6.^{133–137} These biotin labeled probes bind covalently to phosphatases and, thus, allow stringent washing conditions. However, mild release of the enzyme from this kind of probes is impossible and they were used for labeling purposes exclusively thus far. *Huang et al.* showed that modification of a tripeptide sequence around the covalent binding pTyr mimetic could modify binding specificity and suggested the usage of longer peptide sequences.¹³⁶

In this work, it was shown that the high affinity, yet not covalent binder F₂Pmp in a designed cyclic decamer peptide is sufficient for an efficient pull down of endogenous PTP1B, which shows good selectivity in a silver stain of a pull down from U2OS cell lysate.

5 Conclusions and perspectives

The aims of this work were to study the influence of the amino acid composition around the phosphorylated tyrosine of natural substrate sequence for binding to the model phosphatase PTP1B and to use this knowledge to develop a potent inhibitor. It was aspired to evaluate the potential of cyclization of the inhibitory peptide to enhance stability and to introduce fluorescent labels and affinity tags to convert the inhibitor into a chemical tool for biological experiments.

The non-hydrolyzable pTyr mimetic F₂Pmp, developed by Burke and coworkers, was used to generate a highly potent peptidic inhibitor of the model phosphatase PTP1B based, for the first time, on the C-terminal sequence of the Src kinase (526-536), a natural substrate of this phosphatase.¹⁰⁴ Therefore, the synthesis of the required building block N-Fmoc-L-F₂Pmp-OH was optimized to yield gram amounts in an efficient way. The sequence was chosen after detailed comparison of peptides derived from natural substrates of PTP1B, including different peptide lengths, using Michaelis-Menten kinetics.

To better understand the molecular interactions of the C-terminal Src kinase with PTP1B, a detailed analysis of the binding mode of the inhibitory peptide sequence to PTP1B and its most closely related enzyme TCPTP was carried out by alanine- and truncation-scan of the sequence surrounding F₂Pmp (Figure 31). By exchange of the proline at the -2 position to alanine, an extraordinary strong inhibitor (Src-P(-2)A) with around 6-fold higher inhibitory potency compared to the natural Src sequence and the EGFR sequence used in previous studies was detected. In an FP assay with a fluorescently labeled variant of this sequence, a K_d of 61.4 ± 2.0 nM was determined displaying the excellent binding affinity of the peptide to the phosphatase. The peptide proved to specifically bind PTP1B over other protein tyrosine phosphatase like VHR, RPTPα and the SH2 domain of the Src kinase, but could not distinguish the most closely related enzyme TCPTP.

To test the influence of cyclization using a hydrocarbon linker on inhibitory, cell penetration and stability properties, the thiol-ene reaction and copper (I) catalyzed azide-alkyne 1,3-dipolar cycloaddition were evaluated for the synthesis of side-chain to side-chain or head to side-chain cyclized variants of this peptide. Whereas attempts using the thiol-ene reaction were unsuccessful, the copper (I) catalyzed azide-alkyne cycloaddition was successfully applied for the generation of F₂Pmp containing head to side-chain cyclized molecules. Cyclization was induced via a 1,2,3-triazole and a 5- or 1-carbon atoms containing hydrocarbon linker.

The azide group in the 1-carbon linker peptide was introduced efficiently on solid support using the shelf-stable and safe imidazole-1-sulfonyl-azide*HCl reagent, which was reported previously for the amine to azide conversion only in solution.²⁰⁴

The binding affinity and inhibitory potency was compared between the cyclic peptides and their linear precursors and neither a negative nor a positive effect could be observed, suggesting that the hydrocarbon linker is not interfering with peptide binding by the phosphatase.

The bioorthogonal azide-alkyne cycloaddition was evaluated for the usage in the screening for cyclic F₂Pmp-containing peptides with optimal configuration. A protocol to test the ring-closure without the addition of copper *in situ* by incubating the peptide with the enzyme was devised. However, detection of a linear peptide precursor, which was successfully cyclized by this approach remained elusive. A larger library of linear precursor peptides with broader structural diversity, especially in the linker-groups, would need to be tested. This was beyond the scope of this work, but could be addressed in future efforts.

Notably, cyclization was found to be crucial for efficient co-precipitation of endogenous amounts of PTP1B from cell lysates using biotinylated derivatives of the F₂Pmp containing Src sequence (Figures 25 and 26). The cyclic variant with the 5 hydrocarbon containing linker (peptide **95**) was pulling down PTP1B most efficiently and could even be used to pull-down sufficient amounts of the protein to be visualized on a silver stained SDS-polyacrylamide gel. Earlier works with biotinylated probes focused on relatively unselective covalent modification of PTPs by activity-based probes for identification purposes.^{133–137} Probe **95** developed in this work shows potential for a usage to thoroughly analyze the selectivity of the stabilized C-terminal Src sequence as PTP inhibitor in different cell types. Furthermore, it could potentially be used to identify allosteric interaction partners or to analyze the change of posttranslational modifications of PTP1B in the context of different stages in the cell cycle or after exogenous stimulation.

Although head-to-tail cyclized peptides with non-hydrolyzable pTyr mimetics were synthesized before and beneficial bioavailability properties of these molecules were postulated, a detailed analysis of their cell penetration and stability characteristics was missing.^{109,199}

Analysis of cell membrane permeation of fluorescein labeled derivatives of the F₂Pmp-containing Src based peptide sequences with the hydrocarbon linkers before (peptides **82** and **83**) and after cyclization (peptides **84** and **85**) by fluorescence microscopy could not reveal a significant difference in uptake, which was generally low (Figure 19). Certainly, the highly negatively charged F₂Pmp group contributed to the lack of efficient membrane penetration and could have potentially masked a positive effect of cyclization.

Application of the principle of cell penetrating peptides by C-terminal addition of an increasing number of arginine residues (4,6 and 8), and thereby addition of positive charges to the peptide molecule, showed indeed improved cell penetration (Figure 20 **(A)**).^{98,218–220} At the same time, a decrease in binding affinity correlating to the number of inserted arginines was observed (Figure 20 **(B)**). However, the F₂Pmp containing optimized Src sequence with the proline at position -2 exchanged for alanine and 6 C-terminal arginines (**91**) showed colocalization with overexpressed mKate-PTP1B, whereas the F₂Pmp-lacking control peptide (**92**) did not colocalize indicating that **91** is able to penetrate the cell membrane and bind to PTP1B in the cytosol.

Stability measurements of the linker- and F₂Pmp-containing Src sequences before (peptides **82** and **83**) and after cyclization (peptides **84** and **85**) in cell lysate and human serum revealed an extraordinarily high degree of stability of both linear and cyclic variants compared to a control sequence with net positive charge and containing only canonical amino acids. The unnatural and highly negatively charged F₂Pmp was identified to be involved in the gain of stability. An effect of cyclization, however, could not be proven due to the already high degree of stability of the linear variants. This stability is extremely useful with respect to applications of F₂Pmp containing peptides, especially the extraordinary potent Src-P(-2)A sequence, in biological experiments. Furthermore, the peptide based inhibitor, developed in this work, is relatively easy to synthesize and can be converted to a cell permeable molecule by application of the CPP strategy.

In summary, a potent inhibitor of PTP1B based on stabilized natural substrates was successfully developed in this work. The inhibitor can be rendered cell permeable upon fusion to a cell penetrating peptide and can be easily converted to fluorescently-labeled or affinity-tag containing chemical tools. This strategy is in principle applicable to the entire enzyme class.

6 Summary

Protein tyrosine phosphatases (PTPs) are crucial components of cellular signaling processes, and impairment of PTP function is often related to disease development and progress. To gain an understanding of PTP function and regulation it is therefore of great interest to develop PTP inhibitors and other tools to study them. In this work, the goal was to investigate the potential of stabilized natural substrates as easily accessible PTP inhibitors and derived imaging and pull-down tools.

To this end, the prototypical phosphatase PTP1B was chosen as model. A comparative study of a library of phosphotyrosine (pTyr)-peptides from natural substrates against PTP1B and its closest homologue TCPTP using Michaelis-Menten kinetics identified the C-terminal sequence of the Src kinase as the optimal sequence for further investigation. Stabilization of peptide sequences was achieved by replacement of the pTyr by the non-hydrolyzable mimic difluorophosphonomethyl phenylalanine (F₂Pmp) and cyclization via hydrocarbon linkers. This required optimization of the synthesis of the building block N-Fmoc-L-F₂Pmp-OH in gram scale and validation of potentially applicable cyclization methods, which led to the identification of copper (I) catalyzed azide-alkyne cycloaddition as successful ring-closure reaction. The generated linear and cyclic F₂Pmp-containing peptides were used to study the effects of these modifications on binding affinity, inhibition potency and metabolic stability. The influence of the residues surrounding F₂Pmp to binding and inhibition of PTP1B and TCPTP was furthermore investigated by means of alanine- and truncation-scans. In this way an even stronger binding and more potent inhibitory sequence was identified ($K_d = 61.4 \pm 2.0$ nM with respect to PTP1B); selectivity between the two phosphatases was, however, not achieved. The cyclizations using two linkers with a 1,2,3-triazole and a hydrocarbon-chain of different lengths did not have a significant influence on binding and inhibitory potency suggesting that the hydrophobic linkers are not interfering with binding of the phosphatase to the peptides. An effect on metabolic stability was also not observed, because insertion of the F₂Pmp group already rendered the peptide very stable. Subsequent attachment of cell penetrating sequences was carried out to achieve cellular uptake. Fluorescence labeling was performed to enable the use of the inhibitor as tool to detect colocalization with the phosphatase inside cells. Colocalization was shown using the highly potent Src sequence with six C-terminally attached arginine residues. Biotinylated derivatives of the F₂Pmp-containing inhibitory peptides were used for the first time to co-precipitate endogenous PTP1B from cell lysates. Intriguingly, cyclization of the Src derived sequence resulted in highly superior performance of the pull-down tool. This may be caused by a different orientation or conformation of the cyclic peptides compared to the linear ones on the streptavidin beads.

The successful development of a potent inhibitor, in-cell-detection tool and pull-down tool of the model phosphatase PTP1B based on the sequence of a natural substrate was presented in this work. The tool is highly selective against control phosphatases and the SH2 domain of Src, which binds the chosen sequence intramolecularly in vivo. Selectivity against TCPTP was unfortunately not achieved. The applied strategy is potentially applicable to other members of the enzyme class targeting pTyr protein substrates. The synthetic ease enables fast and simple access to these tools.

7 Experimental Section

7.1 General

7.1.1 Chemicals

All chemicals and anhydrous solvents were obtained from Sigma-Aldrich (Steinheim, Germany) and VWR (Darmstadt, Germany) and used without further purification, unless otherwise stated. N-Fmoc-L-4-iodophenylalanine was purchased from Amatek Chemical Co., Ltd. (Zhangjiagang, China). Diethyl bromodifluoromethylphosphonate was obtained from Matrix Scientific (Columbia, USA). Fmoc-protected amino acids and Rink amide AM resin (200-400 mesh, 0.62 mmol/g or 0.57 mmol/g) were purchased from Novabiochem (Darmstadt, Germany).

Following Fmoc protected L-amino acids were used:

Fmoc-Ala-OH, Fmoc-Arg(Pbf)-OH, Fmoc-Asn(Trt)-OH, Fmoc-Asp(*t*Bu)-OH, Fmoc-Cys(Mmt)-OH, Fmoc-Gln(Trt)-OH, Fmoc-Glu(O-2-PhiPr)-OH, Fmoc-Glu(*t*Bu)-OH, Fmoc-Gly-OH, Fmoc-Lys(Alloc)-OH, Fmoc-Lys(Boc)-OH, Fmoc-Lys(Mtt)-OH, Fmoc-Pra-OH, Fmoc-Pro-OH, Fmoc-Ser(*t*Bu)-OH, Fmoc-Thr(*t*Bu)-OH, Fmoc-Tyr(PO(OBzl)OH)-OH, Fmoc-Tyr(*t*Bu)-OH, Fmoc-Val-OH.

Furthermore, 6-azidohexanoic acid, 2-(1H-benzotriazole-1-yl)-1,1,3,3-tetramethyluronium hexafluorophosphate (HBTU), 2-(1H-benzotriazole-1-yl)-1,1,3,3-tetramethylaminium tetrafluoroborate (TBTU) and triisopropylsilane (TIS) were also purchased from Novabiochem. Hydroxybenzotriazole (HOBt) was from Molekula (Shaftesbury, UK). 2-(1H-7-Azabenzotriazol-1-yl)-1,1,3,3-tetramethyl uranium hexafluorophosphate and 1-hydroxy-7-azabenzotriazole (HOAt) were purchased from GL Biochem (Shanghai, China). N-ethyl-N'-(3-dimethylaminopropyl)carbodiimide hydrochloride (EDC*HCl) was from Iris Biotech (Marktredwitz, Germany). D-(+)-biotin was purchased from Alfa Aesar (Karlsruhe, Germany).

7.1.2 Instruments

Peptide synthesis was performed on an automatic peptide synthesizer Syro I from Multisynth (Witten, Germany).

^1H , ^{13}C and ^{31}P nuclear magnetic Resonance (NMR) spectra were recorded on a 400 MHz Bruker Avance DPX. Chemical shifts (δ) are measured in ppm and coupling constants (J) are given in Hz. ^1H and ^{13}C chemical shifts were referenced to the solvent peaks. Splitting patterns are designated as follows: s = singlet, d = doublet, t = triplet, q = quartet, m =

multiplet, dd = doublet of doublet, bs = broad singlet. ^{13}C and ^{31}P spectra were broadband hydrogen decoupled. For ^1H -assignment COSY and HMQC spectra were recorded.

HPLC-MS analysis and HPLC purifications were carried out on a Shimadzu High Performance Liquid Chromatograph/Mass Spectrometer LCMS-2010EV with an UV/Vis Photodiode array detector SPD-M20A Prominence. For analytical and semi-preparative HPLC the solvent delivery module LC-20AD was used. The solvent mixtures were either H_2O and MeCN or H_2O and MeOH, if needed 0.05% TFA was added. RP-HPLC analytical runs were carried out with a Macherey Nagel C18 EC 250/4.0 NUCLEODUR 100-5 C18 ec column and a pump rate of 1.5 ml/min (analytic gradients: X % eluent B for 1 minute and then in 15 minutes to Y % B; unless otherwise stated). For semi-preparative separations a Macherey Nagel C18 VP 250/10 NUCLEODUR 110-5 C18 ec column and a pump rate of 5 ml/min was used (semi-preparative gradients: X % eluent B for 2 minutes and then in 25 minutes to Y % B; unless stated otherwise). Preparative HPLC separations were conducted with solvent delivery module LC-8A, solvent mixtures were either H_2O and MeCN or H_2O and MeOH, if needed 0.05% TFA was added. The column was a Macherey Nagel C18 VP 250/21 NUCLEODUR 100-5 C18 ec column, a pump rate of 25 ml/min was applied (preparative gradients: X % eluent B for 2.5 min and then in 30 min to Y % B; unless stated otherwise).

Mass spectra were recorded on a MALDI micro MX mass spectrometer (Waters, Manchester, UK) equipped with a reflectron analyzer, used in positive ion mode with delayed extraction activated. High resolution mass spectra were recorded on a LTQ Orbitrap Velos (ThermoFisher Scientific, US).

TLC analyses were conducted on Merck precoated silica gel (Merck, 60 F_{254}) using UV light (254nm) or a solution of ceric ammonium molybdate (prepared by addition of 40 mL conc. H_2SO_4 , 360 mL H_2O , 10 g ammonium molybdate and 4 g ceric ammonium sulfate).

Preparative column chromatography was performed using silica gel from Merck (silica 60, grain size 0.063-0.200 mm, 70-230 mesh ASTM).

Melting point determination was done on a Büchi B-540 (Büchi, Essen, Germany) hot stage melting apparatus.

Amplification of DNA molecules by polymerase chain reaction (PCR) was performed on a MJ Research Thermal Cycler PTC-200 from Biozym Diagnostik GmbH (Oldendorf, Germany).

Protein purification was performed with a Äktapurifier 10 system from GE Healthcare (Umeå, Sweden), which was equipped with a P-903 pump, a M-925 mixer, an UV-900 detector and a Frac 950 fraction collected. The system was operated with the UNICORN 5.20 software.

Protein and DNA concentrations in aqueous media were measured on a NanoDrop 1000 Spectrophotometer from PEQLAB Biotechnologie GmbH (Erlangen, Germany).

Confocal microscopy was performed on a Leica TCS SP2 system from Leica Microsystems GmbH (Wetzlar, Germany) with a HCX PL APO CS 40.0x 1.40 oil and a HCX PL APO ibd. BL 63.0x 1.40 oil objective.

For protein transfer from polyacrylamide gels to nitrocellulose membranes the iBlot Dry Blotting System with iBlot Mini Transfer Stacks (nitrocellulose) from Invitrogen (Grand Island, USA) was used.

The film development system was a Kodak RP X-OMAT processor model M6B from Kodak GmbH (Stuttgart, Germany). As chemiluminescent detection reagent

Amersham ECL Western Blotting Detection Reagent and the autoradiographic film was an Amersham Hyperfilm both from GE Healthcare (Buckinghamshire, UK).

Enzymatic assays were performed on a Tecan safire² (Tecan, Salzburg, Austria) plate reader.

Fluorescence polarization assays were measured on an EnVision plate reader from PerkinElmer (Waltham, USA).

For cultivation of eukaryotic cell lines a Heracell 240i CO₂ incubator from ThermoScientific (Waltham, USA) was used.

Following centrifuges were used: Centrifuge 5415 R for 1.5 mL tubes (up to 13,200 rpm) from Eppendorf (Hamburg, Germany), Megafuge 1.0 R for 50 mL tubes (up to 4,000 rpm) tubes from Heraeus (Buckinghamshire, UK) and a Sorvall RC6 (up to 22,000 rpm) from ThermoScientific (Waltham, USA).

For visualization of DNA bands a dual intensity UVP transilluminator from Herolab (Wiesbaden, Germany) was used.

7.1.3 Buffers and Media

PBS

Phosphate buffered saline (PBS) contained 137 mM NaCl, 2.7 mM KCl, 2mM KH₂PO₄, 10 mM Na₂HPO₄, the pH was adjusted to 7.2 with HCl.

Malachite Green assay buffer

The assay buffer contained 15 mM 4-(2-Hydroxyethyl)-1-piperazineethanesulfonic acid (HEPES), 30 mM NaCl, 1.5 mM EDTA and 2 mM DTT. The pH was adjusted to 7.2, DTT was added freshly every day.

pNPP assay buffer

The buffer used for the pNPP competition assay contained 25 mM HEPES, 2.5 mM EDTA, 2mM DTT (was added freshly every day) and 124.5 mM NaCl. The pH was adjusted to 7.2.

TAE

As running buffer for Agarose gels Tris-acetate-EDTA (TAE) containing 40 mM Tris base, 20 mM glacial acetic acid and 1 mM EDTA was used.

SDS-PAGE sample buffer (2 x)

SDS-PAGE sample buffer (2 x) contained 125 mM Tris-HCl (at pH 6.8), 20% (v/v) glycerol, 4% (w/v) sodium dodecyl sulfate (SDS), 10% (v/v) 2-mercaptoethanol, 0.05% (w/v) bromophenol blue.

SDS-PAGE running buffers

As SDS-PAGE running buffers either NuPAGE MOPS SDS (20 x) or MES (20 x) SDS running buffer were used.

Coomassie staining solution

Staining of protein gels was performed with an aqueous solution containing 0.008% coomassie brilliant blue G-250 (Sigma) and 35 mM HCl.

Transfer buffer

Protein transfer buffer for immunoblots contained 25 mM Tris-HCl, 200 mM glycine and 20% (v/v) methanol.

TBS-T

TBS-T buffer contained 10 mM Tris-HCl (pH adjusted to 7.6 with HCl), 137 mM NaCl and 0.1% (v/v) Tween-20.

TCA stock solution

For protein precipitation a trichloroacetic acid (TCA) stock solution was prepared by dissolving TCA (7.1 g, 43.5 mmol) in H₂O (5 mL).

Bacterial culture media

For cultivation of bacteria autoclaved Luria-Bertani (LB) broth was used. The medium was prepared by EMBL's media kitchen and contained 1% (w/v) bacto tryptone, 0.5% (w/v) bacto yeast extract and 170 mM NaCl. The pH was adjusted to 7.6 with NaOH. Depending on the strains resistance the medium was supplemented with the respective antibiotic (100 $\mu\text{g}/\text{mL}$ ampicillin or 30 $\mu\text{g}/\text{mL}$ kanamycin). LB agarose plates were prepared by EMBL's media kitchen and contained 1.5% (w/v) bacto agar and were supplemented with the respective antibiotic (100 $\mu\text{g}/\text{mL}$ ampicillin or 30 $\mu\text{g}/\text{mL}$ kanamycin) for strain selection.

Media and reagents for eukaryotic cell lines

For cultivation of eukaryotic cell lines Dulbecco's modified eagle medium (Gibco-DMEM) from Invitrogen (Grand Island, USA) was used. Starvation medium contained additionally 2 mM L-glutamine (200 mM stock from sigma) and 1% (v/v) penicillin/streptomycin (Gibco, Invitrogen). Growth medium was furthermore supplemented with 10% FBS (Gibco, Invitrogen) and glucose (1 g/L "low glucose" and 4.5 g/L "high glucose").

Detachment of eukaryotic cells from culture vessels was performed with 0.05% Trypsin EDTA (Gibco, Invitrogen).

For DNA transfection or peptide incubation with eukaryotic cells Opti-MEM (Gibco, Invitrogen) was utilized.

Live cell imaging was performed in imaging medium, which contained 20 mM HEPES, 115 mM NaCl, 1.2 mM CaCl_2 , 1.2 mM MgCl_2 , 1.2 mM K_2HPO_4 . The pH was adjusted to 7.4 and the medium was supplemented glucose (2 g/L) directly before usage.

7.1.4 Biological material

Protein gels

For protein separation under denaturing conditions precast NuPAGE® Novex® 4-12% Bis-Tris Gels (1.0 mm thick, 12 or 15 well) from Invitrogen were used.

Antibodies

Anti-PTP1B – Anti-PTP1B (Ab-1) mouse monoclonal antibody FG6-1G was from Calbiochem (La Jolla, USA).

Anti-GFP – Anti-GFP mouse IgG₁ (clones 7.1 and 13.1) was purchased from Roche (Mannheim, Germany).

Secondary HRP-conjugated anti-mouse antibody – Anti-Mouse IgG (Fc specific)-Peroxidase produced in goat was obtained from Sigma-Aldrich (Steinheim, Germany).

Enzymes

Following enzymes were purchased from New England Biolabs (Ipswich, USA): T4 DNA Ligase, T4 Polynucleotide Kinase, Antarctic Phosphatase, Phusion Thermostable DNA Polymerase, *BamHI*, *EcoRI* and *Sall*.

GST-tagged Precision Proteases was provided from the Protein Expression and Purification Core Facility at EMBL (Heidelberg, Germany).

Miscellaneous reagents

Following reagents were purchased from Fermentas (St. Leon-Rot, Germany): Spectra Multicolor Broad Range Protein Ladder as reference for protein gel electrophoresis, GeneRuler 1kb DNA Ladder as reference for DNA gel electrophoresis and 10 mM dNTP mix for addition in PCR reaction mixtures.

For pull down experiments with biotinylated peptides Streptavidine-Sepharose beads from GE Healthcare (Uppsala, Sweden) were used.

Bovine Serum Albumin was from Sigma-Aldrich (Steinheim, Germany).

The transfection reagent FuGENE 6, the protease inhibitor cocktail tablets complete (EDTA free) and the phosphatase inhibitor cocktail tablets PhosSTOP were purchased from Roche (Mannheim, Germany).

DNA oligomers

DNA oligomers were purchased from Eurofins MWG GmbH (Ebersberg, Germany).

DNA sequencing

Sequencing of DNA plasmids was performed by GATC Biotech AG (Konstanz, Germany).

Bacterial strains

For DNA preparations the *E. coli* strains TOP10 and DH5 α , for protein expressions the strain BL21(DE3) were used.

Eukaryotic cell lines

U2OS - human osteosarcoma cell line, adherent, epithelial morphology in 2D culture, from the laboratory of Rainer Pepperkok (EMBL Heidelberg, Germany).

Hela Kyoto – human cervical adenocarcinoma cell line, adherent, epithelial morphology in 2D culture, from the laboratory of Carsten Schultz (EMBL Heidelberg, Germany).

HEK 293 - human embryonic kidney cell line, adherent, epithelial morphology in 2D culture, from the laboratory of Carsten Schultz (EMBL Heidelberg, Germany).

The cell lines were cultured in growth medium (U2OS and Hela Kyoto in low glucose, and HEK 293 in high glucose medium) at 37°C in a humidified incubator at 5% CO₂ and passaged 2-3 times per week.

7.1.5 Software

Microsoft Excel 2008 for Mac (Version 12.3.2) – Microsoft Cooperation (Redmond, USA)

Microsoft Word 2008 for Mac (Version 12.3.2) – Microsoft Cooperation (Redmond, USA)

Microsoft PowerPoint 2008 for Mac (Version 12.3.2) – Microsoft Cooperation (Redmond, USA)

SigmaPlot (Version 11.0) - Systat Software Inc. (San Jose, USA)

KaleidaGraph (Version 4.03) - Synergy Software (Reading, USA)

ImageJ (Version 1.43u) – <http://rsb.info.nih.gov/ij> (NIH, USA)

Mendeley Desktop (Version 1.3) – Mendeley Ltd. (New York, USA)

ChemBioDraw (Version 11.0.3) – CambridgeSoft (Cambridge, USA)

MacPyMOL (Version 0.99rc6) – Schrödinger (Portland, USA)

7.1.6 Cloning, expression and purification of recombinant proteins

General method for DNA amplification by PCR GM 7.1.1

Amplification of specific DNA fragments was performed by PCR using Phusion thermostable DNA polymerase and forward and reverse DNA primers designed for the respective fragment intended to amplify. In a 0.2 mL PCR tube, the DNA template (10-50 ng), forward and reverse primer (0.5 μ M each), dNTPs (200 μ M), Phusion HF buffer (supplied with the enzyme), Phusion polymerase (2 U) and dH₂O (to reach a final volume of 50 μ L) were mixed.

On the thermocycler the DNA template was denatured at 98°C for 30 sec, followed by 29 cycles of denaturation (98°C for 20 sec), annealing (60°C for 1 minute) and elongation (72°C for 1 minute). A final primer extension step (72°C for 10 minutes) was followed by reannealing at 4°C.

General method for the generation of chemically competent bacteria for DNA transformation GM 7.1.2

One liter of LB broth was inoculated with 5 mL over night culture of *E.coli* (TOP10, DH5 α or BL21(DE3)) and propagated until an optical density of 0.3-0.4 at 550 nm was reached. The suspension was divided in 20 aliquots (50 mL each) and incubated on ice for 15 minutes. The bacteria were collected by centrifugation at 3,000 rpm and 4°C for 15 minutes. The pellets were resuspended in 2 mL of ice-cold RF1 buffer. The contents of 5 tubes were pooled and the volume was filled to 50 mL with RF1 buffer resulting in four 50 mL aliquots. After incubation on ice for 10 minutes, the bacteria were collected by centrifugation (3,000 rpm, 4°C, 15 minutes) and resuspended in 2 mL ice-cold RF2 buffer. The contents of all aliquots were pooled and RF2 buffer was added to reach the final volume of 50 mL. The mixture was incubated on ice for 30 minutes and the suspension was distributed in 1.5 mL plastic tubes (200 μ L each). The aliquots were instantly frozen in liquid nitrogen and stored at -80°C.

General method for transformation of plasmid DNA into bacteria GM 7.1.3

An aliquot (200 μ L) of chemically competent *E.coli* (DH5 α or BL21DE3) was thawed on ice. The DNA preparation (5 μ L) was added and incubated on ice for 30 minutes. The cells were heat shocked at 42°C for 90 seconds and placed on ice for another 2 minutes. Then, prewarmed LB medium (500 μ L), was added and the suspension was incubated at 37°C for 30-45 minutes with horizontal shaking. The cells were spinned down at 800 rpm for 3 minutes and 500 μ L of the supernatant was taken off. The cell pellet was resuspended in the remaining liquid and the cells were plated on agar plates containing the appropriate antibiotic.

General method for digestion of double stranded DNA by restriction endonucleases GM 7.1.4

Digestion of double stranded DNA at specific sites by restriction endonucleases was typically performed in 40 μ L volumes following manufacturer's instructions.

General method for the ligation of double stranded DNA fragments GM 7.1.5

Ligation reactions were performed using T4 DNA Ligase (400 U), reaction buffer (supplied with the enzyme), vector and insert DNA (with an approximate molar ratio of 1:3) and dH₂O (to reach a final volume of 10 μ L). The ligation mixtures were incubated at room temperature for at least 2 hours.

General method for the preparation of plasmid DNA GM 7.1.6

For small amounts of plasmid DNA (“minipreps”) 5 mL of LB medium (supplemented with the respective antibiotic for selection) were inoculated with a single bacterial colony and incubated over night at 37°C with constant shaking. The plasmidic DNA was isolated from the bacterial suspension using the commercially available QIAprep Spin Miniprep kit from QIAGEN GmbH (Hilden, Germany).

For bigger amounts of plasmid DNA (“maxipreps”) 250 mL of LB medium (supplemented with the respective antibiotic for selection) were inoculated with 2-5 mL of starting culture and incubated over night at 37°C with constant shaking. The plasmidic DNA was isolated from the bacterial suspension using the commercially available HiSpeed Plasmid Maxi Kit from QIAGEN GmbH (Hilden, Germany).

General method for DNA separation on agarose gels and isolation GM 7.1.7

After PCR or restriction enzyme digest, DNA fragments were separated on 0.8% agarose gels containing 0.05% (v/v) ethidium bromide. The gels were run with TAE buffer at 80-120 mA. The desired band(s) were cut out of the gel, using the UV transilluminator to visualize them, and isolated from the agarose using the commercially available QIAquick Gel Extraction Kit from QIAGEN GmbH (Hilden, Germany).

General method for protein separation on polyacrylamide gels GM 7.1.8

To a 10 μ L protein sample, containing approximately 1.0 μ g of protein, 10 μ L of SDS sample buffer (2 x) were added. After mixing, the sample was boiled at 95°C for 10 minutes and briefly spun down. In the slots of a precast NuPAGE SDS 4-12% Bis-Tris gel 10 μ L of each sample were added and one slot was filled with 5 μ L of Spectra Br protein ladder as reference. The gel was run in an electrophoresis chamber with MOPS or MES SDS running buffer at 200 mA.

General method for staining of protein gels with coomassie GM 7.1.9

If desired, protein gels were stained with the aqueous coomassie brilliant blue solution (see 6.1.3) by mild warming in a conventional microwave to about 60°C and subsequent incubation for at least 10 minutes. Destaining was performed in dH₂O over night.

PTP1B

A clone of human PTP1B encoding amino acids 1-321 (37-kDa PTP1B) in a pET-11a vector was a kind gift from Novo Nordisk (Copenhagen, Denmark). An N-terminal His-tag was fused to the PTP1B cDNA by insertion of a short double stranded DNA stretch, encoding seven

histidine residues along with a methionine encoding start codon, in an *NdeI* site 5' of PTP1B's start codon. The short double stranded DNA stretch was created by annealing the DNA oligomers 1 (5'-TATGCATCATCATCATCATCATAATG-3') and 2 (5'-ACGTAGTAGTAGTAGTAGTATAC-3') through heating up to 96°C and cooling down to 6°C over 1 hour in a thermocycler. Prior to ligation with T4 DNA Ligase, the DNA stretch was phosphorylated with T4 Polynucleotide Kinase and the vector, which was cut with *NdeI*, was dephosphorylated with Antarctic phosphatase. The resulting vector was transformed into *Escherichia coli* strain BL21 DE3 using standard methods. Single colonies were picked and positive clones were identified through sequencing with the T7-3G primer.

A single positive clone was propagated. The cells expressing the recombinant His-PTP1B were lysed by sonication in lysis buffer (20mM Tris-HCl, pH 8.0 containing 150mM NaCl, 10mM imidazole, 1mM dithiothreitol (DTT) and 0.5mM phenylmethylsulfonyl fluoride (PMSF)). The protein was purified using a FPLC Histrap HP 1 ml column (GE Healthcare) using an elution gradient of 10-500mM imidazole gradient (Figure 32). Protein concentration was determined spectrophotometrically by measuring absorbance at a wavelength of 280 nm with the nanodrop system.

TCPTP

A clone of human TCPTP encoding amino acids 1-307 (36-kDa PTP1B) in a pET-11a vector was a kind gift from Novo Nordisk. An N-terminal His-tag was fused to the TCPTP cDNA by insertion of a short double stranded DNA stretch, encoding seven histidine residues along with a methionine encoding start codon, in a *NdeI* site 5' of TCPTP's start codon. The short double stranded DNA stretch was created by annealing the DNA oligomers 1 (5'-TATGCATCATCATCATCATCATAATG-3') and 2 (5'-ACGTAGTAGTAGTAGTAGTATAC-3') through heating up to 96°C and cooling down to 6°C over 1 hour in a thermocycler. Prior to ligation with T4 DNA Ligase, the DNA stretch was phosphorylated with T4 Polynucleotide Kinase and the vector, which was cut with *NdeI* was dephosphorylated with Antarctic phosphatase. The resulting vector was transformed into *Escherichia coli* strain BL21 DE3 using standard methods. Single colonies were picked and positive clones were identified through sequencing with the T7-3G primer.

A single positive clone was propagated. The cells expressing the recombinant His-PTP1B were lysed by sonication in lysis buffer A (50mM Tris-HCl, pH 8.0 containing 150mM NaCl, 20mM imidazole, 1mM dithiothreitol (DTT) and 0.5mM phenylmethylsulfonyl fluoride (PMSF)). The protein was purified using a FPLC Histrap HP 1 ml column (GE Healthcare) using an elution gradient of 20-500mM imidazole gradient in buffer A (Figure 32). Protein concentration was determined spectrophotometrically by measuring absorbance at a wavelength of 280 nm with the nanodrop system.

PTP α

A C-terminally His-tagged fragment of human PTP α (212-503) (34-kDa PTP α) in a pET21b vector was a kind gift of Dr. Anthony Bishop (Amherst College).

The vector was transformed into *Escherichia coli* strain BL21 DE3 using standard methods. A single clone was picked and propagated. The cells expressing the recombinant PTP α -His were lysed by sonication in lysis buffer (20mM Tris-HCl, pH 8.0 containing 150mM NaCl, 20mM imidazole, 1mM dithiothreitol (DTT) and 0.5mM phenylmethylsulfonyl fluoride (PMSF)). The protein was purified using a FPLC Histrap HP 1 ml column (GE Healthcare) using an elution gradient of 20-500mM imidazole gradient (Figure 32). Protein concentration was determined spectrophotometrically by measuring absorbance at a wavelength of 280 nm with the nanodrop system.

GST-tagged SH2 domain of c-Src

The cDNA of human c-Src in a PCI (Promega) expression vector was a kind gift of Dr. Jeffrey Bjorge (University of Calgary). To create a plasmid, which encodes c-Src's SH2 domain with an N-terminally fused Glutathione-S-transferase (GST) separated by a precision cleavage site GST-SH2(Src) (38 kDa), a DNA fragment was generated enclosing the SH2 domain (residues 142-249) flanked by a 5' *Bam*HI and two 3' stop codons (amber and ochre) with an adjacent 3' *Sall* site using PCR and the primers 5'-CGCGGATCCCAGGCTGAAGAGTGGTACTTTGGGAAGATCA-3' and 5'-CACCGCCTCACCAACCGTGTGCTAGTAAGTCGACGTCCGCCATAGCGGCCGCGGAA-3'.

The DNA fragment was ligated into a pGEX-6P-3 vector after digestion of the DNA fragment and the vector with *Bam*HI and *Sall*, subsequently. The vector was transformed into *Escherichia coli* strain BL21 DE3 using standard methods. Single colonies were picked and test digestions were performed to identify positive clones, which was confirmed by sequencing.

A positive clone was propagated and the cells expressing the recombinant GST-SH2 were lysed by sonication in PBS with complete protease inhibitors (Roche). The protein was purified with a GSTrap FF 1 ml column (GE Healthcare) using glutathione containing elution buffer (50 mM TrisHCl, pH 8.0, 10mM glutathione) (Figure 32). Protein concentration was determined spectrophotometrically by measuring absorbance at a wavelength of 280 nm with the nanodrop system.

SH2 domain of c-Src

The 12 kDa c-Src SH2 domain without the GST tag (SH2(Src)) was produced by incubation of a fraction (25 mg) of GST-SH2(Src) with GST-tagged precision protease (500 U) in cleavage buffer (50mM TrisHCl, pH 7.5, 150mM NaCl, 1mM EDTA). The protein by loading the reaction

mixtures on a GSTRap FF 1mL column, whereby all GST containing impurities (GST-precission, GST-SH2(Src) and GST) remain on the column (Figure 32). Protein concentration was determined spectrophotometrically by measuring absorbance at a wavelength of 280 nm with the nanodrop system.

VHR

Human VHR as an N-terminal GST fusion with a thrombin cleavage site in between (48 kDa VHR) was a kind gift of Dr. Rafael Pulido (Centro de Investigación Príncipe Felipe).

The vector was transformed into Escherichia coli strain BL21 DE3 using standard methods. A single colony was picked and propagated. The cells expressing the protein were lysed in PBS containing 1mM DTT and complete protease inhibitors (Roche). The protein was purified with a GSTRap FF 1 ml column (GE Healthcare) using glutathione containing elution buffer (50 mM TrisHCl, pH 8.0, 10mM glutathione) (Figure 32). Protein concentration was determined spectrophotometrically by measuring absorbance at a wavelength of 280 nm with the nanodrop system.

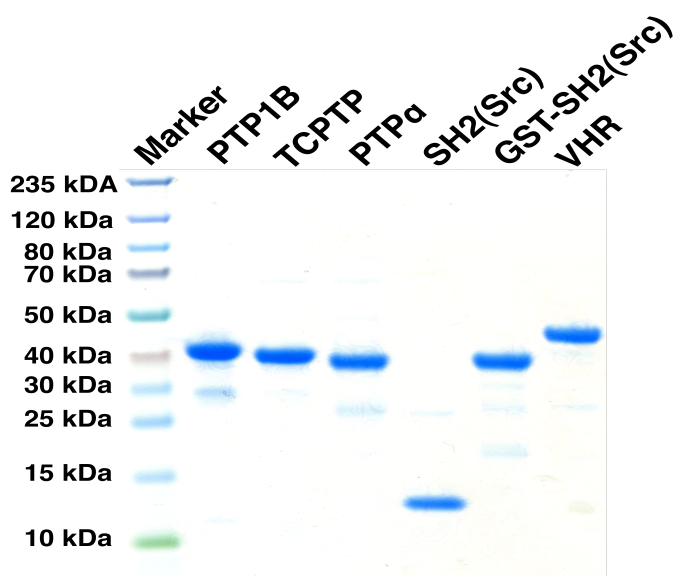


Figure 32: Expressed and purified recombinant proteins on a 4-12% Bis-tris SDS polyacrylamide Gel. PTP1B (37 kDa), TCPTP (36 kDa), PTP α (34 kDa), SH2(Src) (12 kDa), GST-SH2(Src) (38 kDa) and VHR (48 kDa).

7.2 Experiments and methods to chapter 3

7.2.1 Experiments and methods to chapter 3.1.2

General method for the synthesis of phosphopeptides with the automated peptides synthesizer “Syro I” GM 7.2.1

The resin was loaded into a 5 ml reactor with a frit at the bottom. Swelling was performed by dispensing 1 mL DMF and incubating for 15 min (2 x) with 10 seconds shaking every minute. Fmoc deprotection was achieved by treatment with 40% piperidine DMF for 3 minutes and 20% piperidine in DMF for 12 min (10 sec/min shaking). Peptide couplings were carried out by addition of Fmoc-protected amino acids (5 equiv), HBTU (5 equiv), HOBT (5 equiv) and DIPEA (10 equiv) in DMF for 40 minutes (10 sec/min shaking). If present in the sequence, Fmoc-L-Cysteine(Mmt)-OH was coupled using 5 equivalents of the amino acid, DIC (5 equiv) and HOBT (5 equiv) in DMF for 40 minutes (10 sec/min shaking). Double-couplings were performed after each proline and from the fifteenth cycle onwards. N-terminal acetylation was achieved by dispensing 800 μ L of a mixture of acetic anhydride/pyridine (1:9) and reaction for for 2 x 5 minutes (10 sec/min shaking). After each deprotection, coupling or acetylation step 5 washings with DMF (1 minute each with shaking) was performed.

General method for cleavage and side chain deprotection of phosphopeptides GM 7.2.2

After synthesis the resin was transferred in a 5 mL syringe equipped with a frit, 3 washings with DCM (1 minute each) were performed and the resin was dried in high vacuum for at least 30 minutes.

Resin was transferred to a 100 mL round bottom flask and 2 mL of a mixture of TFA and TIS (20:1) was added. The mixture was stirred for 3 hours, 40 mL of toluene was added and solvents were removed in vacuo. The resin was washed consecutively with 10 mL MeOH, 10 mL MeOH/DCM (4:1), 10 mL MeOH/DCM (1:1) and 10 mL MeOH. The collected solvents were evaporated to dryness and the residuum was purified by HPLC.

Ac-Lys-Glu-pTyr-pTyr-Lys-Val-Lys-NH₂ (26)

Resin: Rink amide AM (80mg; L = 0.62 mmol/g)

Purification: Analytical HPLC

(C18; H₂O-MeCN + 0.05% TFA, 5 \rightarrow 20% B in 9 min)

White amorphous solid.

Yield: 3.0 mg (2.6 mmol), 5%.

HPLC (analytical): $t_r = 4.2$ min

(C18; H₂O-MeCN + 0.05% TFA, 10 → 50% B)

C₄₈H₇₇N₁₁O₁₈P₂ (1157.5 g/mol).

ESI-MS: *m/z* calc.: 1158.5 [M+H]⁺
 m/z det.: 1158.4.

MALDI-TOF-MS: *m/z* calc.: 1158.5 [M+H]⁺
 m/z det.: 1159.1.

Ac-Lys-Glu-pTyr-pTyr-Lys-Val-Lys-Glu-Pro-Gly-NH₂ (27)

Resin: Rink amide AM (80mg; L = 0.62 mmol/g)

Purification: Preparative HPLC

(C18; H₂O-MeCN + 0.05% TFA , 10 → 50% B)

White amorphous solid.

Yield: 3.1 mg (2.2 μmol), 4%.

HPLC (analytical): $t_r = 5.7$ min

(C18; MeCN-H₂O + 0.05% TFA, 10 → 50% B)

C₆₀H₉₄N₁₄O₂₃P₂ (1440.6 g/mol).

ESI-MS: *m/z* calc.: 721.3 [M+2H]²⁺
 m/z det.: 721.6.

Ac-Asp-Lys-Glu-pTyr-pTyr-Lys-Val-Lys-Glu-Pro-Gly-Glu-Ser-NH₂ (28)

Resin: Rink amide AM (80mg; L = 0.62 mmol/g)

Purification: Preparative HPLC

(C18; H₂O-MeCN + 0.05% TFA, 5 → 20% B)

White amorphous solid.

Yield: 5.6 mg (3.2 μmol), 7%.

HPLC (analytical): $t_r = 5.9$ min

(C18; MeCN-H₂O + 0.05% TFA, 10 → 50% B)

C₇₂H₁₁₁N₁₇O₃₁P₂ (1771.7 g/mol).

ESI-MS: *m/z* calc.: 886.9 [M+2H]²⁺
 m/z det.: 886.9.

MALDI-TOF-MS: *m/z* calc.: 1772.7 [M+H]⁺
 m/z det.: 1772.8.

Ac-Val-Leu-Pro-Gln-Asp-Lys-Glu-pTyr-pTyr-Lys-Val-Lys-Glu-Pro-Gly-Glu-Ser-NH₂ (29)

Resin: Rink amide AM (80mg; L = 0.62 mmol/g)

Purification: Preparative HPLC

(C18; H₂O-MeCN + 0.05% TFA, 10 → 50% B)

White amorphous solid.

Yield: 10.2 mg (4.6 μmol), 9%.

HPLC (analytical): t_r = 8.9 min

(C18; H₂O-MeCN + 0.05% TFA, 10 → 50% B)

C₉₃H₁₄₆N₂₂O₃₆P₂ (2209.0 g/mol).

ESI-MS: *m/z* calc.: 1105.5 [M+2H]²⁺
 m/z det.: 1105.8.

Ac-Glu-Pro-Gln-pTyr-Gln-Pro-Gly-Glu-Asn-Leu-NH₂ (30)

Resin: Rink amide AM (80mg; L = 0.62 mmol/g)

Purification: Preparative HPLC

(C18; H₂O-MeCN + 0.05% TFA, 10 → 50% B)

White amorphous solid.

Yield: 8.2 mg (6.0 μmol), 12%.

HPLC (analytical): t_r = 7.3 min

(C18; H₂O-MeCN + 0.05% TFA,)

C₅₃H₇₉N₁₄O₂₂P (1294.5 g/mol).

ESI-MS: *m/z* calc.: 1295.5 [M+H]⁺
 m/z det.: 1295.1.

Ac-Asp-pTyr-pTyr-Arg-NH₂ (31)

Resin: Rink amide AM (80mg; L = 0.62 mmol/g)

Purification: Preparative HPLC

(C18; H₂O-MeCN + 0.05% TFA , 5 → 20% B)

White amorphous solid.

Yield: 10.3 mg (13.0 μmol), 26%.

HPLC (analytical): t_r = 4.7 min (C18; MeCN-H₂O + 0.05% TFA, 5 → 20% B)

C₃₀H₄₂N₈O₁₅P₂ (816.2 g/mol).

ESI-MS: *m/z* calc.: 817.2 [M+H]⁺
 m/z det.: 817.1.

Ac-Thr-Asp-pTyr-pTyr-Arg-Lys-Gly-NH₂ (32)

Resin: Rink amide AM (80mg; L = 0.62 mmol/g)

Purification: Preparative HPLC

(C18; H₂O-MeCN + 0.05% TFA , 5 → 20% B)

White amorphous solid.

Yield: 9.8 mg (8.9 μmol), 18%.

HPLC (analytical): t_r = 5.6 min

(C18; MeCN-H₂O + 0.05% TFA, 5 → 20% B)

C₄₂H₆₄N₁₂O₁₉P₂ (1102.4 g/mol).

ESI-MS:	<i>m/z</i>	calc.:	1103.4 [M+H] ⁺
	<i>m/z</i>	det.:	1103.8.

MALDI-TOF-MS:	<i>m/z</i>	calc.:	1103.4 [M+H] ⁺
	<i>m/z</i>	det.:	1103.8.

Ac-Asp-Ala-Asp-Glu-pTyr-Leu-NH₂ (33)

Resin: Rink amide AM (80mg; L = 0.62 mmol/g)

Purification: Preparative HPLC

(C18; H₂O-MeCN + 0.05% TFA, 10 → 50 % B)

White amorphous solid.

Yield: 10.0 mg (12.0 μmol), 24%.

HPLC (analytical): t_r = 5.4 min

(C18; H₂O-MeCN + 0.05% TFA, 10 → 50% B)

C₃₁H₄₆N₇O₁₆P (803.3 g/mol).

ESI-MS:	<i>m/z</i>	calc.:	804.3 [M+H] ⁺
	<i>m/z</i>	det.:	803.9.

Ac-Ala-Ser-Gly-Ala-pTyr-Ala-Gly-Gly-Ser-Ala-NH₂ (34)

Resin: Rink amide AM (80mg; L = 0.62 mmol/g)

Purification: Semi-preparative HPLC

(C18; H₂O-MeCN + 0.05% TFA, 5 → 10% B in 19 min)

White amorphous solid.

Yield: 1.3 mg (1.4 μmol), 3%.

HPLC (analytical): t_r = 5.6 min

(C18; H₂O-MeCN + 0.05% TFA, 5 → 10% B in 9 min)

$C_{35}H_{54}N_{11}O_{17}P$ (931.3 g/mol).

ESI-MS: m/z calc.: 932.3 [M+H]⁺
 m/z det.: 932.5.

7.2.2 Experiments and methods to chapter 3.1.3

Malachite green assay

The dephosphorylation assay was conducted using the colorimetric principle of the malachite green assay, which measures the inorganic phosphate generated by the reaction of the enzyme with the substrate.^{113,165} The detection solution (Biomol Green Solution) used for this assays was purchased from Biomol (Hamburg, German).

Determination of phosphatase concentration and incubation time

Different concentrations (4.0 $\mu\text{g/mL}$, 2.0 $\mu\text{g/mL}$, 1.0 $\mu\text{g/mL}$, 0.5 $\mu\text{g/mL}$, 0.25 $\mu\text{g/mL}$) of both phosphatases (PTP1B and TCPTP) were tested in 96-well microtiter plates against a 1:1 dilution series of the peptide substrate **31**. All 6 substrate concentrations (500 μM \rightarrow 15.6 μM) were measured in duplicates in a final reaction volume of 100 μL in assay buffer. After incubation for 5 (TCPTP) or 6 minutes (PTP1B), 40 μL per well of the Biomol Green solution was added. The low pH of the solution quenched the reaction and absorbance was measured at a wavelength of 620 nm after an additional incubation of at least 15 minutes. From the shape of the resulting curves (absorbance vs. substrate concentration) a phosphatase concentration of 13 nM (0.5 $\mu\text{g/mL}$ for PTP1B and 0.48 $\mu\text{g/mL}$ TCPTP) could be identified for usage in the following experiments.

To determine an appropriate incubation time, PTP1B (0.5 $\mu\text{g/mL}$) and TCPTP (0.25 $\mu\text{g/mL}$) were incubated in assay buffer with CMP1B (15 μM) for varying incubation times before the reaction was stopped by the addition of 40 μL Biomol Green reagent. After an additional incubation time of at least 15 minutes, absorbance was measured at 620 nm. Plotting absorbance against reaction time, and inspection of the resulting graph showed, that an incubation time of 1 minute was suitable for the subsequent experiments, since both curves were in its linear phase at this time point.

Measurement of the substrates against the phosphatase

In 8 wells of a lane of a 96-well microtiter plate the peptide substrates were diluted 1:1 to reach final concentrations from 400 μM to 3.1 μM . Then the phosphatases were added to reach a final concentration of 13 nM each. All substrates were measured at least in triplets with enzyme and at least once without enzyme as blank. After an incubation of 1 minute, 40

μ L biomolgreen solution were added. Absorbance was measured at 620 nm after an additional incubation of 25 minutes.

The blanks were subtracted from the sample values and then plotted versus the substrate concentration. The curve was fitted to the Michaelis-Menten equation using KaleidaGraph.

7.3.1 Experiments and methods to chapter 3.2.1

(S)-2-(trimethylsilyl)ethyl-2-((9H-fluoren-9-yloxy) carbonylamino)-3-(4-(diethoxyphosphoryl) difluoromethyl)phenyl)propanoate (38)

In a mixture of dry CH_2Cl_2 (20 mL) and dry DMF (30 mL) 4.80 g (9.35 mmol) of N-Fmoc-L-4-iodophenylalanine (**37**) were dissolved under argon atmosphere. The solution was cooled on an ice bath, subsequently TMSE (2.50 ml, 25.6 mmol, 2.7 equiv), DMAP (914 mg, 7.48 mmol, 0.8 equiv) and EDC (3.58 g, 23.1 mmol, 2.5 equiv) were added. The reaction was monitored by TLC. After four hours, full conversion of the starting material was observed, CH_2Cl_2 (200 mL) was added to the reaction and the mixture was extracted with aq NH_4Cl (2 x 250 mL) and once with brine. The organic phase was dried (Na_2SO_4) and the solvent was removed under reduced pressure. The resulting brown oil was used in the next reaction without further purification; $R_f = 0.35$ (Cyclohexane–EtOAc, 6:1).

For the next step, cadmium metal (6.00 g, 53.4 mmol, purum p.a. for filling reductors, Sigma-Aldrich) was washed by stirring under argon with 1 N HCl (5 mL, 15 min), H_2O (5 mL, 3 x 1 min) and acetone (5 mL, 3 x 1min). The metal was dried overnight in high vacuum whilst stirring and got a metallic shine. While warming the reaction vessel by hand, dry DMF (10 mL) and Diethyl bromodifluoromethylphosphonate (**40**) (12.5 mL, 31.2 mmol) was added dropwise over 15 minutes to the metal under argon. The reaction proceeded slightly exothermic and was allowed to stir at room temperature for three hours.

TMSE-protected **37** was dissolved in dry DMF (10 mL), then CuBr (2.70 g, 18.8 mmol, 2 equiv) and half of the supernatant solution of the Cd reagent (equates to 1.7 equiv) was added in dropwise manner. After three hours again CuBr (1.40 g, 9.41 mmol, 1 equiv) and the other half of the Cd reagent (**41**) solution was added. The reaction was allowed to stir at room temperature for 19 hours in total. The progress of the reaction was checked by HPLC (Nucleodur C18, 85% MeOH in H_2O , 15 min), the AUC of the peak of the starting material ($R_t = 13.8$ min) was 6.5% compared to the area of the product peak ($R_t = 7.5$ min). The reaction mixture was diluted with EtOAc (250 mL), filtered through celite, extracted with aq NH_4Cl (2 x 250 mL) and brine (250 mL). After drying (Na_2SO_4), the solvents were removed in vacuo. Product **38** was isolated by flash chromatography (cyclohexane-EtOAc, 6:1, then 2:1) as transparent yellowish oil (3.80 g, 5.65 mmol, 60% yield over 2 steps). $R_f = 0.62$ (cyclohexane-EtOAc, 2:1).

^1H NMR (400 MHz, CDCl_3): δ = 7.77 (d, 3J = 7.3 Hz, 2H, 2 ar-H-Fmoc), 7.63-7.51 (m, 4H, 2 ar-H-Fmoc, 2 ar-H-Phe), 7.40 (t, 3J = 7.5 Hz, 2H, 2 ar-H-Fmoc), 7.32 (t, 3J = 7.4 Hz, 2H, 2 ar-H-Fmoc), 7.20 (d, 3J = 7.7 Hz, 2H, 2 ar-H-Phe), 5.26 (d, 3J = 8.0 Hz, 1H, NH-Phe), 4.70-4.60 (m, 1H, α -H-Phe), 4.50-4.34 (m, 2H, CH_2 -Fmoc), 4.34-4.07 (m, 7H, CH-Fmoc, 2 CH_2 -Ethyl, CH_2 -TMSE), 3.27-3.08 (m, 2H, CH_2 -Phe), 1.30 (t, 3J = 7.1 Hz, 6H, 2 CH_3 -Ethyl), 0.97 (t, 3J = 8.3 Hz, 2H, CH_2 -TMSE), 0.04 (s, 9H, 3 CH_3 -TMSE).

^{13}C NMR (100 MHz, CDCl_3): δ = 171.2 (O=C-TMSE ester), 155.5 (O=C-Fmoc), 143.8 (C-F₂P), 143.7, 141.3, 139.0, 131.4 (6 ar-C), 129.5, 127.7, 127.1, 126.5, 125.1, 125.0, 120.0 (12 ar-CH), 66.9 (CH_2 -Fmoc), 64.7 (CH_2 -TMSE), 64.1 (2 CH_2 -Ethyl), 54.7 (α -CH-Phe), 47.2 (CH-Fmoc), 38.0 (CH_2 -Phe), 17.4 (CH_2 -TMSE), 16.3 (2 CH_3 -Ethyl), -1.6 (3 CH_3 TMSE).

^{31}P (126 MHz, CDCl_3): δ = 6.4 (t, J = 115 Hz).

$\text{C}_{34}\text{H}_{42}\text{F}_2\text{NO}_7\text{PSi}$ (673.2 g/mol).

ESI-HRMS: m/z calc.: 696.23284 [M+Na]⁺
 m/z det: 696.23318.

(S)-2-(((9H-fluoren-9-yl)methoxy)carbonylamino)-3-(4-(diethoxyphosphoryl)difluoromethyl)phenyl) propanoic acid, N-Fmoc-F₂Pmp(OEt₂) (39)

Compound **38** (3.80 g, 5.65 mmol) was dissolved in dry CH_2Cl_2 (22.5 mL), then trifluoroacetic acid (7.5 mL, 25%) was added and the mixture was stirred over night. Afterwards, TLC showed complete conversion without the formation of side products. The solvents were removed in vacuo, the remaining oil was dissolved in toluene (40 mL), again evaporated (2 x) and dried in high vacuum. The resulting transparent brownish oil was used in the next reaction without further purification.

R_f = 0.85 (cyclohexane-EtOAc, 1:1).

^1H NMR (400 MHz, CDCl_3): δ = 7.76 (d, 3J = 7.6 Hz, 2H, 2 ar-H-Fmoc), 7.56 (d, 3J = 7.7 Hz, 2H, 2 ar-H-Fmoc), 7.51 (d, 3J = 7.7 Hz, 2H, 2 ar-H-Phe), 7.40 (t, 3J = 7.4 Hz, 2H, 2 ar-H-Fmoc), 7.30 (t, 3J = 7.5 Hz, 2H, 2 ar-H-Fmoc), 7.22 (d, 3J = 7.8 Hz, 2H, 2 ar-H-Phe), 5.49 (d, 3J = 7.8 Hz, 1H, NH-Phe), 4.74-4.65 (m, 1H, α -H-Phe), 4.50-4.43 (m, 1H, CH_2 -Fmoc), 4.40-4.34 (m, 1H, CH_2 -Fmoc), 4.33-4.27 (m, 1H, CH-Fmoc), 4.23-4.09 (m, 4H, 2 CH_2 -Ethyl), 3.30-3.09 (m, 2H, CH_2 -Phe), 1.33-1.23 (m, 6H, 2 CH_3 -Ethyl).

^{13}C NMR (100 MHz, CDCl_3): δ = 173.2 (O=C-carboxy), 155.9 (O=C-Fmoc), 143.9 (C-F₂P), 143.7, 141.4, 139.3, 131.0 (6 ar-C), 129.8, 127.9, 127.2, 126.5, 125.2, 125.1, 120.1 (12 ar-CH), 67.1 (CH_2 -Fmoc), 65.4 (2 CH_2 -Ethyl), 54.5 (α -CH-Phe), 47.3 (CH-Fmoc), 37.7 (CH_2 -Phe), 16.3 (2 CH_3 -Ethyl).

^{31}P (126 MHz, CDCl_3): δ = 6.1 (t, J = 122 Hz).

C₂₉H₃₀F₂NO₇P (573.2 g/mol).

ESI-HRMS: m/z calc.: 574.18007 [M+H]⁺
 m/z det.: 574.18034.

(S)-2-(((9H-fluoren-9-yl)methoxy)carbonylamino)-3-(4-(difluoro(phosphono)methyl)phenyl)propanoic acid, N-Fmoc-F₂Pmp (39)

The material obtained in the previous step was dissolved in dry CH₂Cl₂ (30 mL) and cooled down in an ice bath. Under argon, trimethylsilyl bromide (12.4 mL, 94.0 mmol, 16.6 equiv) was added dropwise. The solution was stirred and allowed to warm to room temperature over night. The solvents were removed in vacuo. This procedure was repeated once more. Then 10% MeCN in H₂O were added, the solution was stirred for 2 hours at room temperature and the solvents were removed by evaporation (2 x). The product **39** was obtained as yellowish glass (2.60 g, 5.03 mmol, 89% yield over 2 steps) in appropriate purity (>90% purity estimated by HPLC) and was used without further purification in solid phase peptide synthesis. R_t = 7.6 min (RP-HPLC, Nucleodur C18, 30% MeOH in H₂O → 70% MeOH in H₂O in 15 min).

¹H NMR (400 MHz, CDCl₃, drops of MeOH-*d*₄): δ = 7.76 (d, ³J = 7.5 Hz, 2H, 2 ar-H-Fmoc), 7.57 (t, ³J = 7.1 Hz, 2H, 2 ar-H-Fmoc), 7.52 (d, ³J = 7.8 Hz, 2H, 2 ar-H-Phe), 7.40 (t, ³J = 7.4 Hz, 2H, 2 ar-H-Fmoc), 7.30 (t, ³J = 6.9 Hz, 2H, 2 ar-H-Fmoc), 7.13 (d, ³J = 7.8 Hz, 2H, 2 ar-H-Phe), 4.59 (dd, ²J = 5.8 Hz, ³J = 8.4 Hz, 1H, α-H-Phe), 4.41 (dd, ²J = 6.7 Hz, ³J = 10.5, 1H, CHa-Fmoc), 4.32 (dd, ²J = 6.7 Hz, ³J = 10.6, 1H, CHb-Fmoc), 4.18 (dd, ²J = 6.3 Hz, ³J = 13.8 Hz, 1H, CH-Fmoc), 3.18-3.04 (m, 2H, CH₂-Phe).

¹³C NMR (100 MHz, CDCl₃, drops of MeOH-*d*₄): δ = 173.3 (O=C-carboxy), 155.8 (O=C-Fmoc), 143.7 (C-F₂P), 143.5, 141.2, 138.5, 131.9 (6 ar-C), 129.3, 127.7, 127.0, 126.3, 124.9, 124.8, 120.0 (12 ar-C), 66.8 (CH₂-Fmoc), 54.6 (α-CH-Phe), 47.0 (CH-Fmoc), 37.8 (CH₂-Phe).

³¹P (126 MHz, CDCl₃, drops of MeOH-*d*₄): δ = 6.1 (t, J = 116 Hz).

C₂₅H₂₂F₂NO₇P (517.1 g/mol)

ESI-HRMS: m/z calc.: 518.11747 [M+H]⁺
 m/z det.: 518.11778.

7.3.2 Experiments and methods to chapter 3.2.2

General method for the synthesis of F₂Pmp containing peptides with the automated peptides synthesizer “Syro I” GM 7.3.2

The resin was loaded into a 5 ml reactor with a frit at the bottom. Swelling was performed by dispensing 1 mL DMF and incubating for 15 min (2 x) with 10 seconds shaking every minute.

Fmoc deprotection was achieved by treatment with 40% piperidine DMF for 3 minutes and 20% piperidine in DMF for 12 min (10 sec/min shaking). Peptide couplings were carried out by double couplings with Fmoc-protected amino acids (5 equiv), HBTU (5 equiv), HOBT (5 equiv) and DIPEA (10 equiv) in DMF for 40 minutes (10 sec/min shaking). If present in the sequence, Fmoc-L-Cysteine(Mmt)-OH was coupled using 5 equivalents of the amino acid, DIC (5 equiv) and HOBT (5 equiv) in DMF for 40 minutes (10 sec/min shaking). At the respective position, Fmoc-F₂Pmp-OH (3 equiv) was coupled in DMF (1 mL) by manual addition using TBTU (3 equiv), HOBT (3 equiv) and DIPEA (6 equiv) for 3 hours, after 3 minutes preactivation. N-terminal acetylation was achieved by dispensing 800 μ L of a mixture of acetic anhydride/pyridine (1:9) and reaction twice for 5 minutes (10 sec/min shaking). After each deprotection, coupling or acetylation step, 5 washings (1 minute each) with DMF was performed (10 sec/min shaking).

General method for cleavage and side chain deprotection of F₂Pmp containing peptides GM 7.3.3

After synthesis the resin was transferred in a 5 mL syringe equipped with a frit, washed with DCM for 1 minute (3 x) and dried in high vacuum for at least 30 minutes.

For cleavage 1 mL of a mixture of TFA and TIS (20:1) was aspirated. The syringe with the mixture was kept on a shaker for 3 hours. Then the liquid phase was filtered into 20 mL of icecold Et₂O. Formed precipitate was centrifuged, washed with ice cold Et₂O (2 x 20 mL) and purified by HPLC.

Ac-Asp-Ala-Asp-Glu-F₂Pmp-Leu-NH₂ (44)

Resin: Rink amide AM (40mg; L = 0.62 mmol/g)

¹H NMR (400 MHz, MeOH-*d*₄): δ = 8.55 (m, NH), 8.17 (d, ³*J* = 7.0 Hz, NH), 8.04 (d, ³*J* = 7.0 Hz, NH), 7.91 (d, ³*J* = 7.0 Hz, 2NH), 7.81 (d, ³*J* = 8.3 Hz, NH), 7.52 (d, ³*J* = 7.5 Hz, 2H), 7.38 (d, ³*J* = 7.4 Hz, 2H), 4.76-4.69 (m, 1H), 4.65-4.51 (m, 2H), 4.37-4.29 (m, 1H), 4.26-4.17 (m, 2H), 3.24-3.05 (m, 2H), 2.97-2.72 (m, 4H), 2.37-2.24 (m, 2H), 2.10-1.87 (m, 5H), 1.72-1.48 (m, 3H), 1.41 (d, ³*J* = 7.4 Hz, 3H), 0.93 (d, ³*J* = 6.7 Hz, 3H), 0.87 (d, ³*J* = 5.7 Hz, 3H).

¹³C NMR (100 MHz, MeOH-*d*₄): δ = 179.4, 176.1, 175.1, 174.3, 173.7, 173.1, 172.7, 172.4, 172.1, 171.6, 151.2, 139.4, 133, 128.9, 126.3, 55.3, 53.8, 51.4, 51.0, 50.0, 40.2, 36.6, 35.3, 34.5, 29.8, 26.0, 24.3, 22.2, 21.1, 20.3, 15.8.

³¹P (126 MHz, MeOH-*d*₄): δ = 5.1 ppm (t, *J* = 112 Hz).

Purification: Semi-preparative HPLC

(C18; H₂O-MeCN + 0.05% TFA, 10 \rightarrow 75% B)

White amorphous solid.

Yield: 9.3 mg (10.6 μ mol), 42%.

HPLC (analytical): t_r = 6.4 min

(C18; H₂O-MeCN + 0.05% TFA, 10 \rightarrow 75% B)

C₃₄H₄₇F₂N₇NaO₁₆P (902.3 g/mol)

MALDI-TOF-MS:	<i>m/z</i>	calc.:	902.3 [M+Na] ⁺
	<i>m/z</i>	det.:	902.5.
	<i>m/z</i>	calc.:	918.4 [M+K] ⁺
	<i>m/z</i>	det.:	918.4.

Ac-Ala-Ser-Gly-Ala-F₂Pmp-Ala-Gly-Gly-Ser-Ala-NH₂ (45)

Resin: Rink amide AM (40mg; L = 0.57 mmol/g)

¹H NMR (400 MHz, D₂O): δ = 7.45 (d, ³J = 7.6 Hz, 2H), 7.25 (d, ³J = 7.6 Hz, 2H), 4.54 (t, ³J = 7.0 Hz, 1H), 4.37-4.31 (m, 2H), 4.23-4.16 (m, 3H), 4.16-4.10 (m, 1H), 3.90 (s, 2H), 3.84 (s, 4H), 3.81-3.73 (m, 4H), 3.17-3.08 (m, 1H), 3.02-2.94 (m, 1H), 1.92 (s, 3H), 1.31-1.23 (m, 9H), 1.41 (d, ³J = 7.1Hz, 3H).

¹³C NMR (100 MHz, D₂O): δ = 180.4, 176.8, 175.6, 175.2, 174.8, 174.3, 173.3, 172.9, 171.7, 171.6, 171.3, 156.8, 138.5, 129.2, 128.5, 126.1, 61.0, 55.6, 54.4, 49.8, 49.6, 43.1, 42.5, 40.0, 21.6, 16.6, 16.5, 16.3.

³¹P (126 MHz, D₂O): δ = 4.2 ppm (t, J = 105 Hz).

Purification: Semi-preparative HPLC

(C18; MeCN-H₂O + 0.05% TFA, 5 \rightarrow 10% B)

White amorphous solid.

Yield: 8.2 mg (8.5 μ mol), 37%.

HPLC (analytical): t_r = 10.0 min

(C18; H₂O-MeCN + 0.05% TFA, 5 \rightarrow 10% B)

C₃₆H₅₄F₂N₁₁O₁₆P (965.4 g/mol)

MALDI-TOF-MS:	<i>m/z</i>	calc.:	966.4 [M+H] ⁺
	<i>m/z</i>	det.:	966.4.
	<i>m/z</i>	calc.:	988.3 [M+Na] ⁺
	<i>m/z</i>	det.:	988.4.

7.4.1 Experiments and methods to chapter 3.3.1

General method for selective side-chain deprotection of the 2-Phenylisopropyl (2-Phipr) group GM 7.4.1

In a 5 mL syringe equipped with a frit, the resin was washed with DCM for 1 minute (3 x). The deprotection was achieved by treatment with 1% TFA and 5% TIS in DCM for 2 minutes (3 x).

General method for the coupling of cystamine to the carboxy group of a glutamate side-chain on solid support GM 7.4.2

In a 5 mL syringe equipped with a frit, 10 equivalents of EDC, HOBt and DIPEA in DMF was added to the solid support for 2.5 hours. Then cystamine (5 equiv), DIPEA (10 equiv) and DMAP (1 equiv) was aspirated in DMF. The coupling was allowed to proceed for 24 hours.

General method for the reduction of cystamine on solid support GM 7.4.3

The solid support was transferred to a flame-dried and argon purged 10 mL round bottom flask. In 1 mL of dry DCM, DTT (8 equiv) and triethylamine (4 equiv) was added. The mixture was stirred over night.

General method for selective side-chain deprotection of the methyltrityl (Mtt) group GM 7.4.4

In a 5 mL syringe equipped with a frit, the resin was washed for 1 minute with DCM (3 x). Mtt deprotection was achieved by treatment with 1.8% TFA in DCM for 3 minutes (10 x). During the deprotection the DCM solution turned yellow.

General method for the coupling of 3-mercaptopropionic acid-4-methoxytrityl to an amine group on solid support GM 7.4.5

In a 5 mL syringe equipped with a frit, 3-mercaptopropionic acid-4-methoxytrityl (3 equiv), HATU (3 equiv), HOAt (3 equiv) and DIPEA (10 equiv) was added to the solid support after preactivation (3 minutes) in DMF. The coupling was performed twice for 40 minutes with an intermediate washing with DMF (3 x 1 minute).

NH₂-Cys-Glu-Pro-Gln-F₂Pmp-Gln-Pro-Gly-Glu-Asn-Leu-Lys(N^ε-allyloxycarbonyl)-NH₂ (46)

Resin: Rink amide AM (80mg; L = 0.62 mmol/g)

Purification: Semi-preparative HPLC

(C18; H₂O-MeCN + 0.05% TFA, 10 → 50% B)

White amorphous solid.

Yield: 3.1 mg (1.9 μ mol), 4%.

HPLC (analytical): t_r = 5.9 min

(C18; H₂O-MeCN + 0.05% TFA, 20% B isocratic)

C₆₅H₉₈F₂N₁₇O₂₄PS (1601.6 g/mol)

MALDI-TOF-MS: *m/z* calc.: 1602.6 [M+H]⁺
 m/z det.: 1602.9.

NH₂-Glu(γ -mercaptoethylamino)-Pro-Gln-F₂Pmp-Gln-Pro-Gly-Glu-Asn-Leu-Lys(N ^{ϵ} -allyloxycarbonyl)-NH₂ (47)

Resin: Rink amide AM (40 mg; L = 0.62 mmol/g)

Purification: Semi-preparative HPLC

(C18; H₂O-MeCN + 0.05% TFA, 20 \rightarrow 30% B)

White amorphous solid.

Yield: 1.2 mg (0.8 μ mol), 3%.

HPLC (analytical): t_r = 10.8 min

(C18; H₂O-MeCN + 0.05% TFA, 20 \rightarrow 30% B)

C₆₄H₉₈F₂N₁₇O₂₂PS (1557.7 g/mol)

MALDI-TOF-MS: *m/z* calc.: 1580.7 [M+Na]⁺
 m/z det.: 1579.7.

Ac-Cys-Glu-Pro-Gln-pTyr-Gln-Pro-Gly-Glu-Asn-Lys(N ^{ϵ} -allyloxycarbonyl)-NH₂ (50)

Resin: Rink amide AM (80 mg; L = 0.62 mmol/g)

Purification: Semi-preparative HPLC

(C18; H₂O-MeCN + 0.05% TFA, 10 \rightarrow 75% B)

White amorphous solid.

Yield: 3.9 mg (2.6 μ mol), 5%.

HPLC (analytical): t_r = 6.2 min

(C18; H₂O-MeCN + 0.05% TFA, 10 \rightarrow 75% B)

C₆₀H₉₉N₁₆O₂₅PS (1496.6 g/mol)

ESI-MS: *m/z* calc.: 749.3 [M+2H]²⁺
 m/z det.: 750.1.

Ac-Lys(N^ε-mercaptopropanamido)-Glu-Pro-Gln-pTyr-Gln-Pro-Gly-Glu-Asn-Lys(N^ε-allyloxycarbonyl)-NH₂ (51)

Resin: Rink amide AM (80 mg; L = 0.62 mmol/g)

Purification: Semi-preparative HPLC

(C18; H₂O-MeCN + 0.05% TFA, 10 → 75% B)

White amorphous solid.

Yield: 4.7 mg (2.9 μmol), 6%.

HPLC (analytical): t_r = 6.6 min

(C18; H₂O-MeCN + 0.05% TFA, 10 → 75% B)

C₆₆H₁₀₀N₁₇O₂₆PS (1609.7 g/mol)

ESI-MS: *m/z* calc.: 805.9 [M+2H]²⁺
 m/z det.: 806.1.

7.4.2 Experiments and methods to chapter 3.3.2

Imidazole-1-sulfonyl-azide*HCl

Was synthesized according to the protocol described by *Goddard-Borger et al.*²⁰⁴

To an ice-cold suspension of 3 g sodium azide (46 mmole) in MeCN (50 mL), 3.7 mL sulfuryl chloride were added dropwise. The mixture was allowed to warm to room temperature and stirred over night. The mixture was again cooled down to 0°C and 6 g imidazole (87.5 mmole) were added successively in small quantities. After additional stirring for 3 hours, the reaction mixture was diluted to 100 mL with EtOAc extracted with H₂O (2 x 100mL) and with saturated aqueous NaHCO₃ (1 x 100 mL). The organic phase was dried over Na₂SO₄ and filtered. A solution of HCl in EtOH, which was prepared by dropwise addition of 14.2 mL AcCl (200 mmole) to 50 mL ice-cooled dry ethanol, was added dropwise to the filtrate. The resulting crystallization product was filtered off, washed with EtOAc (3 x 50 mL) and dried in vacuo, yielding imidazole-1-sulfonyl-azide*HCl in colorless needles.

C₃ClH₄N₅O₂S (209.0 g/mol)

¹H NMR (400 MHz, H₂O-*d*₂): δ = 7.44 (bs, 1H), 7.86 (bs, 1H), 9.16 (m, 1H). Reference:

¹H NMR (600 MHz, H₂O-*d*₂): δ = 7.68 (dd, 1H, *J* = 1.3, 2.2 Hz), 8.09 (dd, 1H, *J* = 1.6, 2.2 Hz), 9.53 (dd, 1H, *J* = 1.3, 1.6 Hz)²⁰⁴

Colorless needles.

Yield: 3.3 g (15.8 mmole), 34%.

M.p.: 96-98°C

Reference m.p.: 94°C (on DSC) and 100-102°C (hot stage melting apparatus)²⁰⁴

General method for the diazotransfer on solid support using imidazole-1-sulfonyl-azide*HCl GM 7.4.6

In a 5mL syringe with frit, the resin was washed for 1 minute each with DCM (2 x), DCM/MeOH (2 x) and MeOH (3 x). Then (for 40 mg resin, loading = 0.62 mmole/g) 1.4 equivalents of imidazole-1-sulfonyl-azide*HCl in 1 mL MeOH and 100 μ l of a saturated and centrifuged solution of CuSO₄*5H₂O was added. After 1 minute, DIPEA (1.8 equiv) was aspirated and the coupling was allowed to proceed for 1 hour and repeated once more with an intermediate washing with MeOH (3 x 1 minute).

General method for the cyclization of peptides by copper catalyzed azide alkyne cycloaddition (CuAAC) GM 7.4.7

Linear precursor peptide was diluted to a concentration of 200 μ M in water. Then 4.5 equivalents of CuSO₄*5H₂O and 7 equivalents of ascorbic acid were added and the solution was stirred at room temperature over night. The product was purified by HPLC and lyophilized.

General method for the cyclization trials *in situ* without the addition of copper by azide alkyne cycloaddition GM 7.4.8

The linear peptides were diluted to a concentration of 50 μ M in pNPP assay buffer, PTP1B (0.4 equiv) or BSA (0.4 equiv), as control, were added and the solutions were incubated by 37°C with gentle shaking over night. The samples were analyzed by HPLC.

6-Azidohexanamido-Glu-Pro-Gln-F₂Pmp-Gln-Pro-Gly-Glu-Asn-Pra-NH₂, “Src-5C” (57)

Resin: Rink amide AM (80 mg; L = 0.57 mmol/g)

Purification: Preparative HPLC

(C18; H₂O-MeCN + 0.05% TFA, 10 \rightarrow 50% B)

White amorphous solid.

Yield: 13 mg (9.2 μ mol), 20%.

HPLC (analytical): t_r = 8.9 min

(C18; MeCN-H₂O + 0.05% TFA, 5 \rightarrow 40% B)

C₅₇H₈₀F₂N₁₇O₂₁P (1407.6 g/mol)

ESI-MS:	<i>m/z</i>	calc.:	704.8 [M+2H] ²⁺
	<i>m/z</i>	det.:	704.7.

ESI-HRMS:	<i>m/z</i>	calc.:	1408.5493 [M+H] ⁺
	<i>m/z</i>	det.:	1408.5538.

2-Azidoethanamido-Gly-Glu-Pro-Gln-F₂Pmp-Gln-Pro-Gly-Glu-Asn-Pra-NH₂, “Src-1C” (58)

Transformation of the terminal amino group to the azide was performed according to GM 7.4.6. Testcleavage and HPLC analysis of the crude before and after the reaction reveal quantitative conversion of the starting material.

Resin: Rink amide AM (80 mg; L = 0.57 mmol/g)

Purification: Preparative HPLC

(C18; H₂O-MeCN + 0.05% TFA, 10 → 50% B)

White amorphous solid.

Yield: 7.8 mg (5.77 μmol), 13%.

HPLC (analytical): t_r = 6.4 min

(C18; H₂O-MeCN + 0.05% TFA, 10 → 50% B)

C₅₃H₇₂F₂N₁₇O₂₁P (1351.5 g/mol)

ESI-MS: *m/z* calc.: 1352.5 [M+H]⁺

m/z det.: 1353.1.

ESI-HRMS: *m/z* calc.: 1352.4867 [M+H]⁺

m/z det.: 1352.4880.

“cyclo-Src-5C” (59)

Was synthesized by cyclization of linear precursor peptide **57** (4.4 μmol) using the general method GM 7.4.7.

Purification: Semi-preparative HPLC

(C18; H₂O-MeCN + 0.05% TFA, 10 → 50% B)

White amorphous solid.

Yield: 2 mg (1.4 μmol), 32%.

HPLC (analytical): t_r = 6.2 min

(C18; H₂O-MeCN + 0.05% TFA, 5 → 40% B)

C₅₇H₈₀F₂N₁₇O₂₁P (1407.6 g/mol)

ESI-MS: *m/z* calc.: 704.8 [M+2H]²⁺

m/z det.: 704.8.

ESI-HRMS: *m/z* calc.: 1408.5493 [M+H]⁺

m/z det.: 1408.5487.

“cyclo-Src-1C” (60)

Was synthesized by cyclization of linear precursor peptide **58** (4.5 μmol) using the general method GM 7.4.7.

Purification: Semi-preparative HPLC

(C18; H₂O-MeCN + 0.05% TFA, 10 \rightarrow 50% B)

White amorphous solid.

Yield: 2.6 mg (1.9 μmol), 42%.

HPLC (analytical): $t_r = 5.0$ min

(C18; H₂O-MeCN + 0.05% TFA, 10 \rightarrow 50% B)

C₅₃H₇₂F₂N₁₇O₂₁P (1351.5 g/mol)

ESI-MS: m/z calc.: 676.8 [M+2H]²⁺

m/z det.: 676.8.

ESI-HRMS: m/z calc.: 1352.4867 [M+H]⁺

m/z det.: 1352.4880.

7.5.1 Experiments and methods to chapter 3.4.1

pNPP competition assay

PTP1B or TCPTP (40nM) were incubated with decreasing concentrations of the inhibitory peptides for 30 minutes at 37 °C in final reaction volume of 100 μL in pNPP assay buffer. After the incubation time 20 μL pNPP was added to reach a final concentration of 10 mM. Absorbance at 405 nm was measured every 30 seconds over 15 minutes. All measurements were done at least in triplicates. The slopes of the initial phases were obtained by linear regression of the data points up to 10 minutes. The reaction rates were plotted versus the decadic logarithm of the inhibitor concentrations and the IC₅₀ values were obtained by fitting the curves using the one site competition model of SigmaPlot.

Ac-Glu-Pro-Gln-F₂Pmp-Gln-Pro-Gly-Glu-Asn-Leu-NH₂ (61)

Resin: Rink amide AM (40 mg; L = 0.62 mmol/g)

Purification: Semi-preparative HPLC

(C18; H₂O-MeCN + 0.05% TFA, 10 \rightarrow 50% B)

White amorphous solid.

Yield: 6.9 mg (5.2 μmol), 21%.

HPLC (analytical): $t_r = 6.6$ min

(C18; H₂O-MeCN + 0.05% TFA, 10 → 50% B)

C₅₄H₇₉F₂N₁₄O₂₁P (1328.5 g/mol)

MALDI-TOF-MS: *m/z* calc.: 1351.5 [M+Na]⁺
 m/z det.: 1351.7.

Ac-Glu-Pro-Gln-F₂Pmp-Gln-Pro-Gly-Glu-Asn-Ala-NH₂ (62)

Resin: Rink amide AM (40 mg; L = 0.62 mmol/g)

Purification: Semi-preparative HPLC

(C18; H₂O-MeCN + 0.05% TFA, 10 → 50% B)

White amorphous solid.

Yield: 10.3 mg (8.0 μmol), 32%.

HPLC (analytical): t_r = 5.6 min

(C18; H₂O-MeCN + 0.05% TFA, 10 → 50% B)

C₅₁H₇₃F₂N₁₄O₂₁P (1286.5 g/mol)

MALDI-TOF-MS: *m/z* calc.: 1309.5 [M+Na]⁺
 m/z det.: 1310.0.

Ac-Glu-Pro-Gln-F₂Pmp-Gln-Pro-Gly-Glu-Ala-Leu-NH₂ (63)

Resin: Rink amide AM (40 mg; L = 0.62 mmol/g)

Purification: Semi-preparative HPLC

(C18; H₂O-MeCN + 0.05% TFA, 10 → 50% B)

White amorphous solid.

Yield: 8.5 mg (6.6 μmol), 27%.

HPLC (analytical): t_r = 7.9 min

(C18; H₂O-MeCN + 0.05% TFA, 10 → 50% B)

C₅₃H₇₈F₂N₁₃O₂₀P (1285.5 g/mol)

MALDI-TOF-MS: *m/z* calc.: 1308.5 [M+Na]⁺
 m/z det.: 1309.0.

Ac-Glu-Pro-Gln-F₂Pmp-Gln-Pro-Gly-Ala-Asn-Leu-NH₂ (64)

Resin: Rink amide AM (40 mg; L = 0.62 mmol/g)

Purification: Semi-preparative HPLC

(C18; H₂O-MeCN + 0.05% TFA, 10 → 50% B)

White amorphous solid.

Yield: 11.4 mg (9.0 μ mol), 36%.

HPLC (analytical): t_r = 7.4 min

(C18; H₂O-MeCN + 0.05% TFA, 10 \rightarrow 50% B)

C₅₂H₇₇F₂N₁₄O₁₉P (1270.5 g/mol)

MALDI-TOF-MS: *m/z* calc.: 1293.5 [M+Na]⁺
 m/z det.: 1294.0.

Ac-Glu-Pro-Gln-F₂Pmp-Gln-Pro-Ala-Glu-Asn-Leu-NH₂ (65)

Resin: Rink amide AM (40 mg; L = 0.62 mmol/g)

Purification: Semi-preparative HPLC

(C18; H₂O-MeCN + 0.05% TFA, 10 \rightarrow 50% B)

White amorphous solid.

Yield: 13.1 mg (9.8 μ mol), 40%.

HPLC (analytical): t_r = 7.5 min

(C18; MeCN-H₂O + 0.05% TFA, 10 \rightarrow 50% B)

C₅₅H₈₁F₂N₁₄O₂₁P (1342.5 g/mol)

MALDITOF-MS: *m/z* calc.: 1365.5 [M+Na]⁺
 m/z det.: 1366.0.

Ac-Glu-Pro-Gln-F₂Pmp-Gln-Ala-Gly-Glu-Asn-Leu-NH₂ (66)

Resin: Rink amide AM (40 mg; L = 0.62 mmol/g)

Purification: Semi-preparative HPLC

(C18; H₂O-MeCN + 0.05% TFA, 10 \rightarrow 50% B)

White amorphous solid.

Yield: 5.0 mg (3.8 μ mol), 15%.

HPLC (analytical): t_r = 7.5 min

(C18; H₂O-MeCN + 0.05% TFA, 10 \rightarrow 50% B)

C₅₂H₇₇F₂N₁₄O₂₁P (1302.5 g/mol)

MALDI-TOF-MS: *m/z* calc.: 1325.5 [M+Na]⁺
 m/z det.: 1326.0.

Ac-Glu-Pro-Gln-F₂Pmp-Ala-Pro-Gly-Glu-Asn-Leu-NH₂ (67)

Resin: Rink amide AM (40 mg; L = 0.62 mmol/g)

Purification: Semi-preparative HPLC

(C18; H₂O-MeCN + 0.05% TFA, 10 \rightarrow 50% B)

White amorphous solid.

Yield: 9.6 mg (7.6 μ mol), 31%.

HPLC (analytical): t_r = 7.6 min

(C18; H₂O-MeCN + 0.05% TFA, 10 \rightarrow 50% B)

C₅₂H₇₆F₂N₁₃O₂₀P (1271.5 g/mol)

MALDI-TOF-MS: *m/z* calc.: 1294.5 [M+Na]⁺
 m/z det.: 1295.0.

Ac-Glu-Pro-Ala-F₂Pmp-Gln-Pro-Gly-Glu-Asn-Leu-NH₂ (68)

Resin: Rink amide AM (40 mg; L = 0.62 mmol/g)

Purification: Semi-preparative HPLC

(C18; H₂O-MeCN + 0.05% TFA, 10 \rightarrow 50% B)

White amorphous solid.

Yield: 10.5 mg (8.3 μ mol), 34%.

HPLC (analytical): t_r = 7.3 min

(C18; H₂O-MeCN + 0.05% TFA, 10 \rightarrow 50% B)

C₅₂H₇₆F₂N₁₃O₂₀P (1271.5 g/mol)

MALDI-TOF-MS: *m/z* calc.: 1294.5 [M+Na]⁺
 m/z det.: 1295.0.

Ac-Glu-Ala-Gln-F₂Pmp-Gln-Pro-Gly-Glu-Asn-Leu-NH₂ (69)

Resin: Rink amide AM (40 mg; L = 0.62 mmol/g)

Purification: Semi-preparative HPLC

(C18; H₂O-MeCN + 0.05% TFA, 10 \rightarrow 50% B)

White amorphous solid.

Yield: 9.1 mg (7.0 μ mol), 28%.

HPLC (analytical): t_r = 7.3 min

(C18; H₂O-MeCN + 0.05% TFA, 10 \rightarrow 50% B)

C₅₂H₇₇F₂N₁₄O₂₁P (1302.5 g/mol)

MALDI-TOF-MS: *m/z* calc.: 1325.5 [M+Na]⁺
 m/z det.: 1326.0.

Ac-Ala-Pro-Gln-F₂Pmp-Gln-Pro-Gly-Glu-Asn-Leu-NH₂ (70)

Resin: Rink amide AM (40 mg; L = 0.62 mmol/g)

Purification: Semi-preparative HPLC

(C18; H₂O-MeCN + 0.05% TFA, 10 → 50% B)

White amorphous solid.

Yield: 7.4 mg (5.8 μmol), 23%.

HPLC (analytical): t_r = 7.3 min

(C18; H₂O-MeCN + 0.05% TFA, 10 → 50% B)

C₅₂H₇₇F₂N₁₄O₁₉P (1270.5 g/mol)

MALDI-TOF-MS: *m/z* calc.: 1293.5 [M+Na]⁺

m/z det.: 1294.0.

Ac-Glu-Pro-Gln-F₂Pmp-Gln-Pro-Gly-Glu-Asn-NH₂ (71)

Resin: Rink amide AM (40 mg; L = 0.62 mmol/g)

Purification: Semi-preparative HPLC

(C18; H₂O-MeCN + 0.05% TFA, 10 → 50% B)

White amorphous solid.

Yield: 8.2 mg (6.8 μmol), 27%.

HPLC (analytical): t_r = 4.7 min

(C18; H₂O-MeCN + 0.05% TFA, 10 → 50% B)

C₄₈H₆₉F₂N₁₃O₂₀P (1215.4 g/mol)

MALDI-TOF-MS: *m/z* calc.: 1338.4 [M+Na]⁺

m/z det.: 1238.6.

Ac-Glu-Pro-Gln-F₂Pmp-Gln-Pro-Gly-Glu-NH₂ (72)

Resin: Rink amide AM (40 mg; L = 0.62 mmol/g)

Purification: Semi-preparative HPLC

(C18; H₂O-MeCN + 0.05% TFA, 10 → 50% B)

White amorphous solid.

Yield: 7.2 mg (6.5 μmol), 26%.

HPLC (analytical): t_r = 5.0 min

(C18; H₂O-MeCN + 0.05% TFA, 10 → 50% B)

C₄₄H₆₂F₂N₁₁O₁₈P (1101.4 g/mol)

MALDI-TOF-MS: *m/z* calc.: 1124.4 [M+Na]⁺

m/z det.: 1124.6.

Ac-Glu-Pro-Gln-F₂Pmp-Gln-Pro-Gly-NH₂ (73)

Resin: Rink amide AM (40 mg; L = 0.62 mmol/g)

Purification: Semi-preparative HPLC

(C18; H₂O-MeCN + 0.05% TFA, 10 → 50% B)

White amorphous solid.

Yield: 7.3 mg (7.5 μmol), 30%.

HPLC (analytical): t_r = 5.0 min

(C18; H₂O-MeCN + 0.05% TFA, 10 → 50% B)

C₃₉H₅₅F₂N₁₀O₁₅P (972.4 g/mol)

MALDI-TOF-MS: *m/z* calc.: 995.4 [M+Na]⁺
 m/z det.: 995.5.

Ac-Glu-Pro-Gln-F₂Pmp-Gln-Pro-NH₂ (74)

Resin: Rink amide AM (40 mg; L = 0.62 mmol/g)

Purification: Semi-preparative HPLC

(C18; H₂O-MeCN + 0.05% TFA, 10 → 50% B)

White amorphous solid.

Yield: 6.4 mg (7.0 μmol), 28%.

HPLC (analytical): t_r = 5.0 min

(C18; H₂O-MeCN + 0.05% TFA, 10 → 50% B)

C₃₇H₅₂F₂N₉O₁₄P (915.3 g/mol)

MALDI-TOF-MS: *m/z* calc.: 938.3 [M+Na]⁺
 m/z det.: 938.6.

Ac-Glu-Pro-Gln-F₂Pmp-Gln-NH₂ (75)

Resin: Rink amide AM (40 mg; L = 0.62 mmol/g)

Purification: Semi-preparative HPLC

(C18; H₂O-MeCN + 0.05% TFA, 10 → 50% B)

White amorphous solid.

Yield: 2.3 mg (2.8 μmol), 11%.

HPLC (analytical): t_r = 4.8 min

(C18; H₂O-MeCN + 0.05% TFA, 10 → 50% B)

C₃₂H₄₅F₂N₈O₁₃P (818.3 g/mol)

MALDI-TOF-MS: m/z calc.: 841.3 [M+Na]⁺
 m/z det.: 841.5.

Ac-Pro-Gln-F₂Pmp-Gln-Pro-Gly-Glu-Asn-Leu-NH₂ (76)

Resin: Rink amide AM (40 mg; L = 0.62 mmol/g)

Purification: Semi-preparative HPLC

(C18; H₂O-MeCN + 0.05% TFA, 10 → 50% B)

White amorphous solid.

Yield: 9.9 mg (8.3 μmol), 33%.

HPLC (analytical): t_r = 11.8 min

(C18; H₂O-MeCN + 0.05% TFA, 10 → 50% B)

C₄₉H₇₂F₂N₁₃O₁₈P (1199.5 g/mol)

MALDI-TOF-MS: m/z calc.: 1222.5 [M+Na]⁺
 m/z det.: 1222.8.

Ac-Gln-F₂Pmp-Gln-Pro-Gly-Glu-Asn-Leu-NH₂ (77)

Resin: Rink amide AM (40 mg; L = 0.62 mmol/g)

Purification: Semi-preparative HPLC

(C18; H₂O-MeCN + 0.05% TFA, 10 → 50% B)

White amorphous solid.

Yield: 8.5 mg (7.7 μmol), 31%.

HPLC (analytical): t_r = 5.4 min

(C18; H₂O-MeCN + 0.05% TFA, 10 → 50% B)

C₄₄H₆₅F₂N₁₂O₁₇P (1102.4 g/mol)

MALDI-TOF-MS: m/z calc.: 1125.4 [M+Na]⁺
 m/z det.: 1125.8.

Ac-Pro-Gln-F₂Pmp-Gln-Pro-NH₂ (78)

Resin: Rink amide AM (40 mg; L = 0.62 mmol/g)

Purification: Semi-preparative HPLC

(C18; H₂O-MeCN + 0.05% TFA, 10 → 50% B)

White amorphous solid.

Yield: 3.4 mg (4.3 μmol), 17%.

HPLC (analytical): t_r = 5.0 min

(C18; H₂O-MeCN + 0.05% TFA, 10 → 50% B)

$C_{32}H_{45}F_2N_8O_{11}P$ (786.3 g/mol)

MALDI-TOF-MS: m/z calc.: 809.3 [M+Na]⁺
 m/z det.: 809.6.

Ac-Gln-F₂Pmp-Gln-NH₂ (79)

Resin: Rink amide AM (40 mg; L = 0.62 mmol/g)

Purification: Semi-preparative HPLC

(C18; H₂O-MeCN + 0.05% TFA, 5 → 10% B)

White amorphous solid.

Yield: 0.6 mg (1.0 μmol), 4%.

HPLC (analytical): t_r = 4.3 min

(C18; H₂O-MeCN + 0.05% TFA, 5 → 10% B)

$C_{22}H_{31}F_2N_6O_8P$ (592.2 g/mol)

MALDI-TOF-MS: m/z calc.: 615.2 [M+Na]⁺
 m/z det.: 615.6.

4-(2-carboxyvinyl)benzamido-Gly-Glu-Leu-NH₂, "CinnGEL" (18)

Was synthesized according to the protocol by Moran *et al.*¹²³

For the preparation of *tert*-butyl-(*p*-carboxy)cinnamate 4 g iodobenzoic acid (16.1 mmole) were combined in a flame dried 25 mL double-neck round bottom flask with 3 mL *tert*-butylacrylate, 4.7 mL triethylamine (33.9 mmole), 36.2 mg Pd(II)acetate (0.16 mmole) and 170 mg triphenylphosphin (0.65 mmole). The mixture was heated at 100°C for 2 hours in argon atmosphere. The mixture was diluted to 25 mL with 3N NaOH and extracted with diethylether (3 x 25 mL). The aqueous layer was brought to pH 4 with 1N HCl and extracted with EtOAc (3 x 100 mL). The combined organic phases were dried over Na₂SO₄, filtered and evaporated to dryness. A total of 2.5 g of the cinnamate (10.2 mmole, yield = 63%) was obtained as yellow amorphous solid and was used in the peptides synthesis without further purification.

Amino acid and *tert*-butyl-(*p*-carboxy)cinnamate couplings and cleavage from the solid support were performed using the standard procedures (GM 7.3.2 and 7.3.3).

¹H NMR (400 MHz, MeOH-*d*₄): δ = 8.11 (d, *J* = 7 Hz, 1H), 7.91 (d, *J* = 7 Hz, 2H), 7.71 (d, *J* = 8 Hz, 2H), 7.68 (d, *J* = 16 Hz, 1H), 6.59 (d, *J* = 16 Hz, 1H), 4.36 (br s, 2H), 4.08 (d, *J* = 17 Hz, 1H), 3.99 (d, *J* = 17 Hz, 1H), 2.45 (t, *J* = 8 Hz, 2H), 2.17 (m, 1H), 1.98 (m, 1H), 1.64 (m, 3H), 0.96 (d, *J* = 6 Hz, 3H), 0.91 (d, *J* = 6 Hz, 3H).

Reference¹²³:

¹H NMR (400 MHz, MeOH-*d*₄): δ = 8.06 (br d, *J* = 5 Hz, 1H), 7.87 (d, *J* = 8 Hz, 2H), 7.65 (d, *J* = 8 Hz, 2H), 7.62 (d, *J* = 16 Hz, 1H), 6.55 (d, *J* = 16 Hz, 1H), 4.32 (m, 2H), 4.02 (d, *J* = 17 Hz, 1H), 3.96 (d, *J* = 17 Hz, 1H), 2.41 (t, *J* = 8 Hz, 2H), 2.15 (m, 1H), 1.96 (m, 1H), 1.64 (m, 3H), 0.92 (d, *J* = 6 Hz, 3H), 0.88 (d, *J* = 6 Hz, 3H).

Resin: Rink amide AM (80 mg; L = 0.62 mmol/g)

Purification: Semi-preparative HPLC

(C18; H₂O-MeCN + 0.05% TFA, 10 → 50% B)

HPLC (analytical): *t*_r = 9.6 min

(C18; H₂O-MeCN + 0.05% TFA, 10 → 50% B)

White amorphous solid.

Yield: 3.5 mg (7.1 μmol), 14%

C₂₃H₃₀N₄O₈ (490.2 g/mol)

ESI-MS: *m/z* calc.: 513.2 [M+Na]⁺
 m/z det.: 513.5.

7.5.3 Experiments and methods to chapter 3.4.2

Fluorescence polarization assay

In a 384-well plate serial dilutions of PTP1B and TCPTP were prepared in PBS buffer with 2 mM DTT and 0.05% Tween. The enzymes were incubated with 10 nM carboxyfluorescein labeled tracer peptides for 15 minutes at room temperature. Measurements were performed with excitation at 494 nm and collection of emission at 522 nm. Parallel and perpendicular fluorescence intensities were obtained and fluorescence polarization data were determined as ratio between parallel minus perpendicular and parallel plus perpendicular fluorescence intensity in arbitrary millipolarization units (mP). Measurements were done at least in triplicates. Dissociation constants (*K*_d) were obtained by plotting polarization against the logarithmic molar protein concentration and fitting of the resulting curve with the Kaleidagraph software using following equation:

$$y = m1 + ([m2 - m1] / [1 + 10^{(\log(m3) - x)}])$$

where *x* = the log [M] of the protein concentration, *y* = the polarization value, *m*₁ = basal signal, *m*₂ = maximal signal and *m*₃ = log [M] of the *K*_d value.

General method for the coupling of 5(6)-carboxyfluorescein to an amine group on solid support GM 7.4.6

Resin bearing a peptide with a free amine group was swelled at least for 15 minutes with DMF in a 5 mL syringe with frit. In DMF 5(6)-carboxyfluorescein (3 equiv), HATU (3 equiv), HOAt (3 equiv) and DIPEA (6 equiv) were dissolved and preactivated for 3 minutes. The solution was aspirated and coupling was allowed to proceed for 1 hour. This step was repeated 4 times.

5(6)-carboxyfluoresceinamido-Asp-Ala-Asp-Glu-F₂Pmp-Leu-NH₂ (80)

Resin: Rink amide AM (40 mg; L = 0.62 mmol/g)

Purification: Semi-preparative HPLC

(C18; H₂O-MeCN + 0.05% TFA, 10 → 75% B)

Yellow amorphous solid.

Yield: 1.6 mg (1.3 μmol), 5%.

HPLC (analytical): t_r = 9.5 min

(C18; H₂O-MeCN + 0.05% TFA, 10 → 75% B)

C₅₃H₅₆F₂N₇O₂₁P (1195.3 g/mol)

ESI-MS: *m/z* calc.: 1196.3 [M+H]⁺

m/z det.: 1195.5.

5(6)-carboxyfluoresceinamido-Ala-Ser-Gly-Ala-F₂Pmp-Ala-Gly-Gly-Ser-Ala-NH₂ (81)

Resin: Rink amide AM (80 mg; L = 0.57 mmol/g)

Purification: Semi-preparative HPLC

(C18; H₂O-MeCN + 0.05% TFA, 10 → 75% B)

Yellow amorphous solid.

Yield: 3.7 mg (2.9 μmol), 6%.

HPLC (analytical): t_r = 7.2 min

(C18; H₂O-MeCN + 0.05% TFA, 10 → 75% B)

C₅₅H₆₂F₂N₁₁O₂₁P (1281.4 g/mol)

MALDI-TOF-MS: *m/z* calc.: 1282.4 [M+H]⁺

m/z det.: 1282.5.

6-Azidohexanamido-Lys(N^ε-5(6)-carboxyfluoresceinamido)-Glu-Pro-Gln-F₂Pmp-Gln-Pro-Gly-Glu-Asn-Pra-NH₂, “K(CF)-Src-5C” (82)

Resin: Rink amide AM (40 mg; L = 0.62 mmol/g)

Purification: Semi-preparative HPLC

(C18; H₂O-MeCN + 0.05% TFA, 10 → 75% B)

Yellow amorphous solid.

Yield: 11.1 mg (5.9 μmol), 24%.

HPLC (analytical): t_r = 12.8 min

(C18; H₂O-MeCN + 0.05% TFA, 10 → 50% B)

C₈₃H₁₀₀F₂N₁₉O₂₈P (1893.7 g/mol)

ESI-MS:	<i>m/z</i>	calc.:	947.9 [M+2H] ²⁺
	<i>m/z</i>	det.:	948.2.

2-Azidoethanamido-Lys(N^ε-5(6)-carboxyfluoresceinamido)-Glu-Pro-Gln-F₂Pmp-Gln-Pro-Gly-Glu-Asn-Pra-NH₂, “K(CF)-Src-1C” (83)

Resin: Rink amide AM (40 mg; L = 0.62 mmol/g)

Purification: Semi-preparative HPLC

(C18; H₂O-MeCN + 0.05% TFA, 10 → 75% B)

Yellow amorphous solid.

Yield: 22.7 mg (12.8 μmol), 52%.

HPLC (analytical): t_r = 11.9 min

(C18; H₂O-MeCN + 0.05% TFA, 10 → 50% B)

C₇₇H₈₉F₂N₁₈O₂₇P (1780.6 g/mol)

ESI-MS:	<i>m/z</i>	calc.:	891.3 [M+2H] ²⁺
	<i>m/z</i>	det.:	891.2.

“cyclo-K(CF)-Src-5C” (84)

Was synthesized by cyclization of linear precursor peptide **82** (4.0 μmol) using the general method GM 7.4.7.

Purification: Semi-preparative HPLC

(C18; H₂O-MeCN + 0.05% TFA, 10 → 75% B)

Yellow amorphous solid.

Yield: 0.6 mg (0.3 μmol), 8%.

HPLC (analytical): t_r = 10.8 min

(C18; H₂O-MeCN + 0.05% TFA, 10 → 50% B)

C₈₃H₁₀₀F₂N₁₉O₂₈P (1893.7 g/mol)

ESI-MS:	<i>m/z</i>	calc.:	947.9 [M+2H] ²⁺
	<i>m/z</i>	det.:	948.3.

“cyclo-K(CF)-Src-1C” (85)

Was synthesized by cyclization of linear precursor peptide **83** (2.5 μ mol) using the general method GM 7.4.7.

Purification: Semi-preparative HPLC

(C18; H₂O-MeCN + 0.05% TFA, 10 \rightarrow 75% B)

Yellow amorphous solid.

Yield: 0.5 mg (0.3 μ mol), 12%.

HPLC (analytical): t_r = 10.3 min

(C18; H₂O-MeCN + 0.05% TFA, 10 \rightarrow 50% B)

C₇₇H₈₉F₂N₁₈O₂₇P (1780.6 g/mol)

ESI-MS:	<i>m/z</i>	calc.:	891.3 [M+2H] ²⁺
	<i>m/z</i>	det.:	891.2.

5(6)-carboxyfluoresceinamido-Glu-Pro-Gln-F₂Pmp-Gln-Pro-Gly-Glu-Asn-Leu-NH₂ (86)

Resin: Rink amide AM (40 mg; L = 0.62 mmol/g)

Purification: Semi-preparative HPLC

(C18; H₂O-MeCN + 0.05% TFA, 10 \rightarrow 75% B)

Yellow amorphous solid.

Yield: 4.2 mg (2.6 μ mol), 10%.

HPLC (analytical): t_r = 8.4 min

(C18; H₂O-MeCN + 0.05% TFA, 10 \rightarrow 75% B)

C₇₃H₈₇F₂N₁₄O₂₆P (1644.6 g/mol)

ESI-MS:	<i>m/z</i>	calc.:	823.3 [M+2H] ²⁺
	<i>m/z</i>	det.:	823.6.

5(6)-carboxyfluoresceinamido-Glu-Ala-Gln-F₂Pmp-Gln-Pro-Gly-Glu-Asn-Leu-NH₂ (87)

Resin: Rink amide AM (40 mg; L = 0.62 mmol/g)

Purification: Semi-preparative HPLC

(C18; H₂O-MeCN + 0.05% TFA, 10 \rightarrow 75% B)

Yellow amorphous solid.

Yield: 6.9 mg (4.3 μ mol), 17%.

HPLC (analytical): t_r = 7.7 min

(C18; H₂O-MeCN + 0.05% TFA, 10 \rightarrow 75% B)

C₇₁H₈₅F₂N₁₄O₂₆P (1618.6 g/mol)

ESI-MS: m/z calc.: 810.3 [M+2H]²⁺
 m/z det.: 810.6.

7.6.1 Experiments and methods to chapter 3.5.1

5(6)-carboxyfluoresceinamido-Glu-Pro-Gln-F₂Pmp-Gln-Pro-Gly-Glu-Asn-Leu-Arg-Arg-Arg-NH₂ (88)

Resin: Rink amide AM (40 mg; L = 0.62 mmol/g)

Purification: Semi-preparative HPLC

(C18; H₂O-MeCN + 0.05% TFA, 10 → 75% B)

Yellow amorphous solid.

Yield: 8.2 mg (3.6 μmol), 15%.

HPLC (analytical): t_r = 7.5 min

(C18; MeCN-H₂O + 0.05% TFA, 10 → 75% B)

C₉₇H₁₃₅F₂N₃₀O₃₀P (2269.0 g/mol)

ESI-MS: m/z calc.: 757.3 [M+3H]³⁺
 m/z det.: 757.8.

5(6)-carboxyfluoresceinamido-Glu-Pro-Gln-F₂Pmp-Gln-Pro-Gly-Glu-Asn-Leu-Arg-Arg-Arg-Arg-NH₂ (89)

Resin: Rink amide AM (40 mg; L = 0.62 mmol/g)

Purification: Semi-preparative HPLC

(C18; H₂O-MeCN + 0.05% TFA, 10 → 50% B)

Yellow amorphous solid.

Yield: 4.9 mg (1.9 μmol), 8%.

HPLC (analytical): t_r = 7.3 min

(C18; H₂O-MeCN + 0.05% TFA, 10 → 75% B)

C₁₀₉H₁₅₉F₂N₃₈O₃₂P (2581.2 g/mol)

ESI-MS: m/z calc.: 1291.6 [M+2H]²⁺
 m/z det.: 1292.3.

5(6)-carboxyfluoresceinamido-Glu-Pro-Gln-F₂Pmp-Gln-Pro-Gly-Glu-Asn-Leu-Arg-Arg-Arg-Arg-Arg-NH₂ (90)

Resin: Rink amide AM (40 mg; L = 0.62 mmol/g)

Purification: Semi-preparative HPLC

(C18; H₂O-MeCN + 0.05% TFA, 10 → 50% B)

Yellow amorphous solid.

Yield: 12.5 mg (4.3 μmol), 17%.

HPLC (analytical): t_r = 7.2 min

(C18; H₂O-MeCN + 0.05% TFA, 10 → 75% B)

C₁₂₁H₁₈₃F₂N₄₆O₃₄P (2893.4 g/mol)

ESI-MS:	<i>m/z</i>	calc.:	965.5 [M+3H] ³⁺
	<i>m/z</i>	det.:	965.9.

7.6.2 Experiments and methods to chapter 3.5.2

Cloning of mKate-PTP1B

Full length human PTP1B (1-435) as an N-terminal mono-EGFP fusion in a pIRES puro 3 vector (Clontech, Mountain View, USA) was a kind gift of Dr. Philippe Bastiaens (MPI, Dortmund, Germany).

A DNA fragment encoding full length PTP1B with a C-terminal *EcoRI* and an N-terminal stop codon together with a *BamHI* recognition site was generated by PCR using

5'-CCGGAATTCAATGGAGATGGAAAAGGAGTTCGAGCAGATCGACAA-3' as forward and

5'-CGCGGATCCCTATGTGTTGCTGTTGAACAGGAACCTGTA-3' as reverse primer. The fragment as well as the mKate-C1 vector (Clontech) were digested with *EcoRI* and *BamHI* and ligated together using the standard methods. The plasmid was transformed into *E.coli* (strain DH5α) using the general method and plated on agar plates containing kanamycin. Several single colonies were picked and a small amount of DNA was isolated ("minipreps"). Successful incorporation of the insert was identified by testdigestion with *EcoRI* and *BamHI* and confirmed by sequencing with the CMV primer (GATC).

Transfection of mKate-PTP1B

U2OS cells were cultured in 35 mm glass bottom dishes from MatTek (Ashland, USA). Per dish 6 μL Fugene 6 reagent was added to 94 μL Opti-MEM, the mixture was vortexed briefly and incubated for 5 minutes at room temperature. Then 1 μg of DNA was added, the mixture was vortexed briefly and incubated for 20 minutes at room temperature. The transfection mixture was added to the cell culture dish and the cells were allowed to grow for at least another 8 hours at 37°C, before the medium was removed.

5(6)-carboxyfluoresceinamido-Glu-Ala-Gln-F₂Pmp-Gln-Pro-Gly-Glu-Asn-Leu-Arg-Arg-Arg-Arg-Arg-NH₂ (91)

Resin: Rink amide AM (80 mg; L = 0.57 mmol/g)

Purification: Semi-preparative HPLC

(C18; H₂O-MeCN + 0.05% TFA, 10 → 75% B)

Yellow amorphous solid.

Yield: 7.3 mg (2.9 μmol), 6%.

HPLC (analytical): t_r = 7.4 min

(C18; H₂O-MeCN + 0.05% TFA, 10 → 75% B)

C₁₀₇H₁₅₇F₂N₃₈O₃₂P (2555.2 g/mol)

MALDI -TOF-MS:	<i>m/z</i>	calc.:	2556.2 [M+H] ⁺
	<i>m/z</i>	det.:	2556.4.

5(6)-carboxyfluoresceinamido-Glu-Pro-Gln-Tyr-Gln-Pro-Gly-Glu-Asn-Leu-Arg-Arg-Arg-Arg-Arg-Arg-NH₂ (92)

Resin: Rink amide AM (80 mg; L = 0.57 mmol/g)

Purification: Semi-preparative HPLC

(C18; H₂O-MeCN + 0.05% TFA, 10 → 50% B)

Yellow amorphous solid.

Yield: 5.0 mg (2.0 μmol), 4%.

HPLC (analytical): t_r = 9.0 min

(C18; H₂O-MeCN + 0.05% TFA, 10 → 50% B)

C₁₀₈H₁₅₈N₃₈O₃₀ (2467.2 g/mol)

Maldi-TOF-MS:	<i>m/z</i>	calc.:	2468.2 [M+H] ⁺
	<i>m/z</i>	det.:	2468.4.

7.6.3 Experiments and methods to chapter 3.5.3

Stability measurement in cell lysate

U2OS cells from two approximately 90% confluent 10 cm dishes were pelleted by treatment with trypsin and subsequent centrifugation (800 rpm, 3 minutes). The cells were lysed by incubation with 4 mL of lysis buffer (50 mM Tris-HCl, pH 7.5, 125 mM NaCl, 5% Glycerol, 1.5 mM MgCl₂, 0.2% NP-40 (Igepal CA-630), 0.5 mM PMSF and PhosSTOP phosphatase inhibitors) for 30 minutes at 4°C on a rotating wheel (10 roundings/minute). The lysate was cleared from cell debris by centrifugation (13,000 rpm, 15 minutes, 4°C).

Each peptide was diluted to a concentration of 1 mM in 50 μL of dH_2O . To these solutions 450 μL of lysate was added to reach a final peptide concentration of 100 μM . The samples were incubated at 37°C. At the respective time points 100 μL sample was removed, TCA stock solution (25 μL) was added immediately and the samples were kept on ice for 10 minutes. A white precipitate was forming, which was spinned down by centrifugation (13,000 rpm, 30 minutes, 4°C). The supernatant was removed carefully (80-100 μL each) and the samples were analyzed by HPLC (analytical C18; MeCN- H_2O + 0.05% TFA, 10 \rightarrow 50% B). Every sample was injected twice (25 μL each). The AUC of the peaks of the peptides were determined and compared. For each peptide the AUC data point 0 was normalized to 100%.

Stability measurement in human serum

Fresh human serum was obtained by taking of a blood sample from a caucasian volunteer. The blood was collected in a Serum-Monovette from Sarstedt (Nümbrecht-Rommelsdorf, Germany), incubated at room temperature for 30 minutes and the cruor was spinned down by centrifugation (2,500 rpm, 10 minutes at 4°C).

The peptides were diluted in the serum to a concentration of 100 μM (from 1 mM stock) and incubated at 37°C. As internal standard 5(6)-carboxyfluorescein was added (50 μM). At the respective time points two samples of each peptide (50 μL each) were taken, immediately frozen in liquid nitrogen and lyophilized. The dried samples were resuspended in 100 μL MeCN/ H_2O (1:1) containing 0.1% TFA. Non-dissolving material was removed by centrifugation (13,000 rpm, 20 minutes, 4°C). The samples were analyzed by HPLC (analytical C18; MeCN- H_2O + 0.05% TFA, 10 \rightarrow 75% B). The peak sizes of the peptides were determined and the value of each sample was corrected to its internal standard. The values at time point 0 were normalized to 100%.

5(6)-carboxyfluoresceinamido-Glu-Pro-Gln-Tyr-Gln-Pro-Gly-Glu-Asn-Leu-NH₂ (93)

Resin: Rink amide AM (40 mg; L = 0.57 mmol/g)

Purification: Semi-preparative HPLC

(C18; H_2O -MeCN + 0.05% TFA, 10 \rightarrow 100% B)

Yellow amorphous solid.

Yield: 0.6 mg (0.4 μmol), 2%.

HPLC (analytical): t_r = 7.3 min

(C18; H_2O -MeCN + 0.05% TFA, 10 \rightarrow 100% B)

$\text{C}_{72}\text{H}_{96}\text{N}_{14}\text{O}_{24}$ (1530.6 g/mol)

MALDI-TOF-MS: m/z calc.: 1553.6 $[\text{M}+\text{Na}]^+$

m/z det.: 1553.8.

7.7 Experiments and methods to chapter 3.6

Western blotting of proteins separated by SDS-PAGE GM 7.7.1

Protein samples were separated according to size by protein SDS-PAGE as described (GM 7.1.7) and blotted on a nitrocellulose membrane (iBlot transfer stack mini) using the iBlot machine in programme P3 (7 minute transfer). The membrane was removed from the stack, kept in transfer buffer and cut into appropriate size. The membrane was blocked in 3% BSA/TBS-T for 1 hour. The primary antibody was added in the respective dilution in 3% BSA/TBS-T and incubated over night at 4°C. The membrane was washed with TBS-T (4 x 4 minutes) and the Secondary HRP-conjugated anti-mouse antibody was added in a dilution of 1:10,000 in TBST containing 3% BSA for 45 minutes at room temperature. After another washing with TBST-T (4 x 4 minutes) Amersham ECL Western Blotting Detection reagent (GE Healthcare) was added for 1 minute at room temperature and the membrane was exposed to Amersham Hyperfilm (GE Healthcare). Exposure times varied depending on the strength of the signals. The film was developed in a Kodak RP X-OMAT processor.

Silver staining of polyacrylamide protein gels GM 7.7.2

After separation of the proteins by SDS-PAGE, the gel was submerged in aqueous fixing solution (MeOH 50%, acetic acid 5%) and incubated for 20 minutes with gentle agitation. The gel was washed first with 50% ethanol/H₂O and then 30% ethanol/H₂O for 5 minutes each, which was followed by another washing with H₂O for 10 minutes. The gel was incubated for exactly 60 seconds in an aqueous sodium thiosulfate solution (0.02%) and then again washed with H₂O (3 x 30 seconds). The gel was incubated for 20 minutes with aqueous silver solution (6 mM silver nitrate, 0.0185% formaldehyde) and washed with H₂O (3 x 30 seconds). The gel was developed with developing (Sodium carbonate 2%, formaldehyde 0.0185%, sodium thiosulfate 0.00004%) solution until saturation of the signals was reached. Development was stopped by submerging the gel in stopping solution (acetic acid 5% in H₂O).

Pull down of PTP1B using biotinylated peptides

One aliquot Streptavidin-Sepharose beads per peptide (30 μ L streptavidine bead medium (binding capacity biotin > 300 nmol/ml medium)) was washed twice with washing buffer (50 mM Tris-HCl, pH 7.5, 125 mM NaCl, 5% Glycerol, 1.5 mM MgCl₂). To remove excess of buffer the beads were spinned down at 1000 rpm for 3 minutes. The tested peptides were diluted in 400 μ L washing buffer to a concentration of 50 μ M from a 1mM stock in dH₂O. The peptide solutions were added to the beads and incubated over night at 4°C on a rotating wheel (10 roundings/minute). U2OS cells were pelleted (from two 90% confluent 10 cm dishes for less than 10 peptide samples and three dishes for more samples) by treatment with trypsin and

subsequent centrifugation (800 rpm, 3 minutes). The cells were lysed by incubation with lysis buffer (50 mM Tris-HCl, pH 7.5, 125 mM NaCl, 5% Glycerol, 1.5 mM MgCl₂, 0.2% NP-40 (Igepal CA-630), 0.5 mM PMSF and complete protease inhibitors) for 30 minutes at 4°C on a rotating wheel (10 roundings/minute). The lysate was cleared by centrifugation for 30 minutes at 13.000 rpm at 4°C. The beads were spinned down, the peptide solution was removed and the beads were washed with washing buffer (2 x) and lysis buffer (as last washing step). Each aliquot was incubated with 800 µL lysate for 2 hours at 4°C on the rotating wheel. The lysate was removed and the beads were washed twice with 800 µL lysis buffer. Excess buffer was removed completely and 30 µL SDS sample buffer (2 x) was added. The beads were boiled at 95°C for 30 minutes. As input sample 20 µL lysate 20 µL SDS sample buffer (2 x) was added and the sample was boiled for 10 minutes at 95°C.

The samples (10 µL each) were run on an SDS-PAGE as described (GM 7.1.7).

Western blotting was performed as described (GM 7.7.1). For the experiments with endogenous or recombinant PTP1B, the PTP1B antibody (FG6-1G) was used in a concentration of 2.5 µg/mL. The fusion proteins eGFP-PTP1B or eGFP-TCPTP were detected with the anti-GFP antibody (Roche) in a dilution of 1:1,000.

EGFP-PTP1B

Full length human PTP1B (1-435) as an N-terminal mono-EGFP fusion in a pIRES puro 3 vector (Clontech, Mountain View, USA) was a kind gift of Dr. Philippe Bastiaens (MPI, Dortmund, Germany).

Cloning of EGFP-TCPTP

Full length human TCPTP (48 kDa) in a pET-GST vector (Merck, Darmstadt, Germany) was a kind gift of Dr. Nickolas Tonks (CSHL, Cold spring harbor, USA).

A DNA fragment encoding amino acids 1-387 of TCPTP (45 kDa) with a C-terminal *EcoRI* and an N-terminal stop codon together with a *Sall* recognition site was generated by PCR using

5'-CCGGAATTCAATGCCACCACCATCGAGCGGGAGT-3' as forward and

5'-GCCGACGTCGACTTAAGGTTGCCAATATAACCACCTTTTTCTTTTTTCGTTTC-3' as reverse primer. The fragment as well as the pEGFP-C1 vector (Clontech) were digested with *EcoRI* and *Sall* and ligated together using the standard methods. The plasmid was transformed into *E.coli* (strain DH5α) using the general method and plated on agar plates containing kanamycin. Several single colonies were picked and a small amount of DNA was isolated ("minipreps"). Successful incorporation of the insert was identified by testdigestion with *EcorI* and *Sall* and confirmed by sequencing (GATC).

General method for the coupling of Biotin to an amine group on solid support GM 7.4.6

Resin bearing a peptide with a free amine group was swelled at least for 15 minutes with DMF in a 5 mL syringe with frit and then washed for 1 minute in NMP (3 x). D-(+)-Biotin (3 equiv), HATU (3 equiv), HOAt (3 equiv) and DIPEA (6 equiv) were dissolved in MPR and preactivated for 3 minutes. The solution was aspirated and coupling was allowed to proceed for 2 hours. This step was repeated 2 times.

6-Azidohexanamido-Lys(N^ε-biotinamido)-Glu-Pro-Gln-F₂Pmp-Gln-Pro-Gly-Glu-Asn-Pra-NH₂, “K(biotin)-Src-5C” (94)

Resin: Rink amide AM (80 mg; L = 0.62 mmol/g)

Purification: Semi-preparative HPLC

(C18; H₂O-MeCN + 0.05% TFA, 10 → 75% B)

White amorphous solid.

Yield: 14.1 mg (8.0 μmol), 16%.

HPLC (analytical): t_r = 9.5 min

(C18; H₂O-MeCN + 0.05% TFA, 10 → 75% B)

C₇₃H₁₀₆F₂N₂₁O₂₄PS (1761.7 g/mol)

ESI-MS:	<i>m/z</i>	calc.:	881.9 [M+2H] ²⁺
	<i>m/z</i>	det.:	882.4.

“cyclo-K(biotin)-Src-5C” (95)

Purification: Semi-preparative HPLC

(C18; H₂O-MeCN + 0.05% TFA, 10 → 75% B)

White amorphous solid.

Yield: 3.1 mg (1.8 μmol), 44%.

HPLC (analytical): t_r = 7.1 min

(C18; H₂O-MeCN + 0.05% TFA, 10 → 75% B)

C₇₃H₁₀₆F₂N₂₁O₂₄PS (1761.7 g/mol)

ESI-MS:	<i>m/z</i>	calc.:	881.9 [M+2H] ²⁺
	<i>m/z</i>	det.:	882.5.

Biotinamido-Glu-Ala-Gln-F₂Pmp-Gln-Pro-Gly-Glu-Asn-Leu-NH₂ (96)

Resin: Rink amide AM (80 mg; L = 0.57 mmol/g)

Purification: Semi-preparative HPLC

(C18; H₂O-MeCN + 0.05% TFA, 10 → 50% B)

White amorphous solid.

Yield: 17.8 mg (12.0 μ mol), 26%.

HPLC (analytical): t_r = 7.7 min

(C18; H₂O-MeCN + 0.05% TFA, 10 \rightarrow 50% B)

C₆₀H₈₉F₂N₁₆O₂₂PS (1486.6 g/mol)

MALDI-TOF-MS:	<i>m/z</i>	calc.:	1509.6 [M+Na] ⁺
	<i>m/z</i>	det.:	1509.7.

Biotinamido-Glu-Ala-Gln-Tyr-Gln-Pro-Gly-Glu-Asn-Leu-NH₂ (97)

Resin: Rink amide AM (80 mg; L = 0.57 mmol/g)

Purification: Semi-preparative HPLC

(C18; H₂O-MeCN + 0.05% TFA, 10 \rightarrow 50% B)

White amorphous solid.

Yield: 13.8 mg (9.9 μ mol), 22%.

HPLC (analytical): t_r = 8.7 min

(C18; H₂O-MeCN + 0.05% TFA, 10 \rightarrow 50% B)

C₆₁H₉₀N₁₆O₂₀S (1398.6 g/mol)

ESI-MS:	<i>m/z</i>	calc.:	1421.6 [M+Na] ⁺
	<i>m/z</i>	det.:	1421.7.

Biotinamido-Asp-Ala-Asp-Glu-F₂Pmp-Leu-NH₂ (98)

Resin: Rink amide AM (40 mg; L = 0.62 mmol/g)

Purification: Semi-preparative HPLC

(C18; H₂O-MeCN + 0.05% TFA, 10 \rightarrow 75% B)

White amorphous solid.

Yield: 7.7 mg (7.2 μ mol), 29%.

HPLC (analytical): t_r = 6.9 min

(C18; H₂O-MeCN + 0.05% TFA, 10 \rightarrow 75% B)

C₄₂H₆₀F₂N₉O₁₇PS (1063.4 g/mol)

ESI-MS:	<i>m/z</i>	calc.:	1062.4 [M-H] ⁻
	<i>m/z</i>	det.:	1062.6.

2-Azidoethanamido-Lys(N^ε-biotinamido)-Glu-Pro-Gln-F₂Pmp-Gln-Pro-Gly-Glu-Asn-Pra-NH₂, "K(biotin)-Src-1C" (99)

Resin: Rink amide AM (80 mg; L = 0.57 mmol/g)

Purification: Preparative HPLC

(C18; H₂O-MeCN + 0.05% TFA, 10 → 50% B)

White amorphous solid.

Yield: 7.5 mg (4.5 μmol), 10%.

HPLC (analytical): t_r = 8.8 min

(C18; H₂O-MeCN + 0.05% TFA, 10 → 50% B)

C₆₇H₉₅F₂N₂₀O₂₃PS (1648.6 g/mol)

ESI-MS:	<i>m/z</i>	calc.:	825.3 [M+2H] ²⁺
	<i>m/z</i>	det.:	825.9.

“cyclo-K(biotin)-Src-1C” (100)

Purification: Preparative HPLC

(C18; H₂O-MeCN + 0.05% TFA, 10 → 50% B)

White amorphous solid.

Yield: 2.1 mg (1.3 μmol), 54%.

HPLC (analytical): t_r = 7.1 min

(C18; H₂O-MeCN + 0.05% TFA, 10 → 50% B)

C₆₇H₉₅F₂N₂₀O₂₃PS (1648.6 g/mol)

ESI-MS:	<i>m/z</i>	calc.:	825.3 [M+2H] ²⁺
	<i>m/z</i>	det.:	825.3.

Ac-Lys(N^ε-biotinamido)-Glu-Ala-Gln-Tyr-Gln-Pro-Gly-Glu-Asn-Leu-NH₂ (101)

Resin: Rink amide AM (40 mg; L = 0.57 mmol/g)

Purification: Preparative HPLC

(C18; H₂O-MeCN + 0.05% TFA, 10 → 50% B)

White amorphous solid.

Yield: 7.4 mg (4.5 μmol), 20%.

HPLC (analytical): t_r = 8.1 min

(C18; H₂O-MeCN + 0.05% TFA, 10 → 50% B)

C₆₈H₁₀₃F₂N₁₈O₂₄PS (1656.7 g/mol)

ESI-MS:	<i>m/z</i>	calc.:	829.4 [M+2H] ²⁺
	<i>m/z</i>	det.:	829.6.

Ac-Lys(N^ε-biotinamido)-Asp-Ala-Asp-Glu-F2Pmp-Leu-NH₂ (102)

Resin: Rink amide AM (40 mg; L = 0.57 mmol/g)

Purification: Preparative HPLC

(C18; H₂O-MeCN + 0.05% TFA, 10 → 50% B)

White amorphous solid.

Yield: 4.5 mg (3.6 μmol), 16%.

HPLC (analytical): t_r = 8.8 min

(C18; MeCN-H₂O + 0.05% TFA, 10 → 50% B)

C₅₀H₇₄F₂N₁₁O₁₉PS (1233.5 g/mol)

ESI-MS: *m/z* calc.: 617.8 [M+2H]²⁺

m/z det.: 617.6.

Biotinamido-Glu-Pro-Gln-F₂Pmp-Gln-Pro-Gly-Glu-Asn-Leu-NH₂ (103)

Resin: Rink amide AM (40 mg; L = 0.57 mmol/g)

Purification: Semi-preparative HPLC

(C18; H₂O-MeCN + 0.05% TFA, 10 → 50% B)

White amorphous solid.

Yield: 6.0 mg (4.0 μmol), 18%.

HPLC (analytical): t_r = 8.0 min

(C18; H₂O-MeCN + 0.05% TFA, 10 → 50% B)

C₆₂H₉₁F₂N₁₆O₂₂PS (1512.6 g/mol)

ESI-MS: *m/z* calc.: 757.3 [M+2H]²⁺

m/z det.: 757.5.

Ac-Lys((N^ε-biotinamido)-Glu-Pro-Gln-F₂Pmp-Gln-Pro-Gly-Glu-Asn-Leu-NH₂) (104)

Resin: Rink amide AM (40 mg; L = 0.57 mmol/g)

Purification: Semi-preparative HPLC

(C18; H₂O-MeCN + 0.05% TFA, 10 → 50% B)

White amorphous solid.

Yield: 5.7 mg (3.4 μmol), 15%.

HPLC (analytical): t_r = 9.1 min

(C18; H₂O-MeCN + 0.05% TFA, 10 → 50% B)

C₇₀H₁₀₅F₂N₁₈O₂₄PS (1682.7 g/mol)

MALDI-TOF-MS: *m/z* calc.: 842.4 [M+2H]²⁺

m/z det.: 842.6.

**6-Azidohexanamido-Lys(N^ε-biotinamido)-Glu-Pro-Gln-Tyr-Gln-Pro-Gly-Glu-Asn-Pra-NH₂,
“K(biotin)-Src-(Y)-5C” (110)**

Resin: Rink amide AM (80 mg; L = 0.62 mmol/g)

Purification: Preparative HPLC

(C18; H₂O-MeCN + 0.05% TFA, 10 → 50% B)

White amorphous solid.

Yield: 12.1 mg (7.3 μmol), 16%.

HPLC (analytical): t_r = 10.6 min

(C18; H₂O-MeCN + 0.05% TFA, 10 → 50% B)

C₇₂H₁₀₅N₂₁O₂₂S (1647.8 g/mol)

ESI-MS: *m/z* calc.: 824.9 [M+2H]²⁺
 m/z det.: 825.4.

“cyclo-K(biotin)-Src-(Y)-5C” (105)

Was synthesized by cyclization of linear precursor peptide **110** (2.4 μmol) using the general method GM 7.4.7.

Purification: Semi-preparative HPLC

(C18; H₂O-MeCN + 0.05% TFA, 10 → 50% B)

White amorphous solid.

Yield: 1.5 mg (0.9 μmol), 38%.

HPLC (analytical): t_r = 8.5 min

(C18; H₂O-MeCN + 0.05% TFA, 10 → 50% B)

C₇₂H₁₀₅N₂₁O₂₂S (1647.8 g/mol)

ESI-MS: *m/z* calc.: 824.9 [M+2H]²⁺
 m/z det.: 825.0.

**2-Azidoethanamido-Lys(N^ε-biotinamido)-Glu-Pro-Gln-Tyr-Gln-Pro-Gly-Glu-Asn-Pra-NH₂,
“K(biotin)-Src-(Y)-1C” (111)**

Resin: Rink amide AM (80 mg; L = 0.57 mmol/g)

Purification: Preparative HPLC

(C18; H₂O-MeCN + 0.05% TFA, 10 → 50% B)

White amorphous solid.

Yield: 16.4 mg (10.7 μmol), 24%.

HPLC (analytical): t_r = 9.4 min

(C18; H₂O-MeCN + 0.05% TFA, 10 → 50% B)

$C_{66}H_{94}N_{20}O_{21}S$ (1534.7 g/mol)

ESI-MS: m/z calc.: 768.4 $[M+2H]^{2+}$
 m/z det.: 768.8.

“cyclo-K(biotin)-Src-(Y)-1C” (106)

Was synthesized by cyclization of linear precursor peptide **111** (2.4 μ mol) using the general method GM 7.4.7.

Purification: Semi-preparative HPLC

(C18; H_2O -MeCN + 0.05% TFA, 10 \rightarrow 50% B)

White amorphous solid.

Yield: 1.6 mg (1.0 μ mol), 42%.

HPLC (analytical): t_r = 9.5 min

(C18; H_2O -MeCN + 0.05% TFA, 10 \rightarrow 50% B)

$C_{66}H_{94}N_{20}O_{21}S$ (1534.7 g/mol)

ESI-MS: m/z calc.: 768.4 $[M+2H]^{2+}$
 m/z det.: 768.3.

Ac-Lys(N^ε-5(6)carboxyfluoresceinamido)-Glu-Pro-Gln-F₂Pmp-Gln-Pro-Gly-Glu-Asn-Leu-NH₂ (107)

Resin: Rink amide AM (80 mg; L = 0.57 mmol/g)

Purification: Preparative HPLC

(C18; H_2O -MeCN + 0.05% TFA, 10 \rightarrow 60% B)

Yellow amorphous solid.

Yield: 5.7 mg (3.1 μ mol), 7%.

HPLC (analytical): t_r = 9.9 min

(C18; H_2O -MeCN + 0.05% TFA, 10 \rightarrow 60% B)

$C_{81}H_{101}F_2N_{16}O_{28}P$ (1814.7 g/mol)

ESI-MS: m/z calc.: 908.4 $[M+2H]^{2+}$
 m/z det.: 909.3.

Ac-Lys(N^ε-5(6)carboxyfluoresceinamido)-Glu-Ala-Gln-F₂Pmp-Gln-Pro-Gly-Glu-Asn-Leu-NH₂ (108)

Resin: Rink amide AM (40 mg; L = 0.57 mmol/g)

Purification: Preparative HPLC

(C18; H_2O -MeCN + 0.05% TFA, 10 \rightarrow 60% B)

Yellow amorphous solid.

Yield: 2.8 mg (1.6 μ mol), 7%.

HPLC (analytical): t_r = 9.7 min

(C18; H₂O-MeCN + 0.05% TFA, 10 \rightarrow 60% B)

C₇₉H₉₉F₂N₁₆O₂₈P (1788.7 g/mol)

ESI-MS: m/z calc.: 895.4 [M+2H]²⁺
 m/z det.: 895.3.

Ac-Lys(N^ε-5(6)carboxyfluoresceinamido)-Asp-Ala-Asp-Glu-F₂Pmp-Leu-NH₂ (109)

Resin: Rink amide AM (40 mg; L = 0.57 mmol/g)

Purification: Preparative HPLC

(C18; H₂O-MeCN + 0.05% TFA, 10 \rightarrow 60% B)

Yellow amorphous solid.

Yield: 2.1 mg (1.5 μ mol), 7%.

HPLC (analytical): t_r = 10.6 min

(C18; H₂O-MeCN + 0.05% TFA, 10 \rightarrow 60% B)

C₆₁H₇₀F₂N₉O₂₃P (1365.4 g/mol)

ESI-MS: m/z calc.: 683.7 [M+2H]²⁺
 m/z det.: 684.2.

8 References

1. Alberts, B., Johnson, A., Lewis, J., Raff, M., Roberts, K. and W.P. *Molecular biology of the cell, 4th edition.* (2002).
2. Hunter, T. Signaling - 2000 and beyond. *Cell* **100**, 113-27 (2000).
3. Fischer, E. Einfluss der Configuration auf die Wirkung der Enzyme. *Ber. Dtsch. Chem. Ges.* **27**, 2985-93 (1894).
4. Lichtenthaler, F.W. 100 Years "Schlüssel-Schloss-Prinzip": What made Emil Fischer use this analogy? *Angew. Chem. Int. Edit.* **33**, 2364–74 (1995).
5. Krebs, E.G. and Beavo, J.A. Phosphorylation-dephosphorylation of enzymes. *Ann. Rev. Biochem.* **48**, 923–59 (1979).
6. Olsen, J.V. et al. Global, in vivo, and site-specific phosphorylation dynamics in signaling networks. *Cell* **127**, 635-48 (2006).
7. Hunter, T. Protein kinases and phosphatases: the yin and yang of protein phosphorylation and signaling. *Cell* **80**, 225-36 (1995).
8. Blume-Jensen, P. and Hunter, T. Oncogenic kinase signalling. *Nature* **411**, 355-65 (2001).
9. Buchdunger, E. et al. Inhibition of the Abl protein-tyrosine kinase *in vitro* and *in vivo* by a 2-Phenylaminopyrimidine derivative. *Cancer Res.* **56**, 100-4 (1996).
10. Carroll, M. et al. CGP 57148, a tyrosine kinase inhibitor, inhibits the growth of cells expressing BCR-ABL, TEL-ABL, and TEL-PDGFR fusion proteins. *Blood* **90**, 4947-52 (1997).
11. Deininger, M.W., Goldman, J.M., Lydon, N. and Melo, J.V. The tyrosine kinase inhibitor CGP57148B selectively inhibits the growth of BCR-ABL-positive cells. *Blood* **90**, 3691-8 (1997).
12. Moen, M.D., McKeage, K., Plosker, G.L. and Siddiqui, M.A.A. Imatinib: A review of its use in chronic myeloid leukaemia. *Drugs* **67**, 299-320 (2007).
13. Hanks, S.K., Quinn, A.M. and Hunter, T. The protein kinase family: conserved features and deduced phylogeny of the catalytic domains. *Science* **241**, 42-52 (1988).
14. Hanks, S.K. and Hunter, T. Protein kinases 6. The eukaryotic protein kinase superfamily: kinase (catalytic) domain structure and classification. *Faseb J.* **9**, 576-96 (1995).
15. Tonks, N.K. Protein tyrosine phosphatases: from genes, to function, to disease. *Nat. Rev. Mol. Cell. Biol.* **7**, 833-46 (2006).
16. Wera, S. and Hemmings, B. Serine/threonine protein phosphatases. *Biochem. J.* **311**, 17-29 (1995).
17. Alonso, A. et al. Protein tyrosine phosphatases in the human genome. *Cell* **117**, 699-711 (2004).
18. Alonso Rojas, A., Godzik, A. and Mustelin, T.A. The dual-specific protein tyrosine phosphatase family. *Top. Curr. Gen.* **5**, 333-58 (2004).
19. Andersen, J. and Mortensen, O. Structural and evolutionary relationships among protein tyrosine phosphatase domains. *Mol. Cell. Biol.* **21**, 7117-36 (2001).
20. Felberg, J. and Johnson, P. Characterization of recombinant CD45 cytoplasmic domain proteins. *Biochem.* **273**, 17839-45 (1998).

21. Blanchetot, C., Tertoolen, L.G., Overvoorde, J. and den Hertog, J. Intra- and intermolecular interactions between intracellular domains of receptor protein-tyrosine phosphatases. *J. Biol. Chem.* **277**, 47263-9 (2002).
22. Jiang, G., den Hertog, J. and Hunter, T. Receptor-like protein tyrosine phosphatase α homodimerizes on the cell surface. *Mol. Cell. Biol.* **20**, 5917-29 (2000).
23. Neel, B.G., Gu, H. and Pao, L. The 'Shp'ing news: SH2 domain-containing tyrosine phosphatases in cell signaling. *Trends Biochem. Sci.* **28**, 284-93 (2003).
24. Frangioni, J.V., Beahm, P.H., Shifrin, V., Jost, C.A. and Neel, B.G. The nontransmembrane tyrosine phosphatase PTP-1B localizes to the endoplasmic reticulum via its 35 amino acid C-terminal sequence. *Cell* **68**, 545-60 (1992).
25. Bottini, N., Bottini, A., Gloria-Bottini, F. and Mustelin, T. LMPTP and human disease: in search of biochemical mechanisms. *Arch. Immunol. Ther. Exp.* **50**, 95-104 (2002).
26. Tootle, T.L. *et al.* The transcription factor Eyes absent is a protein tyrosine phosphatase. *Nature* **426**, 299-302 (2003).
27. Rayapureddi, J.P. *et al.* Eyes absent represents a class of protein tyrosine phosphatases. *Nature* **426**, 295-8 (2003).
28. Li, X. *et al.* Eya protein phosphatase activity regulates Six1-Dach-Eya transcriptional effects in mammalian organogenesis. *Nature* **426**, 247-54 (2003).
29. Denu, J.M., Zhou, G., Guo, Y. and Dixon, J.E. The catalytic role of aspartic acid-92 in a human dual-specific protein-tyrosine-phosphatase. *Biochem.* **34**, 3396-3403 (1995).
30. Lohse, D.L., Denu, J.M., Santoro, N. and Dixon, J.E. Roles of aspartic acid-181 and serine-222 in intermediate formation and hydrolysis of the mammalian protein-tyrosine-phosphatase PTP1. *Biochem.* **36**, 4568-75 (1997).
31. Zhang, Z.Y. and Dixon, J.E. Active site labeling of the Yersinia protein tyrosine phosphatase: The determination of the pKa of the active site cysteine and the function of the conserved histidine 402. *Biochem.* **32**, 9340-5 (1993).
32. Zhang, Z.Y. Protein-tyrosine phosphatases: biological function, structural characteristics, and mechanism of catalysis. *Cr. Rev. Bioch. Mol. Biol.* **33**, 1-52 (1998).
33. Zhou, G., Denu, J.M., Wu, L. and Dixon, J.E. The catalytic role of Cys124 in the dual specificity phosphatase VHR. *J. Biol. Chem.* **269**, 28084-90 (1994).
34. Guan, K.L. and Dixon, J.E. Evidence for protein-tyrosine-phosphatase catalysis proceeding via a cysteine-phosphate intermediate. *J. Biol. Chem.* **266**, 17026-30 (1991).
35. Den Hertog, J., Groen, A. and van der Wijk, T. Redox regulation of protein-tyrosine phosphatases. *Arch. Biochem. Biophys.* **434**, 11-15 (2005).
36. Salmeen, A. and Barford, D. Functions and mechanisms of redox regulation of cysteine-based phosphatases. *Antioxid. Redox. Sign.* **7**, 560-77 (2005).
37. Ostman, A., Frijhoff, J., Sandin, A. and Böhmer, F.D. Regulation of protein tyrosine phosphatases by reversible oxidation. *J. Biochem.* **150**, 345-56 (2011).
38. Lee, S.R., Kwon, K.S., Kim, S.R. and Rhee, S.G. Reversible inactivation of protein-tyrosine phosphatase 1B in A431 cells stimulated with epidermal growth factor. *J. Biol. Chem.* **273**, 15366-72 (1998).
39. Rhee, S.G. *et al.* Intracellular messenger function of hydrogen peroxide and its regulation by peroxiredoxins. *Curr. Opin. Cell. Biol.* **17**, 183-9 (2005).
40. Salmeen, A. *et al.* Redox regulation of protein tyrosine phosphatase 1B involves a sulphenyl-amide intermediate. *Nature* **423**, 769-73 (2003).
41. Ostman, A., Hellberg, C. and Böhmer, F.D. Protein-tyrosine phosphatases and cancer. *Nat. Rev. Cancer* **6**, 307-20 (2006).

42. Kristjansdottir, K. and Rudolph, J. Cdc25 phosphatases and cancer. *Chem. Biol.* **11**, 1043–51 (2004).
43. Saha, S. *et al.* A phosphatase associated with metastasis of colorectal cancer. *Science* **294**, 1343-6 (2001).
44. McParland, V. *et al.* The metastasis-promoting phosphatase PRL-3 shows activity toward phosphoinositides. *Biochem.* **50**, 7579-90 (2011).
45. Saarikangas, J. and Zhao, H. Regulation of the actin cytoskeleton-plasma membrane interplay by phosphoinositides. *Physiol. Rev.* **90**, 259-89 (2010).
46. Cully, M., You, H., Levine, A.J. and Mak, T.W. Beyond PTEN mutations: the PI3K pathway as an integrator of multiple inputs during tumorigenesis. *Nat. Rev. Cancer* **6**, 184-92 (2006).
47. Tonks, N.K., Diltz, C.D. and Fischer, E.H. Purification of the major protein-tyrosine-phosphatases of human placenta. *J. Biol. Chem.* **263**, 6722-30 (1988).
48. Tonks, N.K., Diltz, C.D. and Fischer, E.H. Characterization of the major protein-tyrosine-phosphatases of human placenta. *J. Biol. Chem.* **263**, 6731-7 (1988).
49. Cool, D.E. *et al.* cDNA isolated from a human T-cell library encodes a member of the protein-tyrosine-phosphatase family. *P. Natl. A. Sci. USA* **86**, 5257-61 (1989).
50. Brown-Shimer, S. *et al.* Molecular cloning and chromosome mapping of the human gene encoding protein phosphotyrosyl phosphatase 1B. *P. Natl. A. Sci. USA* **87**, 5148-52 (1990).
51. Frangioni, J.V., Oda, A., Smith, M., Salzman, E.W. and Neel, B.G. Calpain-catalyzed cleavage and subcellular relocation of protein phosphotyrosine phosphatase 1B (PTP-1B) in human platelets. *EMBO J.* **12**, 4843-56 (1993).
52. Flint, A.J., Gebbink, M.F., Franza, B.R., Hill, D.E. and Tonks, N.K. Multi-site phosphorylation of the protein tyrosine phosphatase, PTP1B: identification of cell cycle regulated and phorbol ester stimulated sites of phosphorylation. *EMBO J.* **12**, 1937-46 (1993).
53. Barford, D., Flint, A.J. and Tonks, N.K. Crystal structure of human protein tyrosine phosphatase 1B. *Science* **263**, 1397-404 (1994).
54. Denu, J.M. and Dixon, J.E. Protein tyrosine phosphatases: mechanisms of catalysis and regulation. *Curr. Opin. Chem. Biol.* **2**, 633-41 (1998).
55. Denu, J.M. and Tanner, K.G. Specific and reversible inactivation of protein tyrosine phosphatases by hydrogen peroxide: evidence for a sulfenic acid intermediate and implications for redox regulation. *Biochem.* **37**, 5633-42 (1998).
56. Jia, Z., Barford, D., Flint, A.J. and Tonks, N.K. Structural basis for phosphotyrosine peptide recognition by protein tyrosine phosphatase 1B. *Science* **268**, 1754-8 (1995).
57. Puius, Y.A. *et al.* Identification of a second aryl phosphate-binding site in protein-tyrosine phosphatase 1B: a paradigm for inhibitor design. *P. Natl. A. Sci. USA* **94**, 13420-5 (1997).
58. Salmeen, A., Andersen, J.N., Myers, M.P., Tonks, N.K. and Barford, D. Molecular basis for the dephosphorylation of the activation segment of the insulin receptor by protein tyrosine phosphatase 1B. *Mol. Cell* **6**, 1401-12 (2000).
59. Flint, A.J., Tiganis, T., Barford, D. and Tonks, N.K. Development of “substrate-trapping” mutants to identify physiological substrates of protein tyrosine phosphatases. *P. Natl. A. Sci. USA* **94**, 1680-5 (1997).
60. Stuible, M. and Tremblay, M.L. In control at the ER: PTP1B and the down-regulation of RTKs by dephosphorylation and endocytosis. *Trends Cell. Biol.* **20**, 672-9 (2010).
61. Wälchli, S., Curchod, M.L., Gobert, R.P., Arkinstall, S. and Hooft van Huijsduijnen, R. Identification of tyrosine phosphatases that dephosphorylate the insulin receptor.

- A brute force approach based on "substrate-trapping" mutants. *J. Biol. Chem.* **275**, 9792-6 (2000).
62. Elchebly, M. et al. Increased insulin sensitivity and obesity resistance in mice lacking the protein tyrosine phosphatase-1B gene. *Science* **283**, 1544-8 (1999).
63. Klamon, L.D. et al. Increased energy expenditure, decreased adiposity, and tissue-specific insulin sensitivity in protein tyrosine phosphatase 1B-deficient mice. *Mol. Cell. Biol.* **20**, 5479-89 (2000).
64. Bence, K.K. et al. Neuronal PTP1B regulates body weight, adiposity and leptin action. *Nat. Med.* **12**, 917-24 (2006).
65. Ahima, R.S. and Osei, S.Y. Leptin signaling. *Physiol. Behav.* **81**, 223-41 (2004).
66. Galic, S. et al. Coordinated regulation of insulin signaling by the protein tyrosine phosphatases PTP1B and TCPTP. *Mol. Cell. Biol.* **25**, 819-29 (2005).
67. Haj, F.G., Markova, B., Klamon, L.D., Bohmer, F.D. and Neel, B.G. Regulation of receptor tyrosine kinase signaling by protein tyrosine phosphatase-1B. *J. Biol. Chem.* **278**, 739-44 (2003).
68. Dubé, N., Cheng, A. and Tremblay, M.L. The role of protein tyrosine phosphatase 1B in Ras signaling. *P. Natl. A. Sci. USA* **101**, 1834-9 (2004).
69. Buckley, D., Cheng, A. and Kiely, P. Regulation of insulin-like growth factor type I (IGF-I) receptor kinase activity by protein tyrosine phosphatase 1B (PTP-1B) and enhanced IGF-I-mediated suppression of apoptosis and motility in PTP-1B-deficient fibroblasts. *Mol. Cell. Biol.* **22**, 1998-2010 (2002).
70. Liu, F., Sells, M.A. and Chernoff, J. Transformation suppression by protein tyrosine phosphatase 1B requires a functional SH3 ligand. *Mol. Cell. Biol.* **18**, 250-9 (1998).
71. Lammers, R. et al. Differential activities of protein tyrosine phosphatases in intact cells. *J. Biol. Chem.* **268**, 22456-62 (1993).
72. Boute, N., Boubekeur, S., Lacasa, D. and Issad, T. Dynamics of the interaction between the insulin receptor and protein tyrosine-phosphatase 1B in living cells. *EMBO Rep.* **4**, 313-9 (2003).
73. Romsicki, Y., Reece, M., Gauthier, J.-Y., Asante-Appiah, E. and Kennedy, B.P. Protein tyrosine phosphatase-1B dephosphorylation of the insulin receptor occurs in a perinuclear endosome compartment in human embryonic kidney 293 cells. *J. Biol. Chem.* **279**, 12868-75 (2004).
74. Schmidt-Arras, D. and Bohmer, A. Tyrosine phosphorylation regulates maturation of receptor tyrosine kinases. *Mol. Cell. Biol.* **25**, 3690-703 (2005).
75. Choudhary, C. et al. Mislocalized activation of oncogenic RTKs switches downstream signaling outcomes. *Mol. Cell* **36**, 326-39 (2009).
76. Anderie, I., Schulz, I. and Schmid, A. Direct interaction between ER membrane-bound PTP1B and its plasma membrane-anchored targets. *Cell. Sign.* **19**, 582-92 (2007).
77. Faures, R., Baquiran, G., Bergerons, J.J.M. and Posner, B.I. The dephosphorylation of insulin and epidermal growth factor receptors. Role of endosome-associated phosphotyrosine phosphatase(s). *J. Biol. Chem.* **267**, 11215-21 (1992).
78. Haj, F.G., Verveer, P.J., Squire, A., Neel, B.G. and Bastiaens, P.I.H. Imaging sites of receptor dephosphorylation by PTP1B on the surface of the endoplasmic reticulum. *Science* **295**, 1708-11 (2002).
79. Yudushkin, I.A. et al. Live-cell imaging of enzyme-substrate interaction reveals spatial regulation of PTP1B. *Science* **315**, 115-9 (2007).
80. Chen, K., Kirber, M.T., Xiao, H., Yang, Y. and Keaney, J.F. Regulation of ROS signal transduction by NADPH oxidase 4 localization. *J. Cell. Biol.* **181**, 1129-39 (2008).

81. Eden, E.R., White, I.J., Tsapara, A. and Futter, C.E. Membrane contacts between endosomes and ER provide sites for PTP1B-epidermal growth factor receptor interaction. *Nature Cell. Biol.* **12**, 267-72 (2010).
82. Woodford-Thomas, T.A., Rhodes, J.D. and Dixon, J.E. Expression of a protein tyrosine phosphatase in normal and v-src transformed mouse 313 fibroblasts. *J. Cell. Biol.* **117**, 401-14 (1992).
83. Brown-Shimer, S., Johnson, K.A., Hill, D.E. and Bruskin, A.M. Effect of protein tyrosine phosphatase 1B expression on transformation by the human neu oncogene. *Cancer Res.* **52**, 478-82 (1992).
84. LaMontagne, K.R., Hannon, G. and Tonks, N.K. Protein tyrosine phosphatase PTP1B suppresses p210 Bcr-Abl-induced transformation of rat-1 fibroblasts and promotes differentiation of K562 cells. *P. Natl. A. Sci. USA* **95**, 14094-9 (1998).
85. Arregui, C.O., Balsamo, J. and Lilien, J. Impaired integrin-mediated adhesion and signaling in fibroblasts expressing a dominant-negative mutant PTP1B. *J. Cell. Biol.* **143**, 861-73 (1998).
86. Gu, F. *et al.* Protein-tyrosine phosphatase 1B potentiates IRE1 signaling during endoplasmic reticulum stress. *J. Biol. Chem.* **279**, 49689-93 (2004).
87. Yip, S.-C., Saha, S. and Chernoff, J. PTP1B: a double agent in metabolism and oncogenesis. *Trends Biochem. Sci.* **35**, 442-9 (2010).
88. Wiener, J.R. *et al.* Overexpression of the tyrosine phosphatase PTP1B is associated with human ovarian carcinomas. *Am. J. Obstet. Gynecol.* **170**, 1177-83 (1994).
89. Wiener, J.R. *et al.* Overexpression of the protein tyrosine phosphatase PTP1B in human breast cancer: association with p185c-ErbB2 protein expression. *J. Natl. Cancer I.* **86**, 372-8 (1994).
90. Julien, S.G. *et al.* Protein tyrosine phosphatase 1B deficiency or inhibition delays ErbB2-induced mammary tumorigenesis and protects from lung metastasis. *Nature Gen.* **39**, 338-46 (2007).
91. Bentires-Alj, M. and Neel, B.G. Protein-tyrosine phosphatase 1B is required for HER2/Neu-induced breast cancer. *Cancer Res.* **67**, 2420-4 (2007).
92. Arias-Romero, L.E. *et al.* Activation of Src by protein tyrosine phosphatase 1B is required for ErbB2 transformation of human breast epithelial cells. *Cancer Res.* **69**, 4582-8 (2009).
93. Cortesio, C.L. *et al.* Calpain 2 and PTP1B function in a novel pathway with Src to regulate invadopodia dynamics and breast cancer cell invasion. *J. Cell. Biol.* **180**, 957-71 (2008).
94. Zhang, S. and Zhang, Z.Y. PTP1B as a drug target: recent developments in PTP1B inhibitor discovery. *Drug Discov Today* **12**, 373-81 (2007).
95. Vintonyak, V.V., Antonchick, A.P., Rauh, D. and Waldmann, H. The therapeutic potential of phosphatase inhibitors. *Curr. Opin. Chem. Biol.* **13**, 272-83 (2009).
96. Huyer, G. *et al.* Mechanism of inhibition of protein-tyrosine phosphatases by vanadate and pervanadate. *J. Biol. Chem.* **272**, 843-51 (1997).
97. McLauchlan, C.C. *et al.* Inhibition of acid, alkaline, and tyrosine (PTP1B) phosphatases by novel vanadium complexes. *J. Inorg. Biochem.* **104**, 274-81 (2010).
98. Liotta, A.S., Kole, H.K., Fales, H.M., Roth, J. and Bernier, M. A synthetic trisulfotyrosyl dodecapeptide analogue of the insulin receptor 1146-kinase domain inhibits tyrosine dephosphorylation of the insulin receptor *in situ*. *J. Biol. Chem.* **269**, 22996-3001 (1994).
99. Hiriyanna, K.T., Buck, W.R., Shen, S.S. and Ingebritsen, T.S. Thiophosphorylated RCM-lysozyme, an active site-directed protein tyrosine phosphatase inhibitor, inhibits

- G2/M transition during mitotic cell cycle and uncouples MPF activation from G2/M transition. *Exp. Cell. Res.* **216**, 21-29 (1995).
100. Jenkins, K.E., Higson, A.P., Seeberger, P.H. and Caruthers, M.H. Solid-phase synthesis and biochemical studies of O-boranophosphopeptides and O-dithiophosphopeptides. *J. Am. Chem. Soc.* **124**, 6584-93 (2002).
 101. Marseigne, I. and Roques, B.P. Synthesis of new amino acids mimicking sulfated and phosphorylated tyrosine residues. *J. Org. Chem.* **53**, 3621-4 (1988).
 102. Kole, H.K. *et al.* Protein-tyrosine phosphatase inhibition by a peptide containing the phosphotyrosyl mimetic, L-O-malonyltyrosine (L-OMT). *Biochem. Biophys. Res. Co.* **209**, 817-22 (1995).
 103. Burke, T.R. *et al.* 4'-O-[2-(2-fluoromalonyl)]-L-tyrosine: A phosphotyrosyl mimic for the preparation of signal transduction inhibitory peptides. *J. Med. Chem.* **39**, 1021-7 (1996).
 104. Burke, T.R., Kole, H.K. and Roller, P.P. Potent inhibition of insulin receptor dephosphorylation by a hexamer peptide containing the phosphotyrosyl mimetic F₂Pmp. *Biochem. Biophys. Res. Co.* **204**, 129-34 (1994).
 105. Chen, L. *et al.* Why is phosphonodifluoromethylphenylalanine a more potent inhibitory moiety than phosphonomethylphenylalanine toward protein-tyrosine phosphatases. *Biochem. Biophys. Res. Co.* **216**, 976-84 (1995).
 106. Combs, A.P. *et al.* Structure-based design and discovery of protein tyrosine phosphatase inhibitors incorporating novel isothiazolidinone heterocyclic phosphotyrosine mimetics. *J. Med. Chem.* **48**, 6544-8 (2005).
 107. Ala, P.J. *et al.* Structural basis for inhibition of protein-tyrosine phosphatase 1B by isothiazolidinone heterocyclic phosphonate mimetics. *J. Biol. Chem.* **281**, 32784-95 (2006).
 108. Schmidt, M.F., Groves, M.R. and Rademann, J. Dynamic substrate enhancement for the identification of specific, second-site-binding fragments targeting a set of protein tyrosine phosphatases. *ChemBioChem* **12**, 2640-46 (2011).
 109. Akamatsu, M. *et al.* Potent inhibition of protein-tyrosine phosphatase by phosphotyrosine-mimic containing cyclic peptides. *Bioorg. Med. Chem.* **5**, 157-63 (1997).
 110. Huyer, G. *et al.* Affinity Selection from Peptide Libraries to Determine Substrate Specificity of Protein Tyrosine Phosphatases. *Anal. Biochem.* **258**, 19-30 (1998).
 111. Pellegrini, M. C. *et al.* Mapping the subsite preferences of protein tyrosine phosphatase PTP-1B using combinatorial chemistry approaches. *Biochem.* **37**, 15598-606 (1998).
 112. Espanel, X. & Hooft van Huijsduijnen, R. Applying the SPOT peptide synthesis procedure to the study of protein tyrosine phosphatase substrate specificity: probing for the heavenly match in vitro. *Methods* **35**, 64-72 (2005).
 113. Köhn, M. *et al.* A microarray strategy for mapping the substrate specificity of protein tyrosine phosphatase. *Angew. Chem. Int. Edit.* **46**, 7700-3 (2007).
 114. Sun, H., Tan, L. P., Gao, L. & Yao, S. Q. High-throughput screening of catalytically inactive mutants of protein tyrosine phosphatases (PTPs) in a phosphopeptide microarray. *Chem. Commun.*, 677-9 (2009).
 115. Wälchli, S. *et al.* Probing protein-tyrosine phosphatase substrate specificity using a phosphotyrosine-containing phage library. *J. Biol. Chem.* **279**, 311-8 (2004).
 116. Ren, L. *et al.* Substrate Specificity of Protein Tyrosine Phosphatases 1B, RPTPr, SHP-1, and SHP-2. *Biochem.* **50**, 2339-2356 (2011).
 117. Shen, K. *et al.* Acquisition of a specific and potent PTP1B inhibitor from a novel combinatorial library and screening procedure. *J. Biol. Chem.* **276**, 47311-9 (2001).

118. Szczepankiewicz, B.G. *et al.* Discovery of a potent, selective protein tyrosine phosphatase 1B inhibitor using a linked-fragment strategy. *J. Am. Chem. Soc.* **125**, 4087-96 (2003).
119. Liu, G. *et al.* Selective protein tyrosine phosphatase 1B inhibitors: targeting the second phosphotyrosine binding site with non-carboxylic acid-containing ligands. *J. Med. Chem.* **46**, 3437-40 (2003).
120. Liu, G. *et al.* Fragment screening and assembly: a highly efficient approach to a selective and cell active protein tyrosine phosphatase 1B inhibitor. *J. Med. Chem.* **46**, 4232-5 (2003).
121. Lee, S.Y. *et al.* Design, construction, and intracellular activation of an intramolecularly self-silenced signal transduction inhibitor. *Angew. Chem. Int. Edit.* **44**, 4314-6 (2005).
122. Dufresne, C. *et al.* The development of potent non-peptidic PTP-1B inhibitors. *Bioorg. Med. Chem. Lett.* **14**, 1039-42 (2004).
123. Moran, E., Sarshar, S. and Cargill, J. Radio frequency tag encoded combinatorial library method for the discovery of tripeptide-substituted cinnamic acid inhibitors of the protein tyrosine phosphatase. *J. Am. Chem. Soc.* **117**, 10787-8 (1995).
124. Liljebris, C., Larsen, S.D., Ogg, D., Palazuk, B.J. & Bleasdale, J.E. Investigation of potential bioisosteric replacements for the carboxyl groups of peptidomimetic inhibitors of protein tyrosine phosphatase 1B: identification of a tetrazole-containing inhibitor with cellular activity. *J. Med. Chem.* **45**, 1785-98 (2002).
125. Iversen, L.F. *et al.* Structure-based design of a low molecular weight, nonphosphorus, nonpeptide, and highly selective inhibitor of protein-tyrosine phosphatase 1B. *J. Biol. Chem.* **275**, 10300-7 (2000).
126. Andersen, H.S. *et al.* Discovery and SAR of a novel selective and orally bioavailable nonpeptide classical competitive inhibitor class of protein-tyrosine phosphatase 1B. *J. Med. Chem.* **45**, 4443-59 (2002).
127. Bialy, L. & Waldmann, H. Inhibitors of protein tyrosine phosphatases: next-generation drugs? *Angew. Chem. Int. Edit.* **44**, 3814-39 (2005).
128. Popov, D. Novel protein tyrosine phosphatase 1B inhibitors: interaction requirements for improved intracellular efficacy in type 2 diabetes mellitus and obesity control. *Biochem. Biophys. Res. Co.* **410**, 377-81 (2011).
129. Jia, Z., Barford, D., Flint, A.J. and Tonks, N.K. Structural basis for phosphotyrosine peptide recognition by protein tyrosine phosphatase 1B. *Science* **268**, 1754-8 (1995).
130. Wiesmann, C. *et al.* Allosteric inhibition of protein tyrosine phosphatase 1B. *Nat. Struct. Mol. Biol.* **11**, 730-7 (2004).
131. Tjernberg, A. *et al.* Mechanism of action of pyridazine analogues on protein tyrosine phosphatase 1B (PTP1B). *Bioorg. Med. Chem. Lett.* **14**, 891-5 (2004).
132. Cravatt, B.F. and Sorensen, E.J. Chemical strategies for the global analysis of protein function. *Curr. Opin. Chem. Biol.* **4**, 663-8 (2000).
133. Jeffery, D.A. and Bogoy, M. Chemical proteomics and its application to drug discovery. *Curr. Opin. Biotech.* **14**, 87-95 (2003).
134. Kumar, S. *et al.* Activity-based probes for protein tyrosine phosphatases. *P. Natl. A. Sci. USA* **101**, 7943-8 (2004).
135. Shen, K., Qi, L., Ravula, M. and Klimaszewski, K. Synthesis and peptide incorporation of an unnatural amino acid containing activity-based probe for protein tyrosine phosphatases. *Bioorg. Med. Chem. Lett.* **19**, 3264-7 (2009).
136. Huang, Y., Kuo, C., Chu, C., Huang, Y. and Hu, Y. Development of activity-based probes with tunable specificity for protein tyrosine phosphatase subfamilies. *Tetrahedron* **66**, 4521-9 (2010).

137. Skorey, K., Waddleton, D., Therien, M. and Leriche, T. Enzyme occupancy measurement of intracellular protein tyrosine phosphatase 1B using photoaffinity probes. *Anal. Biochem.* **349**, 49-61 (2006).
138. Tiganis, T. and Bennett, A.M. Protein tyrosine phosphatase function: the substrate perspective. *Biochem. J.* **402**, 1-15 (2007).
139. Zabolotny, J.M. *et al.* PTP1B regulates leptin signal transduction in vivo. *Dev. Cell* **2**, 489-95 (2002).
140. Myers, M.P. *et al.* TYK2 and JAK2 are substrates of protein-tyrosine phosphatase 1B. *J. Biol. Chem.* **276**, 47771-4 (2001).
141. Gu, F. *et al.* Protein tyrosine phosphatase 1B attenuates growth hormone-mediated JAK2-STAT signaling. *Mol. Cell. Biol.* **23**, 3753-62 (2003).
142. Cheng, A. *et al.* Attenuation of leptin action and regulation of obesity by protein tyrosine phosphatase 1B. *Dev. Cell* **2**, 497-503 (2002).
143. Simoncic, P.D., Lee-Loy, A., Barber, D.L., Tremblay, M.L. and McGlade, C.J. The T cell protein tyrosine phosphatase is a negative regulator of janus family kinases 1 and 3. *Curr. Biol.* **12**, 446-53 (2002).
144. Zhu, S., Bjorge, J.D. and Fujita, D.J. PTP1B contributes to the oncogenic properties of colon cancer cells through Src activation. *Cancer Res.* **67**, 10129-37 (2007).
145. Wang, J. *et al.* PTP1B expression contributes to gastric cancer progression. *Med. Oncol.* (2011).
146. Liang, F., Lee, S.Y., Liang, J., Lawrence, D.S. and Zhang, Z.Y. The role of protein-tyrosine phosphatase 1B in integrin signaling. *J. Biol. Chem.* **280**, 24857-63 (2005).
147. Cheng, A., Bal, G.S., Kennedy, B.P. and Tremblay, M.L. Attenuation of adhesion-dependent signaling and cell spreading in transformed fibroblasts lacking protein tyrosine phosphatase-1B. *J. Biol. Chem.* **276**, 25848-55 (2001).
148. Bjorge, J.D., Pang, A. and Fujita, D.J. Identification of protein-tyrosine phosphatase 1B as the major tyrosine phosphatase activity capable of dephosphorylating and activating c-Src in several human breast cancer cell lines. *J. Biol. Chem.* **275**, 41439-46 (2000).
149. Krishnan, N., Fu, C., Pappin, D.J. and Tonks, N.K. H₂S-Induced Sulfhydrylation of the Phosphatase PTP1B and Its Role in the Endoplasmic Reticulum Stress Response. *Science Sign.* **4**, 1-12 (2011).
150. Wiede, F., Russell, S., Godfrey, D. and Tiganis, T. T cell protein tyrosine phosphatase attenuates T cell signaling to maintain tolerance in mice. *J. Clin. Invest.* **121**, 4758-74 (2011).
151. Shields, B.J., Court, N.W., Hauser, C., Bukczynska, P.E. and Tiganis, T. Cell cycle-dependent regulation of SFK, Jak1 and STAT3 signaling by the protein tyrosine phosphatase TCPTP. *Cell Cycle* **7**, 3405-16 (2008).
152. Zabolotny, J.M. *et al.* Transgenic overexpression of protein-tyrosine phosphatase 1B in muscle causes insulin resistance, but overexpression with leukocyte antigen-related phosphatase does not additively impair insulin action. *J. Biol. Chem.* **279**, 24844-51 (2004).
153. Kenner, K. A., Anyanwu, E., Olefsky, J.M. and Kusari, J. Protein-tyrosine phosphatase 1B is a negative regulator of insulin- and insulin-like growth factor-I-stimulated signaling. *J. Biol. Chem.* **271**, 19810-6 (1996).
154. Haj, F.G., Zabolotny, J.M., Kim, Y.B., Kahn, B.B. and Neel, B.G. Liver-specific protein-tyrosine phosphatase 1B (PTP1B) re-expression alters glucose homeostasis of PTP1B *-/-* mice. *J. Biol. Chem.* **280**, 15038-46 (2005).
155. Cicirelli, M.F. *et al.* Microinjection of a protein-tyrosine-phosphatase inhibits insulin action in *Xenopus* oocytes. *P. Natl. A. Sci. USA* **87**, 5514-8 (1990).

156. Meng, T.C., Buckley, D. A., Galic, S., Tiganis, T. and Tonks, N.K. Regulation of insulin signaling through reversible oxidation of the protein-tyrosine phosphatases TC45 and PTP1B. *J. Biol. Chem.* **279**, 37716-25 (2004).
157. Galic, S. *et al.* Regulation of insulin receptor signaling by the protein tyrosine phosphatase TCPTP. *Mol. Cell. Biol.* **23**, 2096-2108 (2003).
158. Tiganis, T., Bennett, A.M., Ravichandran, K.S. and Tonks, N.K. Epidermal growth factor receptor and the adaptor protein p52 Shc are specific substrates of T-cell protein tyrosine phosphatase. *Mol. Cell. Biol.* **18**, 1622-43 (1998).
159. Tiganis, T., Kemp, B.E. and Tonks, N.K. The protein-tyrosine phosphatase TCPTP regulates epidermal growth factor receptor-mediated and phosphatidylinositol 3-kinase-dependent signaling. *J. Biol. Chem.* **274**, 27768-75 (1999).
160. Mattila, E. *et al.* Negative regulation of EGFR signalling through integrin- α 1 β 1-mediated activation of protein tyrosine phosphatase TCPTP. *Nat. Cell. Biol.* **7**, 78-85 (2005).
161. Klingler-Hoffmann, M. *et al.* The protein tyrosine phosphatase TCPTP suppresses the tumorigenicity of glioblastoma cells expressing a mutant epidermal growth factor receptor. *J. Biol. Chem.* **276**, 46313-8 (2001).
162. Merrifield, R. Solid phase peptide synthesis I. The Synthesis of a tetrapeptide. *J. Am. Chem. Soc.* **14**, 2149-54 (1963).
163. Merrifield, R.B. Automated synthesis of peptides. *Science* **150**, 178-85 (1965).
164. Merrifield, R. & Stewart, J.M. Automated peptide synthesis. *Nature* **207**, 522-3 (1965).
165. Harder, K.W. *et al.* Characterization and kinetic analysis of the intracellular domain of human protein tyrosine phosphatase beta (HPTP beta) using synthetic phosphopeptides. *Biochem. J.* **298**, 395-401 (1994).
166. Michaelis, L. and Menten, M.L. Die Kinetik der Invertinwirkung. *Biochem. Z.* **49**, 333-69 (1913).
167. Gordeev, M., Patel, D.V., Barker, P.L. and Gordon E.M. N- α -Fmoc-4-phosphono(difluoromethyl)-L-phenylalanine: a new O-phosphotyrosine isosteric building block suitable for direct incorporation into peptides. *Tetrahedron Lett.* **35**, 7585-8 (1994).
168. Shen, K. *et al.* Acquisition of a specific and potent PTP1B inhibitor from a novel combinatorial library and screening procedure. *J. Biol. Chem.* **276**, 47311-9 (2001).
169. Qabar, M.N., Urban, J. and Kahn, M. A facile solution and solid phase synthesis of phosphotyrosine mimetic L-4-[diethylphosphono(difluoromethyl)]-phenylalanine (F₂Pmp(EtO)₂) derivatives. *Tetrahedron* **53**, 11171-8 (1997).
170. Burke, T.R. Design and synthesis of phosphonodifluoromethyl phenylalanine (F₂Pmp): a useful phosphotyrosyl mimetic. *Curr. Top. Med. Chem.* **6**, 1465-71 (2006).
171. Wrobel, J. and Dietrich, A. Preparation of L-(Phosphonodifluoromethyl)phenylalanine derivatives as non-hydrolyzable mimetics of O-phosphotyrosine. *Tetrahedron Lett.* **34**, 3543-6 (1993).
172. Burke, T.R. *et al.* Nonhydrolyzable phosphotyrosyl mimetics for the preparation of phosphatase-resistant SH2 domain inhibitors. *Biochem.* **33**, 6490-4 (1994).
173. Solas, D., Hale, R.L. and Patel, D.V. An efficient synthesis of N- α -Fmoc-4-(Phosphonodifluoromethyl)-L-phenylalanine. *J. Org. Chem.* **61**, 1537-9 (1996).
174. Smyth, M.S. and Burke, R. Enantioselective synthesis of N-boc and N-fmoc protected diethyl 4-phosphono(difluoromethyl)-L-phenylalanine; agents suitable for the solid-phase synthesis of peptides containing nonhydrolyzable analogues of O-phosphotyrosine. *Tetrahedron Lett.* **35**, 551-4 (1994).
175. Weiming, Q.D. and Burton, D.J. A facile and general preparation of α,α -difluoro benzylic phosphonates by the CuCl promoted coupling reaction of the

- (diethylphosphonyl)difluoromethylcadmium reagent with aryl iodides. *Tetrahedron Lett.* **37**, 2745-8 (1996).
176. Veber, D., Strachan, R. and Bergstrand, S. Nonreducible cyclic analogues of somatostatin. *J. Am. Chem. Soc.* **5**, 8-10 (1976).
177. Veber, D.F. *et al.* Highly active cyclic and bicyclic somatostatin analogues of reduced ring size. *Nature* **280**, 512-4 (1979).
178. Tugyi, R., Mezö, G., Fellingner, E., Andreu, D. and Hudecz, F. The effect of cyclization on the enzymatic degradation of herpes simplex virus glycoprotein D derived epitope peptide. *J. Pept. Sci.* **11**, 642-9 (2005).
179. Nutt, R. and Veber, D. Synthesis of nonreducible bicyclic analogs of somatostatin. *J. Am. Chem. Soc.* **102**, 6539-45 (1980).
180. Liskamp, R.M.J., Rijkers, D.T.S., Kruijtzter, J.A.W. and Kemmink, J. Peptides and proteins as a continuing exciting source of inspiration for peptidomimetics. *ChemBioChem* **12**, 1626-53 (2011).
181. Kessler, H. Conformation and biological activity of cyclic peptides. *Angew. Chem. Int. Edit.* **21**, 512-23 (1982).
182. Gante, J. Peptidomimetics - tailored enzyme inhibitors. *Angew. Chem. Int. Edit.* **33**, 1699-1720 (1994).
183. Chorev, M. and Goodman, M. Recent developments in retro peptides and proteins-an ongoing topochemical exploration. *Trends Biotechn.* **13**, 438-45 (1995).
184. Briand, J.P. *et al.* A retro-inverso peptide corresponding to the GH loop of foot-and-mouth disease virus elicits high levels of long-lasting protective neutralizing antibodies. *P. Natl. A. Sci. USA* **94**, 12545-50 (1997).
185. Walensky, L.D. *et al.* Activation of apoptosis in vivo by a hydrocarbon-stapled BH3 helix. *Science* **305**, 1466-70 (2004).
186. Leone, M., Barile, E., Dahl, R. and Pellecchia, M. Design and NMR studies of cyclic peptides targeting the N-terminal domain of the protein tyrosine phosphatase YopH. *Chem. Biol. Drug. Des.* **77**, 12-19 (2011).
187. Hoyle, C.E. and Bowman, C.N. Thiol-ene click chemistry. *Angew. Chem. Int. Edit.* **49**, 1540-73 (2010).
188. Jonkheijm, P. *et al.* Photochemical surface patterning by the thiol-ene reaction. *Angew. Chem. Int. Edit.* **47**, 4421-4 (2008).
189. Killops, K.L., Campos, L.M. and Hawker, C.J. Robust, efficient, and orthogonal synthesis of dendrimers via thiol-ene "click" chemistry. *J. Am. Chem. Soc.* **130**, 5062-4 (2008).
190. Köhn, M., Benito, J.M., Ortiz Mellet, C., Lindhorst, T.K. and García Fernández, J.M. Functional evaluation of carbohydrate-centred glycoclusters by enzyme-linked lectin assay: ligands for concanavalin A. *ChemBioChem* **5**, 771-7 (2004).
191. Wittrock, S., Becker, T. and Kunz, H. Synthetic vaccines of tumor-associated glycopeptide antigens by immune-compatible thioether linkage to bovine serum albumin. *Angew. Chem. Int. Edit.* **46**, 5226-30 (2007).
192. Jagasia, R., Holub, J.M., Bollinger, M., Kirshenbaum, K. and Finn, M.G. Peptide cyclization and cyclodimerization by Cu(I)-mediated azide-alkyne cycloaddition. *J. Org. Chem.* **74**, 2964-74 (2009).
193. Huisgen, R. Kinetics and reaction mechanisms: selected examples from the experience of forty years. *Pure Appl. Chem.* **61**, 613-28 (1989).
194. Huisgen, R. Kinetik und Mechanismus 1,3-Dipolarer Cycloadditionen. *Angew. Chem.* **75**, 742-54 (1963).

195. Himo, F. *et al.* Copper(I)-catalyzed synthesis of azoles. DFT study predicts unprecedented reactivity and intermediates. *J. Am. Chem. Soc.* **127**, 210-6 (2005).
196. Moses, J.E. and Moorhouse, A.D. The growing applications of click chemistry. *Chem. Soc. Rev.* **36**, 1249-62 (2007).
197. Tron, G.C. *et al.* Click chemistry reactions in medicinal chemistry: applications of the 1,3-dipolar cycloaddition between azides and alkynes. *Med. Res. Rev.* **28**, 278-308 (2007).
198. Cantel, S. *et al.* Synthesis and conformational analysis of a cyclic peptide obtained via i to i+4 intramolecular side-chain to side-chain azide-alkyne 1,3-dipolar cycloaddition. *J. Org. Chem.* **73**, 5663-74 (2008).
199. Choi, W.J. *et al.* Application of azide-alkyne cycloaddition "click chemistry" for the synthesis of Grb2 SH2 domain-binding macrocycles. *Bioorg. Med. Chem. Lett.* **16**, 5265-9 (2006).
200. Manetsch, R. *et al.* *In situ* click chemistry: enzyme inhibitors made to their own specifications. *J. Am. Chem. Soc.* **126**, 12809-18 (2004).
201. Mocharla, V.P. *et al.* *In situ* click chemistry: enzyme-generated inhibitors of carbonic anhydrase II. *Angew. Chem. Int. Edit.* **44**, 116-20 (2004).
202. Mock, W., Irra, T., Wepsiec, J. and Manimaran, T. Cycloaddition Induced by Cucurbituril. A case of Pauling principle catalysis. *J. Org. Chem.* **48**, 3619-20 (1983).
203. Mock, W., Irra, T. and Wepsiec, J. Catalysis by cucurbituril. The significance of bound-substrate destabilization for induced triazole formation. *J. Org. Chem.* **54**, 5302-8 (1989).
204. Goddard-Borger, E.D. and Stick, R.V. An efficient, inexpensive, and shelf-stable diazotransfer reagent: imidazole-1-sulfonyl azide hydrochloride. *Org. Lett.* **9**, 3797-800 (2007).
205. Zhang, Z.Y. Kinetic and mechanistic characterization of a mammalian protein-tyrosine phosphatase PTP1. *J. Biol. Chem.* **270**, 11199-204 (1995).
206. Jameson, D.M. and Ross, J.A. Fluorescence polarization/anisotropy in diagnostics and imaging. *Chem. Rev.* **110**, 2685-708 (2010).
207. Weber, G. Polarization of the fluorescence of macromolecules. *Biochem. J.* **51**, 145-55 (1952).
208. Weber, G. Polarization of the fluorescence of macromolecules. *Biochem J* **51**, 155-67 (1952).
209. Ashkenazi, A. *et al.* Mapping the CD4 binding site for human immunodeficiency virus by alanine-scanning mutagenesis. *P. Natl. A. Sci. USA* **87**, 7150-4 (1990).
210. Cunningham, B.C. and Wells, J.A. High-resolution epitope mapping of hGH-receptor interactions by alanine-scanning mutagenesis. *Science* **244**, 1081-5 (1989).
211. Gibbs, C.S. and Zoller, M.J. Identification of electrostatic interactions that determine the phosphorylation site specificity of the cAMP-dependent protein kinase. *Biochem.* **30**, 5329-34 (1991).
212. K.L. Morrison and Weiss G.A. Combinatorial alanine-scanning. *Curr. Opin. Chem. Biol.* **5**, 302-7 (2001).
213. Sarmiento, M., Zhao, Y., Gordon, S.J. and Zhang, Z.Y. Molecular basis for substrate specificity of protein-tyrosine phosphatase 1B. *J. Biol. Chem.* **273**, 26368-74 (1998).
214. Zheng, X.M., Resnick, R.J. & Shalloway, D. Mitotic activation of protein-tyrosine phosphatase alpha and regulation of its Src-mediated transforming activity by its sites of protein kinase C phosphorylation. *J. Biol. Chem.* **277**, 21922-9 (2002).
215. Zheng, X.M., Resnick, R.J. and Shalloway, D. A phosphotyrosine displacement mechanism for activation of Src by PTPalpha. *EMBO J.* **19**, 964-78 (2000).

216. Wenqing, X. and Harrison, S. Three-dimensional structure of the tyrosine kinase c-Src. *Nature* **385**, 595-602 (1997).
217. Rothbard, J.B. *et al.* Conjugation of arginine oligomers to cyclosporin A facilitates topical delivery and inhibition of inflammation. *Nat. Med.* **6**, 1253-7 (2000).
218. Rothbard, J.B., Jessop, T.C., Lewis, R.S., Murray, B.A. and Wender, P.A. Role of membrane potential and hydrogen bonding in the mechanism of translocation of guanidinium-rich peptides into cells. *J. Am. Chem. Soc.* **126**, 9506-7 (2004).
219. Schmidt, N., Mishra, A., Lai, G.H., and Wong G.C.L Arginine-rich cell-penetrating peptides. *FEBS Lett.* **584**, 1806-13 (2010).
220. Wender, P.A. *et al.* The design, synthesis, and evaluation of molecules that enable or enhance cellular uptake: peptoid molecular transporters. *P. Natl. A. Sci. USA* **97**, 13003-8 (2000).
221. Lu, W., Gong, D., Bar-Sagi, D. and Cole, P.A. Site-specific incorporation of a phosphotyrosine mimetic reveals a role for tyrosine phosphorylation of SHP-2 in cell signaling. *Mol. Cell* **8**, 759-69 (2001).
222. Green, N.M. Avidin. *Biochem. J.* **89**, 585-91 (1963).
223. Rostovtsev, V.V., Green, L.G., Fokin, V.V. and Sharpless, K.B. A stepwise Huisgen cycloaddition process: copper(I)-catalyzed regioselective "ligation" of azides and terminal alkynes. *Angew. Chem. Int. Edit.* **41**, 2596-9 (2002).
224. Payne, G., Shoelson, S.E., Gish, G.D., Pawson, T. and Walsh, C.T. Kinetics of p56lck and p60src Src homology 2 domain binding to tyrosine-phosphorylated peptides determined by a competition assay or surface plasmon resonance. *P. Natl. A. Sci. USA* **90**, 4902-6 (1993).
225. Ellison, S., Mori, J., Barr, A.J. and Senis, Y.A. CD148 enhances platelet responsiveness to collagen by maintaining a pool of active Src family kinases. *J. Thromb. Haemost.* **8**, 1575-83 (2010).
226. Nakagawa, Y. *et al.* Tyrosine phosphatase epsilonM stimulates migration and survival of porcine aortic endothelial cells by activating c-Src. *Biochem. Biophys. Res. Co.* **325**, 314-9 (2004).
227. Pera, I.L. *et al.* The rat tyrosine phosphatase eta increases cell adhesion by activating c-Src through dephosphorylation of its inhibitory phosphotyrosine residue. *Oncogene* **24**, 3187-95 (2005).
228. Somani, A.K., Bignon, J.S., Mills, G.B., Siminovitch, K.A. and Branch, D.R. Src kinase activity is regulated by the SHP-1 protein-tyrosine phosphatase. *J. Biol. Chem.* **272**, 21113-9 (1997).
229. Zambuzzi, W.F. *et al.* Modulation of Src activity by low molecular weight protein tyrosine phosphatase during osteoblast differentiation. *Cell. Physiol. Biochem.* **22**, 497-506 (2008).
230. Vacaru, A.M. and den Hertog, J. Catalytically active membrane-distal phosphatase domain of receptor protein-tyrosine phosphatase alpha is required for Src activation. *FEBS J.* **277**, 1562-70 (2010).
231. Talamonti, M.S., Roh, M.S., Curley, S.A. and Gallick, G.E. Increase in activity and level of pp60c-src in progressive stages of human colorectal cancer. *J. Clin. Invest.* **91**, 53-60 (1993).
232. Hiscox, S. *et al.* Elevated Src activity promotes cellular invasion and motility in tamoxifen resistant breast cancer cells. *Breast Cancer Res. Tr.* **97**, 263-74 (2006).
233. Verdine, G.L. & Hilinski, G.J. Stapled peptides for intracellular drug targets. *Methods Enzymol.* **503**, 3-33 (2012).